Online Fault Detection of a Heavy Duty Diesel Engine with Model-Based Methods

Vom Fachbereich
Elektrotechnik und Informationstechnik
der Technischen Universität Darmstadt
zur Erlangung des Grades eines Doktor-Ingenieurs (Dr.-Ing.)
genehmigte Dissertation

von

Michael Hinrichs, M.Sc.

Referent:	Prof. Dr.-Ing. Dr. h. c. Rolf Isermann
Korreferent:	Prof. Dr.-Ing. Christian Beidl
Tag der Einreichung:	25. Januar 2021
Tag der Prüfung:	8. Juni 2021

D 17 · Darmstadt 2021

Online Fault Detection of a Heavy Duty Diesel Engine with Model-Based Methods

Gemehmigte Dissertation von Michael Hinrichs, M.Sc.

D 17 · Darmstadt 2021

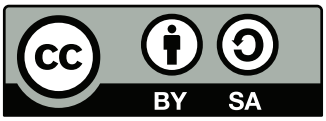

Danksagung

Zunächst möchte ich Herrn Prof. Dr.-Ing. Dr. h. c. Rolf Isermann für die Übernahme der Betreuung meiner Arbeit danken. Durch zahlreiche wissenschaftliche Diskussionen habe ich viel gelernt, nicht nur aus akademischer, sondern auch aus menschlicher Sicht. Der unbändige Wissensdurst und das Beibehalten der kindlichen Neugier bis ins höhere Alter sind ein absolutes Vorbild.

Besonderer Dank gilt auch Herrn Prof. Dr.-Ing. Peter Pickel für das in mich gesetzte Vertrauen. Ab dem ersten Arbeitstag hatte ich unglaublich viele Freiheiten eigene Ideen oder wissenschaftliche Fragestellungen zu verfolgen.

Herrn Prof. Dr.-Ing. Christian Beidl danke ich für das Interesse an meiner Arbeit sowie die Übernahme des Koreferats.

Bedanken möchte ich mich ebenfalls bei Herrn Prof. Dr.-Ing. Michael Günthner für die gute Zusammenarbeit und die Bereitstellung des Motorenprüfstandes an der TU Kaiserslautern. Ebenso danke ich allen Mitarbeitern des VKM/LAF für die Unterstützung und die zahlreichen “interessanten” Kaffeezimmergespräche.

Ein herzliches Dankeschön auch an die “TFZ’ler”, bei denen nicht nur die traditionellen Projekttreffen im Sommer, sondern auch die tägliche Zusammenarbeit sehr viel Spaß gemacht haben.

Der gesamten Abteilung External Relations möchte ich danken für das tolle Arbeitsklima und die moralische Unterstützung in den letzten Jahren. Insbesondere möchte ich mich bei Herrn Dr.-Ing. Philipp Münch für das Korrekturlesen meiner Arbeit und viele interessante Diskussionen und Tipps bedanken.

Vielen Dank auch an das Team in Darmstadt. Speziell bei Frau Ilse Brauer möchte ich mich für die Übernahme unzähliger organisatorischer Angelegenheiten am Lehrstuhl bedanken.

Meiner Freundin Linda danke ich für die große Unterstützung und die Geduld (nicht nur während der Anfertigung dieser Arbeit).

"Twenty years from now you will be more disappointed by the things that you didn't do than by the ones you did do." – Mark Twain

Kurzfassung

Eine schnelle Reduktion des CO_2 Ausstoßes von landwirtschaftlichen Maschinen kann nur gelingen, wenn Dieselmotoren mit Kraftstoffen betrieben werden, die eine geringe CO_2 Gesamtbilanz aufweisen. In der Landwirtschaft eignen sich dazu besonders biogene Kraftstoffe der 1. Generation, wie bspw. naturbelassenes Rapsöl. Dieses kann von Landwirten selbst hergestellt und auf dem eigenen Betrieb eingesetzt werden. Durch kurze Transportwege und dem einfachen Herstellungsverfahren können bis zu 91% der CO_2-Emissionen eingespart werden.
Jedoch haben sich diese Kraftstoffe bisher nicht durchgesetzt. Neben ökonomischen Gründen wurde vielfach die in der Landwirtschaft geforderte Zuverlässigkeit nicht eingehalten. Insbesondere bei kalten Temperaturen führte der Betrieb mit naturbelassenem Rapsöl in der Vergangenheit zu Problemen im Kraftstoffsystem der Maschinen.
Eine Möglichkeit die Zuverlässigkeit der Maschine und die Akzeptanz der Kunden zu erhöhen ist ein Verbrennungsmotor, der die Mischung von herkömmlichen Diesel mit biogenen Kraftstoffen erlaubt. Damit sich der Motor auf die jeweilige Kraftstoffmischung einstellen kann, ist eine Kraftstofferkennung notwendig.

Dazu werden im ersten Teil dieser Arbeit Modelle auf Basis von Sauerstoffsensoren im Abgastrakt (*Oxygen-Mixture Model*) und der Stromaufnahme der Kraftstoffpumpe (*Fuel Pump Current Model*) erstellt. Mit diesen Modellen können Kraftstoffmischungen zwischen Diesel und naturbelassenem Rapsöl sowie Mischungen zwischen Diesel und Rapsmethylester erkannt werden. Darüber hinaus wird ein neues Niederdruck-Kraftstoffsystem entwickelt, welches für den Betrieb der drei Kraftstoffe ausgelegt ist und den Rapsölbetrieb bei kalten Temperaturen deutlich verbessert. Weiterhin werden umfangreiche Anpassungen der Steuer- und Regelfunktionen in der Motorsteuerung vorgenommen, sodass im Betrieb mit Kraftstoffmischungen ein ähnliches Verhalten wie im reinen Dieselbetrieb erreicht wird.

Im zweiten Teil dieser Arbeit werden Modelle entwickelt, um Fehler des Dieselmotors zu erkennen. Dies dient der weiteren Erhöhung der Zuverlässigkeit von landwirtschaftlichen Maschinen. Prinzipiell sind die Modelle auch für naturbelassenes Rapsöl und Rapsmethylester geeignet, jedoch fehlen zum Teil grundlegende Informationen zu diesen Kraftstoffen. Aus diesem Grund werden alle Versuche ausschließlich mit fossilem Dieselkraftstoff durchgeführt.

Insgesamt werden drei Modelle entwickelt, mit denen die eingespritzte Kraftstoffmasse berechnet werden kann. Mit diesen Modellen kann nicht nur Leistungsverlust durch zu geringe Einspritzmengen, sondern auch erhöhte Leistungen durch illegales Motortuning detektiert werden. Da das Manipulieren von Motoren zu frühzeitigen Schäden an Maschinen führen kann, ist eine sichere Motortuning-Erkennung hinsichtlich etwaiger Gewährleistungsansprüche finanziell für den Hersteller von hoher Bedeutung.

Zu den drei entwickelten Einspritzmengenmodellen gehört das *Rail Pressure Based Fuel Estimation Model*, bei dem die Einspritzmenge auf Basis des Raildrucks bzw. Dichteänderungen des Kraftstoffs im Rail berechnet wird.
Ein weiteres Einspritzmengenmodell ist das *Suction Control Valve Model*. Hierbei wird die eingespritzte Kraftstoffmasse auf Basis der Zumesseinheit der Hochdruckpumpe berechnet.
Das dritte Modell ist das *Oxygen-Fuel Model*. Es ist völlig unabhängig von Fehlern im Kraftstoffsystem, da es die eingespritzte Kraftstoffmasse auf der Grundlage des Restsauerstoffgehalts im Abgas und des Luftmassenstroms berechnet.

Ein weiteres Problem, welches die Zuverlässigkeit des Dieselmotors beeinträchtigt, sind Injektorablagerungen. Damit diese im laufenden Betrieb der Maschine erkannt werden können, wird ein *Injector Deposit Detection Model* vorgestellt. Hiermit ist es möglich Injektoren zu klassifizieren und Reparaturstrategien abzuleiten. Die Erkennung von Injektorablagerungen wird hierbei über eine Mehrfachabtastung des Raildrucksignals realisiert.

Insgesamt zeigt diese Forschungsarbeit, dass der Betrieb von biogenen Kraftstoffen auch mit modernen Dieselmotoren möglich ist. Es wird jedoch deutlich, dass ein zusätzlicher Applikationsaufwand für die Motorsteuerung notwendig ist, um einen Motor (der für verschiedene Kraftstoffmischungen geeignet ist) zur Serienreife zu bringen. Ferner zeigen die Ergebnisse der Fehlererkennungsmodelle Potential die Zuverlässigkeit von Dieselmotoren weiter zu erhöhen.

Summary

A rapid reduction in CO_2 emissions from agricultural machinery can only succeed if diesel engines are operated with fuels that have a low CO_2 impact. In agriculture, first generation biogenic fuels such as natural rapeseed oil are particularly suitable. This fuels can be produced by the farmers themselves and used on their own farms. The short transportation distances and simple production process can save up to 91% of CO_2 emissions.
However, these fuels have not yet become established. Apart from economic reasons, the reliability required in agricultural machinery has often not been met. Especially at cold temperatures, the operation with natural rapeseed oil in the past led to problems in the fuel system of the machines. One way to increase machine reliability and customer acceptance is to have an internal combustion engine that allows conventional diesel to be blended with biogenic fuels. In order for the engine to adjust to the respective fuel mixture, fuel detection is necessary.

For this purpose, models based on the oxygen sensors in the exhaust tract (*Oxygen-Mixture Model*) and the current consumption of the fuel pump (*Fuel Pump Current Model*) are created in the first part of this thesis. These models can be used to detect fuel mixtures between diesel and natural rapeseed oil as well as mixtures between diesel and rapeseed methyl ester. In addition, a new low-pressure fuel system is being developed which is designed to operate with the three fuels and significantly improves rapeseed oil operation at cold temperatures.
In addition, extensive adjustments are made to the control and regulation functions in the engine control unit, so that in operation with fuel mixtures a similar behavior is achieved as in pure diesel operation.

In the second part of this thesis, faults of the diesel engine in pure diesel operation are detected. This serves to further increase the reliability of agricultural machines. In principle, the models are also suitable for natural rapeseed oil and rapeseed methyl ester. However, since some important basic information is only available for diesel fuel, all tests are performed with fossil diesel.
In total, three models are being developed with which the injected fuel mass can be calculated. With these models not only the loss of performance due to insufficient injection quantities can be detected, but also increased performance due to illegal chip tuning. Since chip tuning can lead to early damage to machines, a reliable chip tuning detection with regard to possible warranty claims is financially very important for the manufacturer.

One of the three developed injection quantity models is the *Rail Pressure Based Fuel Estimation Model* where the injection quantity is calculated based on the rail pressure or density changes of the fuel in the rail.
Another injection quantity model is the *Suction Control Valve Model*. Here the injected fuel mass is calculated based on the metering unit of the high pressure pump.
The third model is the *Oxygen-Fuel model*. It is completely independent of faults in the fuel system

as it calculates the injected fuel mass based on residual oxygen content in the exhaust gas and the intake air mass flow.

Another problem that affects the reliability of the diesel engine are injector deposits. In order to detect these deposits on the machine, an *Injector Deposit Detection Model* is presented. With this model it is possible to classify injectors and derive repair strategies. The detection of injector deposits is realized by multiple sampling of the rail pressure signal.

Altogether, this research work shows that the operation of biogenic fuels is also possible with modern diesel engines. However, it becomes clear that a high parameterize effort for the engine control unit would be necessary to get an engine (which is suitable for different fuel mixtures) ready for series production. Furthermore, the results of the fault detection models show potential to further increase the reliability of diesel engines.

Contents

Symbols and Acronyms

Symbols

A_c	area of component c (m^2)
$c_{p,s}$	thermal capacity of the substance s ($J\,kg^{-1}\,K^{-1}$)
$E_{\text{fuel,st}}$	air mass based heat input of the fuel for stoichiometric comb. ($kJ\,kg^{-1}$)
E_{f}	bulk modulus of the fuel (GPa)
$f_{\text{max,crank}}$	maximal frequency of crank timing wheel signal (Hz)
F_c	force of cause c (N)
F_{tuning}	tuning factor for storing a fault code (-)
$F_{\text{inj,idd}}$	percentual deviation of the modeled from the desired injection mass (%)
$H_{\text{u},s}$	lower heating value of the substance s ($kJ\,kg^{-1}$)
i_{pump}	current of the electrical fuel pump (A)
$i_{\text{pump,new}}$	current of the electrical fuel pump with new fuel filter (A)
$i_{\text{pump,dirty}}$	current of the electrical fuel pump with dirty fuel filter(A)
$\bar{i}_{\text{scv}}$	mean current for controlling the suction control valve (A)
j	index for multiple injections during one comb. stroke (-)
k	running index for recorded injections of a specific injector (-)
l	running index for recorded injections of all injectors (-)
$L_{\text{st},s}$	stoichiometric air demand of the fuel s (-)
$\text{LGF}(w_{\text{b0}})$	probability for a specific B0 proportion in the fuel (-)
$\dot{m}_{\text{air,th}}$	theoretical air mass flow through all cylinders ($mg\,s^{-1}$)
$\dot{m}_{\text{air,real}}$	real air mass flow through all cylinders ($mg\,s^{-1}$)
$\dot{m}_{\text{hpp}}$	fuel mass flow through high-pressure pump ($mg\,s^{-1}$)
$\dot{m}_{\text{prv}}$	fuel mass flow through pressure relief valve ($mg\,s^{-1}$)
m_c	mass of cause c (kg)
m_{air}	air mass in the cylinder before comb. (mg)
$m_{\text{air,exh}}$	air mass in the cylinder after comb. (mg)
$m_{\text{air,sim}}$	simulated air mass in the cylinder before comb. (mg)
m_{exh}	exhaust gas mass in cylinder after comb. (mg)
$m_{\text{exh,ox}}$	mass of H_2O and CO_2 in cylinder after comb. (mg)
$m_{\text{f,meas}}$	fuel mass measured by weight scale (mg)
$m_{\text{f,oil}}$	total fuel mass in the engine oil (mg)
m_{inj}	inj. fuel mass for one comb. stroke (mg)
$m_{\text{inj},i}$	inj. fuel mass for injector i (mg)
$m_{\text{inj},j}$	inj. fuel mass of the multiple injection j (mg)
$m_{\text{inj},i,k}$	inj. fuel mass of injector i at injection k (mg)
$m_{\text{inj,b0}}$	inj. fuel mass of B0 for one comb. stroke (mg)
$m_{\text{inj,b0,equi}}$	equivalent mass of B0 with same heating value as a specific fuel mixture (mg)

$m_{\mathrm{inj,cfm}}$	inj. fuel mass of the currently used fuel mixture during one comb. stroke (mg)
$m_{\mathrm{inj,ecu}}$	inj. fuel mass for one comb. stroke with which the ECU calculates (mg)
$m_{\mathrm{inj,ecu},j}$	inj. fuel mass for the multiple injection j with which the ECU calculates (mg)
$m_{\mathrm{inj,ecu,post}}$	inj. fuel mass of non-torque generating injection for one comb. stroke (mg)
$m_{\mathrm{inj,ecu,post,j}}$	inj. fuel mass of non-torque generating injection of the multiple injection j (mg)
$m_{\mathrm{inj,leak}}$	leakage fuel mass for one comb. stroke (mg)
$m_{\mathrm{inj,leak},i}$	leakage fuel mass for one comb. stroke returned by injector i (mg)
$m_{\mathrm{inj,nro}}$	inj. fuel mass of NRO for one comb. stroke (mg)
$m_{\mathrm{inj,oil}}$	mass of fuel entering the engine oil for one comb. stroke (mg)
$m_{\mathrm{inj,of}}$	inj. fuel mass based on Oxygen-Fuel Model for one comb. stroke (mg)
$m_{\mathrm{inj,post,j}}$	inj. fuel mass of non-torque generating injection of the multiple injection j (mg)
$m_{\mathrm{inj,post,doc}}$	inj. fuel mass of non-torque generating injection reaching the DOC (mg)
$m_{\mathrm{inj,rbfe}}$	simulated inj. fuel mass based on RBFE model (mg)
$m_{\mathrm{inj,rbfe,idd}}$	simulated inj. fuel mass based on IDD model (mg)
$m_{\mathrm{leak,meas}}$	leakage fuel mass measured by weight scale (mg)
m_{oil}	mass of the engine oil (mg)
m_{pump}	fuel mass pumped by the high pressure pump for one comb. stroke (mg)
$m_{\mathrm{pump,sim}}$	simulated fuel mass pumped by the high pressure pump for one comb. stroke (mg)
m_{r}	fuel mass in rail (mg)
$m_{\mathrm{r,bi},i}$	fuel mass in rail before injection of injector i starts (mg)
m_{RME}	inj. rapeseed methyl ester mass for one comb. stroke (mg)
m_{scv}	simulated inj. fuel mass based on SCV model for one comb. stroke (mg)
M	torque (N m)
M_{ecu}	torque with which the ECU calculates (N m)
M_s	molar mass of the substance s (g mol^{-1})
$\mathrm{MA}(w_{\mathrm{b0}})$	mixture array representing the probability for a specific B0 proportion in the fuel (-)
n_s	number of atoms of substance s (mol)
n_{des}	desired engine speed (rpm)
n_{eng}	engine speed (rpm)
n_{inj}	number of injections (-)
$n_{\mathrm{inj},i}$	number of injections of injector i (-)
$\mathrm{O}_{2,\mathrm{meas}}$	measured oxygen content in exhaust gas (%)
$\mathrm{O}_{2,\mathrm{th}}$	simulated oxygen content in exhaust gas (%)
p_{lpfs}	fuel pressure in the low pressure fuel system (bar)
p_{r}	rail pressure (MPa)
$p_{\mathrm{r},a,k}$	rail pressure in the pressure zone a at recording point k(MPa)
$\bar{p}_{\mathrm{r,bi},i}$	mean rail pressure before injection of injector i over all recorded injections (MPa)
$p_{\mathrm{r,bi},i,k}$	rail pressure before injection k of injector i (MPa)
$p_{\mathrm{r,data},i}$	rail pressure data of all 50 recorded runs fonr injector i (MPa)
$p_{\mathrm{r,data,shift},i}$	rail pressure data of all 50 recorded runs shifted to same starting pressure (MPa)
$p_{\mathrm{r,ecu}}$	rail pressure with which the ECU calculates (MPa)
$p_{\mathrm{r,set}}$	rail pressure set-point of the ECU (MPa)
p_{scv}	fuel pressure before entering the SCV (bar)

$\dot{Q}_{\text{pump}}$	volume flow of the fuel through electrical fuel pump ($\mathrm{L\,h^{-1}}$)
R	universal gas constant ($\mathrm{J\,mol^{-1}\,K^{-1}}$)
R_{tun}	resistance of the rail pressure measuring path with rail tuning (Ω)
R_{ecu}	resistance of the rail pressure measuring path in series condition (Ω)
t_{inj}	injector pulse duration (µs)
$t_{\text{inj,ecu}}$	injector pulse duration with which the ECU calculates (µs)
$t_{\text{cd,ecu}}$	injector needle closing delay with which the ECU calculates (µs)
$t_{\text{cd,sim}}$	simulated injector needle closing delay (µs)
$t_{\text{od,ecu}}$	injector needle opening delay with which the ECU calculates (µs)
$t_{\text{od,sim}}$	simulated injector needle opening delay (µs)
t_{sd}	rail pressure sensor delay (µs)
T	temperature (K)
T_{eip}	time for end of injection pulse (µs)
$T_{\text{eip,ecu}}$	time for end of injection pulse with which the ECU calculates (µs)
T_{eopd}	time for end of pressure drop (µs)
T_{ep}	time of pumping end (µs)
$T_{\text{ep,r}}$	time of pumping end based on measured rail pressure (µs)
T_{exh}	exhaust temperature at exhaust valve (°C)
T_{hps}	fuel temperature in the high pressure fuel system (K)
T_{inc}	time for injector needle closed (µs)
$T_{\text{inc,ecu}}$	time for injector needle closed with which the ECU calculates (µs)
T_{ino}	time for injector needle open (µs)
$T_{\text{ino,ecu}}$	time for injector needle open with which the ECU calculates (µs)
T_{lpfs}	fuel temperature in the low pressure fuel system (°C)
T_{sip}	start of injection pulse (µs)
$T_{\text{sip,ecu}}$	time for start of injection pulse with which the ECU calculates (µs)
T_{sopd}	time for start of pressure drop (µs)
u_{def}	control signal for diesel exhaust fluid (-)
u_{egr}	control signal for exhaust gas re-circulation (-)
u_{eth}	control signal for exhaust throttle (-)
u_{scv}	control signal for suction control valve (-)
$v_{\text{sound,s}}$	speed of sound of the substance s ($\mathrm{m\,s^{-1}}$)
V_{hps}	volume of high pressure fuel system ($\mathrm{mm^3}$)
V_{D}	displacement volume of one cylinder ($\mathrm{m^3}$)
$w_{\text{b0,sim}}$	simulated mass fraction of B0 for one load point (%)
$w_{\text{b0,meas}}$	measured mass fraction of B0 (%)
w_s	mass fraction of the substance s (%)
$w_{\text{H}_2\text{O,ox}}$	proportion of water of the total oxidized mass (%)
$x_{\text{f,oil}}$	measured fuel content in engine oil (%)
ξ_{doc}	efficiency factor for post injection (-)
η_{comb}	percentual difference of energy introduced to combustion chamber (%)
$\eta_{\text{f,oil}}$	percentual proportion of fuel in the engine oil (%)
$\Delta i_{\text{pump,dirty}}$	compensation part for dirty fuel filters (A)

$\Delta m_{\mathrm{f,meas}}$	mass of fuel consumed for a given time period, measured by weight scale (mg)
$\Delta m_{\mathrm{leak,meas}}$	mass of leakage fuel for a given time period, measured by weight scale (mg)
Δp_{bhp}	delta pressure of the Broken High Pressure Pump Model (MPa)
$\Delta p_{\mathrm{r},k}$	rail pressure drop at injection k (MPa)
Δt_{cd}	difference between simulated and set-point closing delay (µs)
Δt_{ino}	difference between simulated and set-point injector needle open duration (µs)
Δt_{od}	difference between simulated and set-point opening delay (µs)
$\Delta T_{\mathrm{doc,meas}}$	measured temperature increase in DOC (°C)
$\Delta T_{\mathrm{doc,sim}}$	simulated temperature increase in DOC based on inj. fuel mass (°C)
η_{V}	volumetric efficiency factor of the air intake
ρ_s	density of the substance s ($\mathrm{kg\,m^{-3}}$)

Acronyms

°CA	crankshaft angle in degree
°BTDC	degree before top dead center
B0	pure fossil diesel (0% biodiesel)
RME	rapeseed oil methyl ester
NRO	natural rapeseed oil
DEF	diesel exhaust fluid
DOC	diesel oxidation catalyst
DPF	diesel particulate filter
ECU	engine control unit
EDID	external diesel injector deposits
EGR	exhaust gas recirculation
FTC	fuel temperature control
IDID	internal diesel injector deposits
LPFS	low pressure fuel system
NO_X	nitrogen oxide
PRV	pressure relief valve
PWM	pulse width modulation
SCR	selective catalytic reduction
SCV	suction control valve
Models:	
BHP	Broken High-Pressure Pump Model
DE	Diesel Oxidation Catalyst Efficiency Model
IDD	Injector Deposit Detection Model
HL	High Pressure System Leakage Detection Model
OF	Oxygen-Fuel Model
OM	Oxygen-Mixture Model
RBFE	Rail Pressure Based Fuel Estimation Model
SCV	Suction Control Valve Model

1 Introduction

Since agriculture and forestry are responsible for about 24% of worldwide man-made CO_2 equivalents, agricultural industry and its impact on environment is receiving more public attention [107]. However, agriculture has a special status regarding climate change. It is one of the largest producers of climate-damaging CO_2 equivalents but simultaneously the economic sector which is most dependent on the environment [82][10]. Effects of climate change have become particularly evident in agriculture in the last years due to droughts and crop failures in Germany [17][18]. Even if these occurred repeatedly in history, scientists agree that the probability for extreme large-scale weather situations has strongly increased by the anthropogenic greenhouse effect [58].
Furthermore, agriculture does not only produce CO_2 but can also serve as a CO_2 sink through sustainable farming [122]. However, at the moment agriculture is responsible for 80% of N_2O, 95% of NH_3 and 60% of CH_4 emissions in Germany which lead to the high CO_2 equivalents [88].

The German government has set sectoral targets for the energy sector, industry, buildings, transport and agriculture in its Climate Protection Plan 2050 to decrease CO_2 emissions [19]. In this context greenhouse gas (GHG) emissions must be reduced by 31-34% compared to 1990 until 2030. Main drivers of climate-damaging emissions in the agricultural sector are the use of fertilizers and animal husbandry [10].
However, more efficient diesel engines of agricultural machines also help to reduce CO_2 impact of agriculture [19]. At the moment there are no CO_2 limits (similar to CO_2 limits for cars in the EU) for agricultural machinery, but in the future there could be a legislation that limits CO_2 emission. Since internal combustion engines are very highly developed, no large steps in fuel consumption are to be expected [125]. Electrification like in the automotive industry seems to be only partially suitable for agricultural machinery (high amount of energy required) [112]. Even if concepts such as cable-guided machines already exist, these machines will not be able to be used comprehensively in the next few years [85][118]. It seems that the requested CO_2 reduction can not be achieved by electrification by 2030 [84].
There is broad agreement in the industry that a rapid CO_2 reduction can only be achieved by using alternative fuels which have a lower CO_2 impact on the environment [50][91][100]. In recent years an increasing number of synthetic fuels (could be produced from surplus electrical energy such as wind power) have been subsidized by the German federal government for this purpose [20].
In the agricultural sector first generation biogenic fuels are still a promising approach. Most reasonable fuel of the first generation in Germany is natural rapeseed oil (NRO) due to regional conditions [16].
When farmers grow rapeseed and use the oil as fuel in their machines, they are both fuel producers and consumers. Resulting short transport distances and simple processes in contrast to diesel (fuel is produced by pressing and filtering rapeseed) greenhouse gas emissions are reduced by at least 57% (depending on used calculation method) [113]. If the entire production process is considered and rapeseed cake (residues of the crop after pressing) is used as a soy substitute, 91% of green-

house gas emissions can be saved with natural rapeseed oil [129]. Furthermore, using rapeseed oil does not require development of new, more efficient processes like the production of synthetic fuels [46]. Therefore a CO_2 reduction could be achieved quickly by changing fossil diesel fuel to rapeseed oil.

However, using fuels other than fossil diesel for non-road engines is practically excluded by current legislation. Currently valid exhaust emission level in the EU (Stage 5) for agricultural machines requires an emission homologation for each type of engine and each usable fuel [26]. Since an engine homologation of every additional fuel is very costly, there are hardly any engines which are approved for rapeseed oil or other environment friendly fuels.
A further innovation of exhaust emission standard Stage 5 compared to previous standards was the "In Service Monitoring". Stage 5 requires manufacturers to ensure exhaust emissions are compliant for a longer period of operation in practice. This further reinforces the trend of more diagnosis systems in the vehicle, which has been ongoing since the 1990s [61]. More diagnosis systems are needed to detect faults in the exhaust system to ensure emission limits.
In addition to legal barriers, these systems complicate the use of alternative fuels because many more parameters in the engine control unit (ECU) have to be adapted to the new fuel. If no changes are made and only the fuel is changed, fuels deviating from diesel lead to incorrectly detected faults (false positives). If this happens, the ECU will probably derate the engine so it becomes useless for practical operation.

Since large quantities of fossil oil are currently being consumed worldwide, it is unlikely that one single product can replace oil. It is more likely, a combination of many approaches is needed to reduce the CO_2 impact.
Generally diesel engines are suitable for a variety of fuels [86]. To enable modern diesel engines operating with different fuels, software adaptations in the ECU (regarding performance, emissions and diagnosis) are necessary. This requires a reliable fuel detection.
Additional sensors for fuel detection increase the costs of combustion engines. Costs for diesel engines have already risen sharply in the last ten years due to rising costs of exhaust aftertreatment without generating any added customer value [25]. A further cost increase of machines will therefore most likely not lead to a better market penetration of biogenic fuels.

Agricultural machines have a significantly longer service life compared to automobiles [121]. Since fuel prices can change clearly over that time, using serial production sensors for fuel detection ensure customers have the option of using the most economical fuel even several years after purchasing the machine. This could be achieved by a software update without changing any hardware and would be a strong purchase criterion for customers. Furthermore, a multi-fuel capable machine reduces customer inhibition to replace a established fuel like diesel with a more environmentally friendly fuel.
In the past, natural rapeseed oil caused problems due to its high viscosity, especially in cold winters [28][49]. If the customer is allowed to choose the fuel freely, diesel can be added in winter ensuring a high reliability of the machine.

Reliability of non-road machines is the most important customer criterion [41]. Perfect operation of agricultural machines is essential in seasonal work peaks, such as harvesting. For example, combine harvesters are only used for a few days in the summer, so downtime means particularly high costs for customers. This is the reason why manufacturers have been trying to reduce the down time of machines for years. Predictive maintenance (failure or wear is detected before machine breaks down), or precise diagnosis of faults (if a fault occurs, technicians do not have to search for the cause and machines are repaired quickly) increase operating time. In both cases a precise vehicle diagnosis is helpful. Using series-production sensors for fuel detection also implies fault and fuel detection can only be considered together. For example faults can lead to an incorrectly detected fuel type.

Besides electrical problems, the fuel system is one of the most common causes of a complete failure of diesel engines [4]. Therefore, fuel system diagnosis should be further improved, independent of different fuels. Diagnosis should not only detect faults leading to breakdown of machines but also faults that endanger operational safety, e.g. fuel leaks. Fuel leaks often lead to fires when machines are used on dry grain fields in combination with dust [70].

Besides random errors due to wear and aging, so-called chip tuning of machines is not unusual in the agricultural sector. Performance is increased or operating costs are reduced by manipulating the engine. Not only significantly worse emissions of these machines are possible, they also lead to an increased number of warranty claims and thus costs for manufacturers.
There are many reasons for chip tuning an engine. It offers farmers more engine power even years after buying the machine. Individual farms are growing steadily, which leads to a trend towards larger machines. Agricultural machinery is one of the biggest cost drivers of modern agriculture [43]. If a larger implement is required, it is often not possible to purchase a larger tractor for this implement at the same time. Engine-tuning is therefore often used to bridge the years between a too small and a larger new tractor.
Another reason is the high price difference between performance classes of tractors within same series. For example, list price difference between a John Deere 6195R (195 hp nominal power) and a 6215R (215 hp nominal power) is currently approx. 10.000€ in Germany [67]. Since both machines have a mechanically identical engine (overall machine is not mechanically identical), many farmers see chip tuning as a cheap possibility to get the same product at a lower price.

Sale and installation of tuning equipment is not prohibited, so manufacturers and dealers of tuning equipment have a very low risk to be prosecuted. However, machines loose their operating license and are not allowed to be moved on public roads. Since there are no controls checking increased performance or deteriorated exhaust emissions, farmers still tune their machines. There is no quantifiable data on chip tuning (percentage of tuned machines, percentual increase in performance, warranty claims due to tuning, etc.). An onboard detection would be desirable to get information about the scope of engine-tuning in practical operation.

Based on this introductory discussion the following research questions can be derived:

1. How can operation and detection of biogenic fuels (especially natural rapeseed oil) be realized with series sensors?
2. How can an onboard chip tuning detection be achieved?
3. How can faults (especially of the fuel system) be detected before the engine fails?

2 State of the Art

In order to derive concrete goals from the problem definition, current state of the art is presented in this chapter. Firstly, used fuels and engines capable of running NRO will be presented. Subsequently, a literature research on injector deposits is carried out and an introduction to chip tuning is given.

2.1 Fuels

An alternative to reduce the CO_2 impact of diesel engines is the capability of using biogenic fuels like vegetable oil as described in chapter 1. Vegetable oil is produced by pressing oily plants. It consists mainly of glycerol esters with fatty acids, so-called triglycerides [38].

Various vegetable oils differ considerably depending on the source plant. For example, Rudolf Diesel himself ran his engine with peanut oil [121]. Peanut oil is not suitable as a fuel in Germany because it starts to flocculate below 10 °C [34].
Natural rapeseed oil (NRO) is especially well suited for fuel use in Germany because of the fuel properties and geographical conditions [35]. It can be produced in industrial oil mills by hot pressing with the use of solvents and subsequent refining. Another way is decentralized cold pressing with aftertreatment to reduce undesirable elements (e.g phosphor) in the fuel [97].

The press cake (remains of the rapeseed after pressing) is approved as animal feed in Germany. Since rapeseed cake contains a lot of protein, soya imports can be reduced by using it as animal feed, which also has a positive influence on the CO_2 impact [113].

However, NRO also has physical disadvantages compared to conventional diesel fuel. In particular, the increased viscosity of NRO repeatedly leads to problems. For this reason, a large proportion of NRO is converted to rapeseed methyl ester (RME) by transesterification with monohydric alcohols such as methanol [35]. This adapts the properties of NRO to those of diesel. Since it is also conceivable that the proportion of RME in Germany will be further increased, this study will examine RME in addition to NRO and pure fossil diesel fuel.
Since the year 2010 commonly used B7 fuel in Germany consists of up to 7 % biodiesel. Biodiesel can consist of various esterified vegetable oils such as NRO, palm oil, soybean oil, jatropha oil, or animal fats and oils. Whenever pure diesel is mentioned in this research work, it refers to fossil diesel with 0% biogenic content (B0).

NRO, RME and B0 will be investigated in this work. Since these fuels differ considerably, most important properties are presented in the next section.

Table 2.1: Fuel Analysis carried out in this research work - κ at 20 °C and atmospheric pressure [81]

fuel	H_u ($\frac{MJ}{kg}$)	L_{st}	w_{H_2} (%)	w_C (%)	w_{O_2} (%)	$E_{fuel,st}$($\frac{MJ}{kg_{air}}$)
B0	43.1	14.6	13.4	86.6	0	2.95
RME	37.3	12.5	11.8	77.8	10.4	2.98
NRO	37.1	12.5	11.7	77.6	10.7	2.97

B0: fossil diesel fuel with 0% biogenic content
RME: rapeseedmethylester
NRO: natural rapeseed oil
w_s: mass fraction of substance s in fuel
H_u: lower heating value
L_{st}: stoichiometric air demand
$E_{fuel,st}$: air mass based heat input

2.1.1 Fuel Properties

NRO is a natural product, so fuel properties vary stronger in contrast to fossil diesel fuel. However, rapeseed is standardized by DIN 51605 so certain minimum requirements must be met by fuel producers. In literature, energy content of rapeseed is estimated between 34.5 and 38 MJ/kg [111][127][89]. This is a percentual deviation of about 10 %, so limits for tolerable performance fluctuations of ±5% can easily be exceeded. Values presented in Table 2.1 are derived from fuel analyses of used test fuels in this study. Analyses correspond approximately to values found in the literature (B0: [133], B7: [65], RME and NRO: [55]). Test data sheets of fuel analyses carried out within the scope of this work can be found in the Appendix.
The main reason for the spread of hydrocarbon-containing fuels is the relatively high energy density. Released energy mainly originates from oxidation of H to H_2O and C to CO_2. When the fuels are oxidized with 1 kg normalized air, air mass based heat input can be calculated for the different fuels with the lower heating value H_u and stoichiometric air demand L_{st} via

$$E_{fuel,st} = \frac{H_u}{L_{st}}. \tag{2.1}$$

All fuels are at a comparable level (Table 2.1).

Gravimetric energy content of fossil diesel is 18% higher than NRO, but volumetric energy content at 15 °C is only increased about 5%. The reason is the higher density of NRO. Since density is dependent on temperature and pressure, an approximate formula for the fuels is presented.

$$\rho(p,T) = a_0 + a_1 \cdot p + a_2 \cdot T + a_3 \cdot p^2 + a_4 \cdot p \cdot T \tag{2.2}$$

Here T is the fuel temperature in Kelvin and p is the fuel pressure in MPa.
Coefficients for density calculation can be found in Table 2.2. The procedure for speed of sound is analogous with coefficients in Table 2.3

$$v_{sound}(p,T) = b_0 + b_1 \cdot p + b_2 \cdot T + b_3 \cdot p^2 + b_4 \cdot p \cdot T \tag{2.3}$$

Table 2.2: Coefficients for approximation formula of densities based on [133] [65] [80] [83] [47] [52]

parameter	ρ_{b0}	ρ_{RME}	ρ_{NRO}	unit
a_0	1030	1082	1092	$kg\,m^{-3}$
a_1	$1.392e^{-01}$	$2.042e^{-01}$	$1.42e^{-01}$	$kg\,m^{-3}\,MPa^{-1}$
a_2	$-6.736e^{-01}$	$-6.78e^{-01}$	$-6.04e^{-01}$	$kg\,m^{-3}\,K^{-1}$
a_3	$1.294e^{-03}$	$-9.76e^{-04}$	$-8.02e^{-04}$	$kg\,m^{-3}\,MPa^{-2}$
a_4	$1.619e^{-03}$	$1.28e^{-03}$	$1.40e^{-03}$	$kg\,m^{-3}\,MPa^{-1}\,K^{-1}$

Table 2.3: Coefficients for approximation formula of speed of sound based on [133] [65] [80] [83] [47] [52]

parameter	$v_{sound,B0}$	$v_{sound,RME}$	$v_{sound,NRO}$	unit
b_0	2325	2290	2300	$m\,s^{-1}$
b_1	1.801	2.548	2.13	$m\,s^{-1}\,MPa^{-1}$
b_2	−3.27	−3.01	−2.87	$m\,s^{-1}\,MK^{-1}$
b_3	$-7.99e^{-03}$	$-6.88e^{-03}$	$3.09e^{-03}$	$m\,s^{-1}\,MPa^{-2}$
b_4	$8.7e^{-03}$	$-6.00e^{-03}$	$4.43e^{-03}$	$m\,s^{-1}\,MPa^{-1}\,K^{-1}$

Measurement data to approximate fuel parameters can be found in literature (Table 2.2). An exception is measurement data of NRO for high pressures and temperatures. This data was provided by the Competence Center for Cogeneration of the *OTH Amberg-Weiden* in the context of this research work. Tabular data can be found in the Appendix. Measurement data not available up to 200 MPa and 380 K is extrapolated for all fuels.

It is noticeable that viscosity for NRO differs strongly from RME and diesel, especially at cold temperatures and high pressures (comp. Figure 2.1, Figure 2.2 and Figure 2.3).
Viscosity cannot be approximated with sufficient accuracy by a second degree polynomial. It is approximated by the MATLAB® function "lowess" (locally weighted scatter plot smoothing function) in practically occurring temperature (270-380 K) and pressure ranges (0-200 MPa). Since viscosity is only required qualitatively in this work, results of the approximation are shown graphically for better comparison.

2.1.2 Engines Capable of Running Natural Rapeseed Oil

NRO engines have been investigated for many years, so a lot of experiences and approaches for the design of suitable engines can be found in literature. There is general agreement that diesel engines are generally well suited for operation with NRO [76][28].

Nevertheless, there are still technical problems that prevent the widespread use of NRO engines. These are mainly cold start problems and not feasible exhaust aftertreatment regenerations [55] [12][120] [6]. For this reason, manufacturers have developed two tank systems as an interim solu-

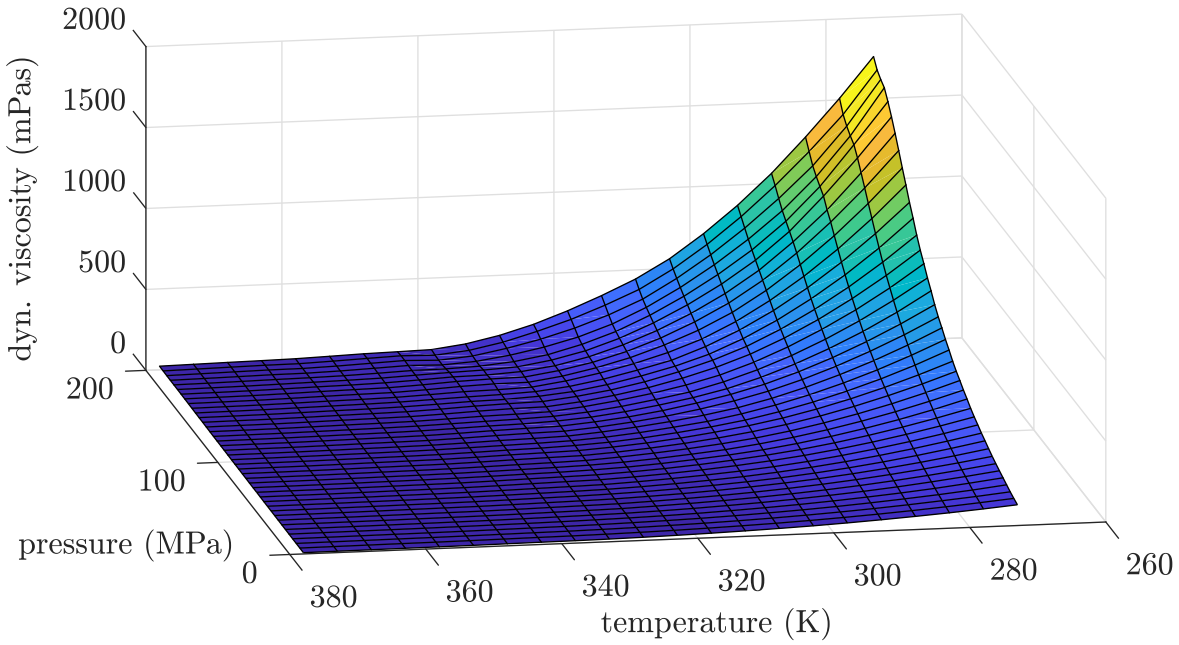

Figure 2.1: Viscosity of NRO [52]

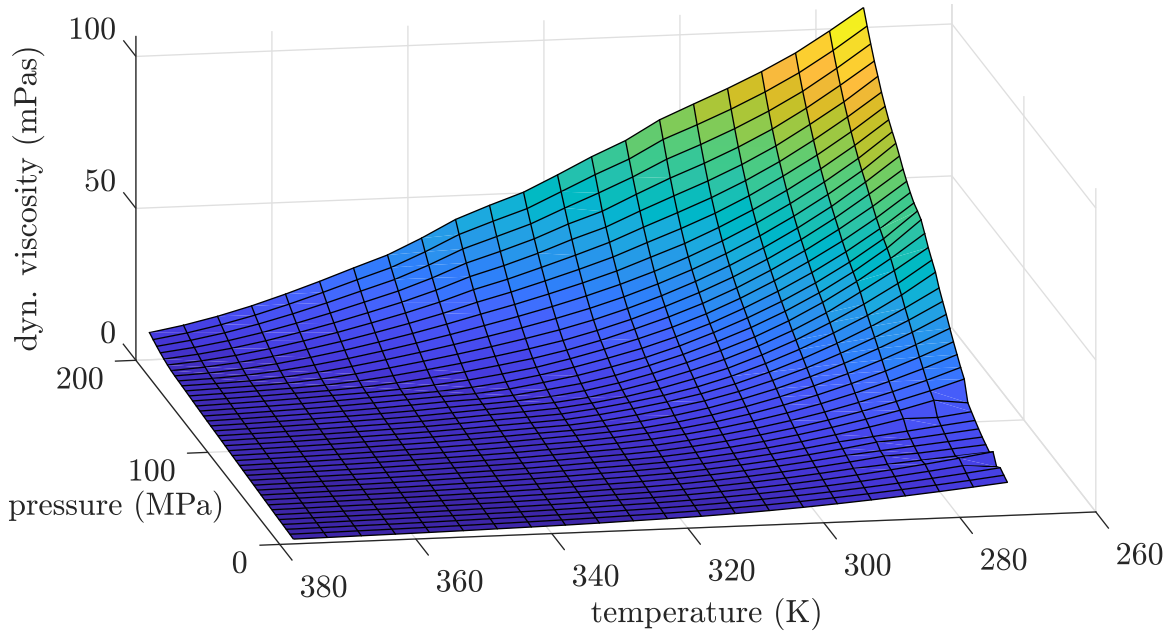

Figure 2.2: Viscosity of RME [39]

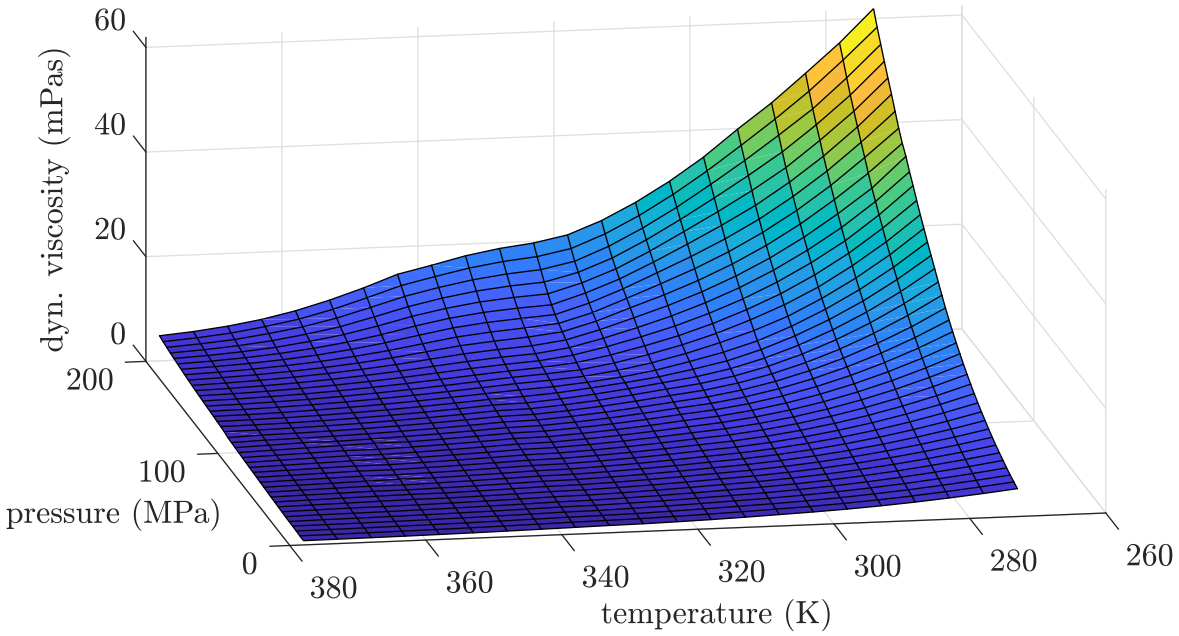

Figure 2.3: Viscosity of fossil diesel [30]

tion. In difficult operating conditions the fuel system switches to a proven fuel such as fossil diesel [35]. As soon as the engine is warm and at a normal operating point (no catalyst heating, no DPF regeneration, no cold start...), it switches to the more environmentally friendly NRO fuel.
However, an additional tank and a second fuel system is associated with high additional costs and prevents the chances of a successful market introduction. The long-term goal should be the development of a cost-effective NRO engine with a 1-tank system. This means that the problems that are solved by the two tank system (cold start and exhaust aftertreatment regenerations) become more important again.

Dönges and Traulsen [28] state that a sufficiently good cold start with NRO can only be achieved with preheating equipment.

Backofen, Braungarten, and Tschöke [6] come to a similar conclusion. Warming up NRO fuel before starting the engine is considered absolutely necessary. Furthermore, it is determined that the cold filter plugging point of NRO is unacceptable at temperatures below 0 °C.

Zahoransky [131] examined NRO in stationary diesel engines and pointed out that only preheated NRO fuel can ensure that the fuel is atomized correctly.

There is agreement in the literature that increased temperatures or a lower viscosity of the NRO has advantages regarding cold start, mixture preparation and emission behavior [109] [6] [49] [120] [131]. The viscosity of NRO reaches the viscosity of fossil diesel (at 15 °C) fuel at about 100 °C (subsection 2.1.1). Nevertheless, the fuel temperature should not be increased to such high values. For example at 75 °C NRO fuel can polymerize [109]. The polymerization leads to long

chain polymers which clog filters. Furthermore, the oxidation stability of NRO fuel decreases with increasing temperature [97].

However, Remmele et al. [98] writes, that cold-start problems in NRO operation is significantly improved if the engine control system is adapted to NRO fuel.

Spicher and Lüft [109] state that the spread and vaporization of an injection jet differs considerably between diesel and NRO fuel. This leads to insufficient mixture formation and incomplete combustion. An adjustment of the injector maps and injection times is therefore necessary.

It becomes clear that a precise adaptation of modern common rail injection systems to the fuel can significantly improve engine behavior. In the past, the injection system was largely not electronically controlled (e.g. diesel engines with pre-combustion chamber). Therefore the fuel had to be adapted to the injection system (e.g. NRO was heated). However, with modern common rail systems the injection can react actively to the fuel and be adjusted.

This is also the result of Ettl et al. [36]. If the engine is adjusted to the characteristics of the fuel used, real emission values of diesel engines operated with NRO do not exceed the permissible limits. Similar emission values indicate similar combustion, so that the necessity of software adaptions becomes clear.

Besides a multitude of emission and performance measurements, literature often mentions engine issues (cold start, dpf regeneration, injector deposits, more NO_x, more soot...) linked to biogenic fuels [74] [71] [104] [22] [130] [116] [76] [51] [42] [99]. This conflicts with the high reliability required for agricultural machinery. In particular, injector deposits seem to increasingly cause problems in operation with biogenic fuels. For this reason, a literature research on injector deposits is carried out in the next chapter.

2.2 Fuel System Errors

Many faults can occur in the fuel system of a combustion engine. In this chapter two faults are presented. Injector deposits, as biogenic fuels are suspected to accelerate them, and intentional faults like chip tuning.

2.2.1 Diesel Injector Deposits

Klaissle [71] claims deposits are the leading cause of engine malfunction along with mechanical wear in general. Some of the deposits can be found on the injectors. Therefore injector deposits have been increasingly researched in recent time [72][8][1][90][7][66][103]. Continuous decreasing diameters and needle geometries inside diesel injectors are the main reason for growing interest because even slight deposits have a significant impact on injector behavior (shifted injector timings, imprecise injection quantity, poor atomization...) [53].

One has to differentiate between internal diesel injector deposits (IDID) and external diesel injector deposits (EDID) [53]. In this work, EDID refers to all deposits that change the flow through injectors (with the same needle opening time). This includes deposits at the injector needle tip and injection holes (section 3.5) and is largely consistent with the definition of Quigley et al. [90].
IDID occur inside the injector and are defined in this research work as deposits that influence the injector needle opening time.
Quigley et al. [90] and Ullmann et al. [124] mention typical areas for IDID as the guidance of the injector needle, control valve and parts around the magnetic coil (section 3.5). Most sensitive components for injector function are the inlet orifice, outlet orifice, control plate and control valve. Even small deposits on these components can have a large effect on injector function such as deviating opening and closing delays. [53]
Deposit formation mechanisms between IDID and EDID differ considerably since the inside of an injector has no direct contact with combustion. Effects of deposits on engine operation are important in order to detect deposits or to create avoidance strategies. For example, deposits on the injector needle have different effects than deposits on the control valve of the injector. [53]

This literature research is roughly divided into the following areas:

1. Deposition formation when using biogenic fuels
2. General causes of deposit formation (independent of the used fuel)
3. Effects of injector deposits on engine operation

Since biogenic fuels have been suspected of forming increased injector deposits for a long time, there are a large number of investigations regarding biogenic fuels. Although this work focuses on RME and NRO, literature on other biogenic fuels (soybean methyl ester, fatty acid methyl ester, hydro treated vegetable oil) is also viewed. The reason for this is the similar chemical composition of biogenic fuels (oxygen content, oxidation stability, etc.).

Li et al. [74] examined natural vegetable oil and found strong injector deposits with a reduction of the nozzle hole diameter. This led to a significant increase in particulate mass (PM) in the exhaust gas (>50% increase after 20 hours of operation). It is concluded that no engine should run on vegetable oil if PM emissions can increase so much after such a short time.

In Klaissle [71] it is stated that formation of deposits is much more pronounced with natural vegetable oil than with fossil diesel fuel. Elements deviating from fossil diesel fuel such as calcium, magnesium and phosphorus in biogenic fuels are considered as a reason. According to the statement, these elements accelerate deposit formation. Also increased surface temperatures cause deposit formation. It is stated that the injector is the most sensitive component regarding deposits in the combustion engine.

Sem [104] carried out investigations on deposit formation with soybean methyl ester (SME). Results show a strongly increased external deposit formation in contrast to fossil diesel. Thermal

decomposition of methyl ester molecules is assumed to be the reason, which leads to solid coking on the injector needle.

Caprotti et al. [22] has investigated deposition formation with RME. A 10% decrease in injection mass due to deposits resulted in 12% less power. However, it is not stated whether the loss of power is due to poorer combustion and atomization of the fuel, or whether secondary effects such as shifted control parameters are the reason.

Wörgetter [130] conducted endurance tests with fatty acid methyl esters (FAME). A clear loss of performance could be determined. This was explained by reduced hydraulic flow and a significant deterioration in atomization. Especially at the beginning of the needle opening phase highly divergent behavior could be observed. Detailed information on injector behavior such as shifted injector delays or changed control parameters of the ECU are not mentioned. Influences of a delayed injection timing were also not considered.

In contrast, Tang [116] state FAME has no influence on the external deposit formation, when high quality fuel is used. Storage and age of the fuel is more important compared to fossil diesel fuel.

Maurer [76] investigated NRO-B0 mixtures. Only external deposits were evaluated. It was not described whether internal deposits were present simultaneously. Interesting is a non-linear deposition rate with increasing mixture ratio between rapeseed and diesel. So it is conceivable that there is a particularly bad mixture regarding injector deposit formation. However, the exact mixing ratio (or reason) is not given in the work.

Hoang and Le [51] conducted tests with jatropha oil (vegetable oil from the seeds of the jatropha nut) at 30 °C and 90 °C fuel temperature. Deposits were formed after 300 hours during operation with 30 °C warm jatropha fuel. At 90 °C fuel temperature, deposit formation with fossil diesel or jatropha oil was clearly less pronounced. However, the cause for reduced deposit formation at warmer fuel temperatures is not given.

Galle et al. [42] examined fatty acid methyl esters (FAME) over 1500 h. Injectors were defective much faster than in operation with fossil diesel fuel. Fuel composition is named as the main reason. Especially alkali metals, water and other contamination in the fuel are main reasons for defective injectors according to the statement. The investigations were accomplished at increased fuel temperatures of 110 °C.

A mixture of 70% fossil diesel and 30% RME produces less deposits than commonly used B7 fuel in Germany according to Richter et al. [99]. It is also stated that deposit formation increase with reduced oxidation stability of the fuel.

Lacey et al. [72] note metal carboxylates in the fuel are the main reason for deposit formation. Furthermore, there are no significant differences between high quality FAME and diesel blends in terms of deposit formation. However, this only applies for fresh fuel. As soon as the fuel ages, deposit formation increases significantly for fuels with FAME content.

Junk et al. [68] conclude the oxygen content in biogenic fuels is responsible for deposit formation. Deposit formation reduced up to 91% in their tests by reducing oxygen dissolved in the fuel. It is also recommended using fuels free of aromatic compounds such as hydrotreated vegetable oil[1] (HVO) at lowest possible fuel temperatures.

However, injector deposits are also of increasing research interest independently of biogenic fuels. The reasons are constantly increasing injection pressures (lead to higher fuel and injector nozzle temperatures) and more precise injectors with smaller diameters [53]. Here, even small deposits can have a major impact on engine performance. Therefore many studies also deal exclusively with fossil diesel.

Tang et al. [117] investigations have shown significantly reduced deposit formation by minimizing flow-optimized rounding of injection holes. The reason is increased cavitation within nozzle holes due to their statement. However, full-load performance is also significantly reduced as hydraulic flow through nozzle holes becomes smaller.
Cavitation during the injection process can also be increased by higher injection pressure so deposit formation should be reduced. However, higher pressures also mean higher temperatures, which are increasing deposit formation. Three main influences for external deposit formation are indicated: Temperature, needle geometry and metals (mainly zinc) in the fuel. It is assumed that with increasing needle temperatures, IDID and EDID increase. [116]

A similar result is reached by Argueyrolles et al. [5]. It is stated, that a limit temperature of 300°C at the injector exists. With higher nozzle temperatures deposit formation increases strongly. Furthermore, general fuel composition and not only zinc is described as a driver of injector deposits.

Caprotti et al. [21] also point to strongly increased deposit formation with higher injector nozzle temperatures. As the reason for higher temperatures strongly increased injection pressures are mentioned. Furthermore, only minor influences of flow-optimized injectors regarding deposit formation, but considerable advantages in fuel efficiency are assumed. This is the reason for widespread use of flow-optimized compared to high cavitation injection nozzles.

Bartz [9] shows increased deposit formation in inner and outer part of injectors after turning off the engine. It is considered particularly bad to switch off a hot engine abruptly. This leads to a hot injector needle tip, so external deposits occur.

The most important causes of injector deposit formation appear to be the structural design of injectors, the fuel and operating mode of the engine (rail pressure, injection quantity...). Since effects on engine operation are of particular importance for deposit detection, these are explained in the following.

Hoffmann [53] notes it is difficult to distinguish between IDID and EDID when only the hydraulic flow of the injector is measured. This is due to counteracting effects such as an increased closing delay caused by IDID, when EDID occurs simultaneously. It is possible that the area of the nozzle

[1] HVO can be produced from NRO by hydrogenating it through a catalytic reaction with hydrogen. In this way the properties of NRO are adapted to the properties (especially viscosity) of diesel fuel.[2]

hole is smaller due to EDID and therefore the hydraulic flow is lower. However, IDID can shift the needle opening and closing time so the needle remains open longer and the same amount of fuel as with a new injector is injected.
The strongest effect of IDID is a changed injector response. This is generally referred to as an extended opening and closing delay. Furthermore, the position at which IDID occurs is important. For example, heavy deposits on nozzle needle guidance greatly increase actuation forces for opening and closing the nozzle needle. The strongest effects of deposits on the nozzle needle are observed at low rail pressures, since the hydraulic forces are not high enough to move the needle instantly. Typically this leads to a rail pressure dependent opening delay (larger deviations from the set-point opening delay at low rail pressures). Furthermore, closing delay is independent on rail pressure with needle guidance deposits because the actuation force is delivered by a spring.
In the worst case of injector deposits the injector remains in a closed or open position. If the needle remains open, catastrophic engine damage can be the result, as uncontrolled large quantities of fuel are injected into the combustion chamber. It is also written that IDID and EDID always occur together. An impairment of the fuel atomization, which can lead to e.g. an uneven engine running, bad cold start behavior or loss of power are mentioned as further effects. [53]

Klaissle [71] also states fuel atomization interference, as well as locally very low lambda values in the combustion chamber when injector deposits are present. These can contribute to an increase in particle mass or increased HC emissions.

2.2.2 Engine (Chip) Tuning

In addition to wear or deposit-related faults, chip tuning is another topic in the agricultural engineering sector. Even if the word chip tuning is not entirely correct (engines can be tuned without an additional chip), it will be used for the sake of simplicity in this research work. The overall goal for chip tuning is always costs saving. For example the surcharge for the next more powerful machine of the same tractor series can be saved by increasing engine performance of the low powered machine. Operating costs can also be reduced through lower fuel or diesel exhaust fluid (DEF) consumption by modifying the engine control system. This is usually done at the expense of increased exhaust emissions (NO_X and particle mass) or the exploitation of safety tolerances.
However, there are hardly any publications on chip tuning in agricultural engineering. Only Prankl and Schaufler [87] examined the effectiveness of tuning chips. It is stated, that chip tuning significantly increases the engine performance with only small deviations in exhaust emissions [87]. Sethanunt and Koetniyom [105] examined an external tuning box which distorts the rail pressure. Since this method is very simple and large profit margins are achieved for tuning equipment sellers (e.g. an electrical resistor with a value <0.05 € is sold for 500 €), this method is often used [115][123][119][13][33][3][29][69]. No literature was found on identification of tuning measures or prevention strategies from manufacturers. The same applies to type and scope of chip tuning in agricultural engineering. However, there is a multitude of dealers selling tuning equipment in Germany, so a certain market size can be assumed [115][123][119][13][33][3][29][69].

Often internet shops are advertised with dubious promises. So lower fuel consumption and undetectable tuning measures are promised [115].

Theoretically a lower fuel consumption is possible, even with pure power increase. Especially if the same work can be done at lower engine speed and higher torque.
At older machines with EU exhaust gas stage 3b chip tuning companies increased the fuel efficiency by deactivating the EGR. In John Deere machines this resulted in significantly better fuel efficiency as a diesel-only strategy with DPF without SCR system was used. Series application was designed for low NO_X emissions so the engine was not operated at maximum fuel efficiency. When EGR was deactivated by aftermarket tuning (sometimes with shifted injection timing) fuel efficiency was significantly better while NO_X emissions increased sharply. As the deactivation of the EGR shifts the particle-NO_X-trade-off, less particles were produced [15]. Since this reduces the frequency of DPF regenerations, it also indirectly improves the fuel efficiency of the machine. For engines with an SCR system this measure usually leads to little improvement in fuel efficiency. The reason are machines designed for high fuel efficiency as standard. Resulting NO_X emissions are neutralized by the SCR system [121].

However, if chip tuning only increases the injected fuel mass, fuel efficiency does not increase for same engine speed and torque. chip tuning companies prove a lower fuel consumption by a lower shown display value after chip tuning has been carried out (translated from german): “Driving experience, if you can talk about it on a tractor, is much better. The Case CVX 1170 drives much easier, does the work in the field more effortlessly and the shown fuel consumption value in the display is one display unit lower than before” [115]. The reason for lower displayed value is due to the fact that the actual fuel consumption is not measured but determined via look-up tables. If fuel injection is increased by a tuning chip, the ECU calculates with a lower injection mass than actually injected. So it is a logical consequence that the displayed fuel consumption decreases at the same load point. Real fuel consumption stays approximately the same.

Often tuning companies give the impression weaker powered machines from the same model range differ from more powerful machines only by software adjustments [93]. It is suggested that chip tuning removes software-side throttling and customers get the same tractor for less money compared to buying bigger machines. However, larger machines of same series have in most cases different hardware than smaller machines. For example, there may be larger cooling packages, stronger transmissions or larger hydraulic pumps.

Performance increase of diesel engines can be achieved with very simple measures compared to gasoline engines. In contrast to most gasoline engines, diesel engines operate with a high level of excess air. So more power can be achieved by increasing the injection quantity, without caring about air being pumped into the cylinder. In addition to power increase, the deactivation of EGR to reduce fuel consumption or switching off of urea dosing is also offered [115][123][119]. These measures increase the exhaust emissions of engines considerably, so emission limits are no longer observed. However, all other measures also represent a modification of the vehicle, so vehicles lose their type approval [37].

Apart from serious consequences for the environment, chip tuning has an economic impact on manufacturers of agricultural machinery. For example, an engine can be damaged by chip tuning within the warranty period. According to the current state of the art there is no possibility to detect or prove chip tuning on board of the machine. So manufacturers often have no other choice than paying for damages within the warranty period.
Furthermore, the proportion of leased machinery in the agricultural sector is rising steadily [79]. Since customers can lease agricultural machinery directly from manufacturers, machines that are heavily worn out as a result of chip tuning have an impact on profit of agricultural machinery manufacturers.
With chip tuning of leased machines there is no financial risk for customers (machines are usually leased in combination with a maintenance contract) , so often much weaker machines are leased than would be needed for the required work. These machines are raised to the desired performance level by chip tuning and returned to manufacturers if a defect occurs. Customers have a financial advantage since less powerful machines have significantly lower leasing rates. In many cases chip tuning manufacturers offer a free back fitting (flashing back original software, or removal of tuning chips), so there is little inhibition for customers to tune a machine [69] [115].
Nevertheless, little has been invested by manufacturers to prevent chip tuning so far. Since it is allowed to advertise freely for tuning equipment and also sale is not forbidden, it cannot be assumed that the proportion of tuned machines will decrease. Quantifiable data are not yet available in the literature. Hardly any customer admits publicly having tuned their machines. Reasons for this are the fear of governmental punishment (the machine no longer has an operating license) and the loss of manufacturer warranty. Furthermore, no literature on onboard detection of chip tuning measures or prevention strategies could be found.

2.3 Conclusions from the State of the Art

Based on literature research, problems are identified and research objectives of this thesis can be defined. These refer to the research questions mentioned in chapter 1.

1. The literature on NRO compatible engines shows that some adjustments should be made for a multi-fuel compatible engine. These include, for example, the adaptation of the fuel system to the respective fuels. Even though the injection can be adjusted at common rail engines, a fuel system that preheats the fuel is useful. At low temperatures fuel filters could clog due to the high viscosity of NRO. Furthermore warm NRO fuel significantly improves the spray properties and the flow behavior in the low-pressure fuel system.

   There is a trade-off in the fuel temperatures used. It seems that the deposit formation increases at higher fuel temperatures because of decreasing oxidation stability. Very low fuel temperatures should also lead to increased deposit formation with highly viscous fuels, as the spray properties deteriorate. Therefore a *constant fuel temperature at medium temperatures* (30-50 °C) would be desirable. This also reduces problems in the low pressure fuel system with high viscosity fuels (clogged filters, defective pumps...) [120].

Due to the costs of agricultural engines mentioned in the introduction, a one tank system should be used. Overall, *as little hardware adaptions as possible* should be made on the production diesel engine so nearly the same price as the fossil diesel engine can be achieved (also advantages in price and availability of spare parts).

The literature also shows that the engine has to be adapted not only to the hardware but also to the software. In pure NRO operation a significantly better starting behavior, low exhaust emissions and the same performance as in diesel operation could be determined if, for example, the *injector maps were adapted to the fuel*. Since a good adaptation to the fuel used is only possible if the fuel is known, the necessity of *reliable fuel detection* is made clear.

2. There is agreement in literature that NRO and RME accelerate *injector deposit* formation. Various reasons are given, such as oxidation stability, age and storage of the fuel.
   Since fuel system problems are already one of the most common causes of engine damage to agricultural machinery, injector deposits or problems with injectors must be detected early to ensure the high reliability of the machines. Therefore, an *onboard injector deposit detection* would be desirable. This not only helps reducing the downtime of machines, but can also help to better understand deposit formation in order to develop avoidance strategies in the future.

   Literature reviewed on deposit formation of biogenic fuels or fuel blends often lacks precise information on fuel composition or fuel temperature. Thus, contradictory statements on deposit tendency are found. However, it is widely agreed that alkali metals in the fuel, fuel temperature and operating mode of the engine have an effect on deposit formation.
   Many studies still do not take into account the superposition of several effects occurring in parallel. Thus, investigations on external deposit formation are usually carried out by measuring the engine power or injection quantity with the same injector pulse duration. However, internal deposits can also lead to a shorter injector needle opening time. If needle position, opening and closing delay of injectors are not measured directly, results can be falsified. For example, internal deposits may cause shorter “needle open time” and therefore reduce the injection quantity, even if no external deposits are present.

3. Overall, fault diagnosis should be expanded. Especially the field of *chip tuning* seems to be a hardly treated topic so far. This has a strong impact on the environment and results in additional costs for manufacturers. Since there are no reliable statistics or statements in the literature about the scope of chip tuning an *onboard chip tuning detection* would be desirable. Herewith statistics could be created and warranty cases could be reduced. In the future geographical influences (e.g. high chip tuning rate near a dealer location, typical customers or application profile of chip tuning etc.) could be determined with an onboard detection in combination with telemetry.
   Thus it is conceivable that not only increased injection quantities can be compensated by chip tuning in terms of control technology, but also that too low injection quantities (deposits etc.) can be neutralized. Since the reliability of agricultural machines has highest priority, as many faults as possible should be detected.

2.4 Goals of this Research Work

Conclusions drawn from state of the art reveal many unsolved problems. Together with the problem definition from the introduction chapter, following sub tasks are derived for this work:

- Enable engine operation with different fuels (NRO, RME, B0) with only slight hardware adaptions
- Software adaptions to enable engine operation with different fuels (injector maps, rail pressures ...)
- On-board fuel type detection system
- On-board chip tuning detection system
- On-board injector deposits detection system
- Fuel and tuning independent fault detection in the high pressure system

3 The Investigated Diesel Engine

This chapter gives an overview of the test engine used in this work. It presents most important mechanical components, actuators and sensors. Furthermore, adjustments are made so that the engine can be used with NRO, RME and B0. It is a typical commercial vehicle diesel engine as used in agricultural machines, so many things are valid in general.

3.1 General Layout

The test engine used in this work is a John Deere 4.5L, 4-cylinder, common rail diesel engine. Current engine configuration is homologated for EU emission stage V for non-road vehicles. Exhaust gas cleaning components include a cooled high-pressure exhaust gas recirculation (EGR), a diesel oxidation catalyst (DOC), a diesel particulate filter (DPF) and a selective catalytic reduction (SCR) system.

Sensors installed at this series production engine are shown in Figure 3.3. Additional sensors are installed at the test bench to measure comparative data or for safety features. These include, for example, additional pressure and temperature sensors in the oil circuit, cooling system or air path. These additional sensors are essential for test bench operation but not important for the results of this thesis.
The test bench (Figure 3.1) itself is largely controlled by the measurement and automation software LabVIEW® from National Instruments (speed, torque, fuel temperatures/pressures ...). Series production ECU takes over the speed control of the engine (accelerator pedal position is specified by LabVIEW®). The torque for braking the engine is generated by a SCHENK W400 water-

Table 3.1: Technical data of the test engine (internal John Deere document)

nominal power (ECE-R120), PS(kW)	135 (99)
nominal power with IPM (ECE-R120) at 2100 rpm, PS(kW)	165 (122)
rated speed, rpm	2100
maximum torque (at 1600 rpm), Nm	632
manufacturer	John Deere Power Systems
aftertreatment	DOC + DPF + SCR
emission level	EU Stage 5
supercharging	series stationary turbocharger
cylinders/displacement	4/4.5 L
injection system	common rail system with up to 200 MPa (2000 bar)

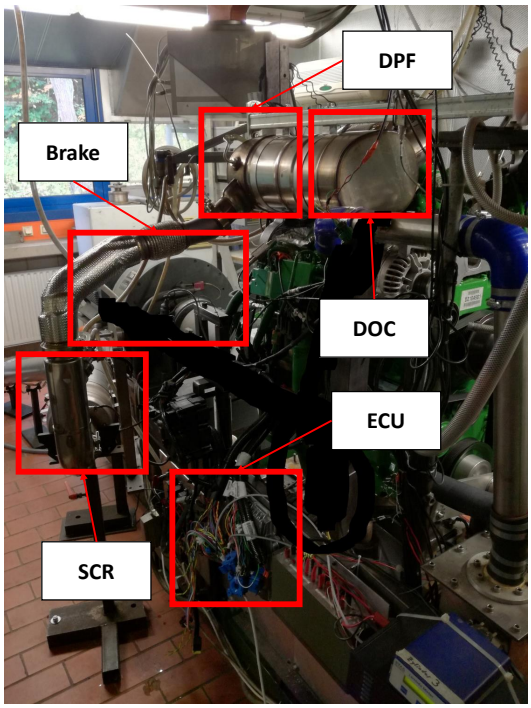

Figure 3.1: Engine installed in test bench with main components of exhaust gas aftertreatment

cooled eddy current brake. The coil current (for generating the magnetic field) is controlled by LabVIEW® via an amplifier circuit. At the brake are strain gauges, so that the torque of the engine can be measured and a closed loop torque control can be realized in LabVIEW®. All actuators of the engine are controlled exclusively via the ECU (Figure 3.2). However, a dSpace MicroAutobox II is connected to the series ECU via CAN so that commands can be sent to the ECU (e.g. change rail pressure set-point). The MicroAutoBox is also connected to the series sensors in parallel with the ECU, so that they can be scanned independently of the ECU (higher scanning rate with MicroAutoBox).

The aspirated air is filtered and compressed by a stationary high and a stationary low pressure turbocharger (Figure 3.3). Boost pressure is limited by a waste gate at the high-pressure turbocharger. Following to air compression by turbochargers, air is cooled with a charge air cooler and mixed with cooled exhaust gas via the EGR control system. It should be mentioned that the engine is not equipped with an air mass flow meter.
The two turbochargers turbines are driven by exhaust gas. At certain load points exhaust gas can be throttled through a flap (u_{eth} in Figure 3.3) installed downstream of the low-pressure turbocharger. This leads to an increasing total pressure in the exhaust manifold so that higher EGR rates are possible at certain load points. In addition, operation points of turbochargers can be shifted and exhaust gas can be heated by throttling the exhaust gas. Afterwards exhaust gas flows through the DOC and DPF. Between the DPF and SCR system urea dosage takes place.

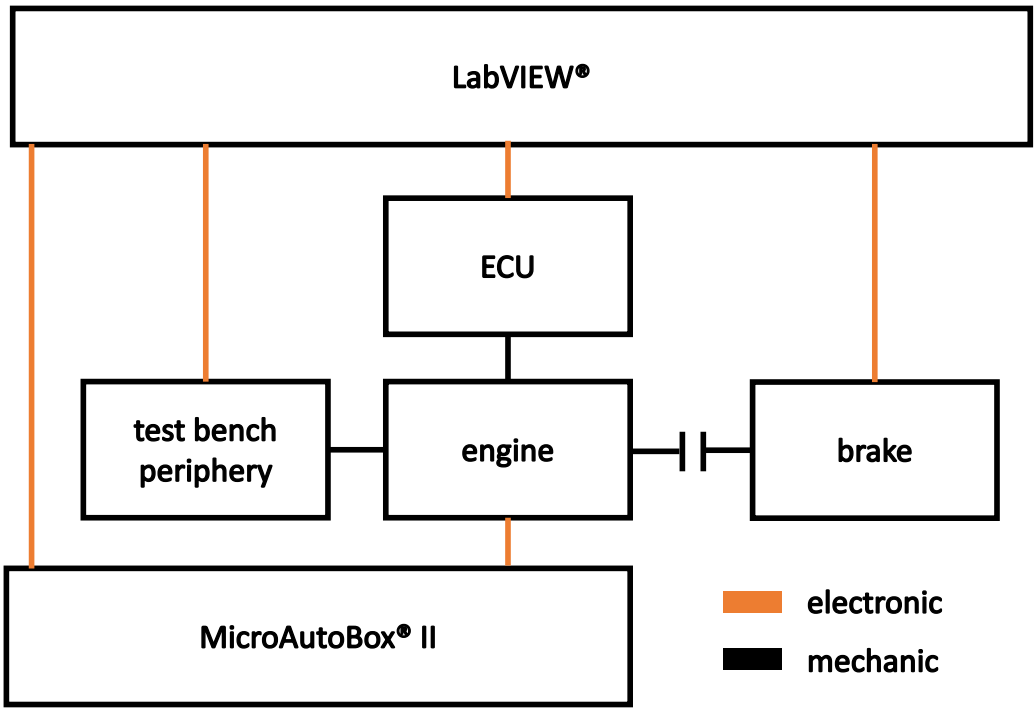

Figure 3.2: Schematic test bench control

3.2 Low Pressure Fuel System

The fuel path starts at the fuel tank of the vehicle. An electrical fuel pump draws in fuel via a prefilter and pumps it through the main filter to the high-pressure pump (Figure 3.4) in the current series system. Fuel flows back into the return line through a throttle in front of the high-pressure pump. Since viscosity of diesel changes only slightly with temperatures occurring in practice, a sufficiently precise pressure in front of the high-pressure pump can be set via this throttle. Furthermore, the fuel system can be vented through the throttle. As soon as ignition is switched on after changing fuel filters, air (which enters the fuel system by changing fuel filters) flows into the fuel tank via return line and does not get into the high-pressure pump.

The LPFS must be adapted to the significantly higher viscosity for operation with NRO. Especially at cold temperatures, high viscosity led to problems in the fuel system in the past. Typical fault messages often indicate a too low fuel pressure upstream of the high-pressure pump. Reasons for this are very narrow mesh sizes of fuel filters (needed due to the high rail pressures in the fuel system) and fuel pumps that are often not designed for NRO operation. For this reason the LPFS is adapted in section 3.3.
Modifications of the LPFS are hardware changes of the machine with correspondingly higher costs. It should be noted that the series system is in principle also suitable for NRO and RME. However, the series system quickly reaches its limits at fuel temperatures $<10\,°C$. The adjustments

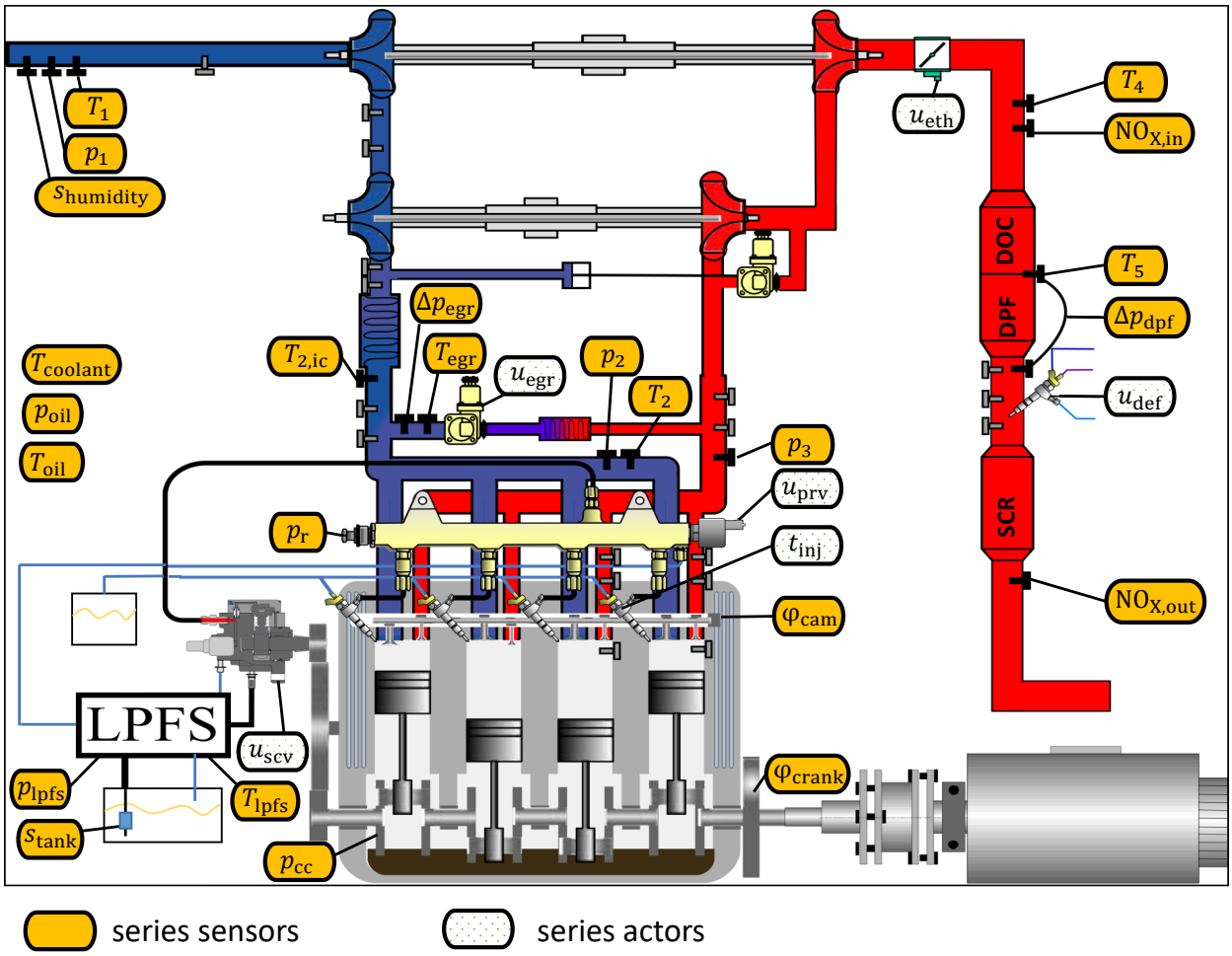

Figure 3.3: Test engine with series sensors and actors

are only intended to ensure operation at cold fuel temperatures. For summer operation (where typically most of the work of an agricultural machine is done), the series fuel system is capable of running NRO.

3.3 Adaption of the Low Pressure Fuel System

The series fuel pump is replaced by a stronger fuel pump (Pierburg E3L) and the fuel prefilter (included water separator) is installed behind the pump (compare Figure 3.6 and Figure 3.4). This reduces suction resistance of the pump.
The Pierburg E3L is a permanent magnet, fuel-cooled screw pump. This design is well suited for highly viscous fuels such as NRO. The electrical fuel pump is operated with constant 12 V (engine off), or 13.5 V (with running engine). Constant voltage (13.5 V) results in the curve shown under Figure 3.5. Since the pump is operated with constant voltage, the pressure downstream of the pump can be determined directly from the current demand. The 13.5 V on-board voltage is constantly regulated by the alternator via a voltage controller.

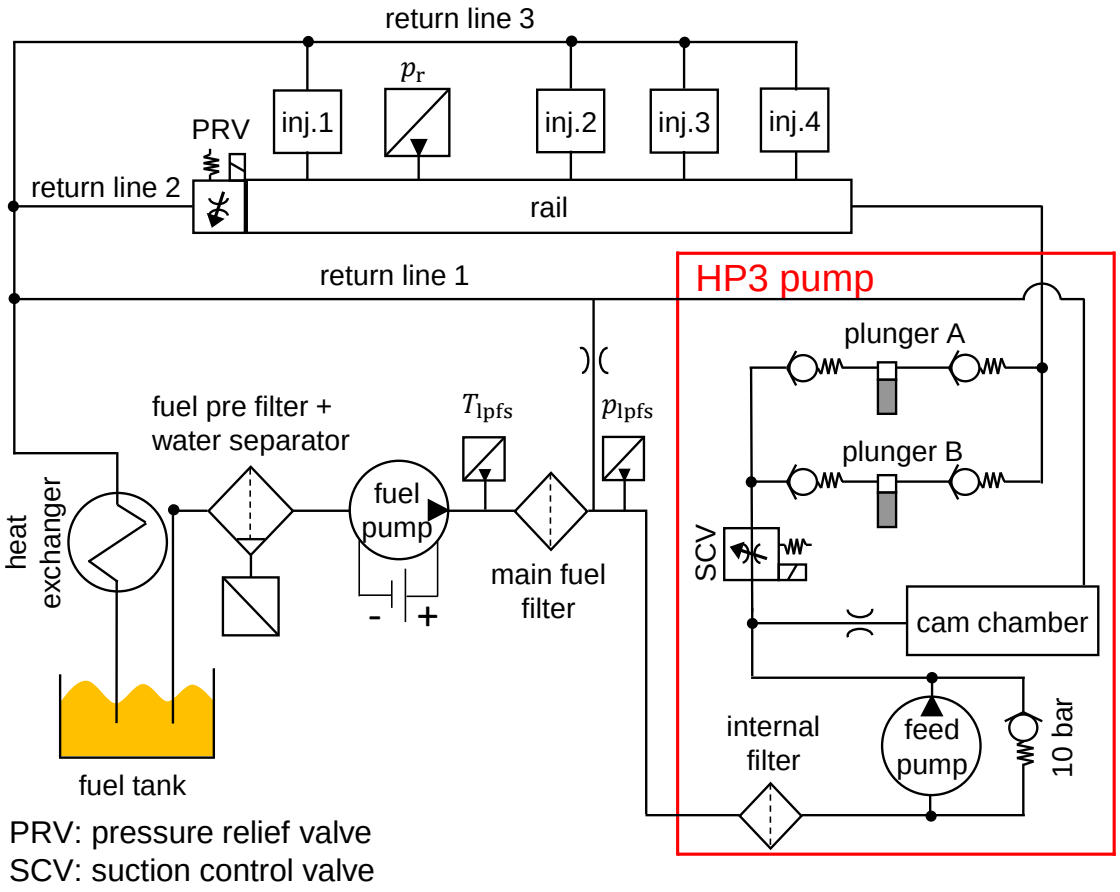

Figure 3.4: Series production fuel system

Figure 3.6 shows the fuel system used at the test bench. Injector leakage flow is collected separately and measured using a second weight scale.

Furthermore, three additional difference pressure valves are installed. These ensure the LPFS is capable of handling NRO over a wide temperature range. A 500 kPa valve is used to protect the electrical fuel pump in case of clogged fuel filters or very cold fuel temperatures (high viscosity of NRO).

A 30 kPa pressure relief valve limits pressure upstream of the high-pressure pump so pressure is within specifications (internal John Deere Document) of the high-pressure pump (between 70 kPa and 140 kPa absolute pressure). The valve is also used for venting the fuel system (e.g. after changing a fuel filter).

A 50 kPa valve ensures pressure in return lines (1,2 and 3) from the high pressure system does not become too high. This could happen due to the high pressure drop across the heat exchanger at cold temperatures.

An ideal electrical fuel pump would generate 0 kPa absolute pressure on the suction side with highly viscous fuel. Theoretically, the electrical fuel pump can therefore suck fuel from upstream of the high-pressure pump (via 50 kPa valve, heat exchanger and return line 4). However, with the 50 kPa valve absolute pressure before the high-pressure pump is still 80 kPa even in the worst case

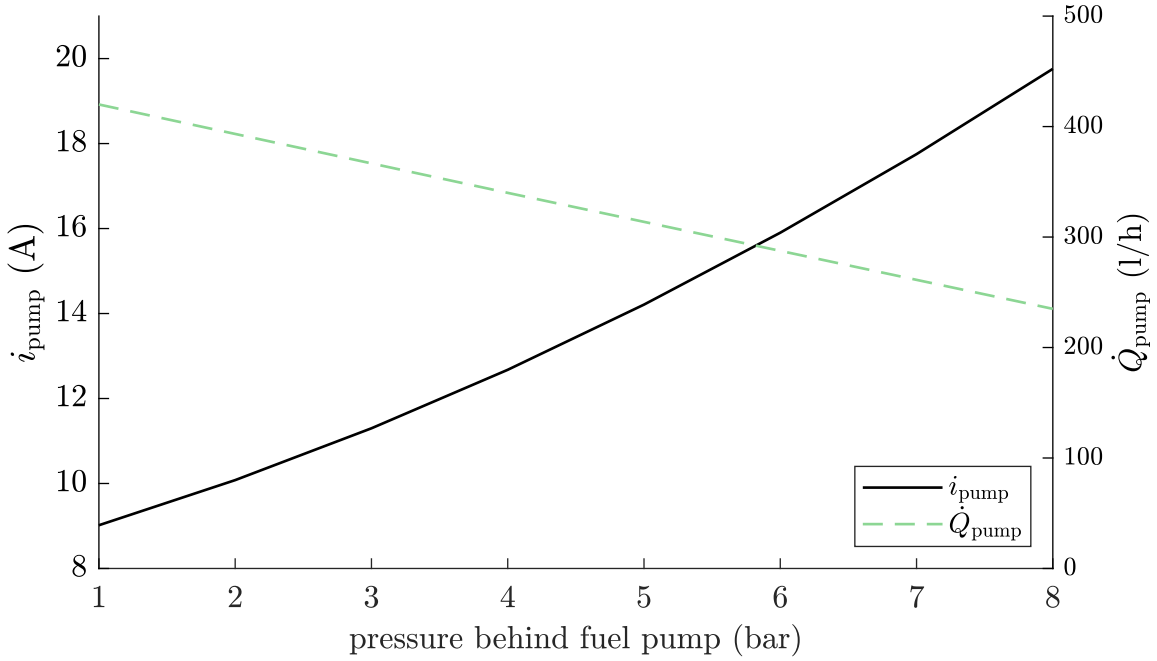

Figure 3.5: Current curve of Pierburg E3L as a function of the pressure at constant 13.5 V with diesel at 20 °C (internal John Deere document)

scenario (pressure before electrical fuel pump 0 kPa and no pressure loss via the heat exchanger), due to the selected valves. Therefore it is still within the specifications of the high-pressure pump. The 50 kPa valve is especially important in the first minutes after a cold start. At very cold temperatures it allows fuel to flow back from the warm return line to the electrical fuel pump (injector leakage is warm immediately after engine start because the high pressure fuel flows back into the return line via a throttle). The electrical fuel pump creates a very low pressure on the suction side if the fuel is highly viscous. If that happens, the valve opens and warm fuel mixes with cold fuel from the fuel tank. This improves the flow through the pump and fuel filters. It also helps warming up the LPFS more quickly.

Constant fuel temperatures are helpful to simplify the engine software to different fuels (viscosity of NRO is highly temperature dependent). This is achieved by a fuel temperature control (FTC) after the fuel pump. On the test bench the fuel temperature control system is equipped with a water cooler and an electrical heater.

In the vehicle fuel conditioning could be carried out with the help of engine cooling water. Potential series production vehicles have a cooling water heater, so water can be warmed up before the first engine start (connection to local power grid via plug). This feature can also be selected as an equipment option as a comfort function (the cabin is heated indirectly via the engine cooling water, so the operator has a warm cabin before starting the engine).

A constantly controlled fuel temperature of 40 °C offers many advantages in practical use of NRO. Due to significantly lower viscosity at elevated temperatures (the viscosity of NRO at 40 °C is half as high as at 20 °C) the pressure drop across the fuel filters is significantly lower. This helps to

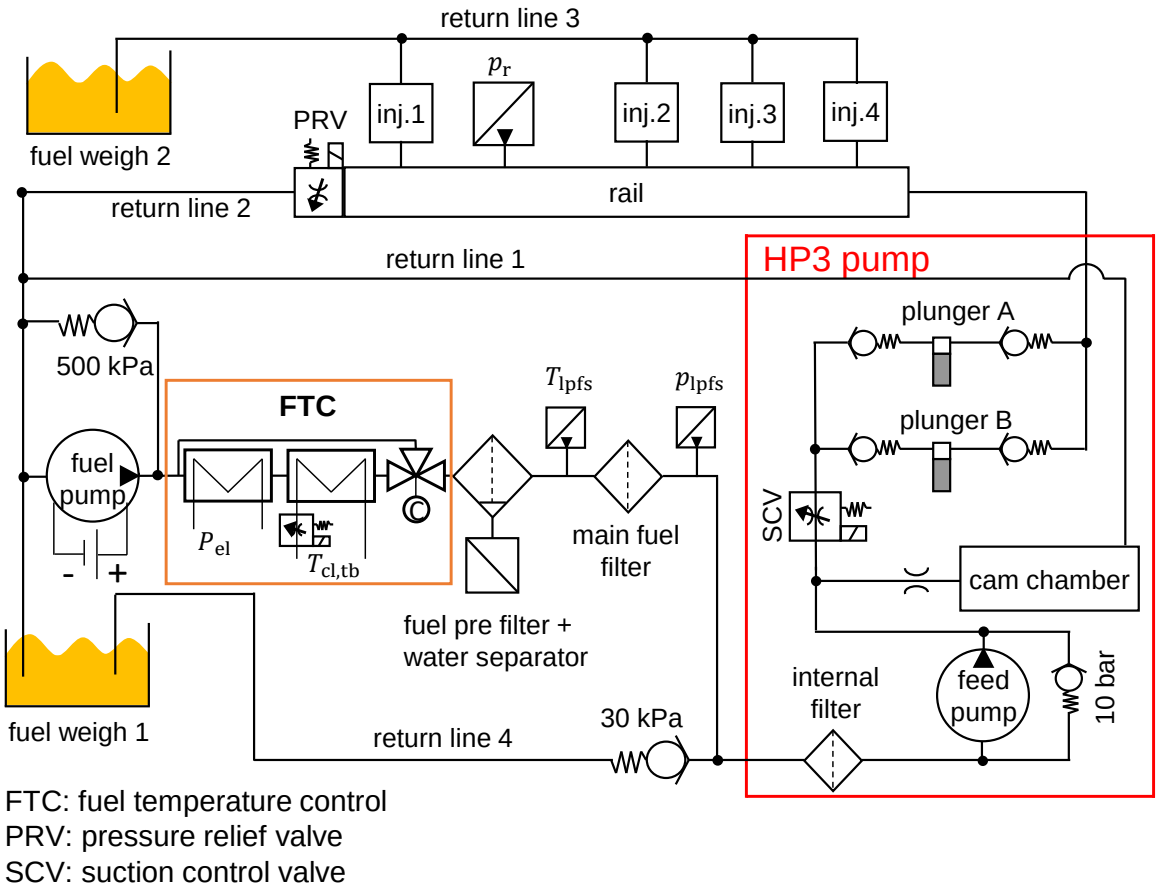

Figure 3.6: Fuel system used at the test bench, which is improved for rapeseed oil usage

prevent errors of a too low pressure upstream of the high-pressure pump.
The most critical point is starting the combustion engine. Even if cooling water can be electrically preheated, fuel in the filters remains cold. Pressure problems can occur in front of the high-pressure pump during the first seconds with the ignition on. However, warm fuel flows through the system and warms up the fuel filters as soon the fuel pump runs. This happens automatically before the engine start in cold temperatures, because the engine has to be electrically preheated via glow plugs (ignition switched on).

3.4 High Pressure Fuel System

This section describes the design and control of the high pressure system. The high pressure pump is of particular importance. The test engine uses a HP3 high-pressure pump of the company Denso. After the fuel enters the high-pressure pump it is pumped by the mechanical feed pump to approx. 10 bar pressure (Figure 3.7). The pressure increased to 10 bar reduces the formation of gas bubbles in the pump chamber (compare Figure 3.10). The feed pump is a trochoid pump as shown in Figure 3.8. Like the two plungers for high pressure generation, it is mechanically driven with the pump-camshaft.

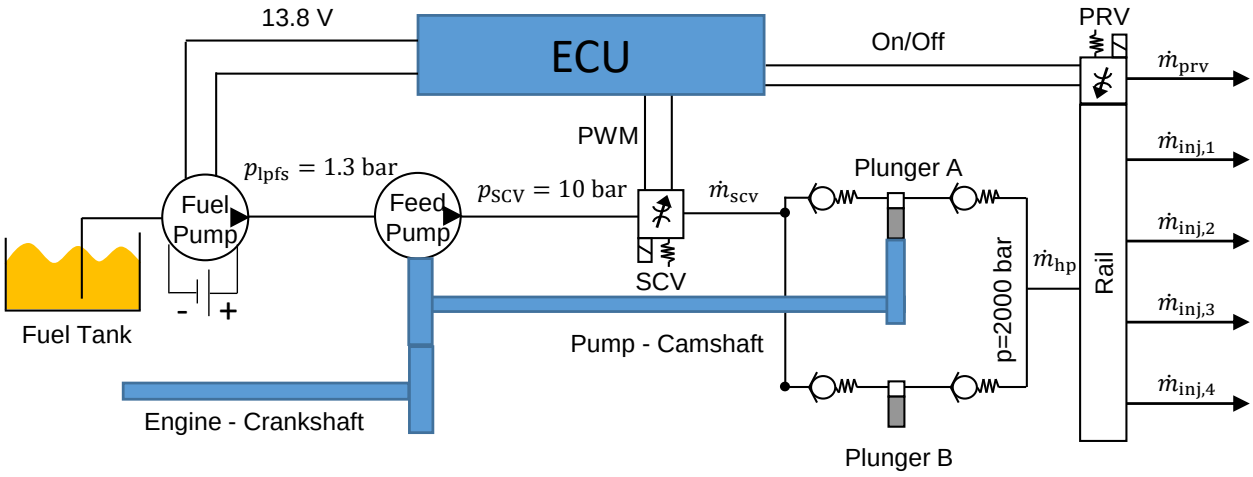

Figure 3.7: Simplified control and pressure overview of the fuel system

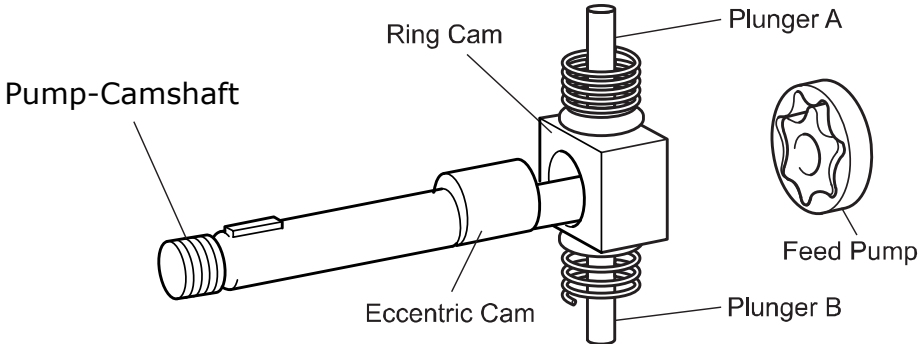

Figure 3.8: High pressure plunger of Denso HP3 high pressure pump (internal John Deere document)

The pump-camshaft is connected to the engine-crankshaft via a gearbox, so that both have the same speed:

$$n_{\text{engine}} = n_{(\text{engine}-\text{crankshaft})} = n_{(\text{pump}-\text{camshaft})} \tag{3.1}$$

The plungers can raise the fuel pressure up to 200 MPa. They are located inside the pump chambers which are offset by 180° (Figure 3.8 and Figure 3.7). The exact physical dependencies for pressure build-up are explained in detail in section 7.4.
A ring cam between the eccentric pump-camshaft and plungers is necessary so no lateral forces are transmitted by rotational movement of the camshaft (Figure 3.8). Since the pump-camshaft rotates with engine crankshaft speed, two pumping operations per 360° crank angle (°CA) or four pumping operations for 720° CA take place. Since this is a 4-cylinder engine with a 4-stroke cycle, the high-pressure pump runs synchronously with fuel injections.

Rail-pressure control is realized by two actuators (Figure 3.7). These include the suction control valve (SCV) and pressure relief valve (PRV). The PRV is installed directly on the rail and is used very rarely as it feeds fuel under high pressure back into the return line via a throttle. This leads to a strong heating of fuel (loss of engine efficiency) which has to be cooled down by the fuel

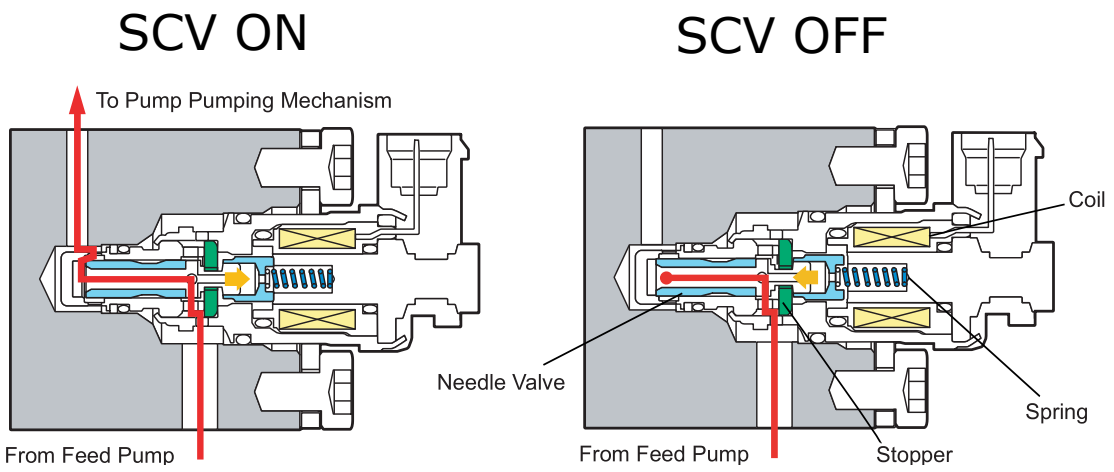

Figure 3.9: Suction control valve (SCV) in open and closed position (internal John Deere document)

cooler afterwards (Figure 3.6). Therefore the PRV is only used in a few cases. One of these cases is e.g. that the engine changes suddenly from high loads (high rail pressures) to idling so the rail pressure needs to be reduced quickly. Another use-case of the PRV is an emergency valve if there is too high pressure in the rail, e.g. due to a faulty SCV or defective injectors.
In faultless cases rail pressure is mainly controlled by SCV. This means plungers of the high-pressure pump are only supplied with as much fuel as required to reach the desired rail pressure. This procedure leads to a significantly improved efficiency compared to overpressure control (via PRV) as it was done in first common-rail generations [94].

When one plunger of the high-pressure pump moves away from top dead center fuel enters the plungers via a suction control valve (SCV). The plungers are pressed in the direction of the bottom dead center by a spring to suck in the fuel (Figure 3.8). This results in the following balance of forces at the plunger (Figure 3.10):

$$m_{\text{plunger}} \frac{dv}{dt} = F_{\text{spring}} + F_{\text{fuel}} - F_{\text{fric}} - F_{\text{amb}} \tag{3.2}$$

In Equation 3.2 only the movement of the plunger during the suction process is considered (there is no force from the ring cam on the plunger). F_{amb} is the force due to the pressure in the pump-camshaft housing.
F_{fuel} depends on the opening cross section of the SCV. If F_{fuel} is very small, the plunger accelerates more slowly so that the plunger only reaches the bottom dead center when SCV is fully open (maximum pumping quantity). With smaller opening cross sections of the SCV the plunger lifts off the cam (small pump quantity). This happens because the ring cam is back in the upward (pressing) motion faster than the plunger reaches its bottom dead center.
When plungers approach the TDC, fuel is compressed until the pressure in the pump chamber is higher than in the rail. This leads to a fuel flow through a discharge valve (Figure 3.10) into the rail.
The SCV itself is electronically controlled by the ECU via pulse-width modulation (PWM) (Figure 3.11). Due to the inertia of the coil, the PWM signal induces a medium current ($\bar{i}_{\text{scv}}$ in the

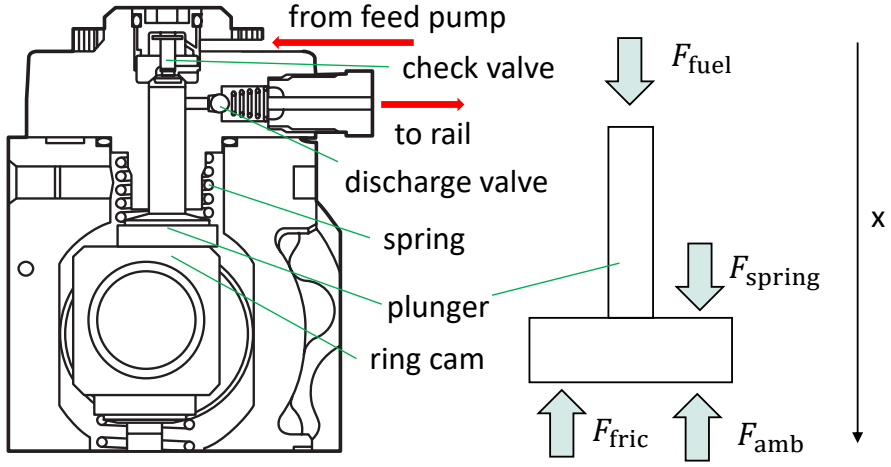

Figure 3.10: Mechanical overview of the suction control valve and forces at the plunger for high pressure generation

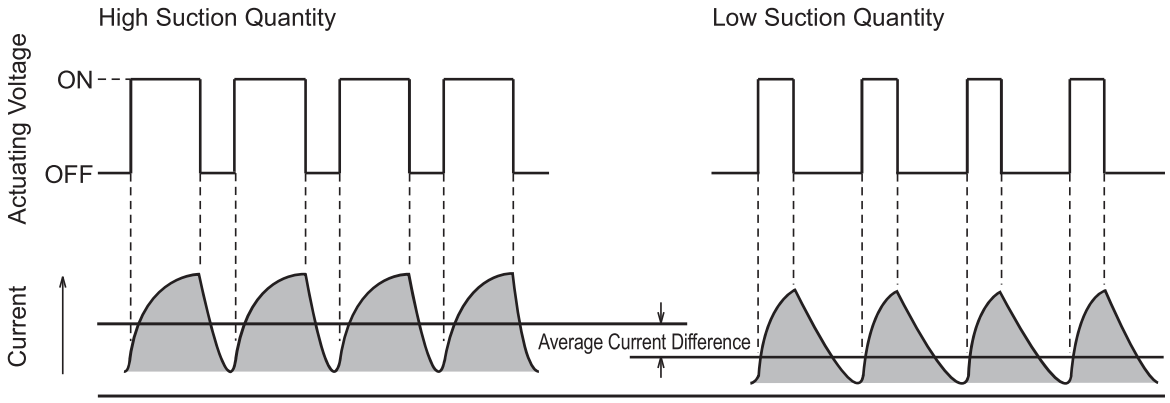

Figure 3.11: PWM control of the suction control valve (internal John Deere document)

following). This creates an electromagnetic force that acts against the spring in the SCV (Figure 3.9). Thus the effective opening cross section of the valve can be adjusted with the PWM signal.

The fuel mass in the high pressure system depends on $\dot{m}_{scv}$, $\dot{m}_{inj,i}$ and $\dot{m}_{prv}$ (see Figure 3.7). All 3 influencing factors can be controlled by the ECU.

SCV is feed-forward controlled via look-up tables based on engine speed, desired rail pressure and desired injection quantity. The closed loop rail pressure control (detailed description of engine controls in section 4.6) in- or decreases $\bar{i}_{scv}$ in order to compensate deviating feed-forward control. Deviations can occur e.g. due to changing fuel temperatures. To close the control loop a rail pressure sensor is needed at the rail (shown in Figure 3.6). It is positioned between the supply line of the first and second injector (p_r in Figure 3.6).

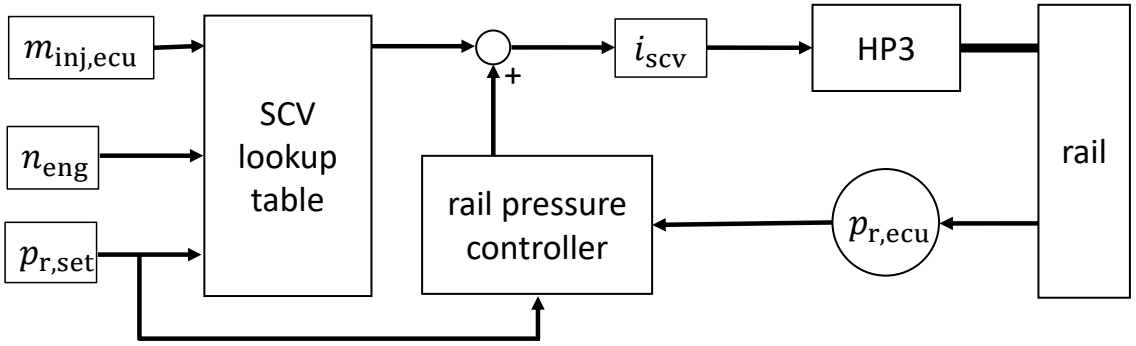

Figure 3.12: Control structure of high pressure system

The pressure relief valve has the same operating principle as a solenoid coil diesel injector (explained in the next section) and has only two states (open and closed). That means that the fuel mass which can be dumped by the PRV is controlled by the control time t_{prv}. The pressure relief valve is open-loop control only. If a limit is exceeded, the PRV opens. For the further course of this work the PRV plays a subordinate role and is only mentioned here for the sake of completeness.

3.5 Fuel Injector

Piezo or solenoid injectors are the state of the art for diesel engines [48]. Piezo injectors offer advantages regarding opening and closing times, whereas solenoid coil injectors have advantages regarding service life and robustness [77]. Since reliability is of high importance, solenoid injectors are installed in the test engine. These are G4S injectors from the company Denso. They are characterized by a clearly reduced leakage quantity compared to previous models but are also more complicated in construction. A control plate was added compared to the old injector in order to reduce leakage quantity and generate a fast response behavior [75]. Injector behavior in engine operation can be roughly divided into 4 states:

1. Control valve closed and needle closed (injector in idle)
2. Control valve open and needle closed (injection starts soon)
3. Control valve open and needle open (fuel injection)
4. Control valve closed and needle open (injection ends soon)

The red areas (Figure 3.13) indicate fuel with the same (high) pressure as in the rail. The green areas at the top of Figure 3.13 show fuel with the pressure of the return line (1-2 bar). The areas A in Table 3.2 are the projected areas in the direction of movement of the needle or control plate. This means that for a lifted needle (needle tip is completely surrounded by fuel and does not cover the injection holes) $A_{\mathrm{needle,top}} = A_{\mathrm{needle,bottom}}$ applies.

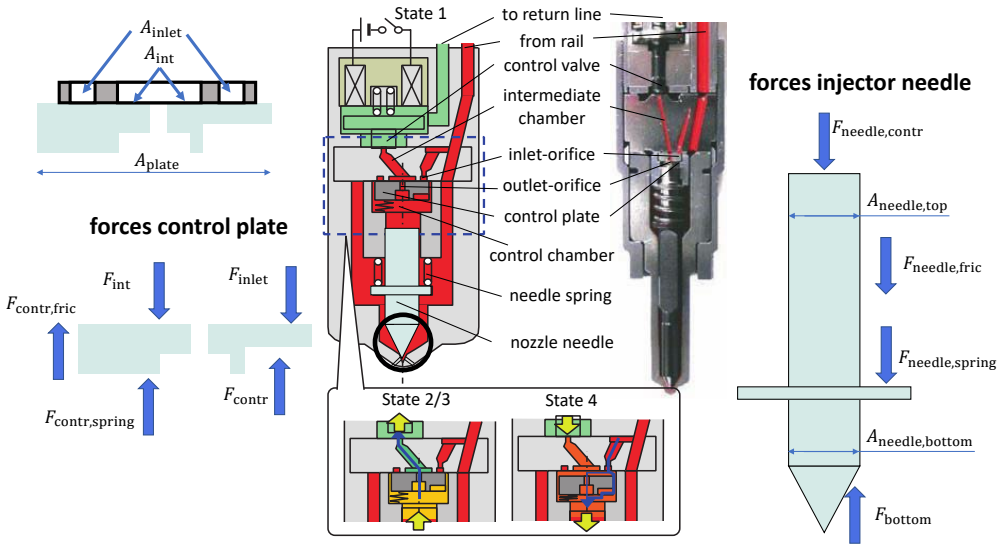

Figure 3.13: Injector function principle with forces to injector needle and control plate. Modified according to [75]

Table 3.2: Correlation of forces and pressures within the injector

symbol	description	pressure correlation
F_{int}	force result. of the pressure in intermediate chamber	$p_{int} \cdot A_{int}$
F_{inlet}	force result. of the pressure in inlet orifice	$p_r \cdot A_{inlet}$
$F_{contr,fric}$	force result. of the friction of control plate	independent of pressure
$F_{contr,spring}$	force result. of the spring at control plate	independent of pressure
F_{contr}	force result. of the pressure in control chamber	$p_{contr} \cdot A_{plate}$
$F_{needle,contr}$	force result. of the pressure in control chamber	$p_{contr} \cdot A_{needle,top}$
$F_{needle,fric}$	force result. of the friction of the injector needle	independent of pressure
$F_{needle,spring}$	force result. of the spring at the injector needle	independent of pressure
F_{bottom}	force on the bottom of the injector needle	$p_r \cdot A_{needle,bottom}$

1. State:
   When the fuel injector is in state 1 (Figure 3.13 top), the entire fuel in the injector has the same pressure as in the rail. This causes the nozzle needle to be pressed against the injection holes. High pressure is canceled in transverse direction of the injector. However, there is a hydraulic force that presses the nozzle needle into the needle seat in the longitudinal direction. The reason for this is that the surface at the top of the injector needle is larger than the surface at the bottom. The part of the needle that closes the injection holes has no surface where the pressure of the fuel can apply (black circle in Figure 3.13). Additionally, a mechanical spring pushes the needle into the seat. It should be noted that the hydraulic forces are many times higher than the spring force and the frictional force (when the needle moves).

The balance of forces of the injector needle (Figure 3.13) for state 1:

$$m_{\text{needle}}\frac{dv}{dt} = F_{\text{needle,contr}} + F_{\text{needle,spring}} + F_{\text{needle,fric}} - F_{\text{bottom}} = 0 \tag{3.3}$$

The following applies:

$$F_{\text{needle,contr}} >> F_{\text{needle,spring}} + F_{\text{needle,fric}} \tag{3.4}$$

The control plate is the most important component for controlling the injector. For this reason a balance of forces (Figure 3.13 left) for state 1 is also set up:

$$m_{\text{plate}}\frac{dv}{dt} = F_{\text{int}} + F_{\text{inlet}} - F_{\text{contr,fric}} - F_{\text{contr,spring}} - F_{\text{contr}} = 0 \tag{3.5}$$

2. State:
If the injector is energized (electro-mechanical behavior is explained in Figure 3.14), the control valve opens and the injector is in state 2 (Figure 3.13 bottom). The electrically operated control valve opens much faster than the hydraulically operated injector needle. The duration from activating the injector until the needle is lifted is called opening delay.
When the control valve opens, fuel flows into the return line of the injector. This is called injector leakage in literature [75]. Since the return flow is approximately at ambient pressure, the throttle (outlet-orifice) of the control plate is very small (to keep leakage rate low). By draining the fuel into the return line $F_{\text{needle,contr}}$ decreases so the needle starts moving:

$$m_{\text{needle}}\frac{dv}{dt} = F_{\text{needle,contr}} + F_{\text{needle,spring}} + F_{\text{needle,fric}} - F_{\text{bottom}} < 0 \tag{3.6}$$

From this follows:

$$F_{\text{bottom}} > F_{\text{needle,contr}} + F_{\text{needle,spring}} + F_{\text{needle,fric}} \tag{3.7}$$

If the dependencies from Table 3.2 are used, the result for pressure in the control chamber (state 2/3 in Figure 3.13 yellow) is:

$$p_{\text{contr}} \cdot A_{\text{needle,top}} < p_{\text{r}} \cdot A_{\text{needle,bottom}} - F_{\text{spring}} + F_{\text{fric}} \tag{3.8}$$

Since $A_{\text{needle,top}} = A_{\text{needle,bottom}}$ applies when the needle is lifted:

$$p_{\text{contr}} < p_{\text{r}} - \frac{F_{\text{spring}} + F_{\text{fric}}}{A_{\text{needle,top}}} \tag{3.9}$$

With the condition Equation 3.4 it results that p_{contr} is only slightly smaller than p_{r}.
The control plate does not move. F_{contr} sinks slightly but at the same time F_{int} sinks very strongly (p_{r} to ambient pressure) so that the control plate is still pressed upwards (in the direction of the control valve).

3. State:
The movement of injector needle releases the injection holes and fuel is injected into the cylinder (state 3). Nothing changes at the described equations from state 2. The injector needle moves further into the control chamber as fuel continues to drain from the control chamber during an injection process. Pressure in the control chamber remains approximately constant.

4. State:
   The control valve closes when the injector pulse is terminated. However, the injector needle remains open until the control chamber is filled with high pressure again (state 4). The duration from end of the injector pulse until the injector needle closing is called closing delay. Since no more fuel can flow out of the control chamber, a pressure balance is established on both sides of the outlet orifice (Figure 3.13). The control plate moves down due to a higher pressure of the in-orifice compared to the control chamber and the in-orifice is released. This leads to a fast pressure equalization between pressure in the rail and control chamber, so the injector needle closes faster compared to previous injector models. An additional mechanical spring is installed in the control chamber in order to achieve a defined initial state. This spring presses the control plate back to the upper seat. There is no large force required because pressure around the control plate is constant after opening the in-orifice.

Out-orifice throttle and rail pressure are decisive for opening delay. Fuel flows faster out of the control chamber with a larger diameter of the throttle or higher rail pressure, so the injector needle opens more quickly. However, since larger leakage rates reduce the efficiency of the engine (heating of fuel), there is a trade-off between opening delay and leakage rate.
The closing delay does not only depend on the in-orifice throttle and rail pressure but also on the duration of the injector pulse. The injector needle has been open further with increasing duration and therefore more fuel must flow through the in-orifice into the control chamber to restore the pressure. The in-orifice should be dimensioned as large as possible in order to keep the closing delay small. However, since a too large in-orifice could cause the control plate to lift out of the seat, there is a trade-off.

The control valve is an electromagnetic valve. The control valve forms the armature. An electrical current flowing through a coil generates a magnetic field in an iron core so that the control valve is attracted (valve opens). A spring is used to reset or close the valve. To open the control valve quickly relatively high currents are necessary [60]. The delay of the electrical pulse to open the

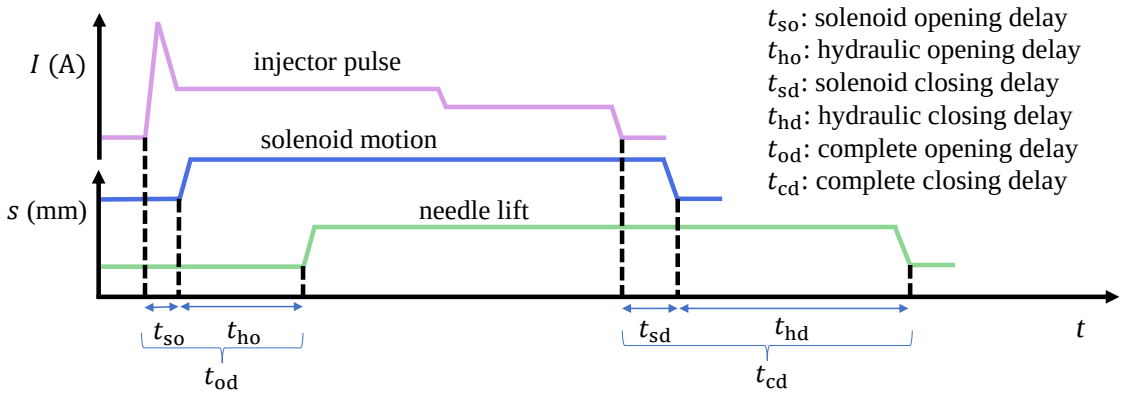

Figure 3.14: Injector delays depending on the components

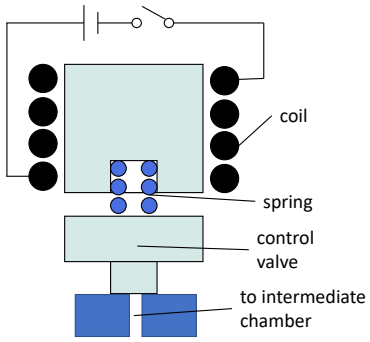

Figure 3.15: Principle of solenoid control valve

control valve is negligible compared to the hydraulic delay. All causes leading to a delayed opening and closing of the injector needle are combined (Figure 3.14). It becomes clear that the closing delay has a large impact on the total needle opening time. Therefore opening and closing delays are stored in look-up tables on the ECU. Necessary pulse duration for triggering the injector can be determined for a desired injection time with stored tables.

3.6 Adaptation of the High Pressure Fuel System

Changes are also being made to the high-pressure pump. However, this is not done in order to adapt the high-pressure pump to different fuels, but to separate pumping and injection processes (independent of the fuel used). This has advantages to later evaluation of the rail pressure signal. In series production the high-pressure pump is synchronous to injections (before every injection an associated pump process takes place). Pumping processes of the high-pressure pump are over as soon as respective pistons in the combustion chamber reach the top dead center. This means that plunger A of the high pressure pump stops the fuel delivery when cylinder 1 and cylinder 4 are at the top dead center. In case of early injection timing, this leads to overlapping pumping processes and fuel injections. Overlapping has no serious consequences for the injection. Theoretically, this setting leads to a smoothed rail pressure curve and thus to a more accurate rail pressure during injection. However, advantages of decoupling pumping and injection processes outweigh disadvantages in this research work. Therefore, the end point of pumping processes is shifted by rotating the high-pressure pump in relation to the drive gear by approx. 30°.

With a shifted angle a pumping process is finished at the latest approx. 30 °BTDC (before the combustion piston reaches the top dead center). Figure 3.16 clarifies that the end of the fuel delivery is before an injection takes place in standard operation. However, it is also clear that at the maximum delivery volumes of the high pressure pump, injection and fuel delivery still overlap. With a fully filled pump chamber, the fuel delivery of the high pressure pump starts after the ring cam is in an upward movement (compare Figure 3.10).

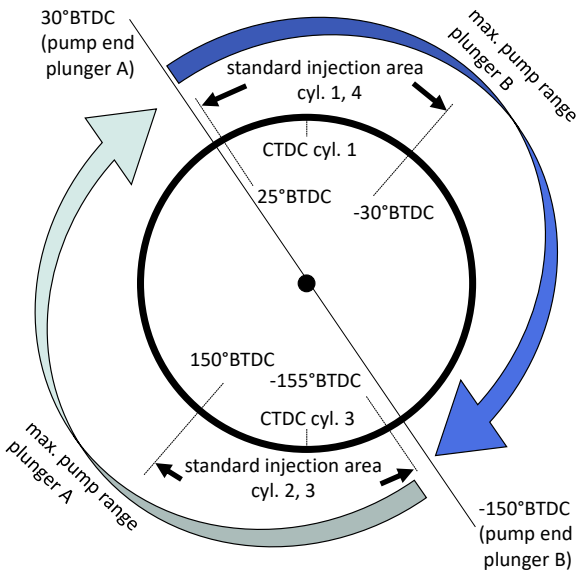

Figure 3.16: Illustration of the pump range after shifting the gears of the high-pressure pump

At constant operating points the maximum consumed fuel of the engine at full load is lower than 150 mm^3/str. So the high pressure pump is oversized for stationary load points (maximum pump quantity is up to 360 mm^3/str). Due to the selected rotation of the high-pressure pump in relation to the crankshaft, the injection and thefuel delivery into the rail are completely separated if the pump quantity is less than 2/3 of the maximum pump quantity. Very large pump quantities (>240 mm^3/str) only occur with a strong increase in the rail pressure set-point with simultaneously high injection quantities (very rare). For all stationary operating points a decoupled injection from the pumping event of the high-pressure pump can be assumed.

3.7 Conclusions of the Investigated Test Engine

Since the series engine from John Deere is approved for biodiesel, no adjustments are necessary for operation with RME. In principle, the engine is also suitable for use with NRO. However, since problems often occurred in the past in operating with NRO, especially in cold temperatures, adjustments to the LPFS were made. For this adjustments only components that are also suitable for RME are used (pumps, valves and seals).
For the overall concept of the work it should be noted that the adjustments for the LPFS were only made for cold temperatures in pure NRO operation. In order to reduce the viscosity of the fuel in cold temperature operation, a mixture with diesel would also be possible. The goal of a low-cost adaptation of the engine to biogenic fuels stated in chapter 1 is therefore still given.
The situation is different with the rotation of the high pressure pump. This is a hardware change with correspondingly high effort. Since the decoupling of pump and injection processes is also valid for pure B0 diesel operation, this change should be adopted for series machines (regardless of whether the machine is operated with different fuels or only diesel).

4 Preparations for Measurement Data Acquisition

In the context of this work, series sensors are to be evaluated more precisely. For this purpose it is necessary to run preliminary investigations as well as developing special strategies for the acquisition of data. These are presented in this chapter. Furthermore, the engine control, as well as the effect of different fuels on the control is explained. Afterwards a strategy for controlling the engine with different fuel mixtures is shown.

4.1 Test Fuels

Fossil diesel, RME and NRO are used in the test engine. B0-NRO and B0-RME mixtures are also used (no RME-NRO mixtures). For fuel properties of blends a linear behavior is assumed within the scope of this thesis to simplify further calculations. Furthermore the assumption states that the volumes of fuels add up perfectly when blended. Investigations by Nguyen, Bazile, and Bessières [80] show that these assumptions are justified for blends between diesel and biodiesel and good results are obtained when interpolating between the fuels.

Fuel mixtures defined for this work are examined in 25% steps. For the investigated fuel mixtures the following notation is used: B0_RME_NRO. Here the number indicates mass-related percentage of the respective fuel. For example, the fuel 75_0_25 equals 75% of fuel mass is B0, 0% RME and 25% is NRO.

Table 4.1: Overview of measured load points for injector maps

fuel	engine speed (rpm)	torque (N m)	fuel temp. (°C)	rail pressure (MPa)
100_0_0	800, 900...2200	0, 100...max	10,20,30,40	series, 100, 150, 200
75_0_25	800, 900...2200	0, 100...max	40	series, 100, 150, 200
50_0_50	800, 900...2200	0, 100...max	40	series, 100, 150, 200
25_0_75	800, 900...2200	0, 100...max	40	series, 100, 150, 200
0_0_100	800, 900...2200	0, 100...max	10, 20, 30, 40	series, 100, 150, 200
75_25_0	800, 900...2200	0, 100...max	40	series, 100, 150, 200
50_50_0	800, 900...2200	0, 100...max	40	series, 100, 150, 200
25_75_0	800, 900...2200	0, 100...max	40	series, 100, 150, 200
0_100_0	800, 900...2200	0, 100...max	10, 20, 30, 40	series, 100, 150, 200

In order to demonstrate the fundamental effects of various fuels, especially regarding injection behavior, engine speeds are measured in 100 rpm and torque in 100 N m steps (Table 4.1). The value “max” for torque in Table 4.1 refers to the maximum torque that can be provided by the engine at corresponding speed and corresponding fuel. Rail pressure is fixed to 100, 150, and 200 MPa (2000 bar), as well as in series mode. In series mode serial look-up tables are used for controlling the rail pressure.

Even if the fuel temperature is controlled on a constant level, injector maps of pure substances are measured at different fuel temperatures. Effects of different fuel temperatures on injector behavior can be determined in this way. In practice, fuel temperatures may be too low directly after starting the engine (fuel temperature control of the LPFS works only with warm engine).
Since respective injection masses or injector maps for individual fuel mixtures are of great importance, following sections present a procedure with which injector-specific injection masses can be calculated.

4.2 Crank-Synchronous Measurements

The crankshaft position forms the basis for controlling an engine. With one sensor (crankshaft timing wheel) the position of the crankshaft or the pistons can be determined by the ECU. Since it is a 4-stroke engine, the current stroke of the engine (position of valves) cannot be determined. For this reason a second sensor (camshaft timing wheel) is attached to a gear rotating at camshaft speed.

The speed sensors are inductive. They consist of a permanent magnet and an induction coil with soft iron core. The movement of the gear wheel changes the magnetic field in front of the sensor and causes a voltage change which is measured by the ECU. The crankshaft timing wheel has 45 (48-3) teeth (Figure 4.1). The distance between the teeth is 7.5 °CA with one exception: After 45 teeth there is a gap (22.5 °CA), so the absolute position of the crankshaft can be determined (gap in measured voltage).
The camshaft timing wheel has 11 bars with an even distance of 30°. The twelfth bar is divided into two smaller ones, so the absolute position can also be determined. By evaluating both signals, the ECU can distinguish between ignition and push-out TDC of the respective piston. A hardware circuit converts the sinusoidal raw signal into a digital signal (Schmitt-Trigger).

The series ECU uses the exact position of the crankshaft to time the injections. Measured values, such as pressures are not recorded synchronously with the crankshaft position by the series ECU. However, measurements taken by the dSpace MicroAutoBox are recorded synchronously with the crankshaft position. For this purpose the pulses of the crankshaft timing wheel are used.
At each edge, i.e. all 7.5 °CA sensor values are hardware triggered recorded.
The most important signal is the rail pressure signal. Since the present test engine has a nominal speed of 2100 rpm, the maximum sampling frequency of the rail pressure sensor with a crankshaft

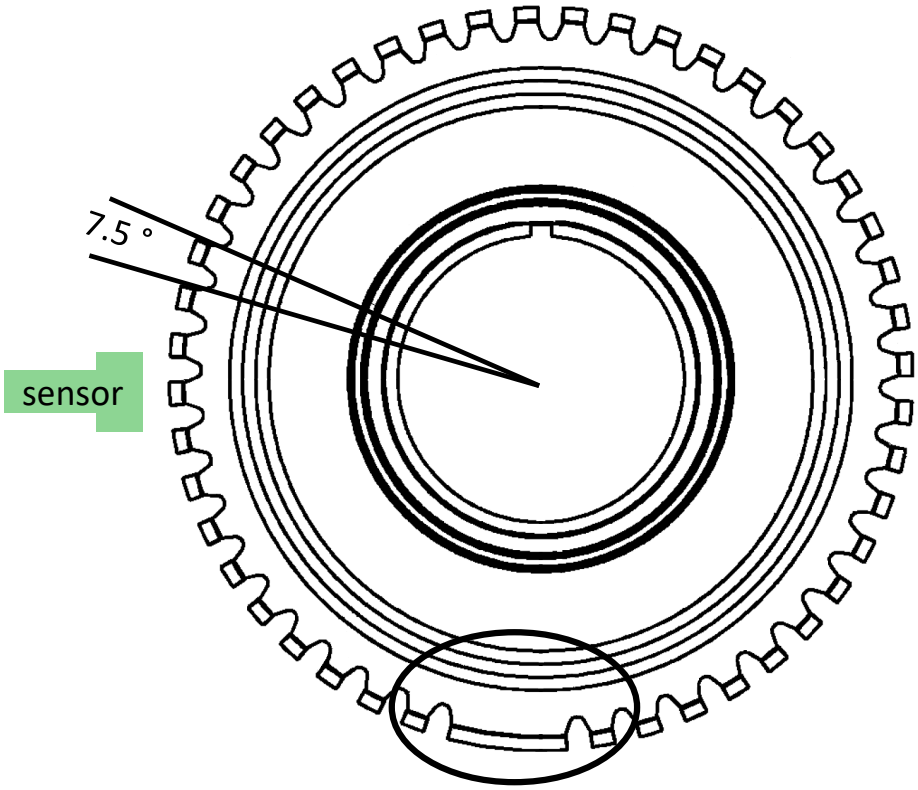

Figure 4.1: Crankshaft timing wheel with gap for absolute position determination

synchronous recording is approx. 1.7 kHz.

$$f_{\text{max,crank}} = \frac{2100\,1/\text{min}}{60\,\text{s}} \cdot 48 = 1680\,\text{Hz} \tag{4.1}$$

4.3 Quasi-Stationary Load Points in Engine Operation

Many diagnostic models only work for quasi-stationary load points in this thesis. Therefore quasi-stationary load points are defined:

1. Speed varies by a maximum of $\pm 5\,\%$
2. Injector pulse duration varies by a maximum of $\pm 5\,\%$ (mean value over 3 injections)
3. Rail pressure fluctuates around $\pm 5\,\%$
4. Minimum duration of the recorded load point is 10 s (first 5 seconds not considered)

For measurement data acquisition the stationary load points should be as long and precisely as possible. If this is the case, average values can be formed and transient effects can be compensated. However, since there is a trade off between long, precise stationary load points and the frequency of their occurrence, a minimum duration of 10 seconds was chosen.

4.4 Determination of Injector-Specific Injection Quantity

In addition to series production sensors, the test bench is equipped with further sensors. A part of the additional sensors is required for control or safety shutdown of the test bench. Other sensors are for the generation of additional measurement data. In addition to speed, torque and air flow meters, fuel weight scales are of particular importance. One weigh measures the fuel leaving the tank:

$$\Delta m_{\mathrm{f,meas}} = m_{\mathrm{f,meas}}(t = 0) - m_{\mathrm{f,meas}}(t = \mathrm{end}) \tag{4.2}$$

A second fuel weight scale measures the return flow of the injectors:

$$\Delta m_{\mathrm{leak,meas}} = m_{\mathrm{leak,meas}}(t = \mathrm{end}) - m_{\mathrm{leak,meas}}(t = 0) \tag{4.3}$$

Both scales are used to create injector maps. Since no injector-specific fuel mass can be measured with this measuring set-up, the fuel consumption is initially averaged over all four injectors. To make these measurements usable, the following procedure is carried out to create injector maps:

1. Adjustment of speed and torque
2. Only one main injection
3. Fixing all ECU set-points (rail pressure, injection timing, EGR etc.)
4. Determination of average injector pulse duration
5. Control all injectors with average injector pulse duration
6. Measurement of fuel consumption for 60 seconds

Step 5 can lead to a slight reduction or increase of the engine torque output. Since this deviation is very small, target torque specification from step 1 is used for all diagrams and tables (for injector maps only rail pressure and injector pulse duration is important). Average injector pulse duration is a set-point value. Injector-specific adjustment of injector pulse duration is still carried out in the ECU like in standard operation (manufacturing tolerances of the injectors).

To determine an injector specific injection quantity, the rail pressure sensor of the engine is evaluated. The sensor is scanned at a high frequency (crank synchronous every 7.5 °CA) so individual injections can be detected in the signal. A simplified rail pressure curve is shown under Figure 4.2 to illustrate the method of injector-specific injection mass determination.

For comparison purposes, Figure 4.3 shows an actually recorded rail pressure curve in a faultless case during operation with diesel fuel.

Each injection of an injector causes a pressure drop $\Delta p_{\mathrm{r},i,k}$ in the rail. In stationary load points the average fuel consumption over all injectors $m_{\mathrm{f,meas}}$ is determined with the fuel weight scale over a longer period of time (Equation 4.2). The return flow of injectors is also measured by a second

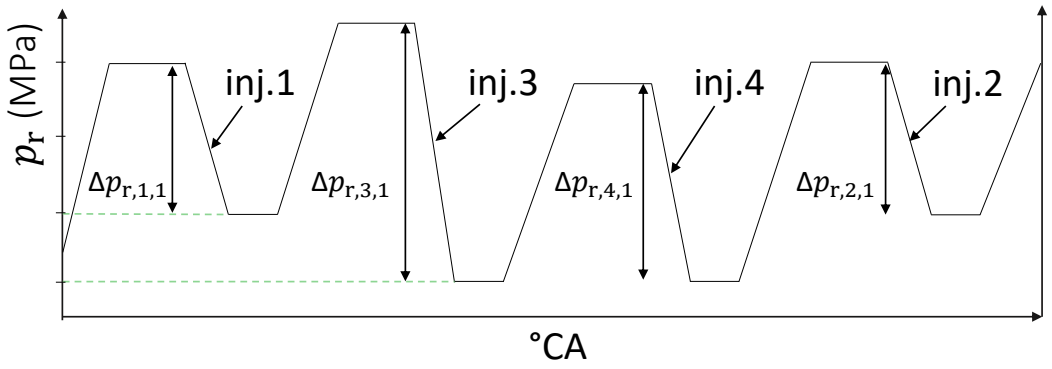

Figure 4.2: Simplified injector specific pressure drop

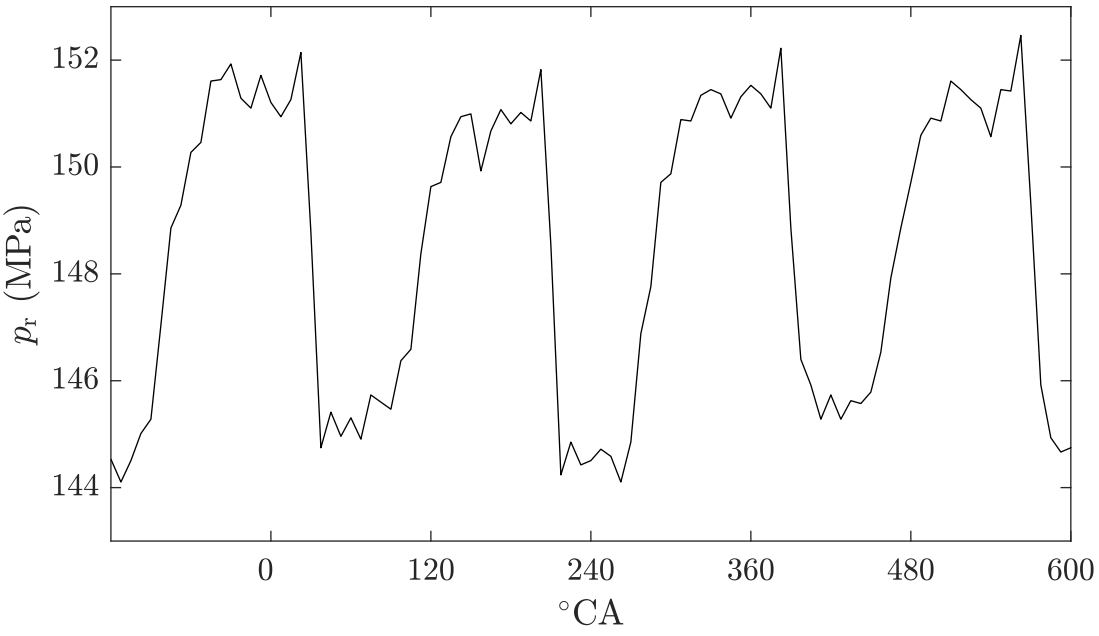

Figure 4.3: Measured rail pressure with pure diesel B0 at 900 rpm and 400 N m

weigh (Equation 4.3).
It is assumed that the return flow quantity is the same for all installed injectors. It would also be conceivable to divide injector leakage quantity based on actual pulse duration of the respective injector. However, differences are so small in relation to injected fuel mass that this influence is neglected. Furthermore it is assumed, that the injected fuel mass by one injection is proportional to the rail pressure drop $\Delta p_{r,i,k}$ (Figure 4.2). Fuel consumption (difference between two fuel weight scales) is divided by the sum of all $\Delta p_{r,l}$ (n_{inj} is the number of all injections in the recorded period) and multiplied by the pressure drop of the respective injection :

$$m_{inj,i,k} = \frac{m_{f,meas} - m_{leak,meas}}{\sum_{l=1}^{n_{inj}} \Delta p_{r,l}} \cdot \Delta p_{r,i,k} \tag{4.4}$$

This is possible because in a stationary load point the PRV is closed and the pressure in the rail can only decrease by injecting fuel or flowing back through the return line into the second weight

scale. The injector-specific injection mass can be calculated approximately for each injection of the respective injector. $m_{\mathrm{inj},i,k}$ is used in the course of this work as a reference value for individual injections.

For the creation of injector maps the average injection quantity of the respective injector is calculated over all injections:

$$m_{\mathrm{inj},i}(p_{\mathrm{r}}, t_{\mathrm{inj,ecu}}) = \frac{\sum_{k=0}^{n_{\mathrm{inj},i}} m_{\mathrm{inj},i,k}}{n_{\mathrm{inj},i}} \tag{4.5}$$

Here $n_{\mathrm{inj,i}}$ indicates the number of injections of the respective injector (0,1,2, or 3).

4.5 Torque Curves

Development and homologation of engines are associated with high costs. These costs are particularly high for low numbers of agricultural machinery. Therefore, many different machine models are equipped with the same engine and adapted by relatively small software and hardware changes to the respective machine. To avoid homologating each power configuration individually, the European Union has proposed an upper and a lower torque curve for non-road mobile machinery [26]. The engine must comply with exhaust emission limits for the upper (maximum torque approved by the manufacturer) and lower (minimal torque approved by the manufacturer) torque curve. These two torque curves are tested in the homologation process. If the engine complies with exhaust emission regulations on these two curves, all torque curves in between the homologated curves are also homologated.
This means that not every power stage of an engine has to be homologated individually, but only test runs with upper and lower curve have to be performed. This reduces the homologation effort considerably.
An example is the test engine (JD 4045). This engine is homologated with the upper curve (up to 730 N m) and lower curve (up to 470 N m) (Figure 4.4). Using this engine, any machine with torque curves between these two can be sold without re-homologating the engine. For example, John Deere sells a 6135R tractor (135 hp rated power) and a 6115R (115 hp rated power) with the same homologated engine.
The present test engine has the middle torque curve shown in Figure 4.4 and is therefore also homologated (because it is between the upper and lower torque curve).

It should be noted that the John Deere machines 6115R and 6135R are not identical machines. They differ not only in different engine control parameters, but also larger cooling packages, stronger gearboxes or a bigger frame. It is therefore not possible to turn a 6115R into a 6135R with a software update. However, if the torque curve of the 6135R is stored on the ECU of the 6115R it has the same performance.

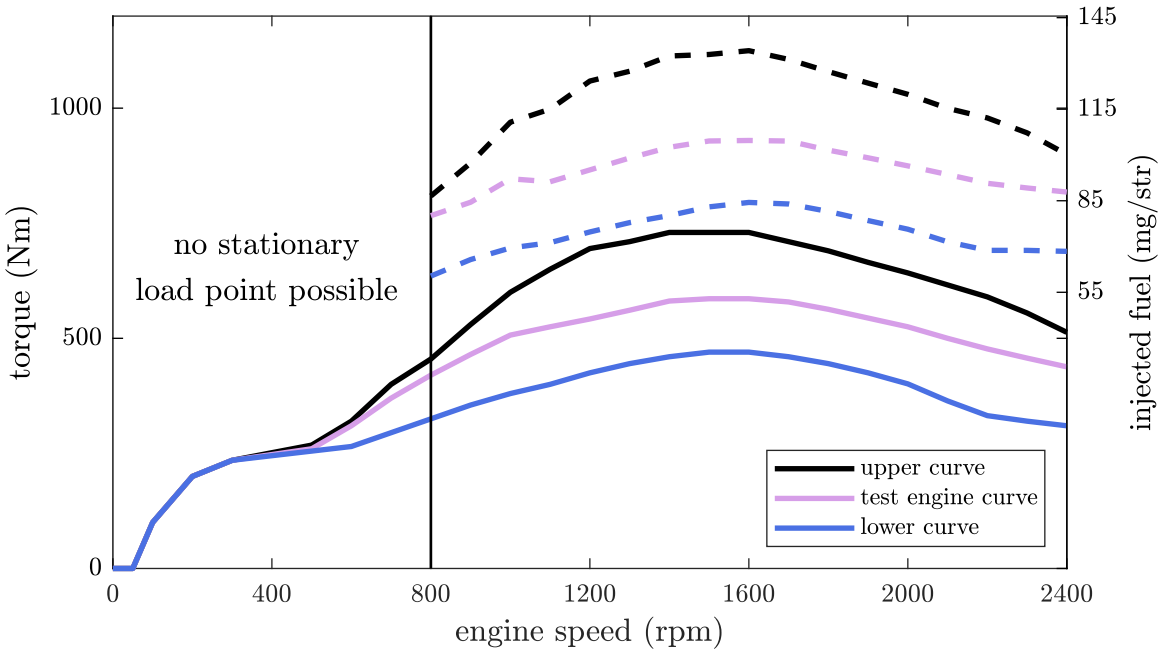

Figure 4.4: Upper and lower test engine curve for homologation

4.6 Engine Control Overview

In this chapter basic engine control structures are shown. The influence of a fundamental change like a different fuel, or tuning should be clarified.
There are many different control modes and operating conditions (cold start, catalyst heating, high altitude, DPF regeneration, no EGR...). For each of these operating conditions there are further conditions and branches such as EGR only in a certain speed range, temperature limits (DEF injection only with sufficiently warm catalyst, less permissible torque because manifold temperatures are too high...) or component limits (maximum turbocharger speed, maximum torque of the transmission...).
In the following the simplified representations are used in “normal” operating mode (all models presented in this thesis take place in this mode). From Figure 4.5 it is obvious that the engine can only be controlled externally by accelerator pedal position α. The ECU has only six manipulable variables which can be used to influence the engine behavior. The air system and the mechanical system can only be controlled passively. For example, closing the exhaust flap u_{eth} in the exhaust tract causes the turbocharger speed to change and thus also the air supplied to the engine changes.

Modern diesel engines use an electronic accelerator pedal. Different control strategies (torque or speed control) can be implemented depending on the application. In the agricultural sector, e.g. power take-off applications often require a constant speed, so an engine speed controller is activated.

Figure 4.6 shows the structure of the speed control. The accelerator pedal position α is converted by a look-up table into a desired speed n_{des}. The difference between desired and measured speed

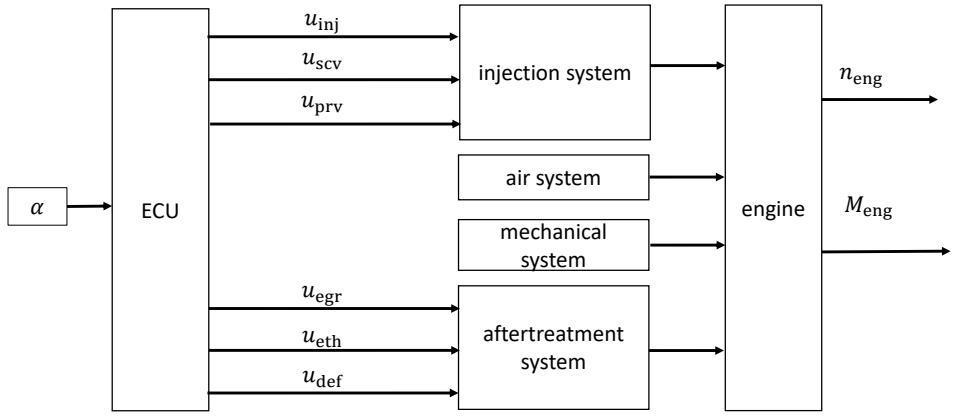

α: throttle position

n_{eng}: engine speed

M_{eng}: generated torque of the engine

u_{inj} : control signal of the injectors

u_{egr} : control signal of the exhaust throttle

u_{scv}: control signal of the suction control valve

u_{eth} : control signal of the exhaust throttle

u_{prv}: control signal of the pressure relief valve

u_{def} : control signal of the diesel exhaust fluid

Figure 4.5: Engine system overview with control signals

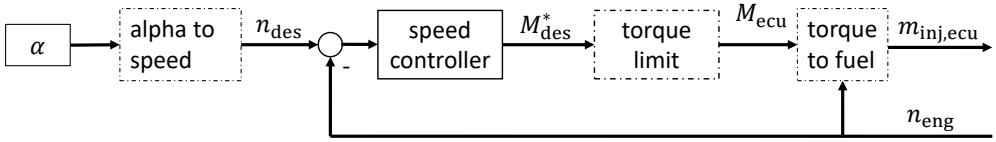

α: throttle position

$m_{\mathrm{inj,ecu}}$: inj. fuel mass with which ECU calculates

n_{eng}: engine speed

M_{ecu}: torque after limit check

n_{des}: desired engine speed

M^*_{des}: torque to reach n_{des} before limit check

Figure 4.6: Engine closed loop speed control

is used as input for the speed controller. Here the torque M^*_{des} is calculated which the engine has to produce to reach the desired speed. If this desired torque does exceed maximum torque curve (section 4.5), the maximum torque is used as the desired torque for further calculations. For example if a torque $M^*_{\mathrm{des}} = 500\,\mathrm{N\,m}$ is needed but the allowed torque is only $400\,\mathrm{N\,m}$ the desired torque is set $M_{\mathrm{des}} = 400\,\mathrm{N\,m}$ (speed does not increase further). This limits the power of the engine.

In another look-up table "torque to fuel" the desired torque is converted to an injection mass $m_{\mathrm{inj,ecu}}$ using the current rpm. Together with n_{eng}, $m_{\mathrm{inj,ecu}}$ is the main input variable used by many other look-up tables and controllers (injection control, EGR control, rail pressure control...).

In Figure 4.7 the injection control is shown in a simplified representation. This test engine can perform up to 5 multiple injections. On the basis of $m_{\mathrm{inj,ecu}}$ and n_{eng} the corresponding injection mass $m_{\mathrm{inj},i}$ and the injection angle $\varphi_{\mathrm{inj,i}}$ are read out in look-up tables for the respective injection.

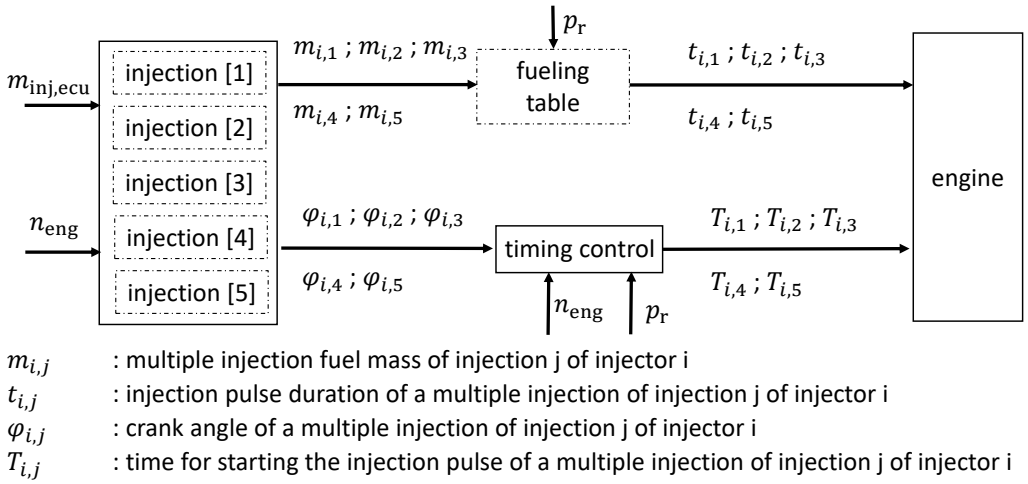

Figure 4.7: Injection control for multiple injections

The necessary injector pulse duration for the corresponding $m_{\mathrm{inj},i}$ is read out in another look-up table "fueling table" together with the rail pressure p_{r}.
The time for the start of the injector pulse T_{sip} is calculated using the speed n_{eng} and look-up tables for the "opening delay". The opening delay depends on the current rail pressure.

4.7 Conclusion of Preparations

In this chapter the used test fuels for this work were defined. Furthermore, the recording principle of crank synchronous measurements was explained. This forms the basis for most of the measurements obtained in this thesis.
Afterwards a strategy was developed to determine single injection masses on the test bench with two fuel weight scales. This strategy is a new approach that works without expensive measurement hardware and still allows the determination of the individual injections.

The section of the ECU controls makes it clear that the engine is mostly controlled based on look-up tables. The most common inputs of all look-up tables on the ECU are the engine speed and the injected fuel mass. Since the injected fuel mass is also based on a look-up table, it is not correct when running with different fuels. Therefore the next chapter will show adjustments of the ECU control.

5 Adapting the Engine Controls to Different Fuels

From the previous chapter it is known that the injected fuel mass is of decisive importance for controlling a diesel engine. As injected fuel is only known for operation with diesel, look-up tables for fuel injection and injector leakage are measured with the fuel mixtures already presented. With these tables the injected fuel mass for known fuel mixtures can be determined with the ECU. Afterwards improved settings of the ECU for the fuels are presented.

5.1 Creation of Injector Maps for Different Fuel-Mixtures

Since actual torque calculation and many further look-up tables of the engine are based on injected fuel mass, knowledge of the injected fuel mass is very important for series engine control. Therefore injector maps are created for all fuel mixtures mentioned in Table 4.1. The procedure described in section 4.4 is used to calculate the actual injected fuel mass of an individual injector. Actual injector temperature is hard to measure at the test engine. However, since LPFS controls the fuel temperature to constant 40 °C, it is assumed that the difference in the injector temperature between the test bench and the real machine is negligible (at same measured low-pressure fuel temperature and load point).

In Figure 5.1 the injector map of diesel and NRO at 40 °C low pressure fuel temperature is shown. The measuring points from Table 4.1 (only constant fuel temperature of 40 °C) were approximated with the Matlab function "lowess". Injected fuel mass in NRO operation (same injector pulse duration and rail pressure) is significantly greater in large parts of the map than in diesel operation. The reason for this is the higher density of rapeseed oil and longer injector closing delays in operation with NRO (proof in section 8.5). This means that the injector needle is open for a longer time in NRO operation during long injector pulse durations in comparison to diesel operation. For better clarity the eight comparison points from Figure 5.1 for NRO and fossil diesel are also shown in Figure 5.2. The comparison points are a part of the measuring points used for the approximation. Differences between fuels regarding injected fuel mass become smaller with smaller injection quantities. With very low injection quantities the injection mass of diesel is even slightly higher than that of NRO. This means that with small injector pulse duration, the higher viscosity of NRO has a greater influence, or the injector needle is not open significantly longer than in diesel operation.
However, the general course of the two fuels is very similar. Since maximum injection mass of the engine in diesel operation is approx. 140 mg, values for higher masses are extrapolated. So the

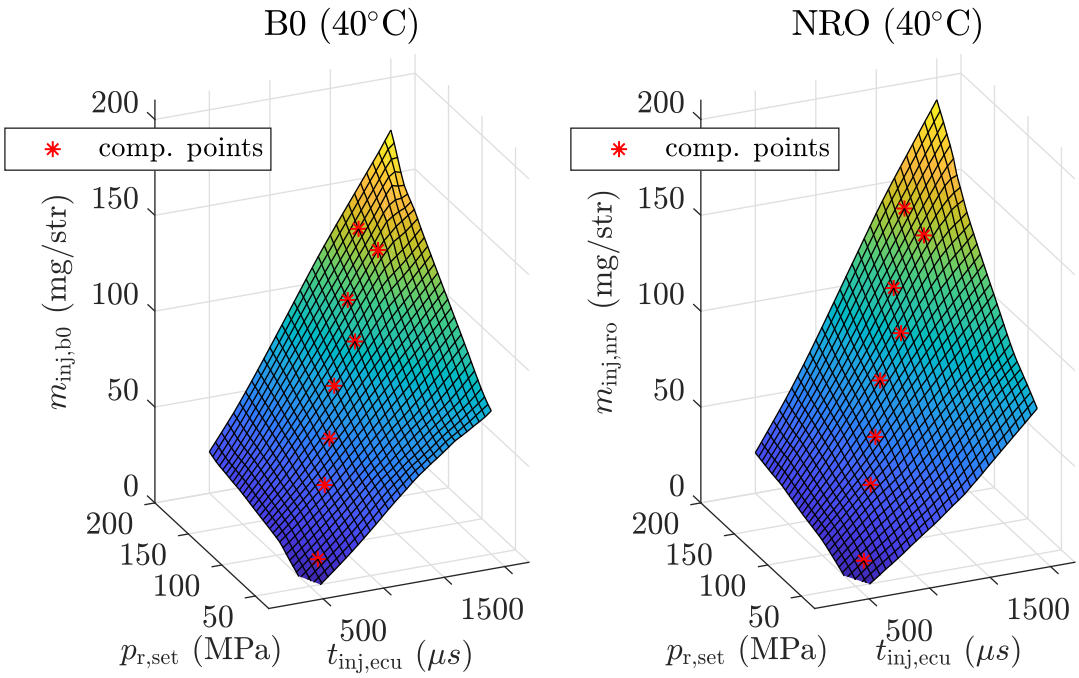

Figure 5.1: Look-up tables for the fuel injection mass for diesel and natural rapeseed oil with comparison points shown in Figure 5.2

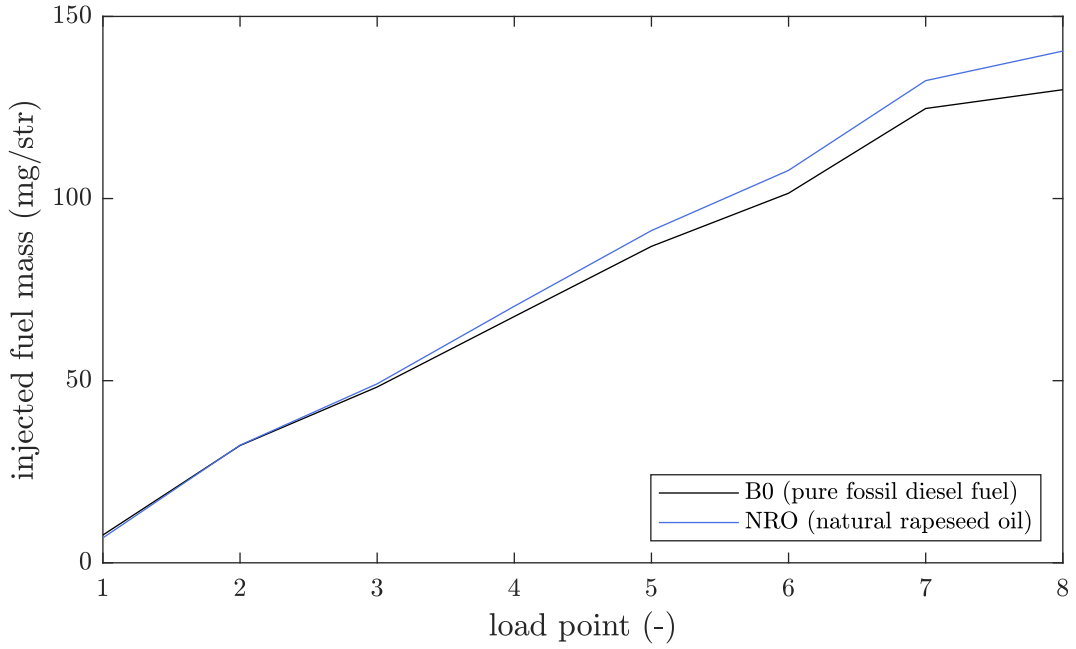

Figure 5.2: Comparsion points for fuel quantity of B0 and NRO from Figure 5.1, $T_{\mathrm{lpfs}} = 40\,^{\circ}\mathrm{C}$

map can also be used for engines with same injectors and larger maximum injection quantities. Measured values in diesel operation are very similar to the injector map stored inside the series ECU (maximum 0.8% deviation). A 3D diagram for a comparison between diesel and RME is shown in section A.3. It only shows little differences.

Injector maps are generated for all 9 fuel mixtures examined (Table 4.1) at 40 °C. For further engine adaptations all 9 measured injector maps are used. An interpolation between the next measured maps is done for fuel mixtures in between the measured values.

5.2 Creation of Injector Leakage Maps for Different Fuel-Mixtures

The injector leakage was measured by a second scale (Figure 3.6). It is assumed that the leakage mass is the same for all injectors if the control of the injectors is identical. Maps for the leakage could be created using the same measuring principle as for the injector maps (comp. Equation 4.5):

$$m_{\mathrm{inj,leak}}(p_{\mathrm{r}}, t_{\mathrm{inj,ecu}}) = \frac{m_{\mathrm{leak,meas}}}{n_{\mathrm{inj}}} \tag{5.1}$$

Here n_{inj} indicates the number of injections and $m_{\mathrm{leak,meas}}$ the measured leakage mass during the measurement period.
Figure 5.3 shows the injector return masses of the three pure fuels from low to higher load points. Although leakage quantities differ slightly (at higher load points leakage quantity for pure NRO tends to be lower than for diesel fuel) it becomes clear that the absolute difference is negligible compared to injected fuel mass. In pure diesel operation an injected fuel mass of 100 mg/str ($t_{\mathrm{inj,ecu}}$=1520 µs and $p_{\mathrm{r,set}}$=150 MPa) results in a leakage mass of 3.33 mg/str. For NRO the leakage quantity is 3.29 mg/str for the same injector pulse duration and rail pressure. The difference is only 0.04 mg/str and is negligible compared to injected fuel mass of 100 mg/str resepective 105.4 mg/str. For this reason the standard diesel look-up table for leakage quantities are used for all fuel mixtures in this research work.

5.3 Basic Engine Adjustments to Different Fuels

If the engine is operated with NRO without ECU adjustments, several effects take place at the same time. An exemplary load point at 1500 rpm and 500 N m is selected in order to clarify the effects. At this load point the EGR is deactivated and there are only two injections per stroke. Since rail pressure is closed loop controlled $p_{\mathrm{r,set}} = p_{\mathrm{r}}$ is assumed. All other control variables are neglected. In this test setup, the test bench controls the torque M to constant 500 N m. The speed control is done by the ECU as described in section 4.6.

In Table 5.1 measurement and control variables are shown for an idealized (real and diesel setpoints are assumed to be the exactly the same) load point at 1500 rpm and 500 N m. The speed control sets the desired fuel mass $m_{\mathrm{inj,ecu}}$ so that $n_{\mathrm{eng}} = 1500$ rpm is reached. The actual torque

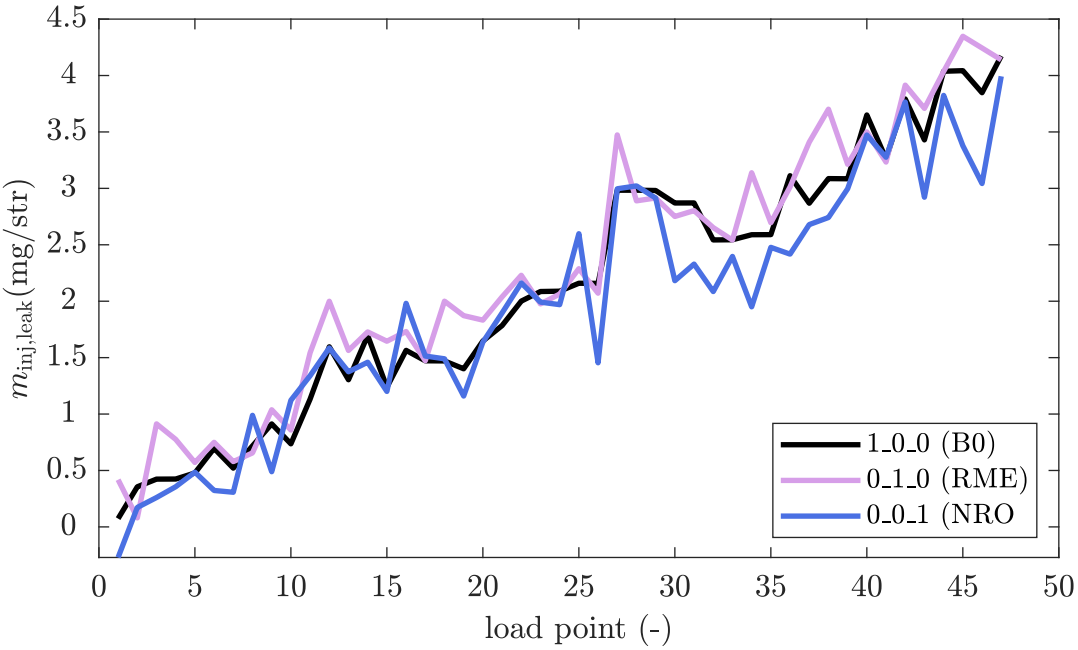

Figure 5.3: Measured leakage quantity comparison between B0, RME and NRO

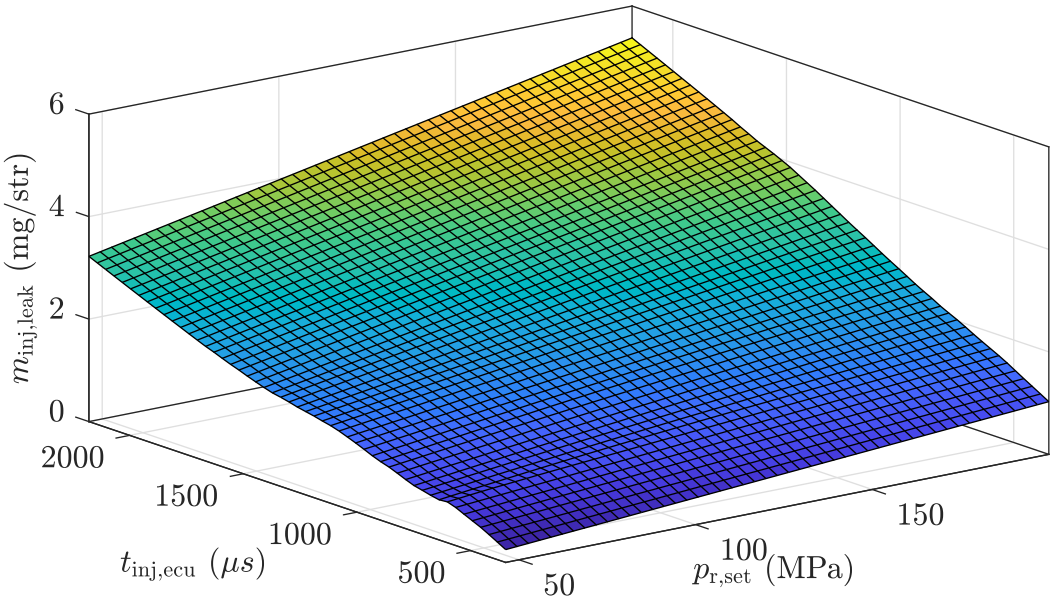

Figure 5.4: Extrapolated injector leakage map for all potential working areas of the injector when using B0

Table 5.1: Measured values and ECU set-points for 1500 rpm and 500 N m

parameter	B0	NRO	unit
M	500	500	N m
M_{ecu}	500	555	N m
m_{inj}	92	109	mg/str
$m_{\mathrm{inj,ecu}}$	92	104	mg/str
$p_{\mathrm{r,set}} = p_{\mathrm{r}}$	172	188	MPa
$m_{\mathrm{inj,1}}$	80	98	mg/str
$m_{\mathrm{inj,ecu,1}}$	80	94	mg/str
$m_{\mathrm{inj,2}}$	12	11	mg/str
$m_{\mathrm{inj,ecu,2}}$	12	15	mg/str

delivered by the engine is not measured in the ECU, but calculated on the basis of $m_{\mathrm{inj,ecu}}$ (section 4.6). The injected fuel mass $m_{\mathrm{inj,ecu}}$ is also not measured, but calculated via a look-up table based on injector pulse duration and rail pressure.

These dependencies on look-up tables is the fundamental problem when changing the fuel. Beside the changed fuel properties which can lead to a changed combustion behavior the following is essential:

Set-points of the ECU are falsified, when changing the fuel.

In diesel operation these look-up tables work with sufficient accuracy. In Table 5.1 the calculated torque M_{ecu} is increased by the speed control in diesel operation until 1500 rpm and 92 mg/str diesel mass is injected. Since the look-up tables are optimized for diesel operation, the desired torque corresponds to the actual torque($M_{\mathrm{ecu}} = M$).

In NRO operation this is not true. The speed control increases the desired torque M_{ecu} until 1500 rpm is reached. These results in a $M_{\mathrm{ecu}} = 555\,\mathrm{N\,m}$ and a calculated injected fuel mass of $m_{\mathrm{inj,ecu}} = 104\,\mathrm{mg/str}$. The real injected fuel mass in NRO operation is $m_{\mathrm{inj}} = 109\,\mathrm{mg/str}$ (at a real torque of $M = 500\,\mathrm{N\,m}$). This means that the values (M_{ecu} and $m_{\mathrm{inj,ecu}}$) do not match the real values (M and m_{real}). The reason for this is that look-up tables are not adapted to NRO.

Influence of falsified calculated values on rail pressure control (compare Figure 3.12):
Since $m_{\mathrm{inj,ecu}}$ is used as an input for further look-up tables, the set-point rail pressure is also falsified. The set-point rail pressure is based on $m_{\mathrm{inj,ecu}} = 104\,\mathrm{mg/str}$ (instead of $m_{\mathrm{inj,ecu}} = 92\,\mathrm{mg/str}$ in diesel operation). This leads to a rail pressure set-point of 188 MPa which is read from the look-up table (for the higher calculated injection mass, rail pressure set-point is also increased). This means that the closed control loop sets a too high rail pressure for the real load point.

Influence of falsified calculated values on injection control (compare Figure 4.7):
The set-point injection quantities for multiple injections $m_{\mathrm{inj,ecu,j}}$ are also based on the desired injection quantity $m_{\mathrm{inj,ecu}}$ (Table 5.1), so set-points differ between NRO and diesel injection. In

diesel operation the total desired injection quantity $m_{\mathrm{inj,ecu}} = 92\,\mathrm{mg/str}$ is divided into two injections ($m_{\mathrm{inj,ecu,1}} = 80\,\mathrm{mg/str}$ and $m_{\mathrm{inj,ecu,2}} = 12\,\mathrm{mg/str}$). However, if the desired fuel is $m_{\mathrm{inj,ecu}} = 104\,\mathrm{mg/str}$, ($m_{\mathrm{inj,ecu,1}} = 94\,\mathrm{mg/str}$ and $m_{\mathrm{inj,ecu,2}} = 11\,\mathrm{mg/str}$) are read from the look-up tables within the injection control. In addition to the changed ratio between first and second injection, the injection times are also simultaneously shifted.

With this simplified example the effect of distorted control variables within the ECU when changing fuel can be illustrated. All set-points are different from standard diesel operation when using NRO (compare desired values in Table 5.1).
Besides the falsified set-points from the look-up tables, engine operation in NRO operation is further falsified because set-points and real injection quantities do not match either. In diesel operation actually $m_{\mathrm{inj}} = 92\,\mathrm{mg/str}$ were injected if the set-point was also $m_{\mathrm{inj,ecu}} = 92\,\mathrm{mg/str}$.
However, in NRO operation the look-up table "fueling table" (compare Figure 4.7) also no longer fits. This means that even with undistorted set-points a mass other than $m_{\mathrm{inj,ecu}}$ could be injected.

The real engine control is much more complex than in this simplified example. EGR, exhaust gas flap, injection timing, pilot control of diesel exhaust fluid dosing, choosing different operating modes or advanced models are adjusted based on M_{ecu} and $m_{\mathrm{inj,ecu}}$.
This means the complete engine control is wrong if the fuel is changed without a new ECU calibration.

If series ECU calibration (fueling table) is used, the percentual difference of the energy introduced into the combustion chamber

$$\eta_{\mathrm{comb}} = \frac{m_{\mathrm{inj,b0}} \cdot H_{\mathrm{u,b0}}}{m_{\mathrm{inj,nro}} \cdot H_{\mathrm{u,nro}}} \tag{5.2}$$

between NRO and B0 based on the control variables p_{r} and $t_{\mathrm{inj,ecu}}$ is shown in Figure 5.5. The difference increase with longer injector pulse duration and thus larger injection quantities. Even if injected NRO fuel mass increases with longer injector pulse duration compared to the diesel mass (Figure 5.1), increased fuel mass cannot compensate the energy difference of the fuels (Figure 5.5).

For a combustion engine the heat introduced into the cylinder is important (not the amount of fuel injected). Mostly the goal of an engine calibration is a desired cylinder pressure curve. Injection quantity and timing are adjusted to achieve the optimum curve.
Since the energy content of the fuels differ, matching the injected fuel mass does not lead to a better calibration of the engine. Since most look-up tables within ECU use injected fuel mass or calculated torque as input, all injection masses of each fuel mixture are converted into a diesel equivalent in the following (instead of a new calibration of all other look-up tables used in the ECU). This means for the calibration of the ECU, that the fueling table is changed to diesel equivalents instead of the injector maps of section 5.1.

$$m_{\mathrm{inj,b0,equi}}(t_{\mathrm{inj,ecu}}, p_{\mathrm{r,ecu}}) = \frac{m_{\mathrm{inj,cfm}}(t_{\mathrm{inj,ecu}}, p_{\mathrm{r,ecu}}) \cdot H_{\mathrm{u,cfm}}}{H_{\mathrm{u,b0}}} \tag{5.3}$$

$m_{\mathrm{inj,cfm}}(t_{\mathrm{inj,ecu}}, p_{\mathrm{r,ecu}})$ is the fuel mass of the currently used fuel mixture. If the mixture ratio of two fuels is known, the injected fuel mass can be determined by the injector maps of section 5.1. $H_{\mathrm{u,cfm}}$ is calculated via interpolation between the fuels.

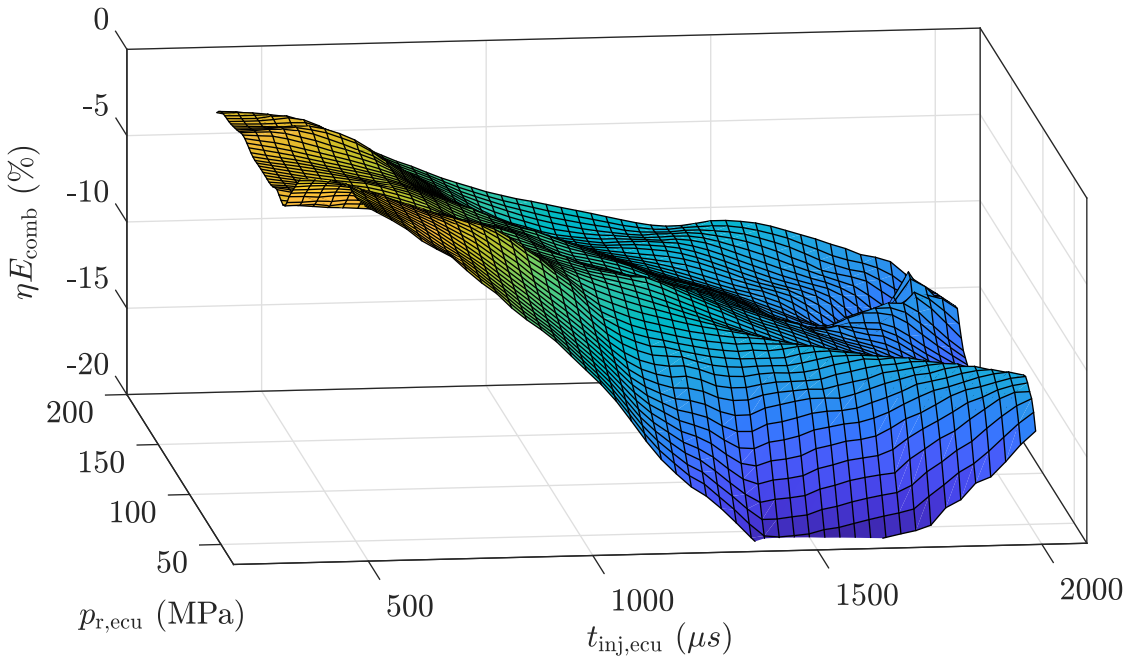

Figure 5.5: Percentual heatvalue difference between pure NRO and B0, calculated via Equation 5.2

For the shown example in Table 5.1 real injected NRO mass is about e.g. 109 mg. Nevertheless a mass of about 92 mg diesel equivalent is used in the injector map. The energy content of 109 mg NRO is approximately the same of 92 mg diesel (subsection 2.1.1).
The conversion to diesel equivalents results in a correct calculated torque within ECU. Furthermore, not all look-up tables which use diesel injection mass as an input have to be changed. So look-up tables (EGR, injection times, rail pressures, number of injections...) are correctly applied regarding injected energy.
However, it is not guaranteed that these maps are optimal for the new fuel. There are still deviations from the originally planned combustion process (cylinder pressure curve), due to deviating combustion characteristics, delayed injector opening times and changed injector pulse duration when using another fuel. For example, to inject 109 mg NRO, the injector must be energized longer as for 92 mg diesel. This results in a shifted center of injection.
However, these deviations are much smaller than the power adjustments of the past (maximum torque curve was shifted so same power was reached). Another advantage of this adjustment is that different fuels only have to be measured once for same injector series. With injector maps for all fuels, rated engine power for each application can be adjusted. For example, there are John Deere 6 cylinder engines 6068 with same injectors as 4 cylinder engines of 4045 series (current test engine). If the injection map is adapted to diesel equivalents in the shown way, all engines with the same injectors should work similar to diesel operation.

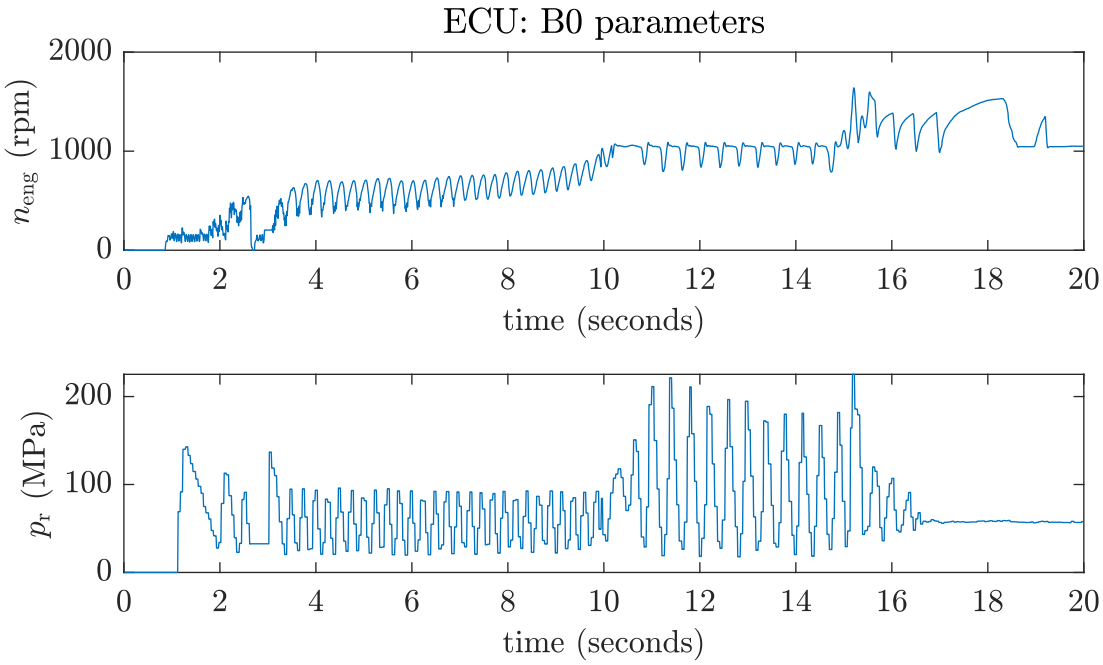

Figure 5.6: Cold start with pure NRO with diesel parameters at $T_{\mathrm{fuel}} = 0\,°\mathrm{C}$

5.4 Improved Controls for Rapeseed Oil Operation

While the engine operation with RME works fine with the adjustments from section 5.3, there are two main problems when running with NRO. These include in particular the cold start and DPF regeneration. To enable practical use of the engine, these are optimized in the following. These are empirical improvements, so that the minimum requirements for engine operation are given.

5.4.1 Cold Start Optimization

Starting the engine at temperatures below 10 °C with series diesel parameters is only possible with great difficulty in NRO operation. Cold start parameters which improve the engine start at cold temperatures were found through empirical tests. These parameters are most likely not optimal parameters, but they allow an engine start up to 0 °C. Tests were carried out in a cold chamber (identical engine as test engine).
In Figure 5.6 the engine start with NRO and diesel (series) parameters at a cooling water temperature of 0 °C are shown. The engine runs after approx. 20 seconds at constant idle. This is unacceptable from a technical (starter motor gets hot, battery discharges, high emissions...) and customer's point of view.
In the lower part of Figure 5.6 one of the problems is shown. The rail pressure curve fluctuates very much and exceeds maximum allowable pressures in the rail.

There are several reasons for this. One is that the rail pressure control is not adapted to the fuel. As the rail pressure fluctuates strongly, a large difference between optimum control parameters

of the PID controller for NRO and diesel operation can be assumed. As maximum pressures are exceeded, the PRV could open which causes further control problems.
Another reason for strong oscillations in the rail are fluctuating speeds when engine is started. With fluctuating engine speed, fuel is drawn into the high pressure chambers with an fluctuating velocity. Since the SCV reacts slow (control is very slow compared to feed-forward control), a wrong rail pressure is generated.

The biggest problem is that individual injections do not take place. Due to cold temperatures and greatly changed fuel properties (high viscosity of NRO), the opening delay can be delayed to such an extent injectors no longer open at all. In the past, expensive injector heaters were installed for this reason [28]. If an injection is not carried out, rail pressures increase more strongly, since the SCV reacts too slow in relation to the injection. As a result, fuel continues to be pressed into the rail even no fuel has left the rail. This also leads to an oscillation of the control loop.
Speed fluctuations are mainly due to two effects. On one hand engine speed drops if injectors do not open (no torque is generated inside combustion chamber). On the other hand the fuel-air mixture does not ignite in the cylinder. This means that fuel is injected but the NRO-air mixture does not burn.
Adjusted parameters lead to a clearly improved starting behavior and rail pressure curve (Figure 5.7). The engine runs after approx. 4 seconds under its own power and from approx. 6 seconds the idle speed is reached. This is an enormous improvement compared to the diesel parameters, where only after about 20 seconds the idle speed is reached. This was achieved by an increased target rail pressure from approx. 50 to 90 MPa and an increased desired fuel by 50 % (only when starting the engine). Furthermore multi injections are deactivated so only one main injection is active. The deactivation of multi injections leads to a longer injector pulse duration, so injectors always open (even with probably heavy enlarged opening delays). The exact amount of injected fuel is unknown but the increased set-point injection quantities together with a higher rail pressure result in a much better starting behavior.

Even if control parameters and feed-forward control of the SCV are not optimal, no maximum permissible pressures are exceeded. However, it is also clear that many further investigations are necessary for a fuel-optimized rail pressure control and improved starting behavior. Since these measures depend on fuel and additionally on fuel temperature, the controller structure currently used in series ECU cannot be used.
However, the enormous improvement through relatively simple changes to the ECU control shows the potential that exists in the starting behaviour of NRO engines.

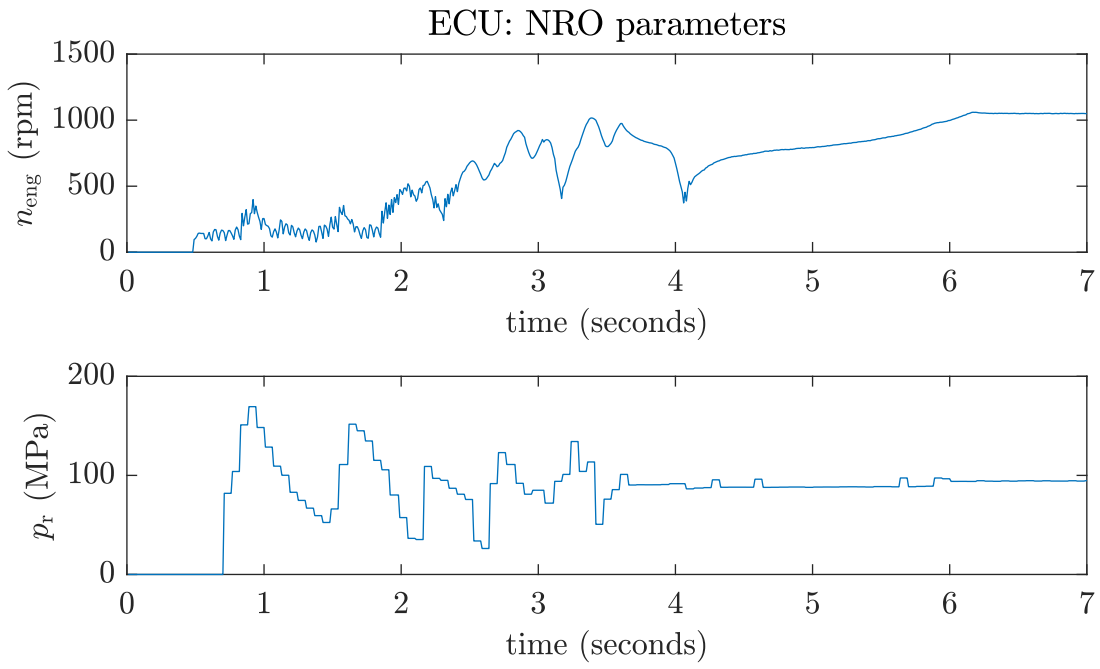

Figure 5.7: Cold start with pure NRO with adjusted parameters at $T_{\mathrm{fuel}} = 0\,^{\circ}\mathrm{C}$

5.4.2 DPF Regeneration Strategy

According to the state of art, DPF does not need to be regenerated when operated with NRO [31]. Increased passive regeneration of the DPF in operation with NRO keeps soot load at a constant level. However, systems with an SCR system require regular increases in exhaust temperatures to remove deposits of crystallized diesel exhaust fluid or sulfur [128][73][114][32].
Furthermore a multi-fuel approach is considered in this research work. In the worst case, the engine is operated with fossil diesel fuel until the load limit of the DPF is reached. Before the DPF regeneration in diesel operation is started, fuel is changed to NRO. If that happens, it cannot be excluded that the maximum load of the DPF is exceeded. A DPF regeneration (sharp increase in exhaust gas temperature) while using NRO and an internal post-injection system is problematic according to the current state of art [31].
The reason for this is the high fuel entry into engine oil. Similar to subsection 5.4.1, measures are presented which make engine operation possible, but should be further optimized.
The delta pressure sensor at the DPF allows to model loading condition of the DPF well (available in series ECU). If loading condition approaches a critical limit, e.g. a display message could prompt the driver to fill up with diesel fuel during next refueling.
Another possibility is a stationary regeneration with NRO. The ECU has a standard feature with which the DPF can be safely regenerated or burnt free. For this purpose the machine has to be parked and the engine is operated in high idle. In practical operation this condition should not occur, since the machine cannot be used during this time. However, if a clogged DPF occurs due to a very unfavorable usage profile of the machine (exhaust gas temperatures too cold), this procedure ensures the DPF can be regenerated. Here the engine is operated in high idle (1800 rpm).

Table 5.2: Series and improved injection parameters for stationary DPF regeneration

parameter	series	improved
number of injections	1	3
injection timing	−180 °CA	−130 °CA,−150 °CA, −180 °CA
rail pressure	60 MPa	150 MPa
engine oil entry	19 %	5.5 %

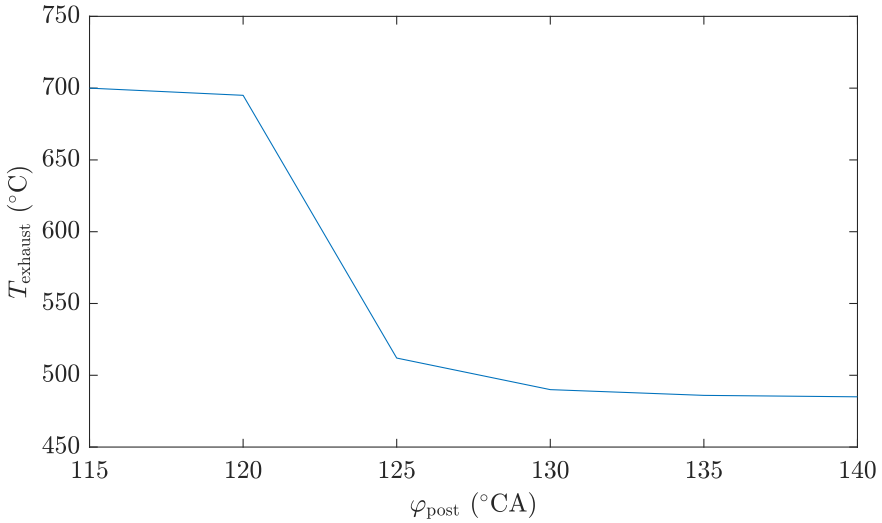

Figure 5.8: Exhaust temperature depending on post injection angle with one post injection

In contrast to series production, injection parameters are adjusted in this section. Parameters shown in Table 5.2 are empirically found. Similar to coldstart parameters these settings are not necessarily optimal for stationary DPF regenerations (sharp temperature increase of the exhaust aftertreament). The basic idea behind adjusting injection parameters is improving vaporization of NRO in the cylinder without burning the fuel. In the optimum case the entire post-injection quantity reaches the DOC in vapor form and is oxidized there.
A higher rail pressure leads to a better atomization of the fuel and thus to a better evaporation (larger surface). For this reason, rail pressure is increased gradually. However, since a higher rail pressure also leads to a deeper penetration depth of the fuel jet, rail pressure cannot be increased at will (danger of fuel hitting cylinder walls increase) [40].
Since the penetration depth of the jet also depends on the air density in the cylinder and at the same time higher temperatures lead to a better evaporation, the injection timing is adjusted as far as possible to an early injection (so that it is as warm as possible in the cylinder, but the fuel does not start to burn).

For this reason, a preliminary examination was carried out, in which the post-injection angle is moved in 5 °CA steps. This is done with a single post-injection of 20 mg.
The measurements (Figure 5.8) show an injection angle of −120 °BTDC to lead to ignition of

Table 5.3: Oil dilution measurements with post injections and pure NRO

$p_{r,set}$ (MPa)	$m_{inj,post,1}$ @ −180 °CA (mg/str)	$m_{inj,post,2}$ @ −150 °CA (mg/str)	$m_{inj,post,3}$ @ −130 °CA (mg/str)	$\eta_{f,oil}$ (%)	$m_{f,oil}$ (mg)	T_{exh} °C
100	19.94	0	0	20.6	3503	421
150	17.89	0	0	14.2	2234	414
200	17.74	0	0	11.1	1686	425
100	10.96	10	0	15.1	2401	481
100	11.21	0	10	14.4	2271	489
100	6.98	5	10	13.1	2035	528
150	9.64	10	0	8.8	1303	492
150	9.03	0	10	7.1	1032	484
150	4.36	5	10	5.5	786	489
200	12.42	10	0	8.9	1319	559
200	12.22	0	10	7.6	1110	568
200	8.12	5	10	6.3	908	597

NRO in the cylinder (increasing exhaust temperatures). Since this should be avoided (increased temperature means fuel is burned in the cylinder), the earliest possible injection angle is set to −130 °BTDC.

A further reduction of penetration depth is possible by reducing injected fuel mass [40]. For this reason a large post-injection quantity is divided into three smaller injection quantities. In Table 5.3 the empirical approach is shown. The injection at −180 °BTDC is the only injection available in series operation. This is controlled by the ECU, so desired DOC outlet temperature is achieved (e.g. in normal DPF regeneration the temperature should be 600 °C). The DOC outlet temperature control stays in its original state (injection quantity of −180 °BTDC is determined via DOC outlet temperature control). The other post-injections were set as set-point values in the ECU. A fixed diesel equivalent was specified as set-point of the post injection quantity.

It becomes clear that the fuel entry into the engine oil can be reduced significantly by these relatively simple adjustments. The best result was achieved with 150 MPa and 3 post injections. At higher rail pressures, fuel entering engine oil increases again. The exact reason for this cannot be determined. On the one hand, an increased rail pressure due to increased outlet velocity could lead to a strong impact on the cylinder wall. On the other hand, more mass has to be injected in total, since a larger part of the fuel is oxidized in the manifold (this can be proven by increased manifold temperatures).
Since the rail pressure applies to all injections, further effects can occur. A changed rail pressure leads to a deviating combustion behavior, so different temperatures are present in the cylinder when the exhaust valve opens. Evaporation effects can also cause the manifold temperature to drop during post-injection (fuel becomes vaporous but does not ignite). A superposition of many effects is likely.

Since the measurements take a long time, only a limited number of oil measurements were carried out. In total the engine oil dilution between series and improved parameters could be reduced by approx. 75% (before optimization approx. 21% fuel of the post injection enters the engine oil to approx. 6% after optimization) in operation with NRO. Since stationary regenerations are only conditionally suitable for practical use, this variant should only be seen as a backup solution. However, if the aftertreatment system has to be burned free, this could be done in NRO operation with a tolerable contribution of fuel to the engine oil.
The adapted parameters show promising approaches for the regeneration of the exhaust aftertreatment system with NRO. In order to develop a multi fuel capable series production engine in the future, regeneration with NRO should be investigated in further scientific work. The same applies to regenerations of the other fuel mixtures. Since the measurements take a long time (warm up, oil sample before, 30 minutes operation with post injections, cold run, oil sample...), a simulative approach should be considered. However, the empirical tests carried out in this work show a great potential for a further reduction of the engine oil input. This applies not only to operation with NRO (or mixtures), but also to pure diesel operation. It is also conceivable that the fuel input into the engine oil can be reduced in pure diesel operation with the adjustments presented.
In the long term, it should also be possible to raise the temperature in the aftertreatment system with the test fuels used in this work, without having to stop the machine (and do a stationary regeneration).

5.5 Conclusion of Adapting the Engine to Different Fuels

In this chapter, fuel injector maps were created for the nine defined test fuels. Afterwards the measured injector maps were converted into equivalent diesel masses within the ECU. Even if this does not correspond to the optimum calibration of the engine for the respective fuel, this adjustment is significantly better than the performance adjustments of the past.

The adjustments result in a performance similar to diesel operation. Since the injected mass is converted to diesel equivalents, transient load points are also correctly adjusted regarding introduced energy into the cylinder. This prevents e.g. very low air ratio values for gas surges.
Theoretically, the engine would have to be re-calibrated for each fuel, i.e. all look-up tables would have to be adapted. However, this solution is not practicable because it requires a huge development effort.
The measured injector maps could also be used for engine simulations in the future, so that not all other maps have to be measured. However, for sufficiently good simulations further work is necessary. In particular, the combustion properties of the fuels (ignition delay, combustion speed, injector delay...) must be known for a sufficiently good simulation.
Two typical problems in operations with NRO were significantly improved. These include an enormous improvement of the cold start and a strategy for the regeneration of the DPF. For the DPF regeneration further improvements are necessary, because the shown solution can not be used in practical operation of the engine. However, the improvements ensure that the engine can basically be operated with all fuels (mixtures).

6 On-Board Fuel Type Detection System

A model-based onboard fuel detection system is considered. For this purpose, a detailed literature research on fuel detection with series sensors is carried out. Furthermore, important characteristics of the test engine for fuel detection are shown. Subsequently, models for fuel detection are presented. The models created are always shown exemplary with B0-NRO mixtures. For B0-RME mixtures the procedure is similar, but with adapted fuel parameters.

6.1 State of the Art of Fuel Detection in Diesel engines

Previous chapters show some major differences between the investigated fuels. Only if the fuel in an engine is known, look-up tables for control can be adapted to the respective fuel properties. For this reason diesel fuel detection (fuels which are not suitable for diesel engines are not considered) has been subject of research for years [126] [132] [11]. Often external sensors (special fuel sensors which are not standard for a diesel engine) have been investigated for this purpose. These are in direct contact with fuel and measure various fuel properties like density, viscosity or electrical conductivity to classify the fuel [27]. Since external sensors increase costs and possibly reduce the reliability of machines, literature research will be limited to approaches using series sensors which are mounted on diesel engines as standard for fuel detection.

Wang et al. [126] used a neuronal network to evaluate the fuel used in the engine. The neural network based on sensor data like engine speed, coolant temperature, pedal position, in-cylinder pressure, ignition delay, indicated mean effective pressure, exhaust air/fuel ratio, smoke sensor signal, exhaust gas temperatures, gas pressures and ECU set-point values was introduced. The classifier was able to distinguish between American ultra low sulfur diesel (ULSD), European diesel according to EN 590 and biodiesel. Disadvantageous of this method is that lots of training data is required for each specific engine variant. Another problem with this method is that it requires a large number of sensors that are not state of the art in agricultural engines. This includes in particular the in-cylinder pressure sensor.

Zhao and Wang [132] determine a ratio of B0-biodiesel mixture based on measured fuel consumption and cylinder pressure, which leads to very accurate results. In addition, they provide another possibility to determine the biodiesel content. Here, different air mass requirements of the fuels are used to determine the mixture ratio via oxygen content in the exhaust gas. For this purpose the oxygen content in the exhaust gas, intake air mass and fuel mass flow is measured. The advantage of this method is the used physical model. Thus, this type of fuel determination can be implemented independently of the engine type.

Beatrice et al. [11] used standard installed cylinder pressure sensors to detect a fuel mixture of RME and diesel. Fuel detection has proven very reliable results. In addition, the closed loop control can be used to control the combustion process in the cylinder independently of different fuels. There is a lot of further literature on closed loop in cylinder pressure control [78][44][59][23][45]. However, in-cylinder pressure sensors are not used in agricultural engines so far, as requirements regarding cost and durability are not fulfilled yet. Engine control and fuel detection via cylinder pressure sensors seem to give the best results of all discussed approaches. When cylinder pressure sensors are installed in series production in the future they shall be used to detect different fuels or other faults due to their considerable advantages (even with fossil diesel fuel).

Conclusion for Fuel Detection with Series Sensors in Literature

Fuel detection with series sensors worked very well in the reviewed literature in some cases. Here procedures can be roughly divided into two areas. On the one hand neural networks are used, which can classify fuels based on series sensors. This comes to quite promising results. Disadvantageous of this method is that neuronal networks have to be trained by a multitude of measurements, which have to be retrained if there are changes in the engine.
On the other hand very good results have been achieved with an internal cylinder pressure measurement in literature. However, since these sensors are currently not in series production for agricultural machinery, fuel detection via the oxygen content in the exhaust gas is evaluated as the most promising approach. With an air mass meter and fuel consumption measurement good detection results have been achieved. These two sensors are not present in the test engine. The air mass flow is currently calculated using a semi physical model. However, the injected fuel mass is only determined via look-up tables.
This leads to the following conflict: To determine the fuel via oxygen content in the exhaust gas, injected fuel mass is needed. Injected fuel mass can only be determined if the fuel or corresponding injector maps are known.
A fuel detection based on oxygen content offers the advantage of being independent of different fuels (in contrast to neural networks that would probably have to be retrained with every new fuel). Thus, all fuels can be detected which differ in oxygen content from fossil diesel. This means that not only biogenic fuels of the first generation such as NRO, but also synthetic fuels such as oxymethylenether (OME) or diemethylether (DME) apply for a oxygen based detection. This method was therefore selected as the most promising one.

6.2 Relevant Characteristics of the Test Engine

For the following fuel detection model the NO_X sensor and the Air-Mass Model of the series test engine are required. For this reason they will be introduced briefly.

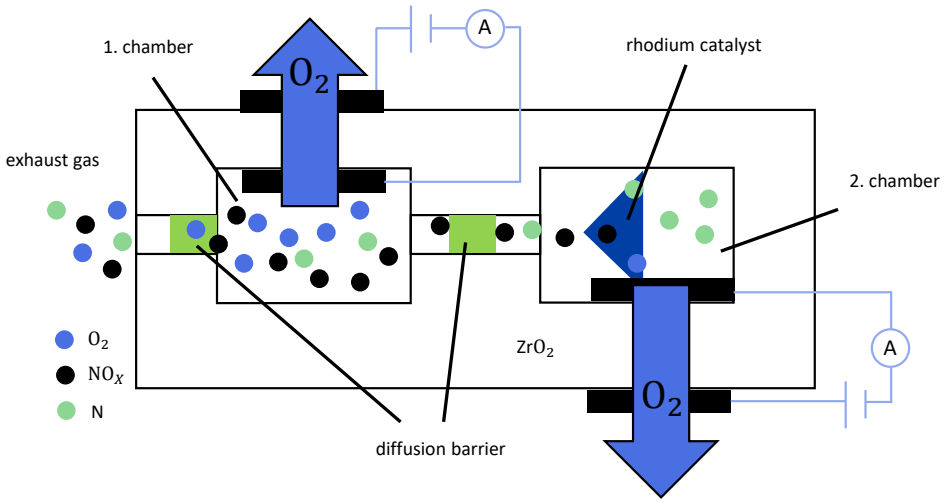

Figure 6.1: Double-chamber NO_X sensor principle. Graphic created based on [56] and [96]

6.2.1 NO_X-Sensor

Almost all modern diesel engines with SCR systems have at least one NO_X sensor installed. This is required to control the injected urea mass. Often two sensors are installed in order to detect faults of the SCR system and to enable a better feed-forward control of the urea dosage. One sensor type frequently used in practice is the so-called double chamber sensor [14]. Since only the measured oxygen value in the exhaust gas is required in the following sections, Figure 6.1 is shown in simplified form. The exact chemical processes and materials used are not necessary for understanding the next sections. However, more detailed explanations can be found under [108] and [95].

The porous layers of the sensor consist of ZrO_2, which has the ability to transmit oxygen ions at temperatures above 700 °C. The exhaust gas enters the first chamber. Here the oxygen is reduced by applying a negative voltage and pumped out of the first chamber electrochemically through the porous layer. The oxygen concentration is proportional to the required current and is thus measured. [108]

At the same time NO_2 is reduced to NO in the first chamber. Since the proportion of nitrogen oxides is much smaller than the proportion of oxygen in the exhaust gas, the influence on the oxygen measurement can be neglected. The NO enters a second chamber where it is split into N_2 and O_2 in the presence of a rhodium catalyst.

$$2NO- > N_2 + O_2 \tag{6.1}$$

Like in the first chamber oxygen is divided into ions by applying a voltage and is then extracted through the porous ZrO_2 layer. Since all the oxygen that is extracted originates from NO, the nitrogen oxide content in the exhaust gas can be determined.

The measurement accuracy of the NO_X, respectively the O_2 sensor is specified by the manufacturer for different air conditions. For example, percentual deviation for a lambda value of 1 according to the 1-sigma value of the Gaussian normal distribution is $\sigma_{O_2} = \pm 0.25\%$ [57]. This means that about 68.27% of sensors will output a value between 0.9975 and 1.0025 at an air ratio of 1. The sensor outputs a value in mole percent.

6.2.2 Air-Mass Model

Since air mass flow is especially important for a fuel detection based on the oxygen content in the exhaust gas, the basic Air-Mass Model is explained briefly. A more detailed description of the model is available in Isermann [61]. It is a semi-physical model in which the volumetric efficiency η_V of the combustion engine has to be stored in the ECU. This means η_V has to be measured with air mass measuring devices in preliminary test bench investigations.
If the engine is modeled in an idealized way, the theoretical air flow through the engine can be described by

$$\dot{m}_{\text{air,th}} = \frac{1}{2} n_{\text{eng}} V_D \frac{p_2}{R_s T_2}, \tag{6.2}$$

where V_D is the engine displacement volume, R_s is the specific gas constant, p_2 is the pressure and T_2 is the temperature in the intake area. Since real flow rates are lower due to throttling effects and transient flow conditions, $\dot{m}_{\text{air,th}}$ is multiplied by the volumetric efficiency factor

$$\eta_V = \frac{\dot{m}_{\text{air,real}}}{\dot{m}_{\text{air,th}}} = \frac{\dot{m}_{\text{air,real}}}{\frac{1}{2} n_{\text{eng}} V_D \frac{p_2}{R_s T_2}}. \tag{6.3}$$

The air mass flow

$$\dot{m}_{\text{air,real}} = \eta_V \cdot V_D \frac{p_2}{R_s T_2} \cdot \frac{1}{2} n_{\text{eng}} \tag{6.4}$$

can be calculated. For the air mass during a combustion cycle

$$m_{\text{air,sim}} = \eta_V \cdot V_D \frac{p_2}{R_s T_2} \tag{6.5}$$

applies.
The model used in series ECU provides good results compared to the air flow mass meter, which is available on the test bench.

Figure 6.2 shows a good agreement between the measured and modeled values of the ECU. On average, the model underestimates the measured air mass flow by about 0.4 %. This is within the measuring accuracy of the air mass sensor used on the test bench.

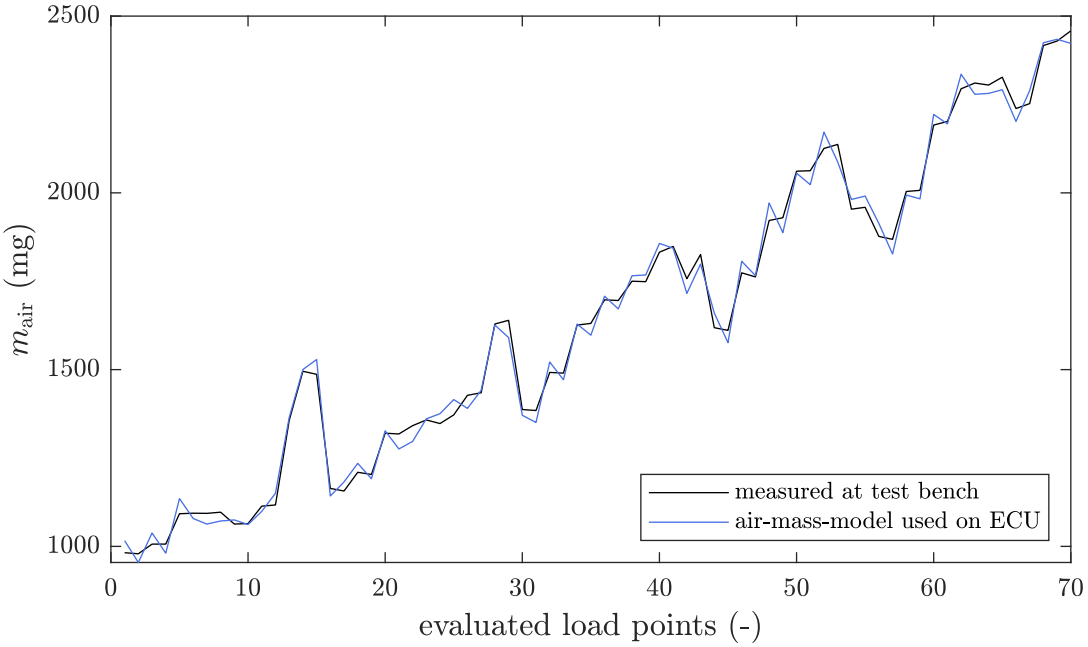

Figure 6.2: Simulated in comparison to measured air mass at test bench for different load points

6.3 Oxygen-Mixture Model (OM Model)

Basis for a fuel detection with O_2 sensors is a model of the complete combustion. It is assumed that all injected fuel is completely oxidized to CO_2 and H_2O and fuel consists only of H, C and O. For a complete combustion holds [102]:

$$C_xH_y + z\ O_2 = x\ CO_2 + 0.5y\ H_2O + (z - x - 0.25y)\ O_2 \tag{6.6}$$

In this chapter the model is carried out using a B0-NRO mixture as an example. For B0-RME blends (or other fuels with an oxygen content) procedure is analogously. If the same mass of NRO instead of diesel is injected into the cylinder, the proportion of oxygen in exhaust gas increases (oxygen demand of NRO is lower). This is due to oxygen dissolved in the fuel, which cannot be oxidized by definition. The idea of the model is to determine the mixture ratio between B0 and NRO based on injected fuel mass, air mass flow and measured oxygen content.
There are two oxygen (NO_X) sensors in the exhaust system. The first is located upstream of the DOC and the second downstream of the SCR system (Figure 3.3). These also measure the O_2 content as described in subsection 6.2.1.

Since injector maps are only accurate for 40 °C LPFS temperature and O_2 sensors require an increased operating temperature, the presented detection model is limited to a warm engine. Furthermore, O_2 sensors react relatively slowly to rapidly changing combustion conditions due to their position in the exhaust system. Therefore, detection is only carried out at stationary load points (section 4.3). Fuel detection is restarted after each tank refueling. A refueling process can

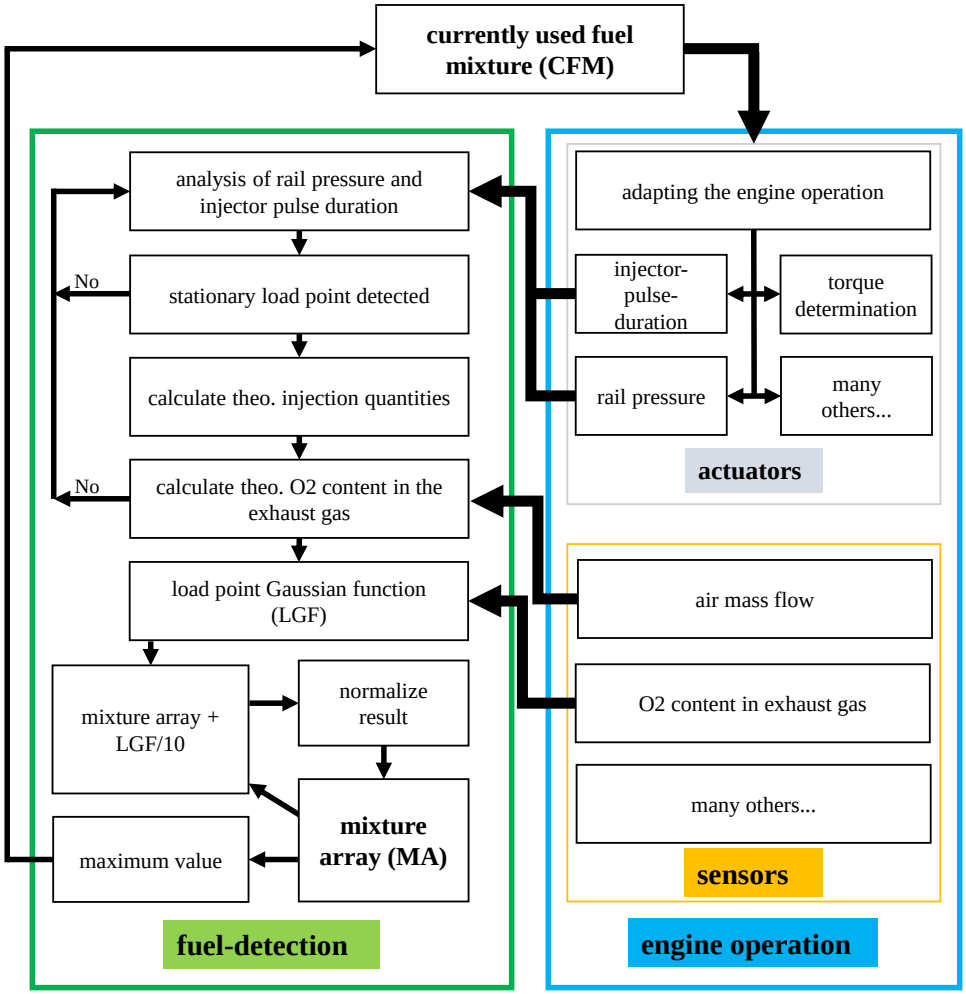

Figure 6.3: Flow chart of the Oxygen-Mixture Model

be detected by a sudden rise of the series production tank level sensor.
When the detection model is started values of rail pressure, injector pulse duration, air mass flow and both O_2 sensors are stored in a ring buffer. If a stationary load point is detected, values are averaged and calculation begins. Since averaging values is a low-pass filter, measurement noise is filtered out. In practical operation both sensors are evaluated. Since the modeling process is identical for both, only the first (DOC inlet) oxygen sensor is used to describe the model in this section.

6.3.1 Theoretical O_2 Content in the Exhaust

Basic procedure of the detection algorithm is shown in Figure 6.3. After a stationary load point is detected injected fuel masses are calculated and stored in 1% steps for all mixture ratios between 0 and 100% diesel using stored injector maps. With the averaged air mass flow rate and the respective injection quantity, a theoretical oxygen content in the exhaust gas is calculated for all mixture ratios between 0 and 100% diesel. This oxygen content is a theoretical value which would

be present in the exhaust gas if the respective fuel mixture would be in the system. If pure NRO is in the tank, a higher fuel mass is injected than in diesel operation at many load points (with the same injector pulse duration and the same rail pressure). This should lead to a lower oxygen content in the exhaust gas. However, since the air requirement of NRO is also much lower, the oxygen content in the exhaust gas can also be higher. For this reason, a theoretical oxygen content is calculated for all mixing ratios. This ensures that each measured oxygen ratio in the exhaust gas can be clearly assigned to a fuel.

The NO_X or O_2 sensor installed in series engines measures the concentration in ppm. Since air is assumed to be a mixture of nitrogen, oxygen and argon, as well as the products H_2O and CO_2 from a complete combustion, oxygen content in the exhaust can be calculated via

$$O_{2,\mathrm{th}} = \frac{n_{O_2,\mathrm{exh}}}{n_{O_2,\mathrm{exh}} + n_{N_2,\mathrm{air}} + n_{\mathrm{Ar,air}} + n_{CO_2} + n_{H_2O}}. \tag{6.7}$$

It is assumed that argon and nitrogen do not participate in the combustion process. Since oxygen is consumed by the oxidation of H and C, the number of oxygen molecules in the exhaust gas is

$$n_{O_2,\mathrm{exh}} = n_{O_2,\mathrm{air}} - n_{CO_2} - 0.5 \cdot n_{H_2O} + n_{O_2,\mathrm{fuel}}. \tag{6.8}$$

Equation 6.8 inserted in Equation 6.7 results in:

$$O_{2,\mathrm{th}} = \frac{n_{O_2,\mathrm{air}} - n_{CO_2} - 0.5 \cdot n_{H_2O} + n_{O_2,\mathrm{fuel}}}{n_{O_2,\mathrm{air}} + 0.5 \cdot n_{H_2O} + n_{O_2,\mathrm{fuel}} + n_{N_2,\mathrm{air}} + n_{\mathrm{Ar,air}}} \tag{6.9}$$

The number of atoms or molecules of the respective substance can be calculated using the molar masses M_s:

$$n_{O_2,\mathrm{air}} = \frac{m_{O_2,\mathrm{air}}}{2M_O} \tag{6.10}$$

$$n_{N_2,\mathrm{air}} = \frac{m_{N_2,\mathrm{air}}}{2M_N} \tag{6.11}$$

$$n_{\mathrm{Ar,air}} = \frac{m_{\mathrm{Ar,air}}}{M_{\mathrm{Ar}}} \tag{6.12}$$

$m_{O_2,\mathrm{air}}$ can be determined via the air composition and the air mass in a cylinder $m_{\mathrm{air,sim}}$ (Equation 6.5).

$$m_{O_2,\mathrm{air}} = m_{\mathrm{air,sim}} \cdot w_{O_2,\mathrm{air}} \tag{6.13}$$

The air composition is assumed to be constant and $w_{O_2,\mathrm{air}}$ is the mass fraction of oxygen in the air (Table 6.1). For $m_{N_2,\mathrm{air}}$ and $m_{\mathrm{Ar,air}}$ the calculation is analogous.

The number of molecules of combustion products can be derived from the equation of complete combustion (Equation 6.6):

$$n_{CO_2} = n_{C,\mathrm{fuel}} \tag{6.14}$$

Table 6.1: Air composition in mass %

$w_{N_2,air}$ (%)	$w_{O_2,air}$ (%)	$w_{Ar_{air}}$ (%)
75.2	23.1	1.7

$$n_{H_2O} = n_{H_2,fuel} \tag{6.15}$$

The fuel composition ($w_{C,b0}$,$w_{H_2,b0}$ etc.) can be found in Table 2.1. Since mixing ratios are given in mass percent, proportions like $w_{C,fuel}$ can be calculated using the following formula:

$$w_{C,fuel} = w_{b0} \cdot w_{C,b0} + (1 - w_{b0}) \cdot w_{C,nro} \tag{6.16}$$

The shares of C, H_2 and O_2 are calculated:

$$n_{C,fuel} = \frac{w_{C,fuel}}{M_C} \cdot m_{fuel} \tag{6.17}$$

$$n_{H_2,fuel} = \frac{w_{H_2,fuel}}{2M_H} \cdot m_{fuel} \tag{6.18}$$

$$n_{O_2,fuel} = \frac{w_{O_2,fuel}}{2M_O} \cdot m_{fuel} \tag{6.19}$$

If all equations are inserted in Equation 6.9 , the result is

$$O_{2,th} = \frac{\frac{w_{O_2,air}}{2M_O} \cdot m_{air} - \frac{w_{C,fuel}}{M_C} \cdot m_{fuel} - 0.5 \cdot \frac{w_{H_2,fuel}}{2M_H} \cdot m_{fuel} + \frac{w_{O_2,fuel}}{2M_O} \cdot m_{fuel}}{\frac{w_{O_2,air}}{2M_O} \cdot m_{air} + 0.5 \cdot \frac{w_{H_2,fuel}}{2M_H} \cdot m_{fuel} + \frac{w_{O_2,fuel}}{2M_O} \cdot m_{fuel} + \frac{w_{N_2,air}}{2M_N} \cdot m_{air} + \frac{w_{Ar,air}}{M_{Ar}} \cdot m_{air}} \tag{6.20}$$

If this equation is summarized, the result is

$$O_{2,th} = \frac{m_{air} \cdot \frac{w_{O_2,air}}{2M_O} - m_{fuel} \cdot (\frac{w_{C,fuel}}{M_C} + 0.5 \cdot \frac{w_{H_2,fuel}}{2M_H} - \frac{w_{O_2,fuel}}{2M_O})}{m_{air} \cdot (\frac{w_{O_2,air}}{2M_O} + \frac{w_{N_2,air}}{2M_N} + \frac{w_{Ar,air}}{M_{Ar}}) + m_{fuel} \cdot (0.5 \cdot \frac{w_{H_2,fuel}}{2M_H} + \frac{w_{O_2,fuel}}{2M_O})} \tag{6.21}$$

With the help of Equation 6.21 the theoretical oxygen content in the exhaust gas can be calculated for each fuel mixture between NRO and B0 in the exhaust gas.

6.3.2 Evaluation of an Exemplary Load Point

First the injected fuel mass $m_{inj,ecu}$ for the respective fuel mixture w_{b0} is entered in Figure 6.4 (e.g. for $w_{b0} = 0$ the injected fuel mass is $m_{inj,ecu} = 56\,mg/str$, for pure diesel fuel (B0) the injected fuel mass is $m_{inj,ecu} = 55\,mg/str$).

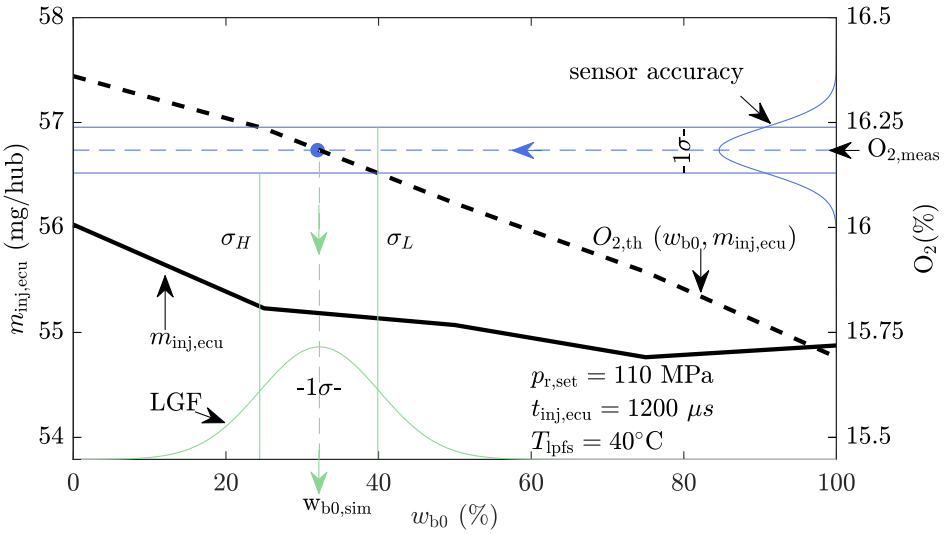

Figure 6.4: Detection resulting in $w_{b0,sim} = 33\%$ at a real mixture $w_{b0,meas} = 25\%$

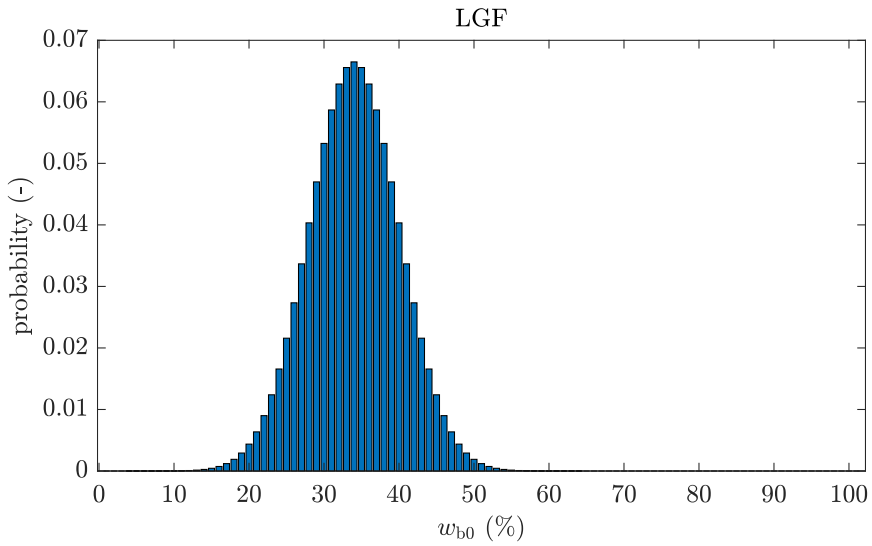

Figure 6.5: Load point Gaussian function (one evaluated load point)

With this injected fuel mass and the air mass flow (independent of fuel composition) the theoretical oxygen content $O_{2,th}(w_{b0}, m_{inj,ecu})$ in the exhaust gas can be calculated for each mixture ratio in 1% steps via Equation 6.21. The values for $O_{2,th}(w_{b0}, m_{inj,ecu})$ are also entered in Figure 6.4.

To find the corresponding mixing ratio w_{b0}, the intersection of $O_{2,th}(w_{b0}, m_{inj,ecu})$ with the measured oxygen value $O_{2,meas}$ is formed. Furthermore, the intersection points of $O_{2,th}(w_{b0}, m_{inj,ecu})$ with the 1-sigma boundaries of the O_2 sensor are formed so that they can be projected onto the x axis σ_L and σ_H (Figure 6.4).

With σ_L, σ_H and $w_{b0,sim}$ a Gaussian function can be formed at the x-axis (Figure 6.5). This load point Gaussian function (LGF) gives the probability for a specific mixing ratio w_{b0}, by assigning a probability to the 101 possible mixing ratios.

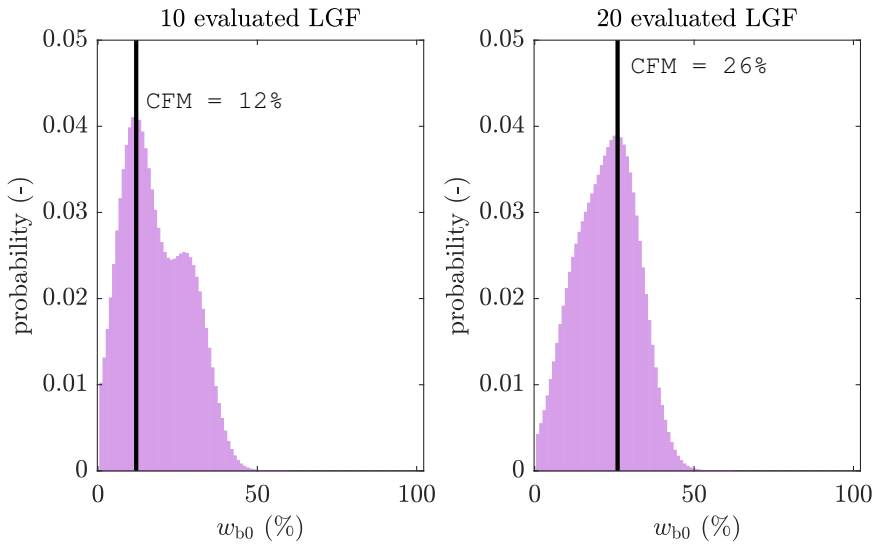

Figure 6.6: Mixture array bar with currently used fuel mixture (CFM) for 10 and 20 evaluated load points

This LGF is generated at each evaluated stationary load point. Since not only one load point is evaluated, but many (whenever the engine is in a stationary load point), the mixture array (MA) is presented in the next section.

6.3.3 Calculating the Mixture Array

The mixture array contains the fuel mixture information for all LGFs already evaluated. It consists of 101 values (0-100% diesel in 1% steps) and a corresponding probability for respective mixture ratio (Figure 6.5). The maximum value in the mixture array (MA) is used as the "currently used fuel mixture (CFM)" for engine control (compare Figure 6.3 and Figure 6.6).

Since either only B0-NRO mixtures or B0-RME mixtures are permitted as fuel, the sum of all values in the mixture array equals 1 (total probability that the mixing ratio is between 0 and 100% is 1).
After evaluating a stationary load point, the mixture array is updated. For this, the probabilities of the LGF (information of one load point) are divided by 10 and added to the mixture array (information of all evaluated load points). The MA is then normalized. This means that a newly evaluated LGF has a 10% weight on the CFM.

$$\mathrm{MA}(w_{b0})_{new} = \frac{\mathrm{MA}(w_{b0})_{old} + \mathrm{LGF}(w_{b0})/10}{\sum_{w_{b0}=0}^{w_{b0}=100}(\mathrm{MA}(w_{b0})_{old} + \mathrm{LGF}(w_{b0})/10)} \tag{6.22}$$

This represents a trade-off between the speed with which the system can react to changing fuel mixtures and the fault tolerance against faulty measurements (if a detected mixture is wrong, the influence on the CFM is only 10%).

On the left side in Figure 6.6 ten LGF's were evaluated with a real fuel mixture of 50_0_50. The CFM indicates a mixture ratio of 44_0_56 with a probability of approximately 4%. The 4% refers to the exact mixing ratio 44_0_56. However, the MA can also be used to determine probabilities for areas. The probability that the detected mixture ratio is in the range between 40-60% diesel is approx. 40% (adding up single probabilities between 40-60% on the left side in Figure 6.6).

On the right side in Figure 6.6 the mixture array is shown after 20 evaluated load points. Here CFM = 49 is calculated, i.e. a mixture ratio of 49_0_51. This is very close to the real mixture ratio of 50_0_50. The probability that the detected mixture ratio is in the range between 40-60% diesel is approx. 70% after 20 evaluated load points.

The mixture array is reset after refueling the machine. If the CFM used in the ECU was e.g. 100% diesel and the fuel tank was half empty, the probabilities in the mixture array after refueling (with any fuel mixture of diesel and NRO) between 50-100% diesel are about 1.96%. All other mixing ratios have the probability 0%.
A new mixture ratio can only be in the range 50-100% diesel, regardless of filled up fuel. Since the total probability of the mixture array equals 1, probability for a value in the possible range is $p = \frac{1}{51} \approx 0.0196$.

6.3.4 Results of the Oxygen-Mixture Model

The accuracy of the model becomes better the more load points are evaluated (Figure 6.7). Load points from Table 4.1 were used for the tests. The load points were approached randomly (as it would be in practical operation). Quality of estimation depends strongly on respective measurement point. The engine was operated directly at high torque, after changing fuel from 25% to 0% diesel. The mixture ratio was immediately calculated correctly. When changing from 50% to 100% diesel the engine was in very low load points for a long time after starting the detection. Because of very high lambda values, the O_2 sensor is relatively inaccurate. For small injection quantities accuracy of injector maps is also reduced. This leads to a 65% diesel estimate instead of the real value of 100% diesel directly after changing the fuel.
After evaluating more stationary load points (including higher load points), the detected mixture approaches the real value. Please note that even a deviation of 100% does not lead to engine failure (in the past, no adjustment was made to the ECU if natural rapeseed oil was used instead of regular diesel).
35% deviation in the first couple of minutes after changing the fuel from 50_0_50 to 100_0_0 shown in Figure 6.7 represents the worst case (fuel detection at very low load points). The theoretically increased maximum power of the engine (if the ECU is set to a CFM = 65%, but there is 100% B0 in the tank) is practically unusable. If the engine is operated at maximum power, the detection will automatically improve. This is because theoretical oxygen content decreases much more strongly with increasing diesel content and high injection quantities. So the estimation via the O_2 sensor in the exhaust gas becomes more accurate. Overall results show a good detection of B0-NRO or B0-RME mixture ratios.

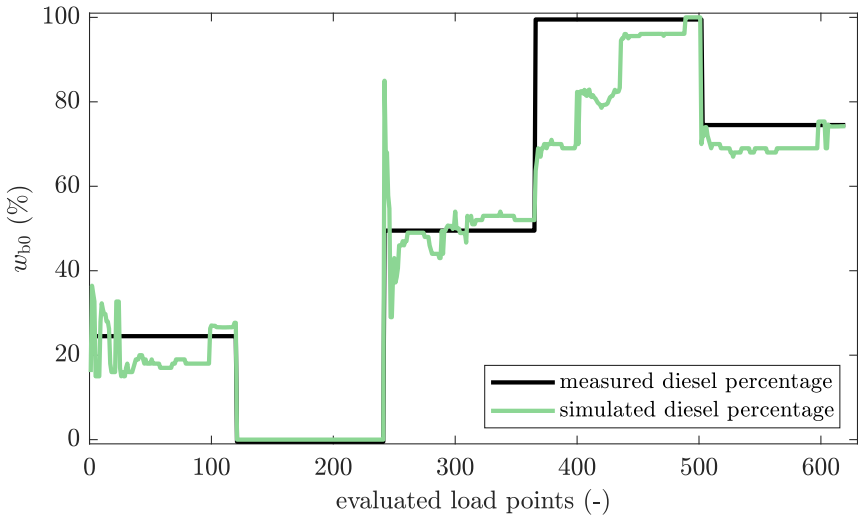

Figure 6.7: Results of the fuel detection of the Oxygen-Mixture Model

The following is especially important for understanding the next section:

> "The percentual composition of the fuel mixture can be detected well with the *OM Model*, but it must be known which two fuels are mixed."

The reason for this is that the calculation of the theoretical oxygen content in the exhaust gas (Equation 6.21) requires physical properties of the two fuels involved in the mixture. However, when the two fuels are known, good fuel mixture detection results are obtained (Figure 6.7).

6.4 Fuel Pump Current Model (FPC Model)

The *OM Model* provides promising results for fuel mixtures from B0-NRO OR mixtures from B0-RME mixtures. However, the *OM Model* cannot be used to determine whether B0-NRO or B0-RME is in the tank.
Detection of the exact composition with the *OM Model* would only work if the air requirements or the injected fuel mass of RME and NRO would differ significantly. However, since the properties of RME and NRO do not differ that much, this chapter presents the *Fuel Pump Current Model* based on current measurement of the electrical fuel pump. This exploits the greatest physical difference between NRO and RME, which is the viscosity as shown in subsection 2.1.1.

A statement can be made about the viscosity of the fuel, by evaluating the measured current of the electrical fuel pump. It is important to distinguish between a high viscosity of fuel and e.g. a clogged fuel filter, which would also increase the current of the pump. If the pressure exceeds 5 bar, an over pressure valve (Figure 3.6) opens, so a clogged fuel filter or a very viscous fuel (NRO at cold temperatures) can be assumed.

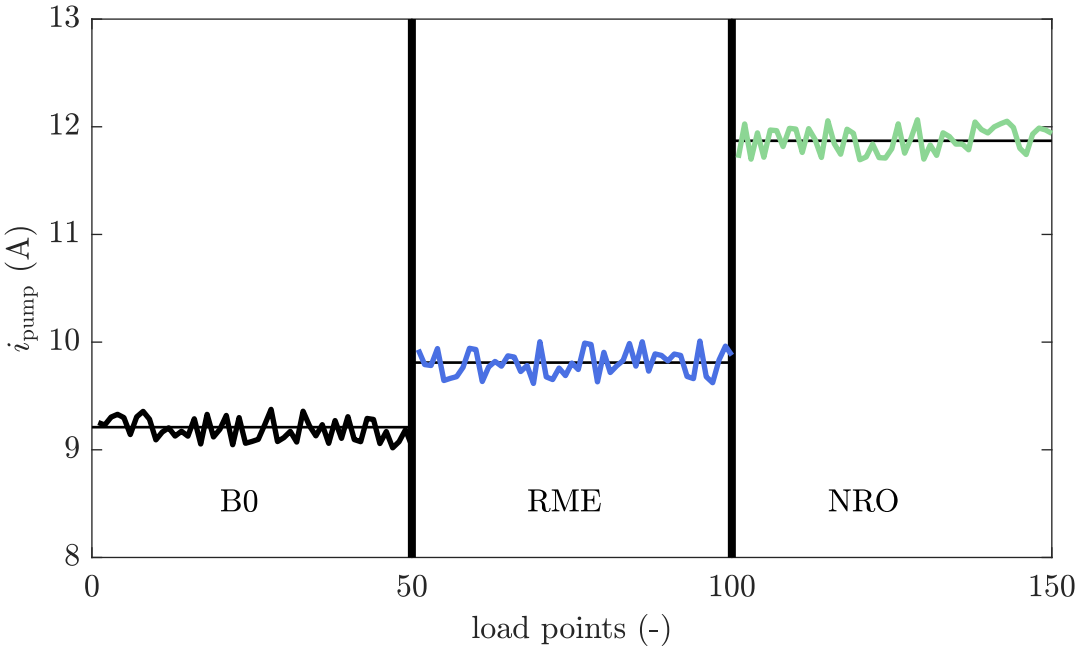

Figure 6.8: Measured fuel pump current values for different fuels

The presented model records the current consumption of the fuel pump with 1 Hz and stores average current values every minute. Since the model is only executed with warm fuel (40 °C) and a running engine (constant voltage), the current of the pump only depends on fuel and the degree of contamination of the filters. Figure 6.8 shows the current curve of the fuel pump for pure fuels with a new filter. It becomes clear that current is the highest for operation with NRO and that the values can be well averaged.
The load points were not recorded in a specific order, but all belong to those shown in Table 4.1. Also it is obvious by looking at Figure 6.8 that the load point is not decisive for the current consumption of the fuel pump because most of the fuel is pumped back into the tank (compare Figure 3.6).

The nine different fuel mixtures (Table 4.1) are measured in the following with new fuel filters (for each fuel a new filter) and the current is recorded and averaged (with warm engine $T_{\text{lpfs}} = 40\,°\text{C}$). In addition, a dirty filter is installed and the pump current is recorded with the pure substances (same filter for all fuels). The results can be seen under Table 6.2.

It is noticeable that interpolation between mixtures is possible for new and dirty filters. Also it becomes clear that the model has a qualitative character. However, the accuracy is sufficient to distinguish between B0-NRO and B0-RME mixtures in the investigated measuring points.

The goal of the *FPC Model* is not to detect an exact fuel composition, but only to support the *OM Model*.

The operation principle of the *FPC Model* together with the *OM Model* is explained using an example (Figure 6.9). There are two instances of the *OM Model* running (B0-NRO-Instance and

Table 6.2: Typical pressures for new fuel filter

fuel	current with new filter ($i_{\text{pump,new}}$) (A)	current with dirty filter ($i_{\text{pump,dirty}}$) (A)
100_0_0	9.32	10.08
75_25_0	9.53	
50_50_0	9.54	
25_75_0	9.74	
0_100_0	9.85	10.67
75_0_25	10.43	
50_0_50	11.17	
25_0_75	11.97	
0_0_100	12.25	14.21

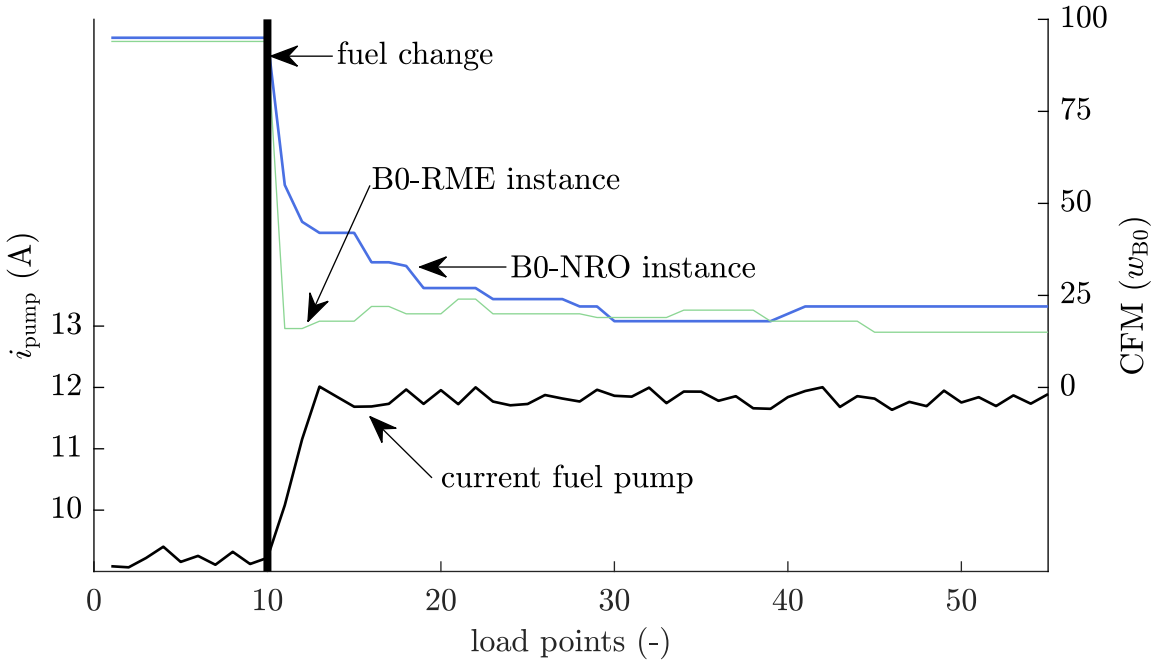

Figure 6.9: Combination of *FPC* and *OM Model*

B0-RME-Instance).
At the first ten load points pure diesel fuel 100_0_0 is in the fuel tank. Now the fuel is changed to a real mixture of 25_0_75 (NRO filled up). The current of the electrical fuel pump is recorded and the *OM Model* is executed after each stationary load point. The ECU is operated with standard diesel parameters for the entire duration of the test.

The only task of the *FPC Model* is to decide whether a B0-RME or B0-NRO mixture is more likely. For this purpose the recorded current value is compared with the values in Table 6.2.
In the first few minutes after changing the fuel, the pump current rises sharply (residues of B0 are still in the lines and filters) until a stationary pump current (only 25_0_75 in the system) is obtained. This pump current averages about 11.8 A.

Table 6.3: Fuel detection results of the two *OM Model* instances for the exemplary used fuel mixture of 25_0_75

instance	detected fuel	current with new filter ($i_{\text{pump,new}}$) (A)	measured current (i_{pump}) (A)	Δi (A)
B0-RME	15_85_0	9.8	11.8	-2
B0-NRO	22_0_78	12.0	11.8	0.2

With nominal values from Table 6.2 it can be decided whether a B0-RME or B0-NRO mixture is more likely. This is done exemplary at load point 55 (far right in Figure 6.9). Here the calculated fuel mixture for the B0-RME instance is 15_85_0 and for the B0-NRO instance 22_0_78.

From interpolated pressure values for a fuel mixture of 15_85_0 (Table 6.2) a target current of 9.8 A results. For a fuel mixture of 22_0_78 (Table 6.2) 12.0 A is obtained via interpolation. The difference to i_{pump} can be calculated with

$$\Delta i = i_{\text{pump,new}} - i_{\text{pump}}. \tag{6.23}$$

It becomes clear that Δi of the B0-NRO instance is way lower (Table 6.3).
In this case the correct *OM Model* instance (B0-NRO) is chosen. A mixture ratio of 22_0_78 would be used in the ECU to set the injector maps, which is close to the real mixture ratio of 25_0_75.

A disadvantage of the *FPC Model* is the dependence on the fuel filter state. If the fuel filter is operated for a very long time (e.g. 500 h), pressure and thus the current of the pump increases due to dirt accumulating in the fuel filters. An increased pressure would shift the *FPC Model* towards the B0-NRO instance of the *OM Model* (dirty fuel filter with B0-RME mixture has the same effect of an rising pump current, as a B0-NRO mixture).

To reduce this effect, a compensation part $\Delta i_{\text{pump,dirty}}$ is calculated for pure B0 operation. This is possible because the *OM Model* can detect the fuel independently from the *FPC Model* if the engine is operated with pure B0 (B0-NRO instance returns the same value as the B0-RME instance when engine is operated with B0). To compensate for smaller deviations $\Delta i_{\text{pump,dirty}}$ is calculated for a B0 content > 95%.

For example, an average current value of $i_{\text{pump}} = 11.32$ A instead of the current value with new filters $i_{\text{pump,new}} = 9.32$ A (compare Table 6.2) is measured with B0. If that happens,

$$\Delta i_{\text{pump,dirty}} = i_{\text{pump}} - i_{\text{pump,new}} = 2 \tag{6.24}$$

is calculated.
The next time a decision is made between B0-NRO or B0-RME instance, $\Delta i_{\text{pump,dirty}}$ will be included:

$$\Delta i = \Delta i_{\text{pump,dirty}} + i_{\text{pump,new}} - i_{\text{pump}} \tag{6.25}$$

In the example shown in Table 6.3 this would lead to a mixture ratio of 15_85_0 instead of 22_0_78 (with dirty filters, $\Delta i_{15\_85\_0} = 0$ and $\Delta i_{22\_0\_78} = 2.2$).

6.5 Diesel Oxidation Catalyst Efficiency Model (DE Model)

In this chapter the fuel used in the engine is determined by a temperature rise in the DOC. For this purpose fuel is injected into exhaust gas at the bottom dead center of the cylinder with a post-injection. This injection does not participate in the combustion process. It is oxidized by the DOC and leads to an increase in temperature.
For this detection model some requirements and assumptions are made:

1. Stationary load point at $t_{\mathrm{inj,ecu}} = 650\,\mu\mathrm{s}$ and $p_{\mathrm{r,set}} = 100\,\mathrm{MPa}$
2. DOC is adiabatic and 100% of fuel energy is converted into heat in the DOC
3. Air consists of 76.5% nitrogen and 23.5% oxygen
4. Exhaust gas consists of air, water and carbon dioxide only
5. Nitrogen has the same heat capacity as air

The same feature of the stationary regeneration (compare subsection 5.4.2) is now being used to detect the fuel via the energy content.

In order to achieve required DOC inlet temperatures for DPF regeneration, exhaust gas flap is used to throttle the exhaust gas mass flow and the injection is set to a late timing. As soon as DOC inlet temperatures rise above 330 °C, post injection starts.

In Figure 6.10 the temperature curve of the DOC inlet and outlet for diesel is shown. Post-injection was used for approx. 5 min. As soon as the DOC outlet temperature stops rising (less than 3 °C in 60 s), post injection stops and the temperature increase is evaluated. For this purpose the last 10 s of DOC inlet and outlet temperatures are averaged and the difference is calculated. The temperature difference $\Delta T_{\mathrm{doc,meas}}$ is approx. 85 °C in shown example.

With the law of conservation of energy theoretical temperature rise for a given fuel can be calculated:

$$\Delta T_{\mathrm{doc,sim}} = \frac{E_{\mathrm{fuel,st}}(w_{\mathrm{b0}}) \cdot m_{\mathrm{inj,ecu,post}} \cdot \xi_{\mathrm{doc}}(w_{\mathrm{b0}})}{m_{\mathrm{exh}} \cdot c_{p,\mathrm{exh}}} \tag{6.26}$$

Here $\xi_{\mathrm{doc}}(w_{\mathrm{b0}})$ indicates the efficiency of the post-injection depending on the fuel mixture.
m_{exh} (gas mass leaving the cylinder every 4 strokes) can be calculated by adding intake air m_{air}, injected fuel quantity for combustion $m_{\mathrm{inj,ecu}}$ and injected fuel quantity $m_{\mathrm{inj,ecu,post}}$ of the post-injection:

$$m_{\mathrm{exh}} = m_{\mathrm{air}} + m_{\mathrm{inj,ecu}} + m_{\mathrm{inj,ecu,post}} \tag{6.27}$$

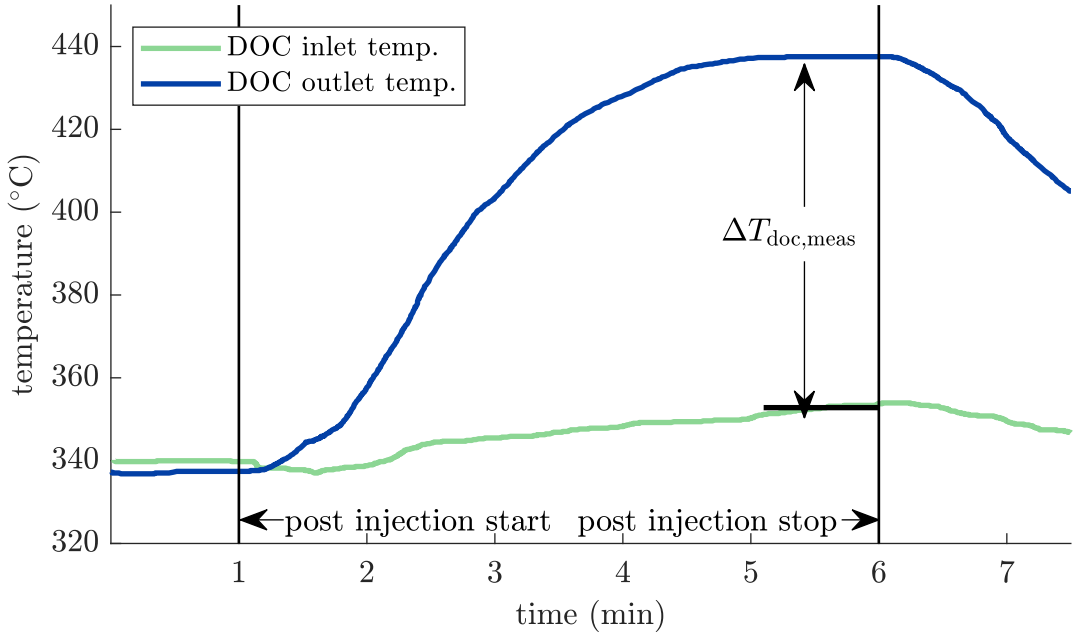

Figure 6.10: Temperature raise during B0 injection at $n_{\mathrm{eng}} = 1800\,\mathrm{rpm}$ and $M = 0\,\mathrm{N\,m}$

The heat capacity of exhaust gas $c_{\mathrm{p,exh}}$ is also required to use Equation 6.26. Exhaust gas pressure in the DOC is approximately assumed to be constant at 1.1 bar absolute pressure. In this case the heat capacity depends only on temperature and exhaust gas composition.
Exhaust gas is assumed to consist of air, water and carbon dioxide. The heat capacity of nitrogen is approximately equal to the heat capacity of air. This assumption can be made because the difference between nitrogen and air is very small (Table 6.4). Between temperatures in Table 6.4 an interpolation is performed.

The heat capacity of the exhaust gas is calculated approximately via:

$$c_{p,\mathrm{exh}} \approx \frac{m_{\mathrm{air,exh}}}{m_{\mathrm{exh}}} \cdot c_{p,\mathrm{air}} + \frac{m_{\mathrm{ox}}}{m_{\mathrm{exh}}} \cdot \left(w_{\mathrm{H_2O,ox}} \cdot c_{p,\mathrm{H_2O}} + (1 - w_{\mathrm{H_2O,ox}}) \cdot c_{p,\mathrm{CO_2}}\right) \tag{6.28}$$

$m_{\mathrm{air,exh}}$ is the air mass in the exhaust gas. Combined mass of H_2O and CO_2 is called oxidized mass m_{ox}. $w_{\mathrm{H_2O,ox}}$ and $w_{\mathrm{H_2O,ox}}$ are the mass fractions of H_2O and CO_2 in m_{ox}.
For residual air mass in the exhaust (with less oxygen content in exhaust gas) the following equa-

Table 6.4: Heat capacities of the exhaust gas components according to [110]

T (°C)	$c_{p,\mathrm{N_2}}$	$c_{p,\mathrm{air}}$	$c_{p,\mathrm{H_2O}}$	$c_{p,\mathrm{CO_2}}$
100	29.12	29.3	33.71	38.17
200	29.2	29.3	34.08	40.13
300	29.35	29.52	34.54	41.83
400	29.56	29.79	35.05	43.33
500	29.82	30.09	35.59	44.66
600	30.11	30.41	36.15	45.85

Table 6.5: Molar masses of the exhaust gas constituents

	M_{N_2}	M_{air}	M_{H_2O}	M_{CO_2}
mole mass (g/mol)	28	28.8	18	44

tion results:

$$m_{air,exh} = m_{air} - 0.235 \cdot L_{st}(w_{b0}) \cdot (m_{inj,ecu} + m_{inj,ecu,post}) \tag{6.29}$$

Here 0.235 is the mass fraction of oxygen in the ambient air. Injected fuel (combustion + post-injection) together with oxygen in air becomes H_2O and CO_2. m_{ox} is approximated by

$$m_{ox} = (m_{inj,ecu} + m_{inj,ecu,post}) \cdot (1 + 0.235 \cdot L_{st}(w_{b0})). \tag{6.30}$$

The proportion of water in oxidation products is calculated via Equation 6.31.

$$w_{H_2O,ox} = \frac{w_{H,fuel} \cdot \frac{M_{H_2O}}{2M_H}}{w_{H,fuel} \cdot \frac{M_{H_2O}}{2M_H} + w_{C,fuel} \cdot \frac{M_{CO_2}}{M_C}} \tag{6.31}$$

With the presented equations $\Delta T_{doc,sim}$ can be calculated (Figure 6.10). If this value is compared with the measured temperature increase, the fuel composition can be determined. However, this only applies if the injected fuel quantity is known. This results in an analogous problem to the *OM Model*. With the energy content it is possible to calculate fuel mixtures between diesel and NRO, but injected fuel mass is needed. This depends on the fuel mixture, so a circular reference is present.
The problem can be solved by calculating the injected fuel mass in 1% steps for all mixture ratios between 0 and 100% diesel using stored injector maps (similar to subsection 6.3.1). This is also done for the stoichiometric air demand, by interpolation from Table 2.1 for the respective fuel ratio. Afterwards it is checked whether a unique mixture ratio can be assigned to the measured $\Delta T_{doc,meas}$.

Even if injected fuel masses can be read from look-up tables, fuel mass arriving the DOC cannot be calculated in this way. A part of the injected fuel mass hits the cylinder wall and enters the engine oil via the piston rings (Figure 6.11) [106].

This fuel proportion also depends on the fuel used. For this reason measurements of fuel entry into engine oil are carried out first. An oil sample is taken and evaluated before and after the post injection is started. Measurements are carried out with 60 min long, stationary load points (main injection of 650 µs and rail pressure of 100 MPa). In diesel (B0) operation this corresponds to an engine speed of approximately 1800 rpm. Furthermore, injector pulse duration of post injections are fixed to $t_{inj,ecu,post} = 512\,\mu s$.

Oil measurement results $x_{f,oil}$ are given in mass percent and can be found under section A.6. Fuel mass in the oil can be calculated by

$$m_{f,oil} = \frac{x_{f,oil} \cdot m_{oil,t=0}}{1 - x_{f,oil}}. \tag{6.32}$$

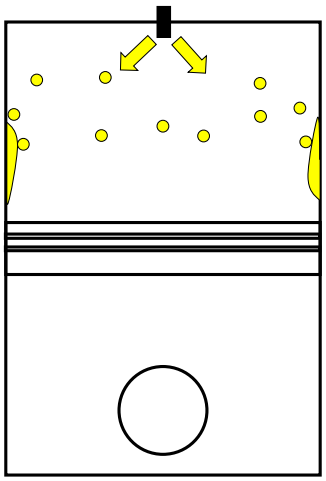

Figure 6.11: Principle of fuel entering engine oil

Table 6.6: Oil dilution measurements during fuel post injections

fuel	m_{inj} (mg/str)	$m_{\mathrm{inj,ecu,post}}$ (mg/str)	$m_{\mathrm{inj,oil}}$ (mg/str)	$\eta_{\mathrm{f,oil}}$ (%)
100_0_0	17.76	10.00	0.31	3.1
50_0_50	17.61	9.52	0.95	9.9
0_0_100	16.99	8.59	1.63	19.0
50_50_0	16.20	7.93	0.36	4.5
0_100_0	16.30	8.26	0.59	7.1

$m_{\mathrm{oil,t=0}}$ is the mass of oil in the engine before regeneration starts. $x_{\mathrm{f,oil}}$ is the measured fuel content of the engine oil analysis. For better comparability oil samples taken after each measurement are converted to quantity per injection. This is done by dividing the total mass of fuel entering the oil by the number of injections.

$$m_{\mathrm{inj,oil}} = \frac{m_{\mathrm{f,oil}}}{n_{\mathrm{inj}}} \tag{6.33}$$

Results are presented in Table 6.6. A considerable part of the injected fuel mass gets into the engine oil, especially with pure NRO. An efficiency factor of post-injection $\xi_{\mathrm{doc}}(w_{\mathrm{b0}})$ is presented for this reason:

$$\xi_{\mathrm{doc}}(w_{\mathrm{b0}}) = \frac{m_{\mathrm{inj,post,doc}}}{m_{\mathrm{inj,ecu,post}}} \tag{6.34}$$

This indicates how much fuel of the post-injection actually reaches the DOC. From measurements in Table 6.6 it is also evident that there is an approximately linear relationship of fuel entry into the engine oil. Therefore, $\xi_{\mathrm{doc}}(w_{\mathrm{b0}})$ is interpolated linearly for different fuel mixtures. It should be noted that these values only apply to the currently used series production ECU software (before optimization from subsection 5.4.2). When the adapted software is used on the ECU, $\xi_{\mathrm{doc}}(w_{\mathrm{b0}})$ is adjusted accordingly.

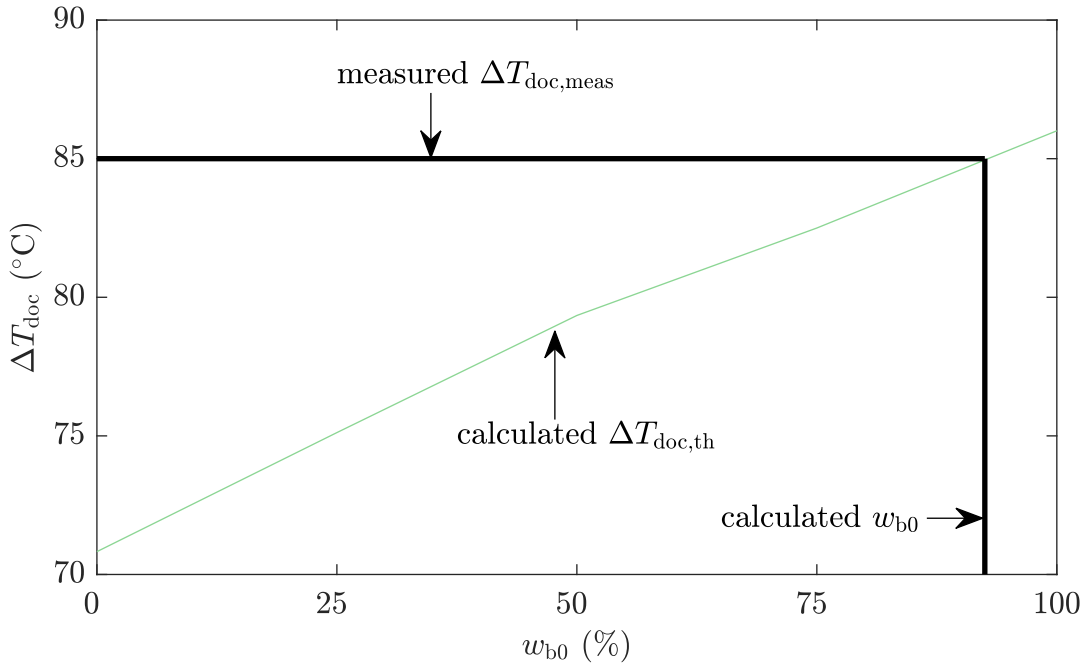

Figure 6.12: Fuel detection of the *DOC-Efficiency Model* based on measured temperature

With the presented equations the theoretical temperature rise $\Delta T_{\mathrm{doc,sim}}$ can be calculated for each fuel mixture according to Equation 6.26. This equation also establishes the connection between the mixing ratio w_{b0} and the measured temperature increase $\Delta T_{\mathrm{doc,meas}}$.
$\Delta T_{\mathrm{doc,sim}}$ is calculated for all mixing ratios in 1% steps and entered in Figure 6.12. Now an intersection between the measured $\Delta T_{\mathrm{doc,meas}} = 85\,°\mathrm{C}$ and $\Delta T_{\mathrm{doc,sim}}$ can be found. This point of intersection is the mixing ratio (result of the model). In the shown example this corresponds to a fuel mixture of about 94 %. The real mixing ratio of Figure 6.12, respectively Figure 6.10 is 100 % diesel.

Another possible application of this model is checking an incorrect injection quantity (e.g. for troubleshooting at the workshop). By transforming the equation Equation 6.26 post-injected fuel mass $m_{\mathrm{inj,ecu,post}}$ can also be determined. Thus, an increased post-injection quantity can be determined (e.g. chip tuning) with known fuel parameters by evaluating

$$m_{\mathrm{inj,ecu,post}} = \frac{m_{\mathrm{exh}} \cdot c_{p,\mathrm{exh}} \cdot \Delta T_{\mathrm{doc,meas}}}{E_{\mathrm{fuel,st}} \cdot \xi_{\mathrm{doc}}(w_{\mathrm{b0}})}. \tag{6.35}$$

6.6 Conclusion of Fuel Type Detection System

Fuel detection via O_2 sensor (*OM Model*) with stored injection maps comes to very good results. Although this initially requires a significantly increased application effort (injector maps must be measured), it has some advantages. For example, a single evaluated steady-state load point of the *OM Model* is sufficient to adapt the entire injection map to the new fuel in the optimum case.

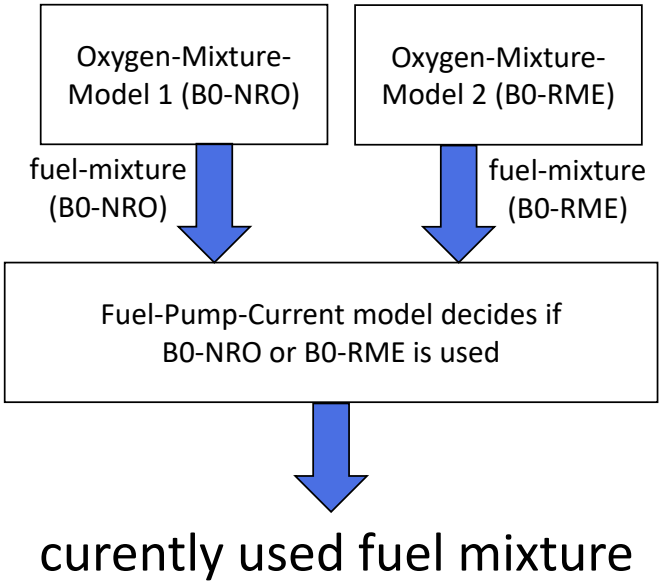

Figure 6.13: Flow chart of the fuel-detection system

The Fuel-Pump-Current model provides important information despite the qualitative statement. A distinction between B0-NRO and B0-RME mixtures can be made. This is possible because the current of the electrical fuel pump in NRO is significantly higher than in B0 or RME operation. The reason is the higher viscosity of NRO (even at constant 40 °C fuel temperature). In combination with the *OM Model*, this model makes it possible to detect B0-NRO OR B0-RME mixtures (and not just one mixture).

The used strategy is a combination of the OM and *FPC Model* (Figure 6.13). The exact mixing ratio, or currently used fuel mixture (CFM), is determined by the *OM Model*. The *FPC Model* decides which of the two CFM (NRO-B0 or RME-B0 instance) is selected.

Both models work with sensors installed in the series production engine. Contrary to the approaches found in the literature, no additional cylinder pressure sensors are required for reliable fuel detection. Furthermore, fuel detection does not require a measurement of fuel consumption.

The *DE Model* (Doc-Efficiency Model) is not used during practical operation of the machine because it is only usable at a constant load point (1800 rpm, 0 N m). However, it can be used for troubleshooting in the workshop, or by evaluating it in parallel with regular stationary DPF regenerations to detect the fuel mixture.
Another possible application of the *DE Model* is the testing of deviating injection masses if the fuel is known. The model could be used with B0 in the workshop to detect chip tuning or other problems that affect the injection mass.
Further injection mass models that can also be used during practical operation (detect chip tuning) are presented in the next chapter.

7 On-Board Chip Tuning Detection System

In this chapter an chip tuning detection system is presented. For this purpose most common chip tuning methods are shown first. Subsequently, various injection mass models are presented to detect undesired deviations of the injected fuel mass. All measurements in this chapter are performed with fossil diesel fuel B0.

7.1 State of the Art of Chip Tuning Detection

No literature could be found on on-board chip tuning detection. As already described in subsection 2.2.2 there are only isolated investigations on effects of chip tuning equipment [87] [105].
For this reason the following sections explain basic tuning procedures. The technical implementation and effects on the engine behavior are discussed. In addition, effects within the engine control system are described.

7.2 Analysis of Typical Chip Tuning Measures

As known from subsection 2.2.2 there are a multitude of chip tuning providers on the market. In spite of the many providers, an increase of the injected fuel mass in diesel engines is essentially achieved by three procedures:

1. Due to a falsification of the rail pressure signal (rail-pressure-tuning)
2. By extending the pulse duration of the injector signal (injector-pulse-tuning)
3. By changing parameters on the ECU (ECU-tuning)

These procedures are presented below and evaluated in terms of their effects on service life of the engine. In general all tuning measures reduce the service life of an engine. For example, higher torque increases load on pistons, engine bearings or transmission.
Also secondary effects can reduce the service life of engines. These can include increased oil, cooling water or exhaust gas temperatures.
Increased oil temperatures lead to reduced lubrication of the engine, so heavy wear can occur. Increased exhaust gas temperatures can damage valves, turbochargers or exhaust after treatment systems, resulting in expensive repairs. Therefore effects of presented tuning measures are always considered in relation to other tuning measures in the following sections.

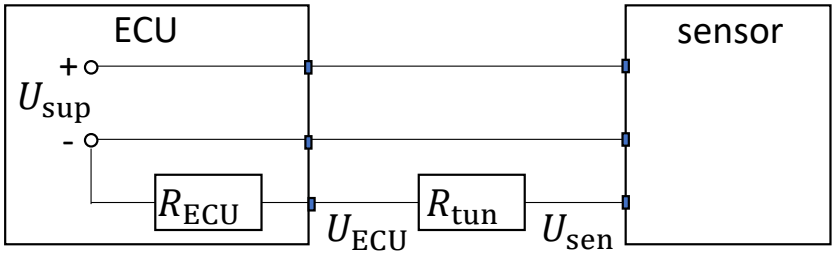

Figure 7.1: Principle of rail-pressure-tuning

7.2.1 Rail-Pressure-Tuning

Rail-pressure-tuning is a procedure in which the measured rail pressure sensor value is falsified. The principle is explained based on the test engine, but applies in general to diesel engines with common-rail injection systems. During normal operation (0-2000 bar) the sensor outputs voltage values between 0.5-4 V (DC-current). During rail-pressure-tuning the voltage measured by the ECU is reduced, so the ECU is increasing real rail pressure due to the closed control loop (Figure 3.12). Higher rail pressure leads to more fuel flow through injectors and power of the engine is increased.

Two general variants were found for investigated rail-pressure-tuning equipment. The simplest variant is the installation of an electrical resistance "R_{tun}" (see Figure 7.1). The resistance causes the measured voltage U_{ecu} to drop so that the real rail pressure is increased by the control loop.
Problematic with this tuning variant is that the real rail pressure can be higher than the maximum permitted pressure of the high pressure system. This reduces the service life of the high-pressure system. In the past rail-pressure-tuning has often led to defective high-pressure pumps.
However, if rail pressure is only slightly falsified, engines will continue to function for some time due to safety factors.

Another variant of rail-pressure-tuning is a variable resistor or an electronic potentiometer. This can be designed so that the resistance value is lower at higher voltages and higher at lower voltages. Advantageous is that maximum permissible pressures are not exceeded, but at low set-point rail pressures a significantly increased injection quantity is generated. Disadvantageous is that the full power of an engine is usually present at high rail pressures. So maximum power of the engine cannot be significantly increased with this method. Since the engine delivers a lot more torque in low speed ranges, this method is offered (the engine can be operated at higher load and lower speed, so fuel can be saved under certain circumstances).

In this thesis the rail-tuning-factor (RTF) is introduced. This describes real rail pressure in relation to rail pressure measured in the ECU.

$$\text{RTF} = \frac{p_{\text{r}}}{p_{\text{r,ecu}}} \tag{7.1}$$

If external influences (temperature, humidity, pressure, etc.) are not taken into account, the resistance of the lines between sensor and ECU can be assumed as constant.

$$R = \frac{U}{I} = \text{const.} \tag{7.2}$$

To increase the rail pressure signal by a desired RTF, the rail pressure sensor input resistance of the ECU must be calculated first. This is done by measuring the current and voltage at the input of the ECU in series condition (without tuning). If the connecting lines are assumed to be without resistance, $U_{\text{ecu}} = U_{\text{sen}}$ applies. If an additional resistor R_{tun} is installed, the circuit is a typically voltage divider (Figure 7.1). The required resistor for a desired RTF can now be set via

$$R_{\text{tun}} = R_{\text{ecu}} \left(1 - \frac{1}{\text{RTF}}\right). \tag{7.3}$$

The selected resistance leads to the desired increase in rail pressure. Since the higher rail pressure leads to an increased injection quantity, an increase in performance can be achieved with very little effort.

Rail-pressure-tuning can lead to strongly changed emissions. Especially at torque peaks the engine is operated close to the soot limit (very rich fuel mixture). This can lead to clearly visible soot, or a rapid clogging of the DPF. However, at stationary load points more air is automatically pumped into the engine due to the higher output of stationary turbochargers, so rail-pressure-tuning hardly leads to increased soot. This agrees with the test of Prankl and Schaufler [87], who only measured stationary load points and have hardly detected any increased emissions.
Another disadvantage of rail-pressure-tuning could be fuel hitting the cylinder wall (fuel enters the engine oil). Reason for this is a significantly increased exit speed of fuel during injection and thus an impact on the cylinder wall cannot be avoided. An increased fuel content in the engine oil leads to increased wear in the entire engine due to the reduced lubricating effect.
If maximum pressures in the rail are exceeded, wear to high-pressure pump, injectors and rail itself will increase. High rail pressures can also lead to washed-out injector holes, which further increase engine power.

The tuning measure of rail-pressure-tuning is a cheap solution, which leads to many errors and reduces the service life of the combustion engine significantly. Therefore, tuning companies have looked for ways to increase engine power without significantly reducing service life. In the next chapter the most common tuning measure according to internal surveys of the company John Deere is presented: Extending the injector pulse duration.

7.2.2 Injector-Pulse-Tuning

Another method to increase diesel engine performance is to extend the injector pulse duration. By extending all injection signals, the injector needle remains open for a longer time and more fuel is injected. As no sensor values are falsified, this behavior does not lead to significantly higher wear in the high-pressure system.

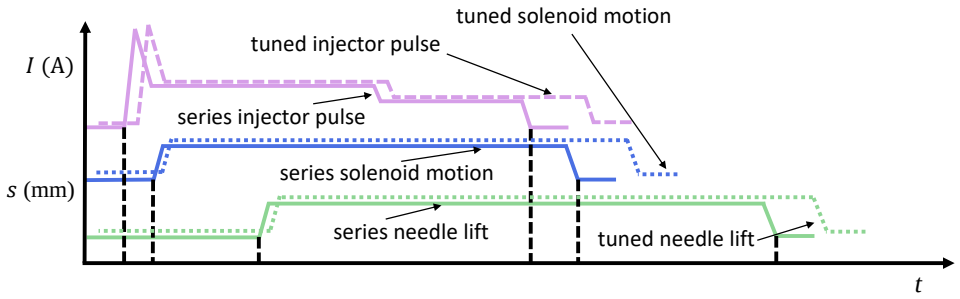

Figure 7.2: Injector delays with injector-pulse-tuning

In contrast to installation of electrical resistors at rail-pressure-tuning, this procedure requires more expensive hardware. A micro controller is connected between the ECU and injectors. If the ECU outputs an injector pulse (electrical voltage), this is also output by the micro controller and the injector is energized. At the same time a counter (to measure original injector pulse duration) is started on the micro controller. When the injector pulse of the ECU is over, the micro controller maintains voltage for a longer period of time and thus extends injector pulse duration. This results in a larger injection quantity and more engine power.
Different qualities of micro controllers are used by tuning equipment manufacturers. Simpler versions have a relatively slow processor. This leads to a delay of the injector signal. With hardware-triggered variants injector signals are passed on almost without delay.
If the micro controller leads to incorrect injection timing or other incorrect control parameters due to hardware restrictions (e.g. inputs/outputs or processor slow), these become particularly apparent when the engine is idling. For this reason many microcontrollers installed in practice often switch off the extension of injector pulse duration when engine is idling. This ensures series idling control of the ECU functions as desired.
However, all injector-pulse-tuning chips have an extended injector pulse duration in common. In Figure 7.2 effects on different parts of the injector are shown.

Analogous to the RTF, the pulse tuning factor (PTF) is introduced. This describes real injector pulse duration t_{inj} in relation to injector pulse duration $t_{\text{inj,ecu}}$ specified in the ECU.

$$\text{PTF} = \frac{t_{\text{inj}}}{t_{\text{inj,ecu}}} \tag{7.4}$$

If injector-pulse-tuning is not exaggerated and power is only moderately increased (e.g. a PTF of 1.1), there are hardly any disadvantages compared to series application of the identical engine with a higher power stage. The engine does not have a significantly lower service life and also emissions are only slightly changed [87]. However, if the engine is operated under extreme conditions such as very long full load periods at high outside temperatures, problems such as insufficient cooling capacity may occur. Since no sensors are falsified, safety algorithms of the ECU run as intended so overheating of the engine is avoided by an fault code or by reducing power.

However, in detail there are some differences compared to series application of identical engines with higher performance level. Injection timing and number of injections are not adjusted in the same way as in series application with engines at higher power levels using the upper curve (Figure 4.4). This can lead to exceeded maximum permissible pressures in the combustion chamber because the injection timing is not shifted based on real injected fuel mass. However, exceeded maximum pressures in the combustion chamber only applies if the most powerful version of the engine was heavily tuned.

Furthermore, at a tuned engine all other actuators continue to be adjusted based on the desired injection quantity (which is calculated) of the ECU and not the increased real injection quantity (due to tuning). This can lead to way too high EGR-rates in the tuned state.
A similar effect can happen if the engine is equipped with a VTG turbocharger. ECU controls the VTG with calculated exhaust gas mass flow and load point of the engine. Since the load point is falsified, turbochargers may operate inefficiently.
However, present test engine only has stationary turbochargers. As injector-pulse-tuning increases pressure in front of the turbochargers, exhaust gas mass driving the turbochargers also increases. Therefore, more air is automatically supplied to the engine during tuning. This has a self-regulating effect regarding low combustion air ratios. Same effects can also be observed during rail-pressure-tuning.
An exception are greatly extended injector pulse durations. With that, performance can be increased much more than with rail-tuning. Since the wastegate opens at a maximum permissible boost pressure, air mass supplied to the engine no longer increases automatically with higher injection quantities. This leads to a very low combustion air ratio in the engine, so exhaust gas temperatures rise sharply. This damages turbochargers and leads to a heavy sooting of the engine.

7.2.3 ECU-Tuning

Changing parameters on the original ECU is the most elegant method to increase performance of diesel engines offered by third parties. This combines advantages of rail-pressure-tuning (low hardware costs) with advantages of injector-pulse-tuning (low impact on engine service life). With ECU-tuning the largest profit margins can be achieved.
There are several variants of ECU tuning. Parameters can be adapted exactly as in series application of the identical engine with a higher power level, by using manufacturer-specific programs. Chip tuning equipment sellers can write ready-made parameter files to the ECU, which are also used by original engine manufacturer. Since this variant requires information by manufacturers, this tuning variant is only possible if there is contact with manufacturers/dealers, or greater development effort.

When no further manufacturer information is available, the ECU memory can be read out and examined e.g. with a HEX editor. Since injection maps from different manufacturers are very similarly structured, a search for related data in typical map form is carried out. For example, injection quantities are often given as a function of speed and desired torque. If suitable numerical values are found, these are increased by e.g. 10%. Afterwards the power of the machine is measured

(often with a PTO brake). This procedure is repeated until the power of the machine is increased (appropriate map is found). A lot of time may be needed for this method. Furthermore, external hardware must be available to measure engine performance, such as a PTO brake. Since this is expensive and requires special know-how, this method is much less common than injector-pulse-tuning. However, if an engine has been successfully increased in performance, ECU-tuning on identical engines can be repeated without measuring power again. This leads to no further costs for chip tuning providers, so high profit margins can be achieved.

In the context of this research work three tuned ECUs are examined. The ECU modified by a tuning manufacturer is read out with the original John Deere tool and compared with the original configuration. On two investigated ECU's the injector maps are increased only. At the third ECU characteristic maps have been changed by the tuning manufacturer which have no effect on performance of the engine. Many maps are more or less randomly increased, such as pre-heating times. Pre-heating tables are increased by 10% in addition to the injector map. This suggests that tuning companies sometimes do not exactly know what they are changing on the ECU, but increasing maps by try and error until the desired result (more power) is achieved.
Since the injector map is also increased by 10%, the tested ECU behaves exactly like an engine modified by injector-pulse-tuning. Therefore, ECU-tuning is summarized with injector-pulse-tuning in the following sections.

The best way to increase power by changing a table in the ECU would be an increased engine torque curve to the upper curve (section 4.5). Since the used test engine is not the most powerful version of the engine, raising maximum permissible torque curve to the upper curve allows the power output to be adjusted without distorting original manufacturer's application. Advantageous of this method is that all downstream look-up tables, which have the injection quantity as input are adapted automatically. However, all investigated ECUs have increased injector maps. Nevertheless, it cannot be excluded that increasing torque curves are also offered by chip tuning manufacturers.
Even if the engine is homologated up to the upper torque curve (section 4.5) and thus emission limits are met, the machine loses its type approval, as other components need not be designed for this power. Especially in Germany the power increase would also result in a loss of approval to operate the machine. Even if the basic engine is designed for a higher power output, durability of the entire machine may no longer be guaranteed. Reasons for this are various hardware changes such as a different gearbox, or a smaller cooling package for the low power class model of the machine.

7.2.4 Conclusion of Chip Tuning Measures

To sum up, increasing performance of diesel engines is far too easy according to the current state of art. ECU-Tuning could be more difficult by encrypting data. However, to establish a secure encryption more powerful hardware is required on the machines. As this increases costs of the machine and does not bring any customer value, there is hardly any effort of manufacturers to change this. To prevent other tuning measures, such as injector-pulse-tuning or rail-tuning, sensors

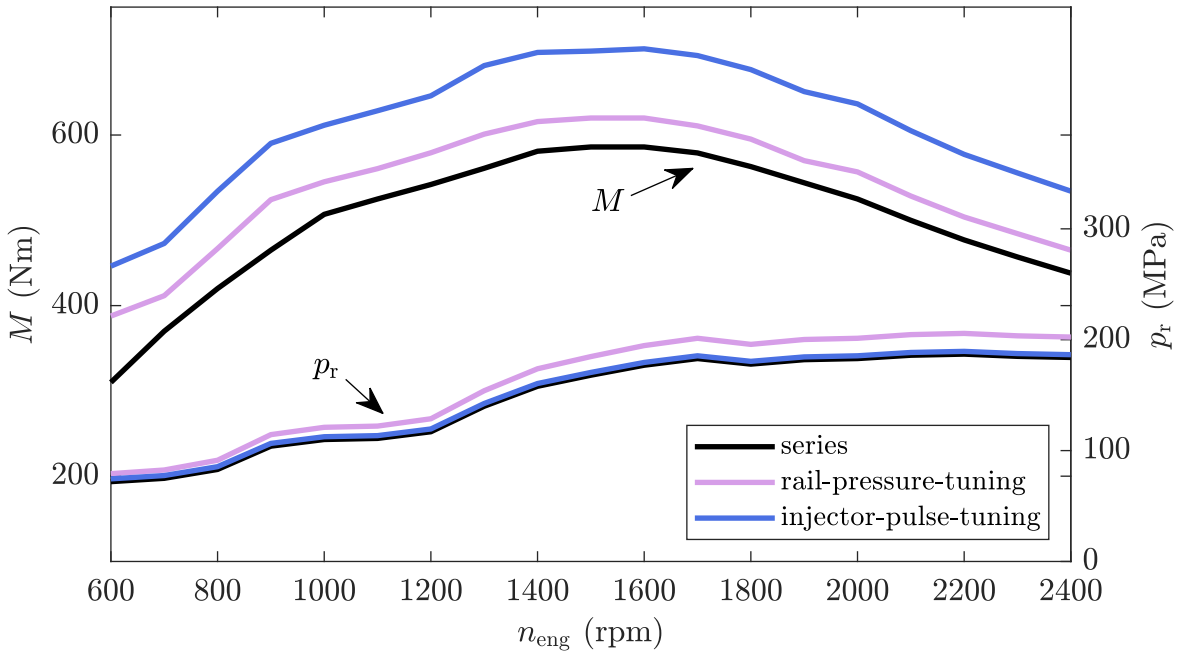

Figure 7.3: Torque curves in series, rail-pressure- and injector-pulse-tuning operation

could also communicate with the ECU in encrypted form. In the end, tuning measures cannot be completely prevented. However, countermeasures can complicate the tuning process to such an extent that significantly more development effort has to be invested in performance improvement. As this means additional costs for many tuning equipment manufacturers, the proportion of tuned machines could significantly decrease.

7.3 Tuning Effects on Engine Characteristics

Effects of presented tuning methods in terms of service life and robustness were described in previous sections. In this section effects on engine characteristics, or reasons why customers buy chip tuning equipment are presented. Since ECU-tuning (injector pulse duration extended by e.g 10%) shows identical behavior as injector-pulse-tuning (injector pulse durations extended by e.g. 10%), effects are summarized below as injector-pulse-tuning.

7.3.1 Torque Curves of Tuned Engines

Figure 7.3 shows the full load curve for the presented tuning variants, as well as respective rail pressure curves in the lower part of the picture.

The test engine used in this thesis is not operated on the upper curve (comp. section 4.5). This means the maximum rail pressure in series state is only 184 MPa and thus below maximum permissible system pressure of 200 MPa. For light rail-pressure-tuning, where the signal is falsified

by 10% (subsection 7.2.1), maximum permissible rail pressures are hardly exceeded. In Figure 7.3 the maximum rail pressure during rail-pressure-tuning is 202 MPa). In case of a light rail-pressure-tuning service life of the engine is not significantly reduced, because the high pressure system is designed for these pressures. However, torque increase of light rail-pressure-tuning compared to series operation is only between 5 and 7% (rail pressure is increased by 10%).
Injector-pulse-tuning has a much greater effect than rail-pressure-tuning. The torque on full load curve has increased between 17 and 20%, even if the injector pulse got extended by only 10%. A generalized statement can still not be made. In other map areas deviations can be much greater or smaller. For example, the influence on closing delays is procentual greater for very small, than for large injection quantities or injector pulse duration.
However, in comparison with section 4.5 it becomes clear that an increased injection quantity from the injector-pulse-tuning is still on the level of the upper torque curve. Thus torque delivered would still be in a range which is not critical for the basic engine.
Both tuning variants increase the torque of the engine over the whole speed range. The customer feels this clearly, as he can move the same machine in a higher gear for the same work, or do the work at a lower engine speed.

7.3.2 Transient Response of Tuned Engines

The so-called transient response behavior is also of great importance to the original engine manufacturer. This is often significantly improved by tuning, so it has a noticeable effect for the customer.
To make this effect quantitatively measurable, the following setup is set on the test bench:

- Engine at constant 1000 rpm
- Eddy current brake constant current applied
- Desired engine speed steps to 1500 rpm

The eddy current brake is applied with a constant current at an engine speed of 1000 rpm. This results in a constant torque at the corresponding speed. Now target speed of the engine is abruptly increased to 1500 rpm and the speed curve in series production and with injector-pulse-tuning is examined. Here it should be noted that the torque of the brake also increases with increasing speed.

In Figure 7.4 the speed curves of series and tuned state (smoothed by MATLAB® smoothing spline) are shown. In tuned case the desired speed is reached much faster (about one second faster than series), even if there is a slightly larger overshoot. The reason for this is the higher injection quantity. Since air mass supplied to the engine reacts slowly in relation to injected fuel mass (build-up of boost pressure), injected fuel mass can only be increased up to the soot limit in series operation (low lambda values lead to soot and increased NO_x production).
With injector-pulse-tuning, injection mass is generally higher, so more torque is generated. In

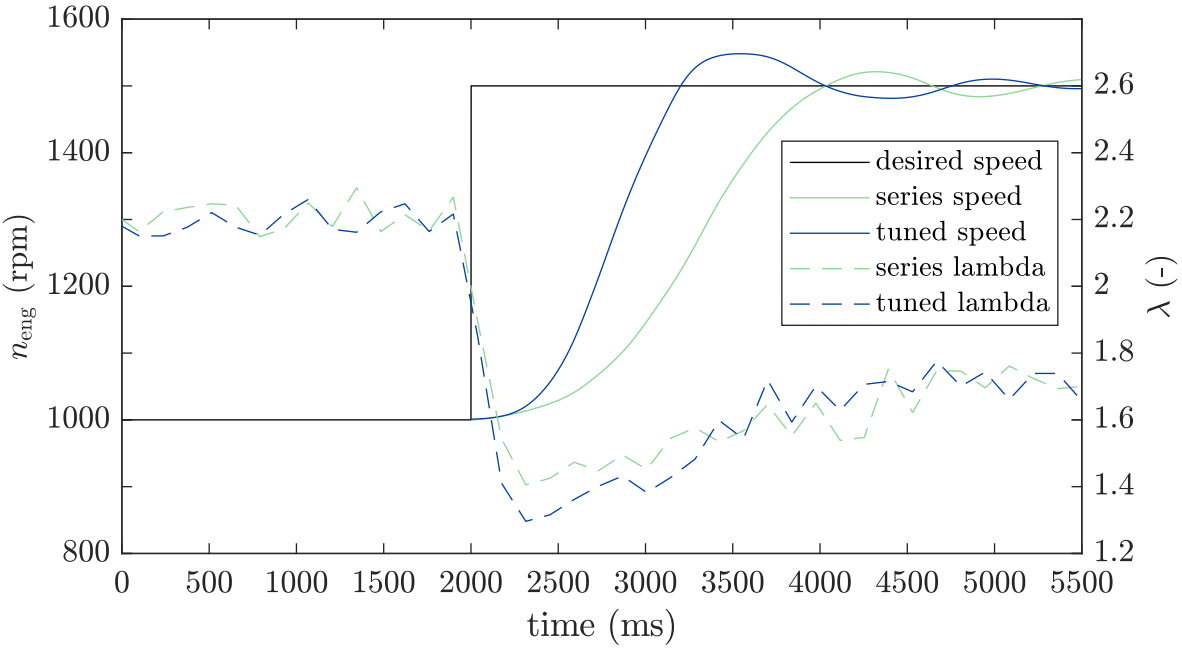

Figure 7.4: Transient response of the engine in series and injector-pulse-tuned condition

Figure 7.4 it can be seen that the lambda value of the engine in tuned mode is close to the soot limit ($\lambda \approx 1.3$) (around 2500 ms). In this case the injector pulse was extended by 10%. With even stronger tuning the soot limit is clearly undercut. As the engine only produces soot for a few combustion strokes and a DPF is installed, customers usually do not notice this. However, customers clearly notice the engine reaching target speed almost one second faster in the shown example. This is often described as a more agile engine.

7.4 Rail Pressure Based Fuel Estimation Model (RBFE Model)

A model which can be used to calculate the actual injected fuel mass is presented in this section. This model is intended to detect increased injection quantities due to tuning, or other faults which affect the injection quantity.
State of the art is an open loop injection quantity control based on look-up tables. Actual injected fuel mass is not measured (shown section 3.5). To inject a desired fuel quantity, the injector is supplied with a certain injector pulse duration at a mean rail pressure. How much fuel is actually injected is not considered in the ECU.

The model is based on a mass balance around the rail

$$\frac{dm_r(t)}{dt} = \dot{m}_{hpp}(t) - \dot{m}_{prv}(t) - \sum_{i=1}^{4} \left(\dot{m}_{inj,i}(t) + \dot{m}_{inj,leak,i}(t)\right) \propto f(p,T), \tag{7.5}$$

where the summands are the high-pressure pump quantity ($\dot{m}_{hpp}$), pressure relief valve flow ($\dot{m}_{prv}$), injector injecting fuel into the combustion chamber ($\dot{m}_{inj,i}$) and the injector leakage ($\dot{m}_{inj,leak,i}$).

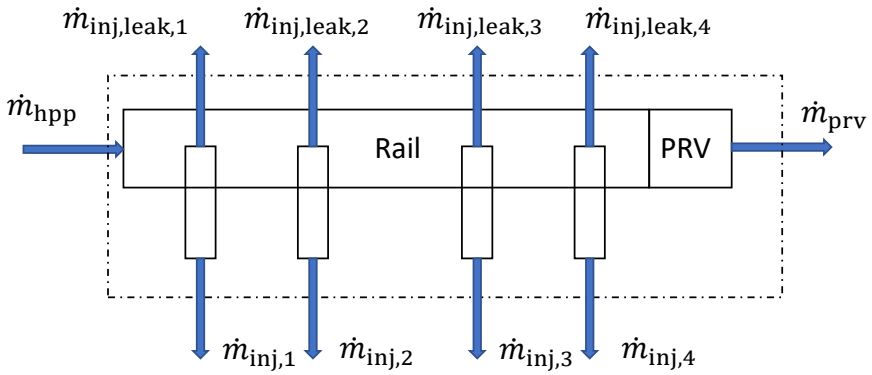

Figure 7.5: Fuel mass balance around the rail

m_{r} only increases when the high-pressure pump pumps fuel into the rail. m_{r} decreases when PRV is opened, fuel is injected into the combustion chamber, or if fuel returns to the tank as an injector leakage. If Equation 7.5 is only considered over the range of one injection (high-pressure pump not delivering fuel, PRV closed)

$$\int_{t=\mathrm{bi},i}^{t=\mathrm{ai},i} \frac{dm_{\mathrm{r}}(t)}{dt} dt = \int_{t=\mathrm{bi},i}^{t=\mathrm{ai},i} \left(\cancelto{0}{\dot{m}_{\mathrm{hpp}}(t)} - \cancelto{0}{\dot{m}_{\mathrm{prv}}(t)} - \sum_{i=1}^{4} \left(\dot{m}_{\mathrm{inj},i}(t) + \dot{m}_{\mathrm{inj,leak},i}(t) \right) \right) dt \tag{7.6}$$

will be obtained, where $t = \mathrm{bi}, i$ is the moment before and $t = \mathrm{ai}, i$ after injector i injects fuel. By solving the integral

$$\int_{t=\mathrm{bi},i}^{t=\mathrm{ai},i} \frac{dm_{\mathrm{r}}(t)}{dt} dt = -m_{\mathrm{inj},i} - m_{\mathrm{inj,leak},i} + m_{\mathrm{r,bi},i} \tag{7.7}$$

is obtained, where $m_{\mathrm{r,bi},i}$ is the fuel mass in the rail before injector i injects fuel.

If the mass flow into the rail is positive (Figure 7.5), the pressure in the rail increases. Power required for compression of the fuel originates from the combustion engine itself, since it drives the two plungers via the crankshaft. The fuel density inside the rail is related to the rail pressure via

$$\mathrm{d}p_{\mathrm{r}} = \frac{E_{\mathrm{f}}}{\rho} \cdot \mathrm{d}\rho \tag{7.8}$$

,where E_{f} is the bulk modulus and ρ is the density of the fuel [24]. A mass balance around a closed volume can also be be calculated with the density and the following equation [63]:

$$\frac{dm_{\mathrm{r}}(t)}{dt} = \frac{d}{dt}(V_{\mathrm{hps}} \cdot \rho(t)) = \cancelto{0}{\frac{dV_{\mathrm{hps}}}{dt}} \rho(t) + \frac{d\rho(t)}{dt} V_{\mathrm{hps}} \tag{7.9}$$

Here V_{hps} is the total high pressure volume (rail, pipes, high pressure pump), and ρ is the density of the fuel. If V_{hps} is assumed to be constant (expansions due to different pressures are neglected), Equation 7.9 simplifies to:

$$\frac{dm_{\mathrm{r}}(t)}{dt} = \frac{d\rho(t)}{dt} V_{\mathrm{hps}} \tag{7.10}$$

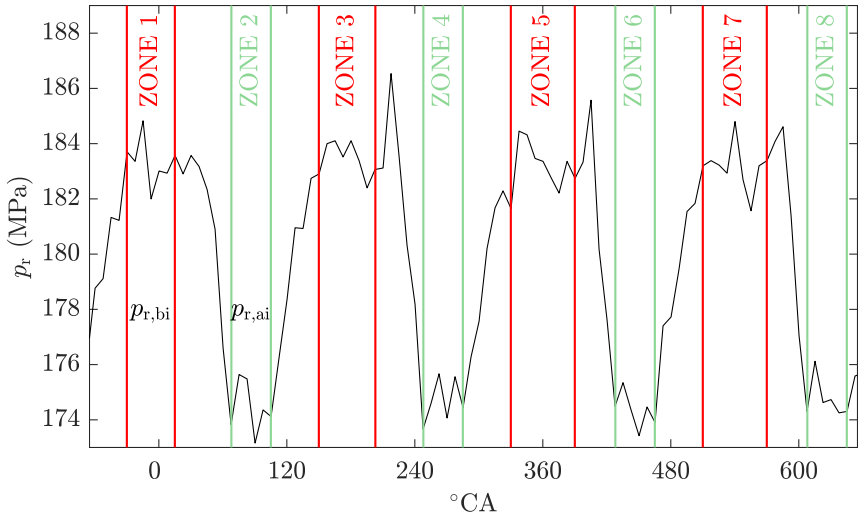

Figure 7.6: Rail pressure depending on crankshaft angle with zones assuming a constant pressure

For the fuel mass which has left the rail in the range of one injection

$$\int_{t=\mathrm{bi},i}^{t=\mathrm{ai},i} \frac{dm_\mathrm{r}(t)}{dt}\,dt = \int_{t=\mathrm{bi},i}^{t=\mathrm{ai},i} \frac{d\rho(t)}{dt} V_\mathrm{hps}\,dt = (\rho_{\mathrm{ai},i} - \rho_{\mathrm{bi},i}) \cdot V_\mathrm{hps} + m_{\mathrm{r,bi},i} \tag{7.11}$$

applies, where $\rho_{\mathrm{bi},i}$ is the fuel density inside the rail before the injection starts, $\rho_{\mathrm{ai},i}$ is the fuel density after the injection (at a lower rail pressure) and V_hps the total high pressure volume.
In contrast to the comparative approaches in [62] and [64] (where injections are compared with each other and a comparison is made with a local linear net), the goal here is to calculate an actual injected fuel mass.
By inserting Equation 7.7 in Equation 7.11 the fuel mass injected into the cylinder is obtained:

$$m_{\mathrm{inj},i} = (\rho_{\mathrm{bi},i} - \rho_{\mathrm{ai},i}) \cdot V_\mathrm{hps} - m_{\mathrm{inj,leak},i} \tag{7.12}$$

To calculate $\rho_{\mathrm{bi,real}}$ and $\rho_{\mathrm{ai},i}$ via Equation 2.2, the rail pressure before an injection ($p_{\mathrm{r,bi}}$) and after an injection ($p_{\mathrm{r,ai}}$) must be known (the relation from Equation 7.8 is already considered by the approximation formula). For this purpose the rail pressure sensor is sampled with a significantly higher frequency than in series operation (with dSpace MicroAutobox). The rail pressure signal is recorded crankshaft synchronously with a crank angle of 7.5° (see. section 4.2) instead of time-based sampling.

Since the high-pressure pump has two chambers and is driven at crankshaft speed, there are four pumping processes within 720 °CA (section 3.2). Test engine is a four-stroke four cylinder engine, so four injections within 720 °CA take place (in Figure 7.6 injections can be seen between the zones, when pressure drops).
In every zone the pressure should be constant. Within these pressure zones, the measured values are averaged in order to filter measurement noise. Since the characteristics of individual zones differ on pump quantity (with very small pump quantities, green low-pressure zones become significantly longer, since pumping process starts later) and injection time (very late injections shorten

Table 7.1: Determining the boundaries for the assumed constant pressure zones

boundaries	procedure
start red zone (1,3,5,7)	fixed crank angle (approx. 30 °BTDC)
stop red zone (1,3,5,7)	7.5 °CA before first injection pulse
start green zone (2,4,6,8)	7.5 °CA before the first increase after last injection pulse (after pressure drop)
stop green zone (2,4,6,8)	3 increasing samples in a row detected. 7.5 °CA before first increase

green and enlarge red pressure zones), zone boundaries are adaptively shifted. Thus, as many measured values as possible within a zone can be used for the evaluation. In Table 7.1 criteria for respective boundary are presented.

End of the red pressure zone is set 7.5 °CA before the first injection pulse. One sampling point in front of an injection is used, since the electrical injection pulse is inducing noise in the pressure signal. End of injection, or start of an even pressure zone, is set to the crank angle where the rail pressure no longer drops (after last injection pulse). This can be done since there is a pressure oscillation in the rail after injection due to the Joukowsky shock [92].

In Figure 7.6 $p_{\mathrm{r,bi}}$ and $p_{\mathrm{r,ai}}$ are marked for the first injection. To calculate $\rho_{\mathrm{bi,real}}$ and $\rho_{\mathrm{ai},i}$ the fuel temperature in the high pressure system is needed. Fuel temperature in the high pressure system depends on many factors like injection quantity, low-pressure fuel temperature, ambient temperature, rail pressure, air flow and the operating point of the engine (e.g. radiant heat significantly increases during active DPF regeneration). Since an exact modeling with all influencing factors would become very complex, a simplified model for the mean high-pressure temperature T_{hps} is used.

Three influences on the average fuel temperature in the high pressure system are assumed:

1. Temperature of the low pressure fuel system
2. Fuel absorbs heat due to the warm engine
3. Fuel heats up by compression of high pressure pump

To 1.:
The low pressure fuel temperature is measured at the fuel filter, so T_{lpfs} is used.
To 2.:
As an approximation, it is assumed that the absorbed heat is proportional to the injected fuel quantity $m_{\mathrm{inj,ecu}}$ (total engine emits more heat at higher load points).
To 3.:
It is assumed that the heating of the fuel by the high-pressure pump is proportional to the rail pressure p_{r}.
Thus, the searched function has the form:

$$T_{\mathrm{hps}}(T_{\mathrm{lpfs}}, m_{\mathrm{inj,ecu}}, p_{\mathrm{r}}) = T_{\mathrm{lpfs}} + X \cdot m_{\mathrm{inj,ecu}} + Y \cdot p_{\mathrm{r}} \tag{7.13}$$

Since T_{hps} cannot be measured at the test bench, it is calculated so that it can serve as a reference for regression.
If Equation 7.12 is changed according to the densities, all terms on the right side are known by measurements on the test bench:

$$\rho_{\mathrm{bi},i} - \rho_{\mathrm{ai},i} = \frac{m_{\mathrm{inj},i} + m_{\mathrm{inj,leak},i}}{V_{\mathrm{hps}}} \tag{7.14}$$

If the polynomial for calculating the density from Equation 2.2 is inserted in Equation 7.14 and resolved to T, T_{hps} results:

$$T_{\mathrm{hps}} = \frac{m_{\mathrm{inj},i} + m_{\mathrm{inj,leak},i}}{V_{\mathrm{hps}} \cdot a_4(p_{\mathrm{bi},i} - p_{\mathrm{ai},i})} - a_1(p_{\mathrm{bi},i} - p_{\mathrm{ai},i}) - a_3(p_{\mathrm{bi},i}^2 - p_{\mathrm{ai},i}^2) \tag{7.15}$$

The coefficients a_1,a_3 and a_4 can be found in Table 2.2.
These calculations are done for a test data set on the test bench in a fault-free case (B0 (pure fossil diesel), no faults or tuning). With the measured data T_{lpfs}, m_{inj} and p_{r} (individual injections are neglected) a linear regression can be performed in MATLAB®. The regression yields

$$T_{\mathrm{hps}} = T_{\mathrm{lpfs}} + 0.4069\,\mathrm{K\,mg^{-1}} \cdot m_{\mathrm{inj}} + 0.02\,\mathrm{K\,MPa^{-1}} \cdot p_{\mathrm{r}}. \tag{7.16}$$

Although desired fuel may vary from real value due to tuning, effect on temperature in the HPS is relatively small. Since the *RBFE Model* calculates a difference between two densities, a slightly wrong fuel temperature inside the HPS has only a very small influence on modeled injection quantity. The calculation of the mean fuel temperature in the high-pressure system based on desired fuel has therefore proven to be useful.

With the regression, m_{inj} can also be calculated for other data (not only the test data set) via Equation 7.12 for each individual injection. For injection 1 with zone 1 ($p_{\mathrm{r,bi}}$) and zone 2 ($p_{\mathrm{r,ai}}$) for injection 3 with zone 3 and zone 4 (ignition sequence 1-3-4-2) and so on (compare Figure 7.6). The calculated injection quantity by the *RBFE Model* is referred by $m_{\mathrm{inj,rbfe}}$ in the following. The results are shown in Figure 7.7.

Each load point was measured stationary for 30 seconds and modeled injected fuel mass was averaged over all injectors. The mean deviation between measured and the modeled injection quantity in range of injector-pulse-tuning is -0.33 mg/str or in percent approx. 0.51%. The modeled value slightly underestimates the real injected fuel mass, but is within a tolerable range. However, the relatively large difference between the standard deviation (3.3 mg/str) and mean deviation also implies that the model should run for a longer period of time. If the model is evaluated over a long time period, the engine was operated in many stationary load points and thus mean deviation is small.
Tuning is only stored in the ECU if for the tuning factor

$$F_{\mathrm{tuning}} = \frac{\sum_{i=1}^{50} \frac{m_{\mathrm{inj,rbfe}}}{m_{\mathrm{inj,ecu}}}}{50} > 1.05 \tag{7.17}$$

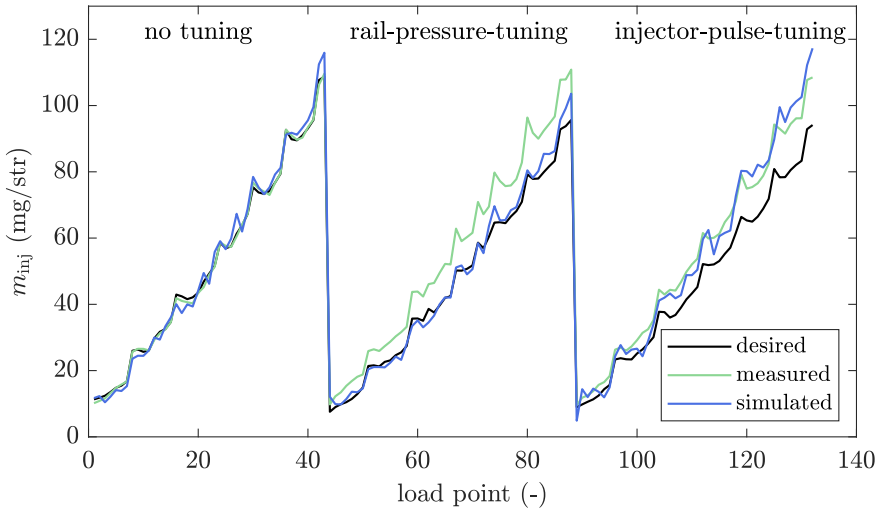

Figure 7.7: Simulated injections quantities of the RBFE Model compared to desired and measured fuel quantities

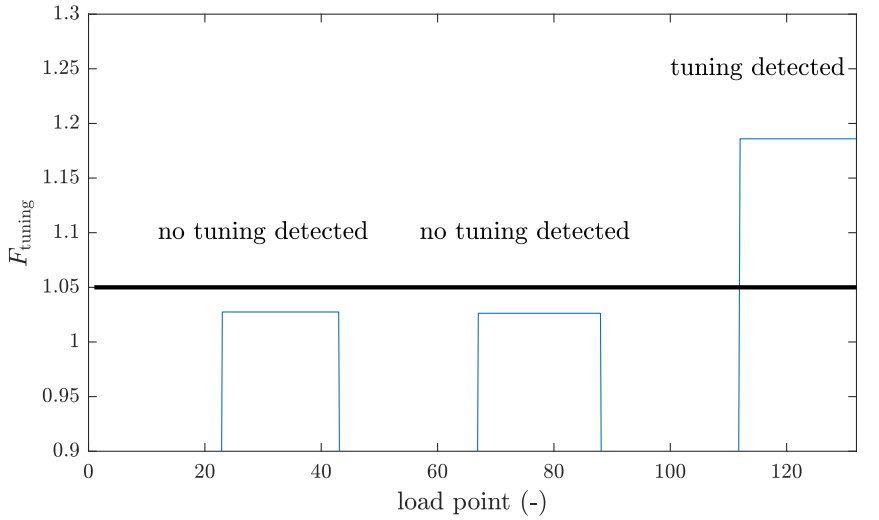

Figure 7.8: Result of RBFE tuning detection (same load points as in Figure 7.7)

applies. In this case i specifies the number of a stationary load point to which applies:

$$m_{\mathrm{inj,ecu}} > 50\,\mathrm{mg/str} \tag{7.18}$$

Figure 7.8 shows that injector-pulse-tuning can easily be detected by a large factor F_{tuning} . This factor is determined over 50 stationary load points with injection quantity >50 mg/str. Figure 7.8 shows that tuning is detected even after fewer load points (in Figure 7.8 only 20 load points were averaged). 50 load points are selected so that there is a greater safety against inaccurately modeled injection quantities (no false positives stored in ECU). After 50 stationary load points with an injection quantity >50 mg/str have been evaluated, values for F are overwritten, so that it is a moving average.

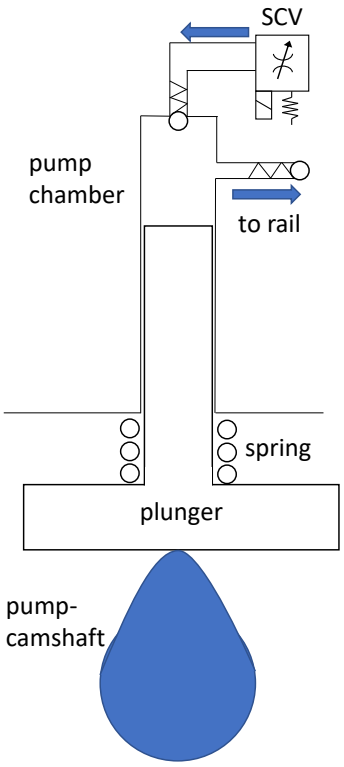

Figure 7.9: Operating principle of the suction control valve (SCV)

Injector-pulse-tuning can be reliably detected with the *RBFE Model*. However, rail-pressure-tuning cannot be detected (proof in the Appendix). Therefore, further models for determining the injected fuel mass in rail-tuning operation are presented in the following.

7.5 Suction Control Valve Model (SCV Model)

In this section a model with calculates injected fuel mass based on the suction control valve (metering valve) of the high-pressure pump is presented. The position of the SCV is feed-forward controlled by look-up tables, as described in section 3.2.

To calculate the pump quantity (m_{pump}) at the test bench (direct measurement is complicated) the following equation is assumed for a stationary load point:

$$m_{\text{pump}} = m_{\text{inj,meas}} + m_{\text{inj,leak}} + \cancelto{0}{m_{\text{prv}}} \tag{7.19}$$

In order to calculate the pump quantity on the real machine, a regression is performed. The input variables used are engine speed n_{eng}, the SCV position u_{scv} and the rail pressure $p_{\text{r,ecu}}$, since these have the greatest influence on the pump quantity. The influence of this variables can be illustrated by Figure 7.9. U_{scv} controls the cross section of the SCV (the larger the opening the more fuel flows into the pump chamber). n_{eng} has an influence, as it affects the time available to fill the

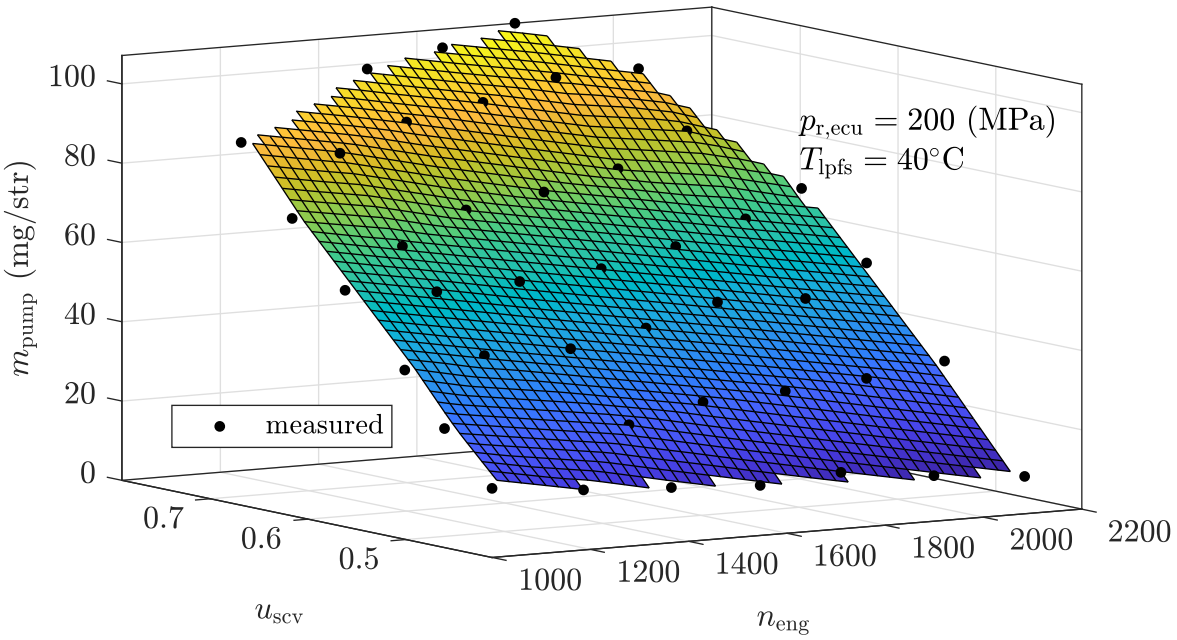

Figure 7.10: Simulated injection quantities of the *SCV Model* compared to measured validation points

pump chamber. If the pump-camshaft rotates so fast that the cam lifts off the plunger, not all of the pump chamber is filled with fuel and the pump quantity decreases. Rail pressure has the lowest influence. It determines the fuel mass that remains in the dead volume (pump-camshaft at top dead center). Furthermore, the pressure has an influence on the gas formation in the fuel, which can be caused by the rapid reduction in pressure as the plunger moves downwards (Compare [24] for more detailed description). Fuel temperature would also have a significant effect on the SCV flow, especially with highly viscous canola fuel. However, since fuel temperature is constantly controlled at 40 °C, the influence can be neglected in the regression (model can only be used with warm engine).

At a constant rail pressure and fuel temperatures, measurements of the fuel weight scale show a linear behavior with respect to engine speed and SCV command (compare Figure 7.10). So a multiple linear regression can be performed well. In Figure 7.10 the behavior for fossil diesel fuel B0 is shown.

The following approximation formula results:

$$m_{\text{pump,sim}} = b_1[\text{mg}] + b_2[\frac{\text{mg}}{\text{rpm}}] \cdot n_{\text{eng}} + b_3[\frac{\text{mg}}{\%}] \cdot u_{\text{scv}} + b_4[\frac{\text{mg}}{\text{MPa}}] \cdot p_{\text{r,ecu}} \tag{7.20}$$

Parameters for the respective fuel mixture resulting from regression are shown under Table 7.2. In this section only 100_0_0 is used. Parameters for the other fuels are shown for the sake of completeness.

The injected fuel mass

$$m_{\text{inj,scv}} = m_{\text{pump,sim}} - m_{\text{inj,leak}} \tag{7.21}$$

Table 7.2: Regression parameters of the *SCV Model* for different fuels

fuel	b_1	b_2	b_3	b_4
100_0_0	-103.98	-0.050	566.58	-0.20
75_0_25	-124.11	-0.055	604.55	-0.09
50_0_50	-119.05	-0.062	624.89	-0.03
25_0_75	-127.88	-0.061	638.75	-0.02
0_0_100	-122.91	-0.065	633.34	-0.01
75_25_0	-95.83	-0.053	579.55	-0.18
50_50_0	-112.66	-0.053	602.94	-0.21
25_75_0	-113.26	-0.057	616.01	-0.19
0_100_0	-106.43	-0.059	616.81	-0.20
0_75_25	-122.49	-0.060	641.94	-0.14
0_50_50	-137.37	-0.069	704.09	-0.07
0_25_75	-94.14	-0.062	603.34	-0.06

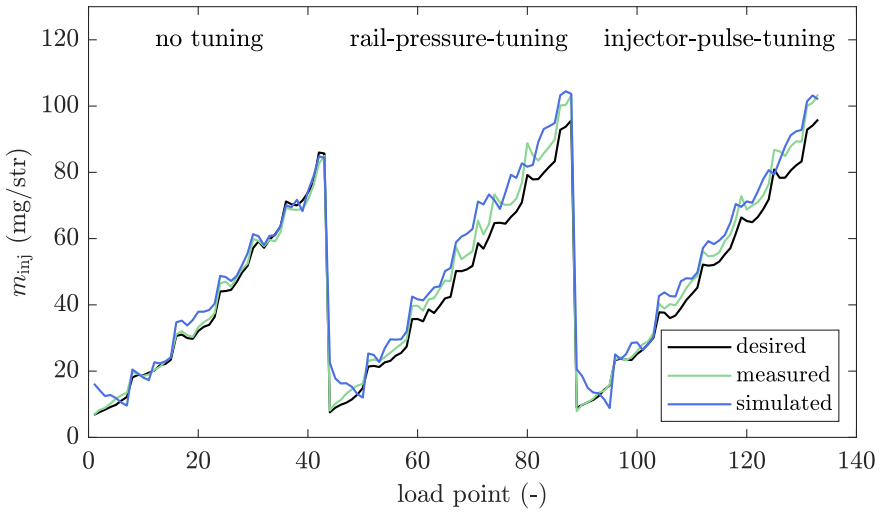

Figure 7.11: Simulated injection quantities of the *SCV Model* compared to desired and measured fuel quantities

can be calculated after switching Equation 7.19 using the leakage maps from Figure 5.4 and the simulated injection quantities of Figure 7.11 (names of the variables adjusted).

In Figure 7.11 results of the regression are plotted together with desired injection quantity and fuel mass measured on test bench. The regression shows weaknesses in low load points with low fuel flows through the SCV. Reasons for this are a larger percentual deviation of the SCV actuator at smaller opening cross sections and a non-linear behavior due to turbulence occurring at high speeds and very small opening cross sections. Since a linear regression was performed, non-linear behavior cannot be described. However, the model is sufficiently accurate for larger pump quantities.

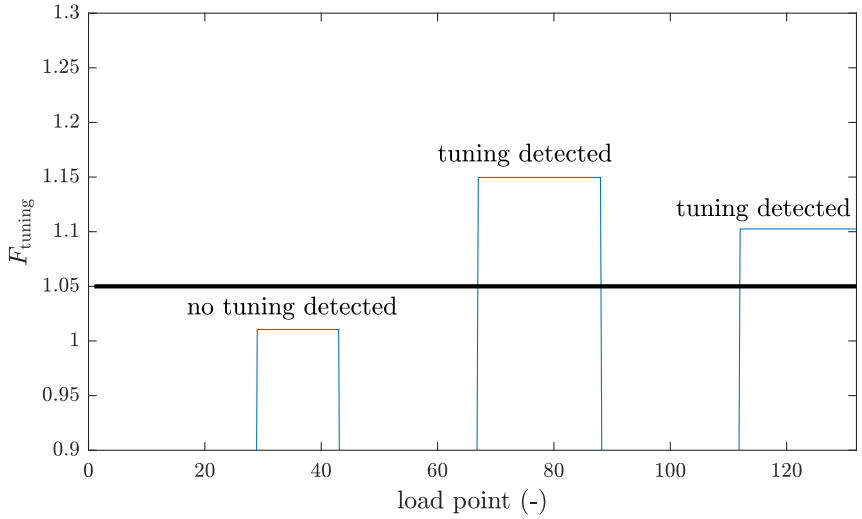

Figure 7.12: Result of the tuning detection based on the *SCV Model*

Overall, the model matches with actual injected fuel mass quite good. However, since the SCV valve is used to set the rail pressure, the model values must be averaged over a longer period of time in order to make a statement about deviating injection quantities (if, for example, only one injection is evaluated, the model value can be much higher than desired fuel, because desired rail pressure was increased in same period of time). Furthermore, the model is designed for constant LPFS temperatures of 40 °C, so it can only be executed with a warm engine.
Disadvantageous of the *SCV Model*, in addition to larger model deviations at low pump quantities, is a slight dependence on rail pressure. This means the model becomes less accurate if the rail pressure is incorrect. A regression was also performed without rail pressure influence (only n_{eng} and u_{scv} used to create regression). This also allows rail pressure tuning detection (with the advantage that the rail pressure has no influence on the model). However, the regression neglecting the rail pressure has a lower accuracy in case of undistorted sensor values than the regression with rail pressure as input variable. Since rail pressure tuning is only one case that affects the injection quantity, the regression with rail pressure was chosen.

However, rail-pressure-tuning has a much greater effect on the injected fuel mass than on the regression so rail-pressure-tuning can still be detected. The procedure for detecting tuning is analogous to that of the *RBFE Model*. In contrast to the *RBFE Model* the tuning factor F is clearly above the limit value of 1.05 with rail-pressure-tuning.

7.6 Oxygen-Fuel Model (OF Model)

Another possibility to determine injected fuel mass is evaluating the O_2-sensor (similar to *OM Model* in section 6.3). For this purpose Equation 6.21 is converted to m_{inj} with the assumption that

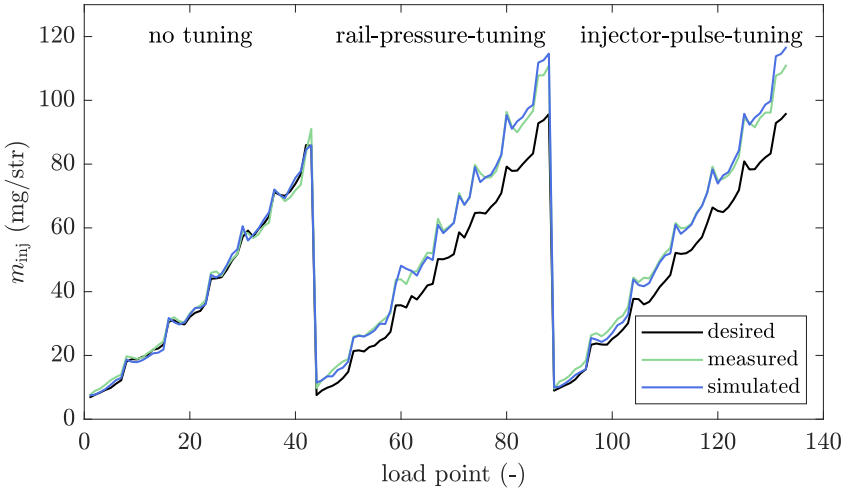

Figure 7.13: Simulated injection quantities of the *Oxygen-Fuel Model* compared to desired and measured fuel quantities

$O_{2,meas} = O_{2,th}$ applies:

$$m_{inj,of} = \frac{m_{air,sim} \cdot \left(\frac{w_{O_2,air}}{2M_O} - O_{2,meas} \cdot \left(\frac{w_{O_2,air}}{2M_O} + \frac{w_{N_2,air}}{2M_N} + \frac{w_{Ar,air}}{M_{Ar}} \right) \right)}{\left(0.5 \cdot \frac{w_{H_2,fuel}}{2M_H} + \frac{w_{O_2,fuel}}{2M_O} \right) \cdot O_{2,meas} + \left(\frac{w_{C,fuel}}{M_C} + 0.5 \cdot \frac{w_{H_2,fuel}}{2M_H} - \frac{w_{O_2,fuel}}{2M_O} \right)} \tag{7.22}$$

If the fuel composition is known (multi fuel is excluded), injected fuel mass can be calculated with Equation 7.22. Since this chapter uses exclusively fossil diesel fuel, the result for diesel is shown in Figure 7.13. A very good match between actual injected fuel mass and modeled fuel mass can be observed. The biggest advantage compared to other presented models is the complete independence of tuning measures and faults of the fuel system (e.g. injector deposits or falsified rail pressure). Burned fuel mass is calculated via air mass flow and oxygen content in exhaust gas only. Disadvantageous is that the model can only be used in stationary load points with engine at operating temperature (NO_x-Sensors need to be warm and react relatively slowly compared to fuel injection). However, in practice these stationary load points occur frequently. A further disadvantage is that air mass available to the engine must be known and not falsified. Since the used air mass model (show in Figure 6.2) is very accurate, modeled fuel quantity of the *OF Model* has also good conformity.
The results are presented analogously to the previous models (Figure 7.14). Even if the *OF Model* has the highest accuracy (compared to other models), tuning is only evaluated at load points with an injection level >50 mg/str. Here the deviation between $m_{inj,OF}$ and $m_{inj,ecu}$ is the highest.

7.7 Conclusion of Chip Tuning Detection

The analysis of typical tuning measures shows that an increase in diesel engine performance is relatively easy to implement by chip tuning-companies. Slight increases in performance can be determined with a moderate influence on the engine's service life. Even with rail-pressure-tuning

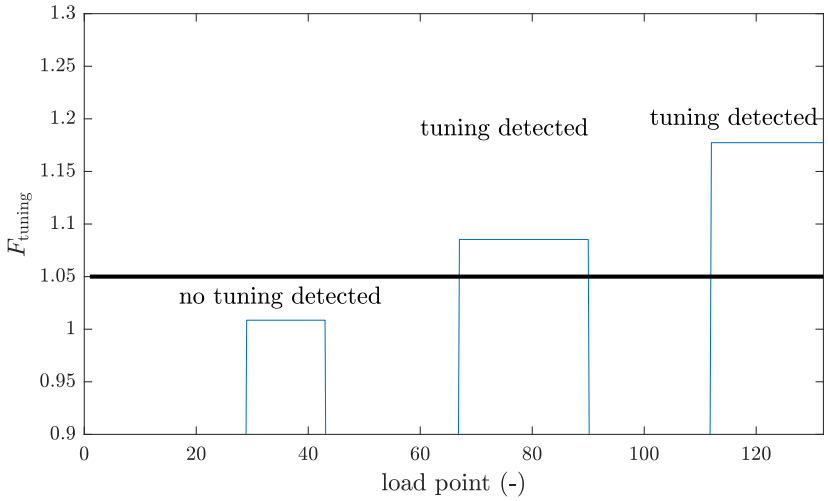

Figure 7.14: Result of tuning detection with the *Oxygen-Fuel Model*

(with only slight falsification of the rail pressure), all specifications are met. If the power should be increased a lot, rail pressure must be strongly falsified (real pressure increases very much). This leads to exceeded maximum pressures in the high-pressure system, making engine damage more likely.

With injector-pulse-tuning the power can be increased more than with rail-pressure-tuning. At the same time injector-pulse-tuning has a smaller effect on the service life of the engine. However, the effects on the overall service life of the machine cannot be estimated, as many components are not designed for the high performance.

In addition to the increased maximum power, a significant improvement in the transient response was also observed. This illustrates the reasons why customers are tuning their machines. Tuning is cheap compared to the more powerful motorized machine and a clear effect is noticeable.

The three models presented help to detect deviating injection quantities. The most common tuning variant (injector-pulse-tuning) can be good detected in particular, as no sensor values are distorted. Rail-pressure-tuning cannot be detected with the presented *RBFE Model*. However, rail tuning detection is possible with the *SCV* and *OF Model*.

Since three independent injection mass models were developed, a “two out of three” test can be performed in a potential series application. This means that if a sensor is drifting or gives wrong values, this can be detected. For example, if the *RBFE* and *SCV model* both detect an increased injection mass of 10%, but the *OF Model* detects 0%, a fault message for the oxygen sensor can be issued.

To sum up, increased injection quantities can be detected well. Since tuning is only stored if 50 stationary load points with a too high mean injection mass are detected, the risk of incorrectly stored tuning is relatively low. The reason for 50 minimum load points is that a “false positive” should be avoided. Since customer claims of warranty are partly about high amounts of money, chip tuning should only be stored if the risk for a false detection is low. This is also important regarding the image, respectively reputation of a company. Since tuning measures usually do not change after they have been installed once, a delayed detection is not a problem.

8 Onboard Injector Deposits Detection System

Injector deposits are a growing problem with modern diesel engines. To further increase the reliability of engines an onboard procedure is presented to determine injector faults with series sensors. In particular, the model includes a way to determine qualitative changes in opening and closing delays of injectors, from which deposits can be identified.

8.1 State of the Art of Diesel Injector Deposit Detection

Currently, no possibility is known with which injector deposits can be detected directly on board of the machine. The majority of injector deposits in currently used agriculture heavy duty production machines are not counteracted. As long as the engine operation does not deteriorate considerably, no fault is detected and the machine continues to operate. If problems with the injection occur, an fluctuating engine speed and/or a reduction in power is noticed by the driver, injectors are replaced.
However, approaches for optimized injection strategies to compensate effects of injector deposits can be found in literature [54] [101]. The key content of these studies are changed rail pressures or injector pulse durations to compensate decreasing power of the engine. The real injector condition is not taken into account or measured. Instead, characteristic curves are stored, which increase the rail pressure (or injector pulse duration) with increasing operating time of the engine.
If the engine operation deteriorates although rail pressure and injector pulse duration were changed, injectors are replaced with new ones. For machines, where a reliable operation of the engine must be guaranteed (engine failure is more expensive than additional injectors), all injectors are often replaced at the same time.

8.2 Time-Based Sampling Principle

Strong external deposits can already be detected by the *RBFE Model* (reduced injection quantity). However, internal deposits do not necessarily lead to lower injection quantities, so these cannot be detected by the *RBFE Model*.
Since internal diesel injector deposits (IDID) can cause significantly changed opening and closing delays (delayed injection times), IDID should be detectable to ensure fault-free engine operation. Furthermore, IDID can lead to a complete failure of injectors (e.g. the injector does not open or

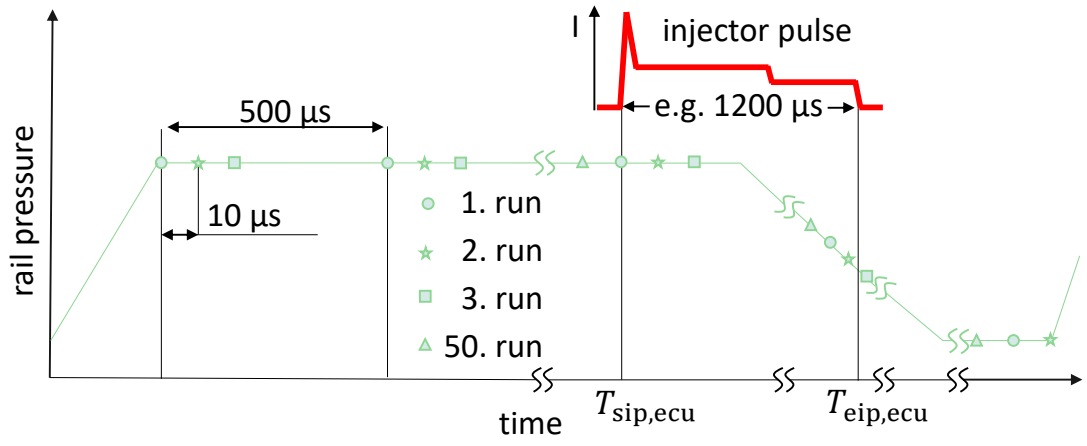

Figure 8.1: Principle of multiple sampling of the rail pressure signal

remains in an open position).
Since the rail pressure sensor is the only series sensor installed in the high pressure system, it will be used to detect injector deposits. The impact on rail pressure between an injector with a high level of deposits and a new injector is very small [53]. A high sampling rate is required to record certain phenomena like differences in opening delays between new and deposit injectors, via the rail pressure sensor. Through preliminary investigations with an oscilloscope, a minimum sampling interval of 10 µs could be identified.However, the maximum possible sampling rate of the ECU (2 kHz or T_0= 500 µs) is too low. In the following a possibility to realize a high sampling rate with the series ECU is presented. This method is based on a repeatedly sampled rail pressure signal and is based on the following assumption:

> With identical injector pulse duration and constant mean rail pressure, the rail pressure signal during a fuel injection is always the same.

Since the needed minimum sampling interval is 10 µs, the signal will be sampled repeatedly 50 times in a row with an sampling interval of 500 µs.

Only one injector is examined at the same time. For this injector multiple injections are deactivated for the duration of the deposit detection. In every run the signal is sampled at 2 kHz (500 µs interval) but shifted compared to injection pulse by 10 µs (Figure 8.1). A run is defined as the time from the end of pumping process for one injection up to the next pumping process of the high-pressure pump for the next injector (Figure 8.1 and Figure 8.2). Thus only the area around one injection is recorded.
The time at which the high-pressure pump is at the upper top dead center is determined by the transmission ratio of the high-pressure pump. At this point, the recording of the first run starts. The procedure is shown in Figure 8.1.

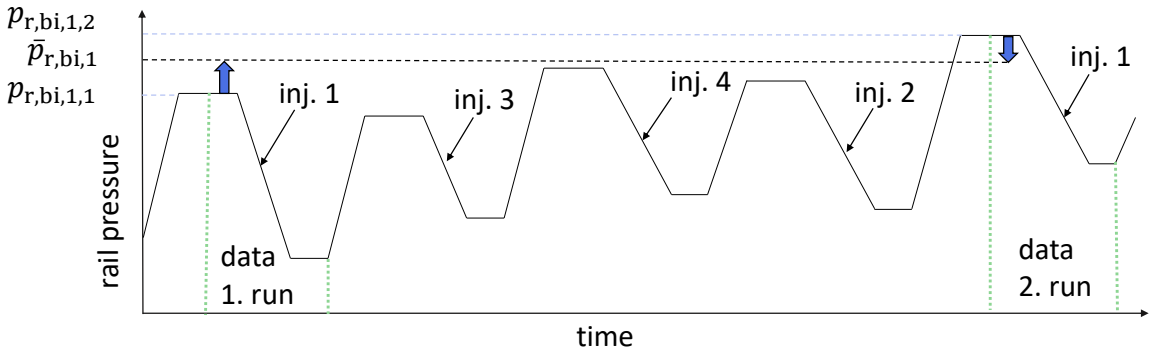

Figure 8.2: Simplified rail pressure fluctuations and corrective action

At the second run (next injection of examined injector), the start of sampling is shifted by 10 µs relative to the start of injection. This is carried out until the 50th run, so the injection signal of the examined injector is sampled with an even distance of 10 µs. The requirement for repeated scanning is an identical signal. Since the injection process in common rail systems is independent of crank angle, an identical injection process can be influenced by the ECU. This can be done by a constant rail pressure set-point and an identical injector pulse duration. For an identical pulse duration and thus an identical injection mass (pulse at same rail pressure), delivered engine torque must be (almost) stationary.

Since only one injector is examined for deposits at a time, slight torque fluctuations can be compensated by lowering or increasing injector pulse duration of remaining injectors. In this case a difference of set-point injection quantity between injectors of ±10% is allowed. In an agricultural machine this leads to barely noticeable additional vibrations.

Injector pulse duration is set very precisely by the ECU. Instead, rail pressure is subject to slight fluctuations. These fluctuations can result from an inaccurate metering unit of the high-pressure pump, speed fluctuations or unequal injections of remaining injectors. This effect is shown schematically in Figure 8.2. In areas with an increasing rail pressure, the pumping processes of the high-pressure pump take place. In areas with a decreasing rail pressure, injections of individual injectors take place. Pressure $p_{r,bi,1,1}$ in the first run of injector 1 is much lower than $p_{r,bi,1,2}$ of the same injector in the second run (compare left side in Figure 8.2 with right side). $p_{r,bi,real,1}$ gets calculated by averaging all measured values before an injection takes places. Since there is some sensor delay (the measured rail pressure lags behind the real rail pressure), the first 300 µs of the recorded data points are ignored.

Since the signal should be identical (same starting pressure at every injection), all recorded data of the 50 runs are linearly shifted to the same starting pressure $\bar{p}_{r,bi,i}$.

For this purpose, all starting rail pressures of the 50 runs are averaged:

$$\bar{p}_{r,bi,i} = \frac{\sum_{k=1}^{50} p_{r,bi,i,k}}{50} \tag{8.1}$$

Subsequently, all recorded data is shifted thus each recorded run has the rail pressure $\bar{p}_{\mathrm{r,bi},i}$ before an injection (Figure 8.2).

$$p_{\mathrm{r,data,shift},i}(t) = p_{\mathrm{r,data},i}(t) + \bar{p}_{\mathrm{r,bi},i} - p_{\mathrm{r,bi},i}(t) \tag{8.2}$$

This means that the entire record of the respective run has been moved so that $p_{\mathrm{r,bi},i}$ now corresponds to $\bar{p}_{\mathrm{r,bi},i}$. Since all 50 runs now have $\bar{p}_{\mathrm{r,bi},i}$ as pressure before an injection, all 50 recorded injections of an injector can be combined into one signal.
This can be done because there is only a small difference between real and shifted rail pressures. Differences in injector behavior (e.g. higher injection quantity, because of higher rail pressure) are so small that they can be neglected.
However, $p_{\mathrm{r,bi,i}}$ is not constant, too. The mean value from all data points before an injection is calculated for one run in order to compensate rail oscillations or measuring noise. In the shown example in Figure 8.1 that would be 6 data points for the first run (7th data point is at the start of the injection). The number of measuring points for the creation of $p_{\mathrm{r,bi,i}}$ results from the fixed end of the pump process and the injection time.

In practical operation approximately constant load points are very often present. This means that the detection program can be carried out during normal engine operation without affecting the work of the machine. However, fixed rail pressure, fixed injector pulse duration of one injector and deactivation of multiple injections can worsen exhaust emissions. This should be considered in series production to stay inside the emission regulations. Since effects of injector deposits are particularly well detectable with large injection quantities, detection mode is only started with an injection quantity $m_{\mathrm{inj,ecu}}$ of at least 50 mg/str.

8.3 Injector Deposit Detection Model (IDD Model)

The ECU has a processor with a certain clock frequency. Thus all tasks within the ECU are time-based. For example, a “desired start injection angle” within the ECU is converted into a time-based injection. Since the injection does not start instantaneously when energizing the injector (section 3.5), the ECU contains tables for opening and closing delay of the injector. These tables are based on rail pressure and injector pulse duration. For a “desired start of injection angle”, the ECU calculates the set-point start of injection pulse $T_{\mathrm{sip,ecu}}$. Based on this injection pulse, the starting point of sampling is shifted (see. Figure 8.1).
Furthermore, the duration of the pulse is determined based on desired injection quantity and current rail pressure (section 4.6). Since each injector is slightly different, correction factors are stored in the ECU. These are provided by manufacturers for each injector. This compensates differences in opening delay, closing delay and injector flow rate, as long as injectors are new. With stored data, “set-point end of injection pulse” ($T_{\mathrm{eip,ecu}}$) can be calculated. As these injector characteristics are only known for diesel fuel, onboard injector diagnosis is only carried out with diesel in this work. However, if the set-point injector characteristics are known for other fuels, presented methods are in principle possible for any fuel.

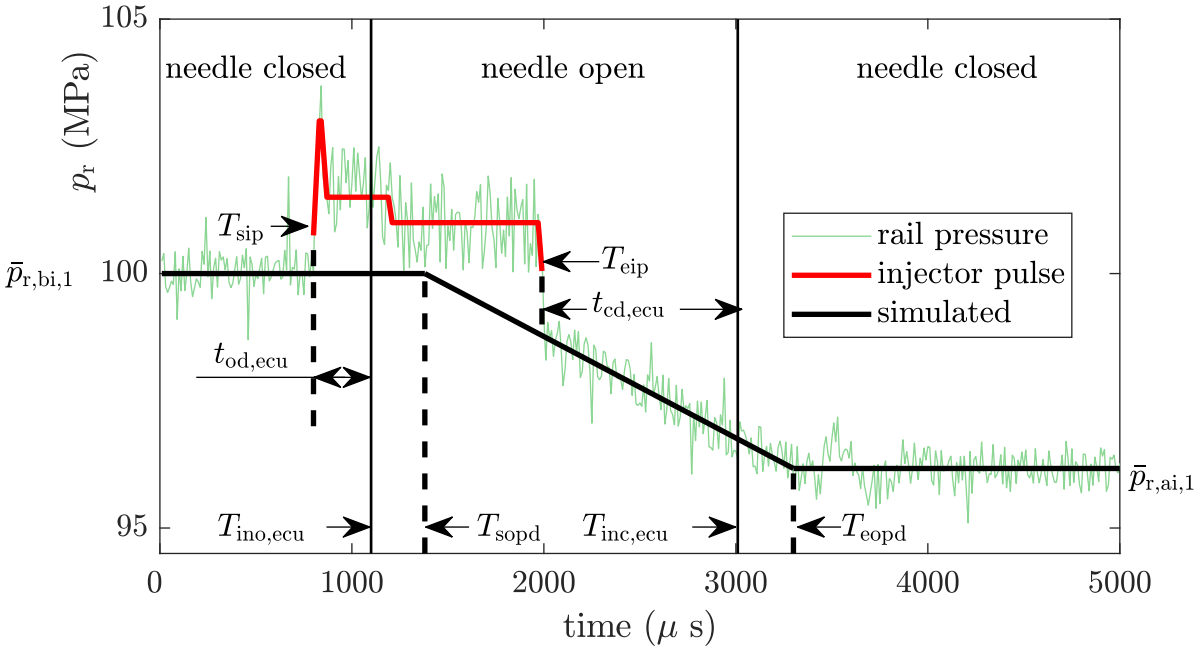

Figure 8.3: 50 recorded injections combined to high resolution rail pressure signal with new injector

8.3.1 Calculating Model Parameters

After recording 50 runs the measured data is merged into a virtual rail pressure signal (Figure 8.3). As an example, only injector 1 is examined in this chapter at the following load point: $t_{inj,ecu} = 1200\,\mu s$ and $p_{r,ecu} \approx 98\,MPa$.

The high-resolution rail pressure signal generates a lot of information on injector behavior, which is not recorded in series operation. It is noticeable that the rail pressure rises before it drops. The reason for this is the high current of the injector actuation, which has a large disturbance influence on the rail pressure signal measurement. This interfering signal cannot be prevented without changing the standard wiring harness and ECU. The cause of this error could not be clarified conclusively, since the signal is already disturbed on the ECU. A larger noise of the signal can be explained by inductance and the pulse width modulated controlled injector current. However, the offset cannot be explained by inductance. Since the interference signal already affects the supply voltage of the rail pressure sensor, interactions between the high injector current and the voltage controller are likely.

A typical injector current curve of a solenoid coil injector can be seen in the rail pressure signal (Figure 8.3 red). The noisy signal prevents direct determination of T_{sopd} (time at the start of pressure drop) from the signal. Advantageous of the disturbance signal is that the actual pulse duration sent to the injector can be measured. So the desired pulse duration can be compared with the actual measured pulse duration. Since the interference signal cannot be eliminated without hardware changes and is therefore also present in series vehicles, the signal is not suppressed on the test bench (potentially possible by shielded cables and external voltage supply of the sen-

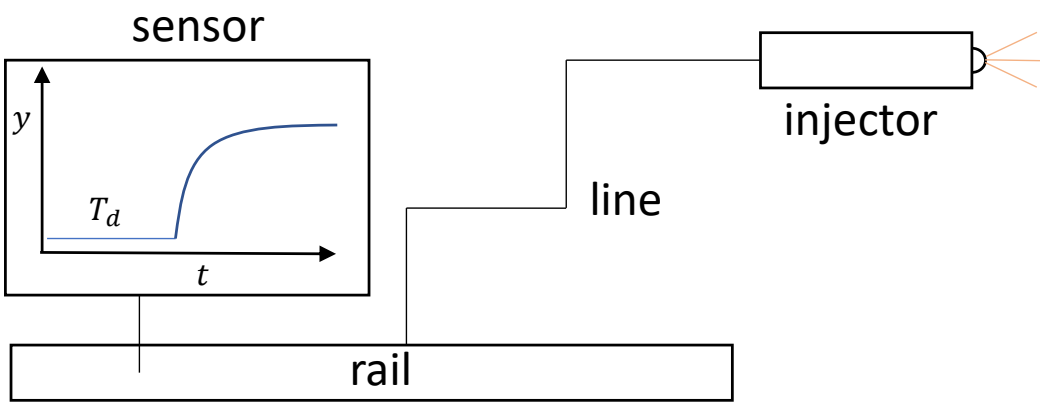

Figure 8.4: Principle of delayed rail pressure measurement

sor). In a fault-free condition the real injector pulse starts at the same time as defined in the ECU $T_{\text{sip,ecu}} = T_{\text{sip}}$. The same applies to the end of the pulse $T_{\text{eip,ecu}} = T_{\text{eip}}$.
The high-resolution injector signal is mathematically evaluated in the following. For better illustration the calculated values are entered in Figure 8.3.

The set-point opening delay $t_{\text{od,ecu}}$ is stored in the ECU (for illustration also drawn in Figure 8.3), so that the right time can be chosen to energize the injector. The time at which the injector needle should be open

$$T_{\text{ino,ecu}} = T_{\text{sip,ecu}} + t_{\text{od,ecu}} \tag{8.3}$$

can be calculated. With set-point closing delay ($t_{\text{cd,ecu}}$), the time at which needle should be closed ($T_{\text{inc,ecu}}$), can be calculated analogously from:

$$T_{\text{inc,ecu}} = T_{\text{eip,ecu}} + t_{\text{cd,ecu}} \tag{8.4}$$

It is obvious that the time from the end of the pressure drop (T_{eopd}) does not match $T_{\text{inc,ecu}}$ (Figure 8.3). The reason for this is the measurement delay between the rail pressure sensor and real pressure (Figure 8.4). The main reason for the delayed measurement is the distance the pressure wave has to travel from the tip of the injector to the position of the rail pressure sensor. In addition, there is a relatively short dead time (response time) T_{d} of the sensor. Figure 8.4 shows the principle procedure.

However, this sensor delay can be measured indirectly. The end of the pumping process is always at the same crank angle due to a fixed transmission ratio between high-pressure pump and crankshaft (section 3.2). By measuring the time from the moment at which the high-pressure pump is at the top dead center $T_{\text{ep},i}$ (via engine speed sensor) to the end of the pumping process determined by the rail pressure signal $T_{\text{ep,r},i}$, the sensor delay

$$t_{\text{sd,meas,i}} = T_{\text{ep,r},i} - T_{\text{ep},i} \tag{8.5}$$

can be determined (comp. Figure 8.5).

The principle is explained in Figure 8.5. At $T_{\text{ep},1}$ the piston of the high pressure pump is at the top dead center. The end of the pressure increase is measured at the time $T_{\text{ep,r},1}$ due to the sensor

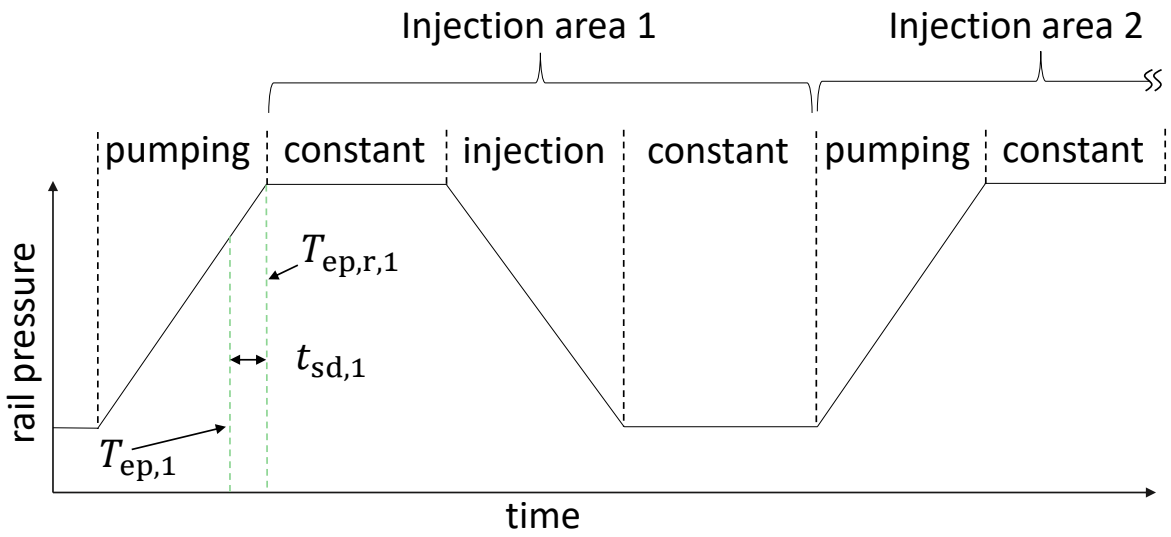

Figure 8.5: Sensor delay measurement principle (moment of pump end $T_{ep,1}$ determined by fixed gear ratio and engine speed sensor for injector 1)

delay. The sensor delay measured in this way is assumed to be constant for the entire injection area 1 (Figure 8.5). A new sensor delay is measured at the next injection of the next injector. The slight differences in speed of sound due to different rail pressures (before and after an injection) are neglected.

To classify the injector, real opening delay ($t_{od,real}$), closing delay ($t_{cd,real}$), total needle opening time (t_{ino}), as well as injected fuel mass (m_{inj}) must be determined.
Individual calculation steps are described below (all refer to a single injector for which the data were recorded by 50 runs):

Step 1:

Start (T_{sip}) and end (T_{eip}) of the injector pulse can be determined by maximum and minimum slope of rail pressure signal in the range of an injection. Mathematically, this is done by forming a difference quotient where f is the recorded signal:

$$T_{sip} = \text{index}\left(\max\left(\frac{f(t+10\,\mu s)-f(t)}{10\,\mu s}\right)\right) \tag{8.6}$$

$$T_{eip} = \text{index}\left(\min\left(\frac{f(t+10\,\mu s)-f(t)}{10\,\mu s}\right)\right) \tag{8.7}$$

Step 2:

By comparing set-point times ($T_{sip,ecu}$, $T_{eip,ecu}$) of the injector control with T_{sip} and T_{eip}, an incorrect injector pulse can be detected. A tolerance of $\pm 20\,\mu s$ is allowed for start and end points, due to measurement frequency. If the deviation is greater, a fault is detected. This fault will be used in section 8.6 and has no influence on deposit detection since measured values for injector pulse (T_{sip} and T_{eip}) are used. A reason for a large deviation between $T_{sip,ecu}$ - T_{sip} and $T_{eip,ecu}$ - T_{eip} could be e.g. chip tuning with enlarged pulse durations or other electrical problems.

Step 3:

To be able to determine T_{sopd}, despite the injector interference signal, an equalizing line is created in the undisturbed injection area after the injection pulse (Figure 8.3 green). To calculate the gradient during an injection, measured values 30 µs after T_{eip} (to make sure there is no interference) up to $T_{\text{inc,ecu}}$ (to make sure there is still a decreasing rail pressure) are used.

Step 4:

T_{sopd} can be determined by the time at which the equalizing line reaches the value $\bar{p}_{\text{r,bi},i}$.

Step 5:

The average pressure after injection ($\bar{p}_{\text{r,ai},i}$) is calculated by averaging all measured values between 1500 µs after $T_{\text{inc,ecu}}$ up to end of data (high-pressure pump delivering fuel). This ensures that the mean value is calculated after T_{eopd} and any rail vibrations that occur due to closing the needle do not falsify the calculation.

Step 6:

T_{eopd} is calculated by the time at which the equalizing line reaches the value $\bar{p}_{\text{r,ai},i}$.

Step 7:

Total needle opening duration can be calculated with:

$$t_{\text{ino}} \approx t_{\text{ino,sim}} = T_{\text{eopd}} - T_{\text{sopd}} \tag{8.8}$$

Relative calculations in this context are not entirely accurate since different rail pressures at T_{sopd} and T_{eopd} have an influence on speed of sound of the fuel and thus on sensor delay. However, the difference can be neglected in comparison to the sampling rate of 10 µs.

Calculated needle opening time (1920 µs) for the new injector in Figure 8.3 corresponds well with the set-point needle opening time (1908 µs) from ECU tables.

Step 8:

Analog to section 7.4 the injected fuel mass can be calculated.

$$m_{\text{inj,rbfe,idd}} = (\rho_{\text{bi}} - \rho_{\text{ai}}) \cdot V_{\text{hps}} - m_{\text{leak}} \tag{8.9}$$

Densities and m_{leak} are calculated from look-up tables analog to section 7.4. The calculated mass for the new injector was 52.0 mg in the example load point of Figure 8.3. This is at the same level as measured injection mass of 51.6 mg. With 51.4 mg the injection quantity set-point was slightly below the measured value. Slight deviation between set-point and measured fuel consumption could be due to a lack of temperature adjustment in the ECU or measurement noise.

Step 9:

Opening delay ($t_{\text{od,sim}}$) of the injector can be calculated:

$$t_{\text{od,sim}} = T_{\text{sopd}} - t_{\text{sd,meas}} - t_{\text{sip}} \tag{8.10}$$

For the new injector in the shown example an opening delay of $t_{\text{od,sim}} = 300\,\mu\text{s}$ is calculated. This is very accurate compared to the theoretical opening delay of 302 µs. The closing delay is calculated analogously:

$$t_{\text{cd,sim}} = T_{\text{eopd}} - t_{\text{sd,meas}} - t_{\text{eip}} \tag{8.11}$$

The model calculates a closing delay $t_{\text{cd,sim}} = 1000\,\mu\text{s}$. Set-point closing delay $t_{\text{cd,ecu}}$ is 1010 µs, so the model is one sampling point off.

Step 10:
In the last step, differences between computed parameters and set-points are calculated. The set-point opening delay ($t_{\mathrm{od,ecu}}$) is subtracted from the calculated opening delay:

$$\Delta t_{\mathrm{od}} = t_{\mathrm{od,sim}} - t_{\mathrm{od,ecu}} \tag{8.12}$$

The difference in closing delay is

$$\Delta t_{\mathrm{cd}} = t_{\mathrm{ino,sim}} - t_{\mathrm{cd,ecu}}, \tag{8.13}$$

wherein the set-point closing delay ($t_{\mathrm{cd,ecu}}$) is subtracted from modeled closing delay. Difference in the needle open time can be calculated analogously by subtracting the set-point of needle open duration $t_{\mathrm{ino,ecu}}$:

$$\Delta t_{\mathrm{ino}} = t_{\mathrm{ino,sim}} - t_{\mathrm{ino,ecu}} \tag{8.14}$$

Percentual deviation of the simulated injection mass $m_{\mathrm{inj,rbfe,idd}}$ from the desired injection quantity $m_{\mathrm{inj,ecu}}$ is represented by a factor:

$$F_{\mathrm{inj,idd}} = \frac{m_{\mathrm{inj,rbfe,idd}} - m_{\mathrm{inj,ecu}}}{m_{\mathrm{inj,ecu}}} \tag{8.15}$$

EDID are not detected based on $F_{\mathrm{inj,idd}}$. There are theoretically injector states where effects of EDID are compensated by IDID (e.g. EDID reduces flow through injector. Parallel longer total needle opening times, because of IDID, increases injected fuel so $F_{\mathrm{inj,idd}} \approx 0$).
For this reason the dimensionless size

$$\gamma = \frac{A_{\mathrm{dep}}}{A_{\mathrm{new}}} \tag{8.16}$$

relates the cross section of injection holes between new injector (no deposits) and an injector with deposits.
It is assumed that the injector opening time is proportional to the injection mass and γ has a linear effect on injection mass, too. This assumption can be made if nozzle holes are considered simplified as an orifice. For an orifice (according to Bernoulli and law of conservation of mass) applies

$$Q = \alpha \cdot A \cdot \sqrt{\frac{2\Delta p}{\rho}}, \tag{8.17}$$

where Q is the volume flow, α is a flow coefficient, A is the cross-section, ρ is the fluid density and Δp is the pressure drop across the orifice. γ is considered as a reduction of A, so γ has a linear influence on volume flow. It is assumed, that the density does not change during an injection ($V_{\mathrm{hps}} >> m_{\mathrm{inj}}$). An extended needle opening time can be considered just like a smaller cross section of the injector holes as a linear effect on mass flow.
To be able to make a statement about EDID the difference in cross section is assumed as

$$\gamma = F_{\mathrm{inj,idd}} - \frac{\Delta t_{\mathrm{ino}}}{t_{\mathrm{ino,ecu}}}. \tag{8.18}$$

That means if the mass flow through the injector decreases in the same proportion as the injector needle opening time, EDID is not assumed (IDID more likely).

Table 8.1: Limits of simulated parameters for injector classification

class	injector status	Δt_{od} (µs)	Δt_{cd} (µs)	Δt_{ino} (µs)	γ (%)
A	injector new	<10	<30	<30	> -2
B	injector still good	<15	<50	<50	>-7
C	change/clean injector at next service	<25	<80	<80	>-10
D	replace injector as quickly as possible	≥25	≥80	>80	<-10

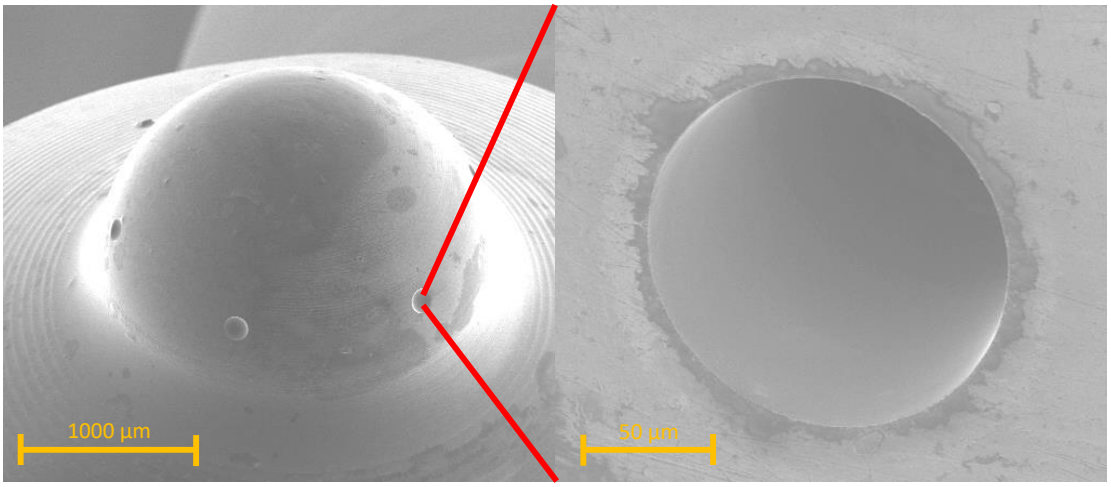

Figure 8.6: New injector: overview (left), nozzle hole (right)

Δt_{od}, Δt_{cd}, Δt_{ino} and γ are stored on the control unit. To classify the injector, mean values over 10 evaluated load points of Δt_{od}, Δt_{cd}, Δt_{ino} and γ are calculated. This compensates influence of relatively inaccurate recording resolution. A record value shifted by one measuring point can result in a relatively large deviation, especially at the opening delay.
Four classes are distinguished. If all mean values lie within a tolerable range, the injector is classified as “Injector new”. As soon as individual variables deviate, a distinction is made between “Injector still good”, “Change/clean injector at next service” and “Replace injector as quickly as possible” depending on deviation. Limit values for respective averaged parameters are shown in Table 8.1.

The worst case always determines the injector status. If three features classify the injector as “Injector new” and one parameter indicates an “Change/clean injector at next service”, the total classification will be “Change/clean injector at next service”.

The reason for a very good matching of the model to nominal values of the ECU in the shown example is the new condition of the injector. A scanning electron microscope image of the new injector is shown in Figure 8.6 in order to have a comparison to deposit injectors. The picture shows the surface of the injector nozzle is clean and smooth. There are sharp edges on the injector nozzle holes. These lead to a good flow of fuel and a good spray. Around the nozzle hole slight color changes can be seen. These are not deposits but material changes due to the manufacturing process of nozzle holes.

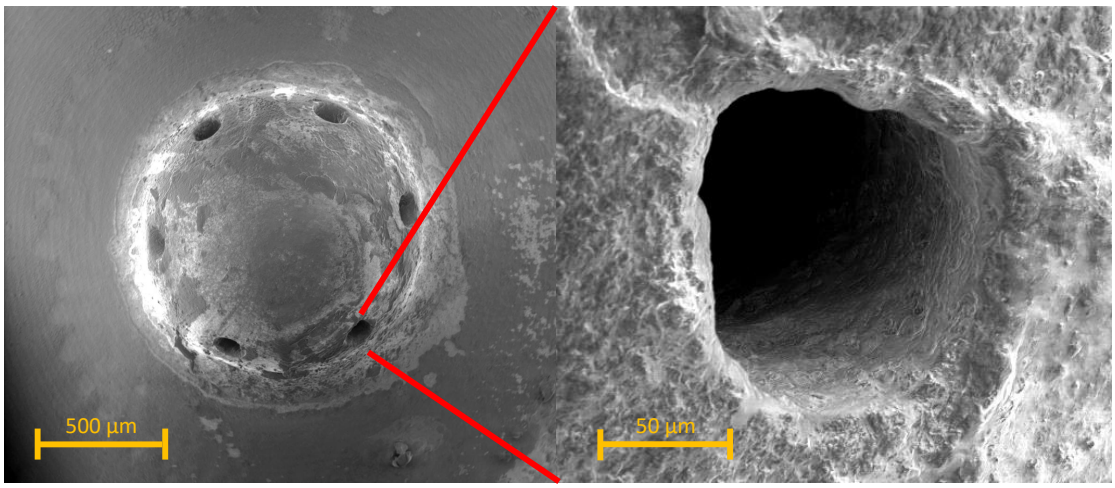

Figure 8.7: Deposit injector: overview (left), nozzle hole (right)

8.3.2 Results for Injector Deposit Detection

The presented detection algorithm is tested with an injector having deposits in this section. Deposits of the investigated injector were produced by approx. 500 h operation in a tractor with canola oil fuel according to DIN 51605 without fuel additives. After this time, internal and external deposits formed (Figure 8.7). External deposits are relatively easy to see through an electron microscope on the nozzle tip and injection holes. A slight coking on nozzle tip has no direct influence on injector function.
However, deposits in or at the nozzle holes (right picture) reduce the effective cross section and injector flow. Compared to the new injector (Figure 8.6), the cross-sectional area is reduced by 0.5-11%, depending on examined nozzle hole. The strongest reduction of 11% is shown in Figure 8.7 on the right. Due to a changed shape of the nozzle hole and deformed edges it can be assumed that the spray pattern is significantly deteriorated. This leads to a disturbed combustion and therefore to an increased fuel consumption and increased HC and CO emissions.

For better comparability, the deposit injector is operated under identical conditions (same rail pressure and injector pulse duration) as the new injector from Figure 8.6. Since the deposit injector is not the very same injector, the injection quantity set-point belonging to injector pulse duration of 1200 µs is not the same. Due to different injector correction factors, the target injection quantity is 50.6 mg compared to 51.4 mg of the new injector. The rail pressure curve hardly differs from the curve of the new injector (Compare Figure 8.3 and Figure 8.8). Biggest difference to the new injector can be seen in distance of $T_{\mathrm{inc,ecu}}$ to T_{eopd}. The values for T_{eopd} and $\bar{p}_{\mathrm{r,ai},i}$ of the injector from Figure 8.3 are entered in Figure 8.8 as “no deposits”. Measured fuel consumption of 47.7 mg is approx. 5.7% lower than target value of 50.6 mg. Detection model calculates a fuel consumption of 47.2 mg and is thus ca. 1% to low compared to measured value.
For an injector classification at least 10 load points should be evaluated. For this reason the deposit injector is operated at different load points and the detection algorithm is started. Load points and calculated features are shown in Table 8.2.

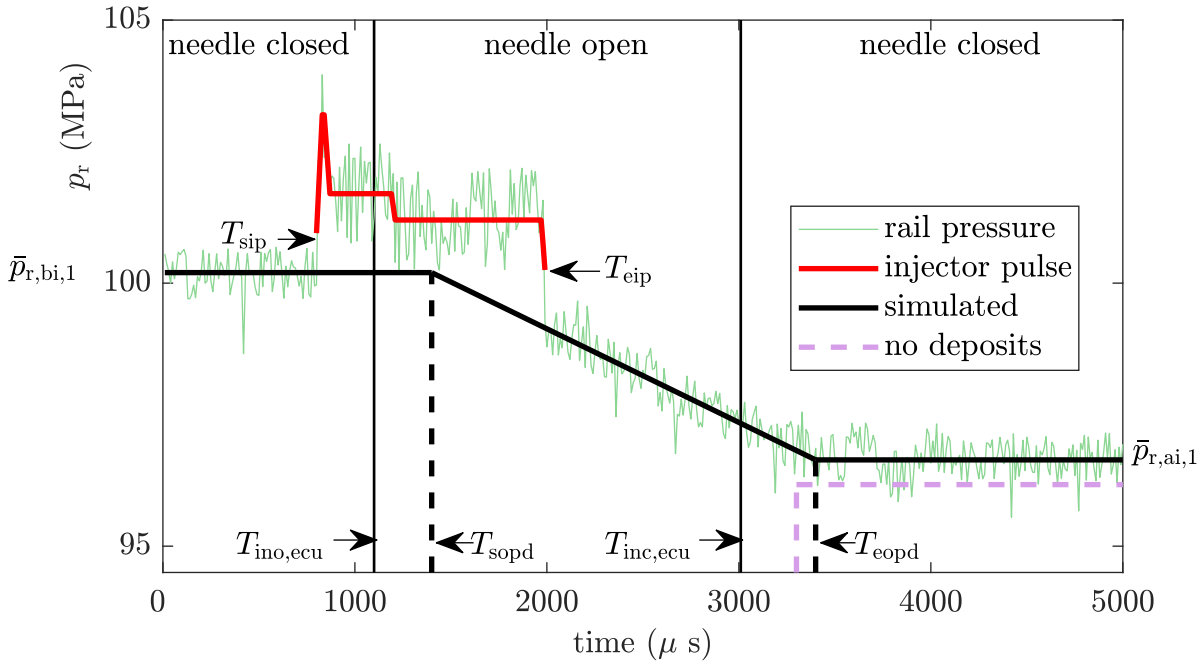

Figure 8.8: 50 recorded injections combined to high resolution rail pressure signal with deposit injector (T_{eopd} enlarged, $\bar{p}_{r,ai,i}$ higher in comparison to Figure 8.3)

Table 8.2: Simulated data of the *Injector Deposit Detection Model* for 10 evaluated load points

$p_{r,set}$ (MPa)	t_{inj} (µs)	$t_{od,ecu}$ (µs)	Δt_{od} (µs)	$t_{cd,ecu}$ (µs)	Δt_{cd} (µs)	$t_{ino,ecu}$ (µs)	Δt_{ino} (µs)	Δm (%)	γ (%)
50	1200	322	28	796	84	1674	56	-2.6	-6.0
50	1800	322	18	1230	80	2708	62	-4.1	-6.4
50	2400	322	18	1680	70	3758	52	-5.7	-7.1
100	1200	302	18	1010	80	1908	62	-3.5	-6.8
100	1800	302	-2	1629	71	3127	73	-3.7	-6.0
100	2000	302	8	1853	77	3551	69	-4.8	-6.8
150	1200	285	15	1149	61	2064	46	-4.4	-6.6
150	1400	285	5	1380	70	2495	65	-4.9	-7.5
200	800	273	-3	761	69	1288	72	-0.2	-5.8
200	1200	273	7	1288	82	2215	75	-2.7	-6.1
mean value			11.2		74.4		63.2		-6.5
classification			B		C		C		B

After averaging over 10 examined load points, the injector is classified as “"Change/clean injector at next service”. A reason for significantly increased closing delay could not be fully clarified. Most likely are increased actuating forces of the injector needle. This is indicated by the tendency towards higher opening delays at low rail pressures and closing delays independent of the rail pressure. For the classification of the injector the cause of the deposits is not important as long as the injector deviates from its normal behavior.

8.4 Conclusion of the On-Board Injector Deposits Detection System

The *IDD Model* shows great potential and good results for higher load points. The injectors are classified so that the operator of the machine can decide if injectors should be changed for higher reliability or remain installed.
Advantageous of the presented model is that a high resolution can be achieved with an initially limited sampling rate of the ECU. A disadvantage is that the assumption the injector behaves identically with each pass of sampling. Especially with injectors with deposits it could happen that shifted opening and closing delays do not occur identically with every injection. It is therefore conceivable that deposits on the injector needle sometimes lead to an extended opening delay and sometimes not. If this occurs within the 50 recorded injections, a highly noisy overall signal in the T_{eopd} range will be produced. This behavior did not occur in the performed tests but it should be considered in a possible serial development. Therefore many tests are still necessary for a potential series application. However, results of the *IDD Model* show great potential for cost-effective onboard detection of injectors.

It is also conceivable that the model will only be executed at the dealer. In this way, defective injectors can be detected or the service life of injectors can be estimated. Since no injectors have to be removed to classify the condition, the downtime of machines can be reduced considerably. In addition, injectors can be replaced as required, instead of changing all. This significantly reduces operating costs.
As the presented on board injector classification is a fundamentally new approach, a lot of information regarding injector deposit formation can be collected. Especially with telemetry many different machines at different operating conditions can be evaluated. Thus, the injector status of many machines worldwide can be stored and evaluated regarding external influences. This could give a competitive advantage over other engine manufacturers regarding the development of new injection systems or strategies to prevent deposit formation.

Another small limitation is that the model only works for higher injection masses. With small injection masses the pressure difference is not sufficient to make an exact statement. Therefore the model is only started at minimum injection masses $m_{\mathrm{inj,ecu}}$ of 30 mg/str.

To use the detection model with fuels deviating from diesel, injector data has to be provided by injector manufacturers. The accuracy of the model is not sufficient for determining set-point

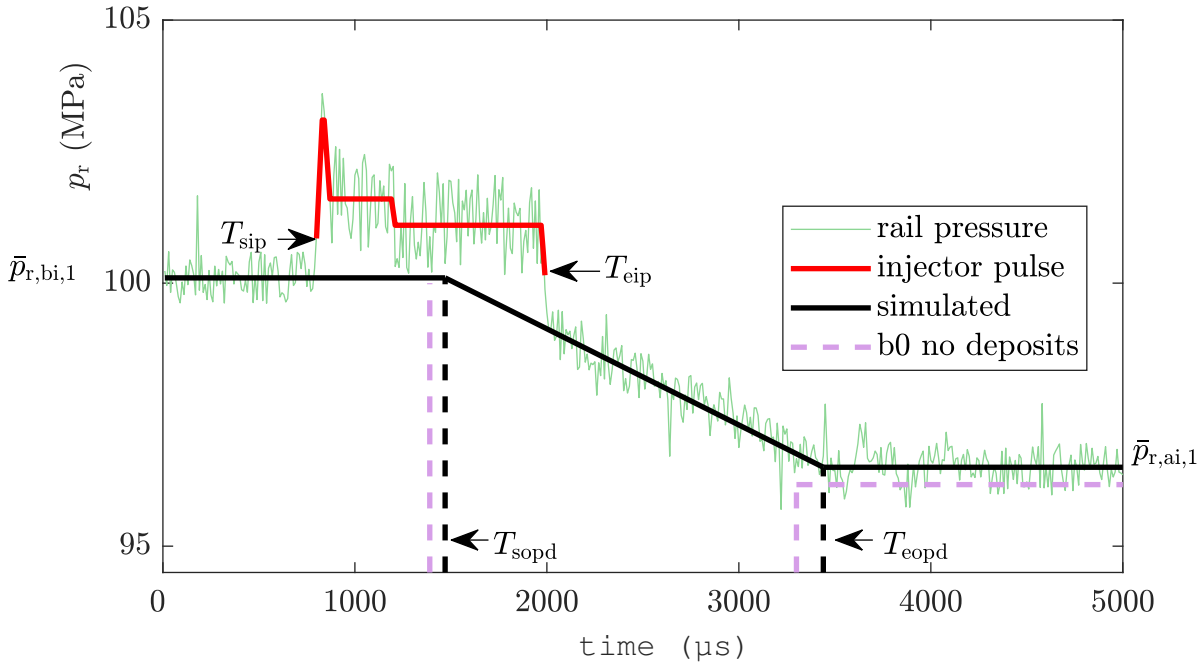

Figure 8.9: 50 recorded injections combined to high resolution rail pressure signal with new injector in NRO operation at $t_{inj,ecu} = 1200\,\mu s$ and $p_r = 100\,MPa$

values (measured values for a new injector could be regarded as set-points), so presented model only works for pure diesel fuel. However, with the appropriate injector data the model should work for all fuels in principle.
In the next section, the *IDD Model* was operated with NRO in order to have a comparison to the injector behavior with diesel.

8.5 Using IDD Model with Natural Rapeseed Oil

As already described, important injector information for NRO (set-points opening delay, set-points closing delay) is missing for deposit detection in NRO operation. However, in the following the new injector from Figure 8.3 was tested with NRO. Only calculated values are entered in Figure 8.9. The comparison to Figure 8.3 reveals the later opening T_{sopd} and closing T_{eopd} time of the injector. With the same injector pulse duration as in B0 mode, the time in which the injector needle is open is approx. 80 µs or approx. 6% greater in NRO operation (closing delay is more increased than the opening delay).
The injected fuel mass is increased by approx. 1% in the NRO operation (compare also Figure 5.1). This means that with the help of the *IDD Model* the injection behavior in NRO operation can be understood better. In further work it has to be investigated, if extended injector closing delays are valid for all load points and different fuel temperatures in NRO operation.
This example shows that the *IDD Model* can be used not only for the detection of deposits but also for further investigations of the injection process.

8.6 Note on Injector-Pulse-Tuning Detection with IDD Model

As described in section 8.3 the injector pulse interferes with the rail pressure signal. This means that the real injector pulse duration can directly read out the measured rail pressure signal. In this way injector-pulse-tuning can be determined. For this purpose the desired injector pulse duration is compared with the duration of the disturbance signal (Equation 8.6). If T_{sip} or T_{eip} deviates by more than $\pm 20\,\mu\mathrm{s}$, a fault is detected. If there is a big deviation (real injector pulse is much longer, than set-point value), chip tuning could be stored in the ECU.

However, by isolating cables of rail pressure and injector signals this detection can be easily bypassed. Also the absence of the disturbance signal can be detected as a fault or interference in the engine system. With clever isolation or by installing tuning chips close to injectors, the original interference signal can be preserved, although the real injector pulse duration is significantly longer. It can also not be excluded that the interference will be eliminated with new engine generations by the manufacturer. In order to be able to detect chip tuning nevertheless, the already presented chip tuning detection models are necessary.

9 Tuning Independent Fault Detection in the High Pressure System

There are many other faults that affect the detection models already presented. The two most common ones are leaks in the high pressure system and a defective high pressure pump. These affect especially the chip tuning detection. In this chapter two models are presented with which a leakage and a defective high pressure pump can be detected independently of the chip tuning detection.

9.1 High Pressure System Leakage Detection Model (HL Model)

As already described in chapter 1, fuel leaks during engine operation are not only dangerous for the environment, but also increase the risk of fire on machines and thus are a danger to the driver. A leakage in the high pressure system leads to a further open SCV (closed control loop of the high pressure system). Therefore an increased fuel mass, due to a leakage, could be detected with the *SCV Model* from section 7.5. However, it is not possible to differentiate between chip tuning and leakage with the *SCV Model* only. For this reason, a method is presented to detect leaks in the high-pressure system of a common rail engine independently of the used fuel and probably existing tuning measures.
In the test series carried out, a leakage was caused on purpose by a damaged seal in the connecting line from the high-pressure pump to the rail. A similar algorithm as that of the *RBFE Model* (section 7.4) is used for detection. In contrast to averaging rail pressures inside constant pressure zones, a gradient within the rail pressure zone is evaluated.
Pressure zones have a constant rail pressure in average between pumping and injection processes in fault-free state. If pressure values drop within a zone as crankshaft rotation progresses, a leakage is indicated. The principle is shown in Figure 9.1.

Since the rail pressure signal is disturbed by the injector pulse (section 8.3), only values before the injector pulse occcurs (start time of injector pulse is known in the ECU), are used for the gradient. The calculation is done by forming a straight line (using the least squares method) within each rail pressure zone:

$$p_{\mathrm{r}}(\varphi) = p_{\mathrm{r,start}} + g_a \cdot \varphi \tag{9.1}$$

The start of the straight line can be calculated via

$$p_{\mathrm{r,start}} = \bar{p}_{\mathrm{r,a}} - g_a \cdot \bar{\varphi}_a, \tag{9.2}$$

where g_a can be calculated via:

$$g_a = \frac{\sum_{k=1}^{n} (\varphi_{a,k} - \bar{\varphi}_a)(p_{\mathrm{r},a,k} - \bar{p}_{\mathrm{r},a})}{\sum_{k=1}^{n} (\varphi_{a,k} - \bar{\varphi}_a)^2}. \tag{9.3}$$

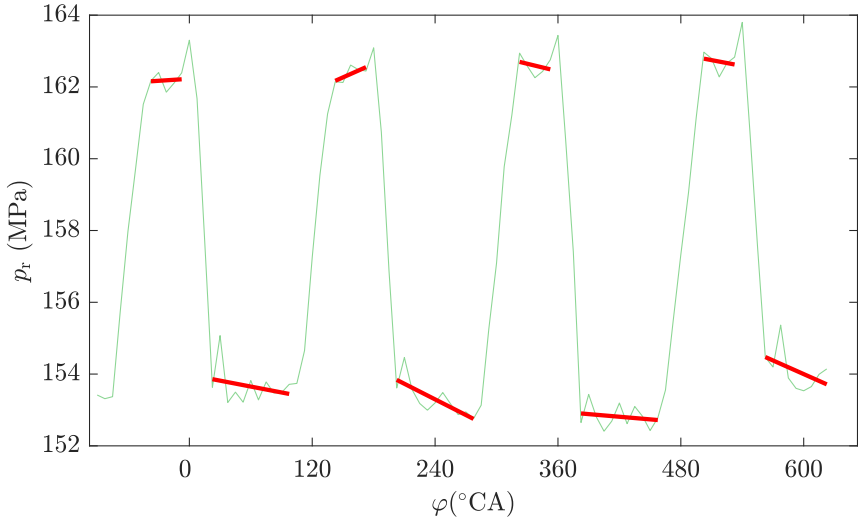

Figure 9.1: Rail pressure signal with intentional constant leakage and plotted gradients in the contant pressure zones

In this equation φ is the crankshaft angle, n is the number of measuring points within a pressure zone and a the number of the recorded rail pressure zone. As can be seen in Figure 9.1, the gradient can be positive even if a leakage is present (approx. −30 °CA and 150 °CA). The reason for this is the relatively slow scanned rail pressure signal (one data point every 7.5 °CA). Errors can occur in the data due to superposition effects or rail pressure oscillations. Therefore, all recorded gradients are subsequently averaged over 100 rail pressure zones.

$$\bar{g} = \frac{\sum_{a=1}^{100} g_a}{100} \tag{9.4}$$

Measurement inaccuracies and fluctuations are compensated this way. Since the zones are only fully developed at larger injection quantities, the detection model is only started for injection quantities of at least 30 mg.
In the shown example (Figure 9.1) the averaged gradient is −0.0028 MPa/°CA. If 100 rail pressure zones have been recorded in a stationary load point, the leakage quantity can be calculated for one crankshaft revolution

$$m_{\text{leak,hps}} = (\rho(\bar{p}_r) - \rho(\bar{p}_r + \bar{g} \cdot 360\,°\text{CA})) \cdot V_{\text{hps}}, \tag{9.5}$$

where $\bar{g}$ is the gradient and $\bar{p}_r$ the mean rail pressure over all recorded data points.
In the example shown, this corresponds to a leakage of approx. 12 mg per revolution. Compared to injected fuel mass approx. 6% of the fuel is lost through leakage (injected fuel mass is approx. 100 mg/str). In order for the model to function independently of the fuel and also in unsteady load points, a leakage is only detected based on mean gradient. A leakage is detected if

$$\bar{g} < -0.002\,\text{MPa}/°\text{CA} \tag{9.6}$$

applies. Measurements have shown that the model works in all load points with an injection quantity above 30 mg and single injection. However, effects become particularly apparent at higher rail pressures (leakage quantity increases).

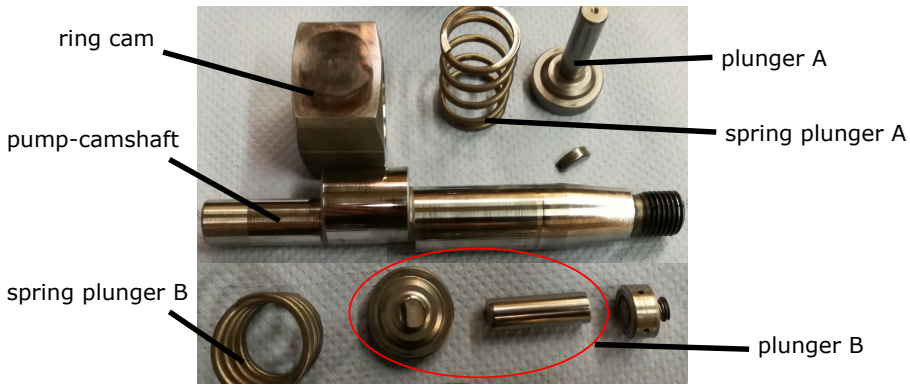

Figure 9.2: Broken plunger of test engine

If a leakage is detected, the chip tuning detection models are deactivated. This prevents a false positive chip tuning detection.

9.2 Broken High-Pressure Pump Detection Model (BHP Model)

Another fuel and tuning independent model can detect a defective high-pressure pump. Analyses of repairs, carried out by John Deere workshops, revealed a typical defect in the high pressure pump. One of two plungers (section 3.2), which are responsible for fuel compression, breaks. Since the high-pressure pump is over sized, this defect does not initially lead to engine failure or fault messages.
However, the absence of a plunger leads to a worse transient response of the engine because rail pressure cannot be raised as quickly to the desired rail pressure. This is partly due to the reduced maximum pumpable fuel mass since only one plunger is available. Another reason is a wrong look-up table for feed forward control of the SCV (SCV should be opened approximately twice as wide to get the same amount of fuel into the rail as with two plungers).
If the second plunger fails after a certain operating time, there is immediately a total failure of the machine. A broken plunger also appeared unplanned on the test bench directly after setting up the engine.

In Figure 9.2 elements of the high pressure pump used on the test bench can be seen. The damage pattern is similar to that of many high-pressure pumps examined in-house, namely a smooth fracture of the plunger. A smooth fracture could indicate a lateral load on the plunger. A plausible explanation would be adhesion forces holding the plunger on the ring cam during the first rotation of the engine. This leads to engines leaving the factory with broken plungers.
It is also conceivable that too little lubrication on the plunger is applied at the first run of the engine. This could be a lack of fuel and therefore lateral forces press on the plunger. It also cannot be ruled out that this is a material or manufacturing defect of the pump producer. To prevent defective engines from leaving the factory and to ensure defective plungers can be detected during practical use of machines, an on-board detection is carried out in the following.

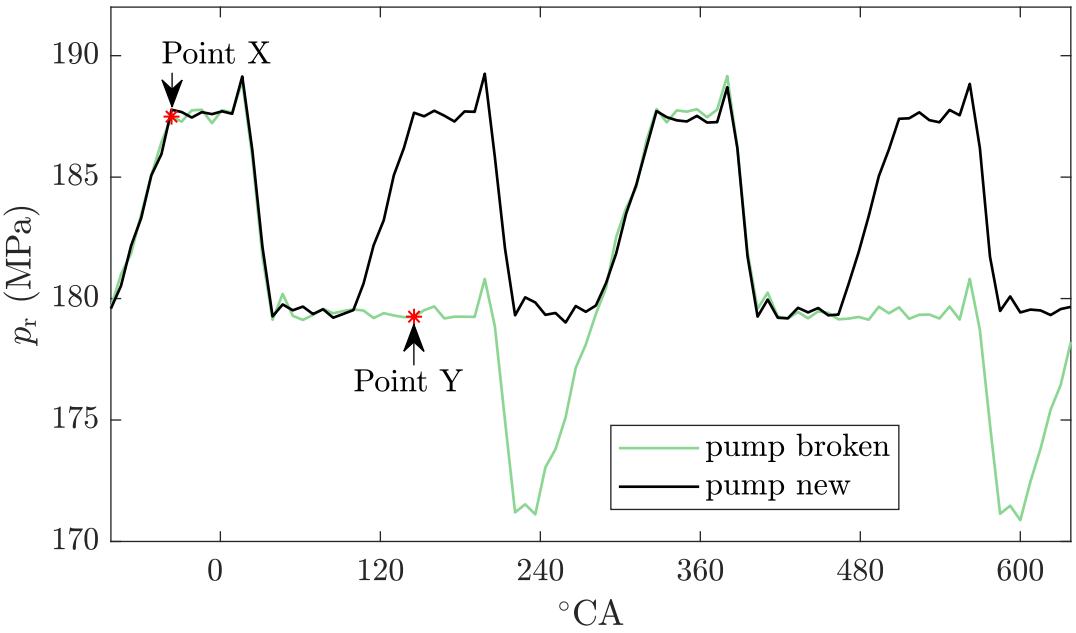

Figure 9.3: Rail pressure curve with broken plunger B in comparison to the faultless rail pressure curve

The test with the broken high pressure pump was performed at the constant load point 1600 rpm and 600 N m. The most obvious effect of a broken plunger is an uneven rail pressure curve (Figure 9.3). The absence of the second plunger is clearly visible, since there are only two instead of four pressure increases in 720 °CA (Figure 9.1). Unequal rail pressures before injections lead to different injection masses between individual injectors, since the injector pulse duration depends only on average rail pressure.

It is easy to distinguish whether plunger A or plunger B (section 3.2) is defective by evaluating the position of pressure rises. If plunger A is fine and plunger B is defective (shown in Figure 9.3), the following behavior is characteristic: In the area before 0 and 360 °BTDC pressure increases take place, as well as no strong pressure increases in the area before 180 and 540 °BTDC.

Mathematically this will be done with a comparison of the pressure curve:

$$\Delta p_{\mathrm{bhp}} = \frac{1}{30\,^{\circ}\mathrm{CA}} \int_{-30\,^{\circ}\mathrm{CA}}^{0\,^{\circ}\mathrm{CA}} p_{\mathrm{r}}(\varphi) - p_{\mathrm{r}}(\varphi - 180\,^{\circ}\mathrm{CA})\mathrm{d}\varphi \tag{9.7}$$

The integral is formed by the absolute angles. That means at 0 °CA, the piston of the first cylinder is at the top dead center. Limits of -30 - 0 °CA were chosen because in this area the pump process of plunger A is completed and the pump process of plunger B has not yet started (if plunger B does not pump more than 2/3 of the maximum volume, which is never the case in stationary load point with an intact pump). Theoretically, it would make sense to compare point X (plunger A at top dead center and plunger B at bottom dead center) with point Y (plunger B at top dead center and plunger A at bottom dead center) because no pumping can be done at this point (compare Figure 9.3). Since this is sensitive to noise and the pump does not deliver maximum pumping

Table 9.1: Decision criterion for the *Broken High-Pressure Pump Detection Model* whether plunger A or B is defective

R_{bhp}	result
>3	plunger A defect
<-3	plunger B defect

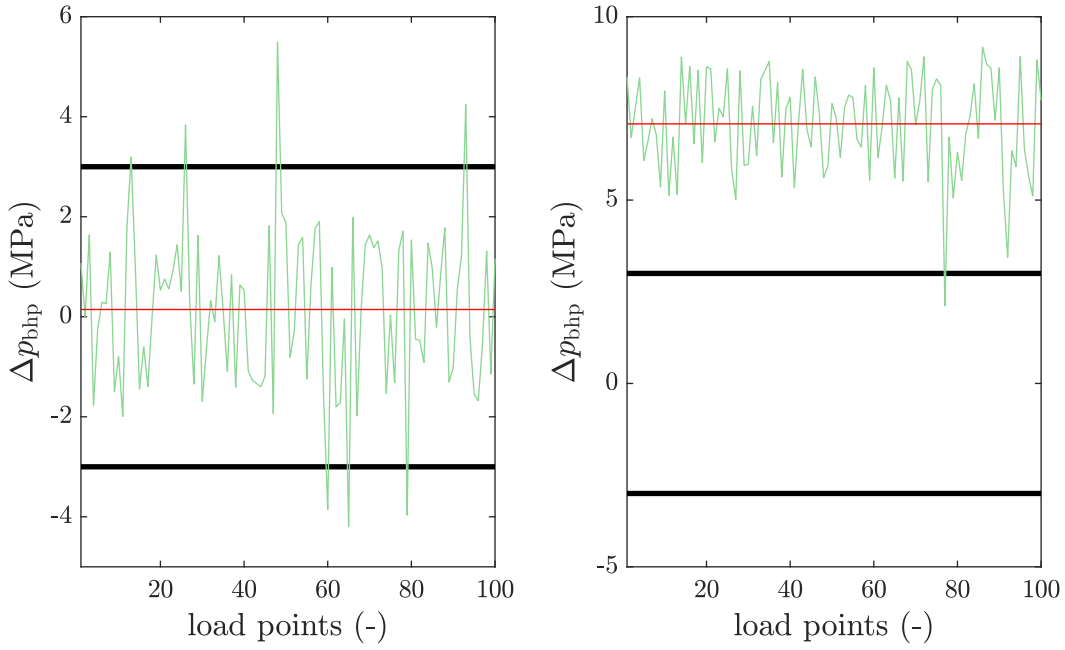

Figure 9.4: Residuum R_{bhp} shown for undamaged pump (left) and broken plunger B (right)

quantity in stationary engine operation, the range between -30 - 0 °CA is selected.
Furthermore, the model is only executed if a stationary load point with $m_{\text{inj,ecu}} > 30\,\text{mg/str}$ applies. For smaller injection quantities the pressure curve is not distinct enough.

A defective high pressure pump is detected when

$$|R_{\text{bhp}}| = |\frac{1}{100}\sum_{l=1}^{100}\Delta p_{\text{bhp},l}| > 3\,\text{MPa} \tag{9.8}$$

applies. The residual is averaged over 100 injections so that sporadically occurring model errors are minimized (compare anomalies in Figure 9.4).
In Figure 9.4 the course of Δp_{bhp} in operation with a faultless (left) and a defective high pressure pump (right) is shown. It is the same stationary load point as in Figure 9.3. R_{bhp} is shown in red. In the left image $|R_{\text{bhp}}| < 3$ applies, so no fault is detected. In the right image $R_{\text{bhp}} \approx 7$ applies, so that a defective plunger B is detected (which is correct).

The model shown is very simple and can be run on the standard ECU. Each John Deere engine is started once before leaving the factory. By executing the model inside the factory it can be ensured

that no defective engine (broken plunger) is installed in new machines. Furthermore, the model can be executed in practical use in regular intervals. If there is a plunger defect, a fault code is stored and the high pressure pump can be changed during the next stay in the workshop.

9.3 Conclusion of Tuning Independent Fault Detection

In this chapter two simple (series ECU capable) models were presented. The first model detects leaks in the high pressure system and prevents incorrectly stored tuning fault messages. Since the model evaluates the rail pressure zones of the *RBFE Model*, hardly any additional computing power is required.

The *BHP Model* can detect a defective high-pressure pump with great certainty. Since the engine can also be operated with only one plunger, the machine does not fail directly. The model can be used to provide an indication so that the machine can be repaired at the nearest workshop.
Since each engine is operated for a short time before being installed in a machine, the *BHP Model* can be used at the end of production line. This prevents that already defective high-pressure pumps are delivered to customers. As this reduces the failure of pumps in the field, the reliability of engines is further increased.

10 Overview of Fault Detection

In the previous chapters, models for specific faults were developed. Good detection results could be achieved. However, only one specific detection model with the corresponding fault was tested. In this chapter the combination of all models with different faults is examined. For this purpose, a fault-symptom table is developed, which shows the effect of different faults on the other fault detection models. Subsequently, cross dependencies are examined while several faults occur at the same time.

Since most engines in the agricultural industry run on conventional diesel and many of the fault models presented in the previous chapters only work for pure diesel, biogenic fuels are not considered in this chapter.

The symptoms of the individual injection mass models (*Oxygen-Fuel, Rail Pressure Based Fuel Estimation, Suction Control Valve* and *DOC Efficiency Model*) are created by comparing the simulated injection mass against the desired fuel quantity which is calculated in the ECU (set-point tables). Results from the *Injector Deposit Detection Model* are also compared against the nominal values of a new injector (set-point values are stored in the ECU too). The broken high pressure pump model symptom is not calculated by comparison with a set-point but by comparison of the rail pressure between two injections (see section 9.2). An exception is the high pressure leakage model which can only output two states: No leakage (0) and leakage detected (1). For the sake of completeness it is included in Table 10.1.

Table 10.1: Overview of symptoms for fault detection via the presented Models

symptom description	calculation
diff. between simulated and desired fuel quant. calculated via *OF Model* using O_2 sensor 1	$s_{\text{of},1} = m_{\text{of},1} - m_{\text{des}}$
diff. between simulated and desired fuel quant. calculated via *OF Model* using O_2 sensor 2	$s_{\text{of},2} = m_{\text{of},2} - m_{\text{des}}$
diff. between simulated and desired fuel quant. calculated via *RBFE Model*	$s_{\text{inj,rbfe}} = m_{\text{inj,rbfe}} - m_{\text{inj,ecu}}$
diff. between simulated and desired fuel quant. calculated via *SCV Model*	$s_{\text{scv}} = m_{\text{inj,scv}} - m_{\text{inj,ecu}}$
diff. between simulated and desired fuel quant. calculated via *DOC Efficiency Model*	$s_{\text{inj,doc}} = m_{\text{inj,doc}} - m_{\text{inj,ecu}}$
diff. of injector opening delay via *IDD Model*	$s_{\text{od,idd}} = t_{\text{od,idd}} - t_{\text{od,ecu}}$
diff. of injector closing delay via *IDD Model*	$s_{\text{cd,idd}} = t_{\text{cd,idd}} - t_{\text{cd,ecu}}$
diff. of injector open time via *IDD Model*	$s_{\text{ino,idd}} = t_{\text{ino,idd}} - t_{\text{ino,ecu}}$
diff. in cross section of the injector holes via *IDD Model*	γ_{idd}
comparison of two injections by Broken High-Pressure Pump Model	$s_{\text{bhp}} = \frac{1}{30\,^\circ\text{CA}} \int_{-30\,^\circ\text{CA}}^{0\,^\circ\text{CA}} p_{\text{r}}(\varphi) - p_{\text{r}}(\varphi - 180\,^\circ\text{CA})\text{d}\varphi$
symptom of high-pressure leakage model, based on gradient	$\begin{cases} s_{\text{hl}} = 1 & \text{if} \quad \bar{g} < -0.002\,\text{MPa}/^\circ\text{CA} \\ s_{\text{hl}} = 0 & \text{if} \quad \bar{g} \geq -0.002\,\text{MPa}/^\circ\text{CA} \end{cases}$

Table 10.2: Fault symptom table (only one fault present at the same time)

symbol	fault	$s_{of,1}$	$s_{of,2}$	$s_{inj,rbfe}$	s_{scv}	s_{doc}	s_{bhp}	s_{hl}	$s_{od,idd}$	$s_{cd,idd}$	$s_{ino,idd}$	$F_{inj,idd}$	γ_{idd}
high inj. quant. general	F1	+	+	+	+	+	0	0	0	0	0	+	+
high inj.quant. 1 injector	F2	(+)	(+)	+	+	0	0	0	0	0	0	+	+
injector-pulse-tuning	F3	+	+	+	+	+	0	0	0	0	0	+	0
rail-pressure-tuning	F4	+	+	0	+	+	0	0	0	0	0	0	0
low inj. qua. general	F5	-	-	-	-	-	0	0	0	0	0	-	-
low inj. qua. 1 injector	F6	(-)	(-)	-	(-)	0	0	0	0	0	0	-	-
HPP plunger defect	F7	0	0	0	0	0	+	0	0	0	0	0	0
suction control valve faulty	F8	0	0	0	+/-	0	0	0	0	0	0	0	0
internal injector deposits	F9	(-)	(-)	(-)	(-)	0	0	0	+	+	+	(-)	0
external injector deposits	F10	(-)	(-)	(-)	(-)	0	0	0	0	0	0	-	-
leakage HPS	F11	0	0	+	+	0	0	1	0	0	0	(+)	(+)
O_2 sensor 1 faulty	F12	+/-	0	0	0	0	0	0	0	0	0	0	0
O_2 sensor 2 faulty	F13	0	+/-	0	0	0	0	0	0	0	0	0	0

0, +, - : Symptom is zero, positive or negative
1: HL-Model detected leakage
(): tendency
+/-: sign depends on operation point

In Table 10.2 the effects of faults on different models are shown. It becomes clear that faults influence different models simultaneously. However, as long as only one fault occurs at the same time, each fault can be detected individually. This is only possible if the injector signal can still be measured indirectly via the interference signal (see. section 8.6). As soon as the interfering signal is prevented (e.g. by special tuning measures mentioned in section 8.6), an e.g. washed-out injector hole (high injection quantity) cannot be distinguished from an injector pulse tuning anymore.
However, if it is not about warranty claims, a detection of deviating injection masses is completely sufficient, so that the injection system can be checked at the next workshop visit.

It is getting even more difficult to isolate individual faults when they overlap each other. For this reason Table 10.3 shows which faults can still be detected with other faults present. The fault in the respective line in Table 10.3 should be detected. If there is a fault (in the column of Table 10.3) at the same time, a “1” indicates that the fault can still be detected. A “0” indicates that the fault cannot be isolated from the other fault. The fault description can be found in Table 10.2.

Many faults can be detected even if another fault is active. For example, fault F1, where the total injection quantity is too high (e.g. washed out injector holes), can still be detected if one injector deviates from the others (as is the case with fault F2). This is possible because the *RBFE Model* can calculate the injection quantity of each injector.
For certain combinations of faults, such as strong external injector deposits and injector pulse tuning, the presented models cannot detect any intervention in the engine control (in the worst case, the reduced injection quantity of the deposits exactly equalizes the increased injection quantity of the injector pulse tuning).
As soon as three or more faults influence the sensors of the injection models (rail pressure, air mass flow, O_2 sensor 1, O_2 sensor 2, fuel temperature and SCV position), no injection mass related faults can be detected (distinguished from each other).
For example, if both O_2 sensors and the SCV value is incorrect at the same time, it is not possible to distinguish which of the three injection models delivers the correct value (*Oxygen-Fuel, Rail Pressure Based Fuel Estimation,* or *Suction Control Valve Model*). In this case the engine could be put into emergency mode similar to current series status, so the next workshop can be reached.

In contrast, there are faults that can be detected even if several sensor values fail or are distorted. For example, a defective high-pressure pump can still be detected even if all faults specified in Table 10.2 are present at the same time. For the *HL Model* only the relative rail pressure curve is important (even if the absolute rail pressure curve is falsified due to e.g. rail pressure tuning).

Table 10.3: Cross check between faults (two faults present at the same time). Fault description in Table 10.2

faults	F_1	F_2	F_3	F_4	F_5	F_6	F_7	F_8	F_9	F_{10}	F_{11}	F_{12}	F_{13}
F_1	-	1	1	1	-	1	1	1	1	1	1	1	1
F_2	1	-	1	1	1	1	1	1	1	1	1	1	1
F_3	1 (0)	1	-	1 (0)	1 (0)	1	1	1	1	1	1	1	1
F_4	1	1	1	-	0	1	1	1	0	0	1	1	1
F_5	-	1	1	0	-	1	1	1	1	1	1	1	1
F_6	1	1	1	1	1	-	1	1	1	1	1	1	1
F_7	1	1	1	1	1	1	-	1	1	1	1	1	1
F_8	1	1	1	1	1	1	1	-	1	1	1	1	1
F_9	1	1	0	0	1	1	1	1	-	1	1	1	1
F_{10}	0	1	0	0	1	1	1	1	1	-	1	1	1
F_{11}	1	1	1	1	1	1	1	1	1	1	-	1	1
F_{12}	1	1	1	1	1	1	1	1	1	1	1	-	1
F_{13}	1	1	1	1	1	1	1	1	1	1	1	1	-

0: fault cannot be detected if second fault is present at the same time

1: fault can be detected if second fault is present at the same time

(): if the injector pulse could not be measured with method from section 8.6

11 Summary

Switching from fossil diesel to alternative fuels is becoming increasingly difficult as modern diesel engines become more complex. Where in the past engines could be operated with different fuels without any adaptations, modern ECU's have many monitoring and diagnostic functions. All these functions were developed for pure diesel fuel only. If the fuel is changed without adapting the ECU, a lot of faults are indicated. These contradict the high level of reliability demanded from agricultural machinery.
In order to ensure the operation of different fuels with high engine reliability, the presented work is divided into a part of *fuel detection*, as well as a part of regular *fault detection*. All detections were carried out with sensors installed in series production.

11.0.1 Fuel Detection

In order to develop a multifuel-capable engine, the fuel system was adapted so that it is suitable for operation with different fuels. In addition, cold starting was improved so that it is possible to start engines running on rapeseed oil at temperatures down to $-5\,^{\circ}\mathrm{C}$.

Within the fuel detection system two models detect the fuel mixtures. The first model does this based on the oxygen content in the exhaust gas. In contrast to previous works, the fuel mixture can be detected without an additional measurement of the fuel consumption. This is achieved by a iterative approach to determine the injection mass. Here, the injected fuel mass is calculated based on look up tables for each possible mixing ratio (at 1% intervals) and the resulting theoretical oxygen content in the exhaust gas is compared with the measured oxygen content.

The second model evaluates the current of the electric fuel pump, so that the different viscosities of the fuels can be used to make a statement about the fuel mixture.

Together, mixtures of diesel and rapeseed oil as well as diesel and rapeseedmethylester can be reliably detected so that ECU parameters can be adjusted to them. Since the models work with series sensors, a cost-effective multi-fuel solution is conceivable with the models presented.

11.0.2 Fault Detection

In the second part of this thesis, new approaches to fault diagnosis for pure diesel fuel are presented. This includes especially the detection of injector deposits as well as detection of chip tuning. There is hardly any literature on chip tuning in the field of agricultural engineering. Therefore most common chip tuning variants are presented first. After most common methods are known,

three models are presented, with which injected fuel mass can be modeled.

1. The first model calculates the injected fuel mass based on the rail pressure signal. By evaluating the pressure drop during a fuel injection (density change of the fuel), the injected fuel mass can be modeled.
2. The second model calculates the injected fuel mass based on the metering unit of the high pressure pump. By a regression the fuel mass pumped into the rail can be calculated. Together with look-up tables for injector leakage the injected fuel mass can be determined.
3. The third model calculates the injected fuel mass based on the measured oxygen amount in the exhaust gas. A combustion model is used to calculate the burnt fuel mass in combination with the intake air flow of the engine.

Knowledge of the actual injected fuel mass offers a multitude of additional diagnostic possibilities. chip tuning (too high injection masses) can be detected as well as too low injection masses which can occur due to faults or wear.

Too low injection masses can also be detected by the presented *Injector Deposit Detection Model*. In addition, the model presents a fundamentally new approach which allows to detect faulty injector behavior (e.g. injector deposits) onboard of the machine. Especially injector opening and closing delays can be calculated with sufficient accuracy. This also opens up other new diagnostic possibilities. Replacing injectors before they fail (predictive maintenance), but also maintaining operation with worn injectors by countermeasures initiated by the ECU, could be applied.
Another advantage is that injectors can be inspected directly in the machine. This enables much shorter maintenance time, as not every single injector has to be removed and examined on an injector test bench.

12 Outlook

Like the main part of the work, the outlook is divided into two parts. The first part presents research questions that need to be addressed if multi-fuel capable engines should go into series production. The second part are research questions that need to be addressed for further improvements to increase the reliability of diesel engines.

Multi-Fuel-Engine:

- Fuel properties which are important for modern fuel systems (injector delay, ignition delay, combustion speed, spray properties...) must be researched for alternative fuels. The aim should be that all simulations which are currently performed for the design and parameterization of a modern diesel engines can also be performed with biogenic fuels.
- New ECU structures for multi fuel capable engines have to be created, so that all parameters can be optimized for the respective fuel. These should be independent of specific fuels, as the fuel mix could increase in the next years. An example could be combustion-controlled engines (e.g. in-cylinder pressure control). These could contribute to a better spread of environmentally friendly fuels because the engine operation can be controlled independently of the fuel.
- Exhaust emission measurements for biogenic fuels, where all parameters are optimized for the respective fuel should be done in the future. A changed emission behavior with biogenic fuels is repeatedly cited by critics, although the reason may not be the fuel but incorrect adaption of the engine. Furthermore, modern control procedures inside the ECU should be investigated with biogenic fuels. If emission measurements are carried out with different fuels and a cylinder pressure control, it is conceivable that e.g. the nitrogen oxide emissions of NRO fuel hardly differ from those of conventional diesel.
- Regeneration of the exhaust aftertreatment system and the cold start should be further improved for the operation with natural rapeseed oil. The parameterizations empirically found in this work have significantly improved the cold start as well as the DPF regeneration. However, for a production machine, DPF regeneration has to work in normal operation without any restrictions for customers.
- The shown fuel detection model based on oxygen concentration should also be tested with other oxygenated fuels. Especially synthetic fuels (with an oxygen content) have been increasingly investigated in the recent past, so that the detection model can bring advantages for a quicker market introduction.

In addition to technical challenges, there are also political obstacles to be overcome. Political incentives are needed to ensure that a more environmentally friendly fuel like natural rapeseed

oil is actually used on a larger scale. In Germany, this could be a reduction of the energy tax for farmers who produce their own fuel. In addition, machines that meet EU Stage 5 emissions standards could be approved for natural rapeseed oil operation without an extra homologation.
It is also conceivable that one defined fuel mixture is allowed without a new homologation of the engine. This could be a e.g. 50% natural rapeseed oil and 50% diesel blend. In this way the engine can be applied to this specific mixture and at the same time CO_2 footprint of agriculture is reduced with reasonable effort.

Fault detection:

- The presented models should be further investigated. Many of the models shown are sufficiently precise in high load points only. Especially the *Injector Deposit Detection Model* has great potential to avoid injector failure. However, there are some limitations regarding suitable load points, multiple injections or externally induced rail vibrations, which should be eliminated with series introduction.
- The presented models have the potential to detect many more faults (see Table 10.2). Combinations of faults and models should be investigated in further work. Especially if several sensor values are falsified at the same time (e.g. by sensor drifts), a reliable detection with the presented models is only possible to a limited extent.
- Results of all models of the onboard detection should be evaluated centrally (via internet connection of the machines).

With a central evaluation of the injector deposit detection system the formation process of deposits for different conditions (fuel quality, high altitude, application profile, etc.) can be better understood. The same could be done with the injected fuel mass models. At the moment there are no quantifiable statistics that capture the true extent of chip tuning. With the models presented, tuning measures (How big is the power increase? How many machines? Regional differences?) could be evaluated. These results can be used to increase the reliability of agricultural machinery and reduce the cost of warranty claims in the future.

Appendix

A.1 Fuel Analysis

The fuels used in this work were analyzed. The investigations were carried out externally. The results are shown under Table A.1.

Table A.1: Fuel Analysis carried out in this research work

fuel	test parameters	test method	test result	unit
B0	upper heating value (Ho,v)	DIN 51900-1 :2000 mod.	45793	J/g
	heating value (Hu,p)	DIN 51900-2 :2003 mod.	43120	J/g
	density (15 °C)	DIN EN ISO 12185 :1997	835.1	kg/m³
	carbon content	DIN 51732 :2014	86.6	% (m/m)
	hydrogen content	DIN 51732 :2014	13.4	% (m/m)
	nitrogen content	DIN 51732 :2014	<0.5	% (m/m)
	oxygen content	DIN 51732 :2014	<0.5	% (m/m)
B7	upper heating value (Ho,v)	DIN 51900-1 :2000 mod.	45725	J/g
	heating value (Hu,p)	DIN 51900-2 :2003 mod.	42840	J/g
	density (15 °C)	DIN EN ISO 12185 :1997	835.5	kg/m³
	carbon content	DIN 51732 :2014	85.6	% (m/m)
	hydrogen content	DIN 51732 :2014	13.3	% (m/m)
	nitrogen content	DIN 51732 :2014	<0.5	% (m/m)
	oxygen content	DIN 51732 :2014	1.1	% (m/m)
RME	upper heating value (Ho,v)	DIN 51900-1 :2000 mod.	39989	J/g
	heating value (Hu,p)	DIN 51900-2 :2003 mod.	37341	J/g
	density (15 °C)	DIN EN ISO 12185 :1997	879.5	kg/m³
	carbon content	DIN 51732 :2014	77.8	% (m/m)
	hydrogen content	DIN 51732 :2014	11.8	% (m/m)
	nitrogen content	DIN 51732 :2014	<0.5	% (m/m)
	oxygen content	DIN 51732 :2014	10.4	% (m/m)
Rapeseed	upper heating value (Ho,v)	DIN 51900-1 :2000 mod.	39746	J/g
	heating value (Hu,p)	DIN 51900-2 :2003 mod.	37112	J/g
	density (15 °C)	DIN EN ISO 12185 :1997	916.2	kg/m³
	carbon content	DIN 51732 :2014	77.6	% (m/m)
	hydrogen content	DIN 51732 :2014	11.7	% (m/m)
	nitrogen content	DIN 51732 :2014	<0.5	% (m/m)
	oxygen content	DIN 51732 :2014	10.7	% (m/m)

A.2 Fuel Properties of Rapeseed Oil

The following data were provided by the University of Applied Sciences Amberg-Weiden in the context of this research work. Table A.2 shows the most important properties of natural rapeseed oil for a typical temperature and pressure range of a diesel engine.

Table A.2: Fuel Properties of Rapeseed Oil

T	p	ρ	iso. K	E	C_p	adiab. K	u	η
(K)	(bar)	($kg\,m^{-1}$)	(1/bar)	(bar)	($J\,kg^{-1}$)	(1/bar)	($m\,s^{-1}$)	(mPa s)
293.15	0	916.74	5.80E-5	17229.34	2051.89	5.04E-5	1470.53	67.6
293.15	200	926.97	5.25E-5	19023.91	2045.65	4.51E-5	1536.42	94.08
293.15	400	936.49	4.80E-5	20818.46	2039.42	4.08E-5	1599.37	124.46
293.15	600	945.39	4.42E-5	22613.03	2033.18	3.72E-5	1659.81	162.3
293.15	800	953.76	4.09E-5	24407.59	2026.95	3.41E-5	1718.08	209.78
293.15	1000	961.67	3.81E-5	26202.15	2020.71	3.14E-5	1774.46	267.7
293.15	1200	969.18	3.57E-5	27996.71	2014.48	2.91E-5	1829.18	344.02
293.15	1400	976.32	3.35E-5	29791.27	2008.24	2.71E-5	1882.43	445.3
293.15	1600	983.15	3.16E-5	31585.83	2002.01	2.53E-5	1934.37	570.02
293.15	1800	989.68	2.99E-5	33380.39	1995.77	2.37E-5	1985.16	718.82
293.15	2000	995.96	2.84E-5	35174.95	1989.54	2.23E-5	2034.9	894.5
313.15	0	903.94	6.42E-5	15560.82	2147.23	5.61E-5	1403.33	33.4
313.15	200	915.07	5.76E-5	17355.38	2140.28	4.97E-5	1472.37	43.64
313.15	400	925.34	5.22E-5	19149.94	2133.34	4.46E-5	1538	54.36
313.15	600	934.89	4.77E-5	20944.50	2126.39	4.03E-5	1600.75	66.24
313.15	800	943.84	4.39E-5	22739.06	2119.44	3.67E-5	1661.03	80.48
313.15	1000	952.25	4.07E-5	24533.62	2112.48	3.37E-5	1719.19	98.8
313.15	1200	960.21	3.79E-5	26328.18	2105.54	3.11E-5	1775.51	118.32
313.15	1400	967.77	3.55E-5	28122.74	2098.60	2.88E-5	1830.2	143.06
313.15	1600	974.96	3.34E-5	29917.30	2091.65	2.68E-5	1883.45	171.86
313.15	1800	981.84	3.15E-5	31711.86	2084.60	2.50E-5	1935.44	205.94
313.15	2000	988.43	2.98E-5	33506.42	2077.75	2.34E-5	1986.3	248.9
333.15	0	891.14	7.11E-5	14048.28	2241.60	6.25E-5	1339.1	18.9
333.15	200	903.24	6.31E-5	15842.84	2233.88	5.48E-5	1411.45	21.14
333.15	400	914.32	5.67E-5	17637.41	2226.17	4.86E-5	1479.84	25.36
333.15	600	924.56	5.14E-5	19431.96	2218.44	4.36E-5	1544.93	30.48
333.15	800	934.10	4.71E-5	21226.52	2210.73	3.95E-5	1607.23	36
333.15	1000	943.05	4.34E-5	23021.08	2203.03	3.60E-5	1667.16	42
333.15	1200	951.47	4.02E-5	24815.64	2195.31	3.30E-5	1725.04	50.56
333.15	1400	959.44	3.75E-5	26610.20	2187.60	3.05E-5	1781.13	59.36
333.15	1600	967.01	3.52E-5	28404.76	2179.88	2.82E-5	1835.65	68.72
333.15	1800	974.23	3.31E-5	30199.32	2172.17	2.63E-5	1888.79	79.5
333.15	2000	981.13	3.12E-5	31993.88	2164.44	2.45E-5	1940.71	93.1

T (K)	p (bar)	ρ (kg m^{-1})	iso. K (1/bar)	E (bar)	C_p (J kg^{-1})	adiab. K (1/bar)	u (m s^{-1})	η (mPa s)
353.15	0	878.33	7.88E-5	12680.28	2336.56	6.97E-5	1277.83	12.2
353.15	200	891.48	6.90E-5	14474.85	2328.02	6.03E-5	1353.65	13.64
353.15	400	903.43	6.14E-5	16269.41	2319.48	5.30E-5	1424.87	14.96
353.15	600	914.40	5.53E-5	18063.97	2310.94	4.71E-5	1492.32	19.68
353.15	800	924.56	5.03E-5	19858.53	2302.40	4.24E-5	1556.64	19.06
353.15	1000	934.04	4.61E-5	21653.09	2293.86	3.84E-5	1618.3	22.1
353.15	1200	942.93	4.26E-5	23447.65	2285.32	3.50E-5	1677.7	24.58
353.15	1400	951.33	3.96E-5	25242.21	2276.78	3.22E-5	1735.13	29.28
353.15	1600	959.28	3.69E-5	27036.77	2268.23	2.97E-5	1790.86	34.56
353.15	1800	966.84	3.46E-5	28831.33	2259.60	2.76E-5	1845.09	39.48
353.15	2000	974.06	3.26E-5	30625.89	2251.16	2.56E-5	1898	43.8
373.15	0	865.53	8.73E-5	11445.38	2432.94	7.76E-5	1219.55	8.5
373.15	200	879.81	7.55E-5	13239.95	2423.52	6.62E-5	1298.98	9.3
373.15	400	892.67	6.65E-5	15034.51	2414.09	5.76E-5	1373.09	10.52
373.15	600	904.39	5.94E-5	16829.07	2404.66	5.08E-5	1442.91	11.72
373.15	800	915.19	5.37E-5	18623.63	2395.21	4.53E-5	1509.22	12.94
373.15	1000	925.22	4.89E-5	20418.19	2385.79	4.08E-5	1572.58	14.7
373.15	1200	934.60	4.50E-5	22212.75	2376.36	3.71E-5	1633.44	16.7
373.15	1400	943.42	4.16E-5	24007.31	2366.92	3.39E-5	1692.15	18.58
373.15	1600	951.75	3.87E-5	25801.87	2357.50	3.12E-5	1749.02	20.7
373.15	1800	959.66	3.62E-5	27596.43	2348.07	2.88E-5	1804.27	23.28
373.15	2000	967.19	3.40E-5	29390.99	2338.64	2.68E-5	1858.1	26.4
393.15	0	852.73	9.67E-5	10332.13	2529.81	8.65E-5	1164.24	6.3
393.15	200	868.23	8.24E-5	12126.69	2519.42	7.26E-5	1247.44	7.02
393.15	400	882.04	7.18E-5	13921.25	2509.03	6.24E-5	1324.51	7.74
393.15	600	894.54	6.36E-5	15715.81	2498.64	5.46E-5	1396.72	8.54
393.15	800	906.10	5.71E-5	17510.37	2488.25	4.83E-5	1464.99	9.42
393.15	1000	916.59	5.17E-5	19304.93	2477.86	4.33E-5	1530.01	10.3
393.15	1200	926.45	4.73E-5	21099.49	2467.46	3.91E-5	1592.28	11.34
393.15	1400	935.70	4.36E-5	22894.05	2457.08	3.56E-5	1652.23	12.74
393.15	1600	944.42	4.05E-5	24688.61	2446.69	3.26E-5	1710.17	14.3
393.15	1800	952.67	3.77E-5	26483.18	2436.30	3.01E-5	1766.38	15.98
393.15	2000	960.51	3.53E-5	28277.74	2425.91	2.78E-5	1821.08	17.9
413.15	0	839.93	1.07E-4	9329.070	2622.82	9.62E-5	1111.891	4.9
413.15	200	856.73	8.99E-5	11123.64	2611.40	7.95E-5	1199.07	4.66
413.15	400	871.55	7.74E-5	12918.20	2599.96	6.75E-5	1279.18	5.24
413.15	600	884.86	6.79E-5	14712.76	2588.54	5.85E-5	1353.81	5.81
413.15	800	896.98	6.05E-5	16507.32	2577.12	5.14E-5	1424.06	6.23
413.15	1000	908.13	5.46E-5	18301.88	2565.69	4.58E-5	1490.72	6.71
413.15	1200	918.48	4.97E-5	20096.44	2554.27	4.12E-5	1554.39	7.11
413.15	1400	928.16	4.56E-5	21891.00	2542.84	3.73E-5	1615.54	7.68
413.15	1600	937.25	4.22E-5	23685.56	2531.42	3.41E-5	1674.54	8.36
413.15	1800	945.84	3.92E-5	25480.12	2519.98	3.13E-5	1731.69	9.04
413.15	2000	953.99	3.66E-5	27274.68	2508.56	2.88E-5	1787.24	9.61

A.3 Injector Map Comparison B0-RME

The injector map comparison for B0 and RME is shown here for the sake of completeness. In comparison with Figure 5.1 the significantly smaller difference between the injection quantities can be seen.

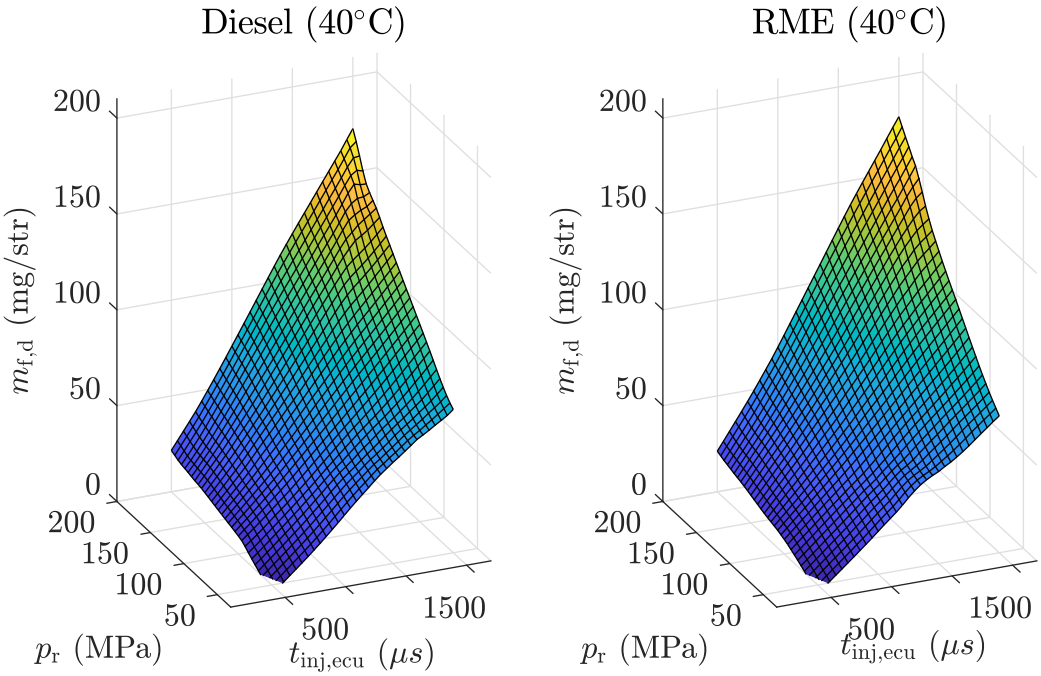

Figure A.1: Fuel quantity comparsion B0-RME

A.4 Formula Derivation of Oxygen-Mixture Model

The NO_X or O_2 sensor installed in series measures the concentration in ppm. Since air is assumed to be a mixture of nitrogen, oxygen and argon, as well as the products H_2O and CO_2 from a complete combustion, the measured oxygen value is calculated:

$$x_{O_2,meas} = \frac{n_{O_2,exh}}{n_{O_2,exh} + n_{N_2,air} + n_{Ar,air} + n_{CO_2} + n_{H_2O}} \tag{A.1}$$

It is assumed that argon and nitrogen do not participate in the combustion process, so that the same number of atoms as in the intake air are present in the exhaust gas.

$$n_{O_2,exh} = n_{O_2,air} - n_{CO_2} - 0.5 \cdot n_{H_2O} + n_{O_2,fuel} \tag{A.2}$$

Equation A.2 inserted in Equation A.1 results in:

$$x_{O_2,meas} = \frac{n_{O_2,air} - n_{CO_2} - 0.5 \cdot n_{H_2O} + n_{O_2,fuel}}{n_{O_2,air} + 0.5 \cdot n_{H_2O} + n_{O_2,fuel} + n_{N_2,air} + n_{Ar,air}} \tag{A.3}$$

The number of atoms, of the respective substance can be calculated using the molar masses:

$$n_{O_2,air} = \frac{m_{O_2,air}}{M_{O_2}} \tag{A.4}$$

$$n_{N_2,air} = \frac{m_{N2}}{2M_N} \tag{A.5}$$

$$n_{Ar,air} = \frac{m_{Ar}}{M_{Ar}} \tag{A.6}$$

$$n_{CO_2} = n_{C,fuel} \tag{A.7}$$

$$n_{H_2O} = n_{H_2,fuel} \tag{A.8}$$

$$n_{C,fuel} = \frac{w_{C,fuel}}{M_C} \cdot m_{fuel} \tag{A.9}$$

$$n_{H_2,fuel} = \frac{w_{H_2,fuel}}{2M_H} \cdot m_{fuel} \tag{A.10}$$

$$n_{O_2,fuel} = \frac{w_{O_2,fuel}}{2M_O} \cdot m_{fuel} \tag{A.11}$$

$$n_{O_2,air} = \frac{w_{O_2,air}}{2M_O} \cdot m_{air} \tag{A.12}$$

$$n_{N_2,air} = \frac{w_{N_2,air}}{2M_N} \cdot m_{air} \tag{A.13}$$

$$n_{Ar,air} = \frac{w_{Ar,air}}{M_{Ar}} \cdot m_{air} \tag{A.14}$$

If all equations in Equation A.3 are inserted, the result is

$$x_{O_2,meas} = \frac{\frac{w_{O_2,air}}{2M_O} \cdot m_{air} - \frac{w_{C,fuel}}{M_C} \cdot m_{fuel} - 0.5 \cdot \frac{w_{H_2,fuel}}{2M_H} \cdot m_{fuel} + \frac{w_{O_2,fuel}}{2M_O} \cdot m_{fuel}}{\frac{w_{O_2,air}}{2M_O} \cdot m_{air} + 0.5 \cdot \frac{w_{H_2,fuel}}{2M_H} \cdot m_{fuel} + \frac{w_{O_2,fuel}}{2M_O} \cdot m_{fuel} + \frac{w_{N_2,air}}{2M_N} \cdot m_{air} + \frac{w_{Ar,air}}{M_{Ar}} \cdot m_{air}} \tag{A.15}$$

Converted to m_{fuel} results in

$$m_{fuel} = m_{air} \cdot \frac{\frac{w_{O_2,air}}{2M_O} - O_{2,meas} \cdot (\frac{w_{O_2,air}}{2M_O} + \frac{w_{N_2,air}}{2M_N} + \frac{w_{Ar,air}}{M_{Ar}})}{(\frac{w_{C,fuel}}{M_C} + 0.5 \cdot \frac{w_{H_2,fuel}}{2M_H} - \frac{w_{O_2,fuel}}{2M_O}) + O_{2,meas} \cdot (0.5 \cdot \frac{w_{H_2,fuel}}{2M_H} + \frac{w_{O_2,fuel}}{2M_O})} \tag{A.16}$$

A.5 Invalid Load Points of the Oxygen-Mixture Model

Load points with a very flat falling theoretical oxygen content, or load points where measuring accuracy of the sensor is of great importance are automatically weighted weaker than load points with a strongly falling theoretical oxygen content, by using the LGF.

At certain load points theoretical oxygen content does not fall linearly with increasing diesel content of the mixture ratio (Figure A.2). As a result theoretical oxygen value cross the measured oxygen value (measured by O_2- sensor) for different mixing ratios.
Reason for this are non-linear injection quantities over different fuels (a mixture of 75% diesel and 25% NRO has a lower injection mass than 100% diesel in Figure A.2). Identical theoretical oxygen values in exhaust gas mean no clear mixing ratio can be determined via oxygen content. This effect is additionally reinforced by measurement inaccuracy of the O_2 sensor (comp. Figure A.2). A wide range of theoretical mixing ratios would result in the measured O_2 value in the shown example.
Theoretical oxygen content between about 45-75% diesel would satisfy the measured O_2 value range. Even if there are areas in the shown load point where only one mixture ratio meets the exact O_2 value (e.g. with a measured oxygen content of 7.5%, only a mixture ratio of approx. 90% diesel would have the same theoretical oxygen content), load points with a non-monotonically decreasing theoretical oxygen content are not evaluated. This simplifies the model, because valid ranges in which the O_2-value can be clearly assigned to a mixture ratio do not have to be detected. Since fuel does not change abruptly there is enough time to evaluate further load points. Since approx. 90% of the load diagram in “NRO - diesel operation” and approx 99% in “RME - diesel operation” consists of valid load points, this procedure of not evaluating every load point has no major disadvantages.

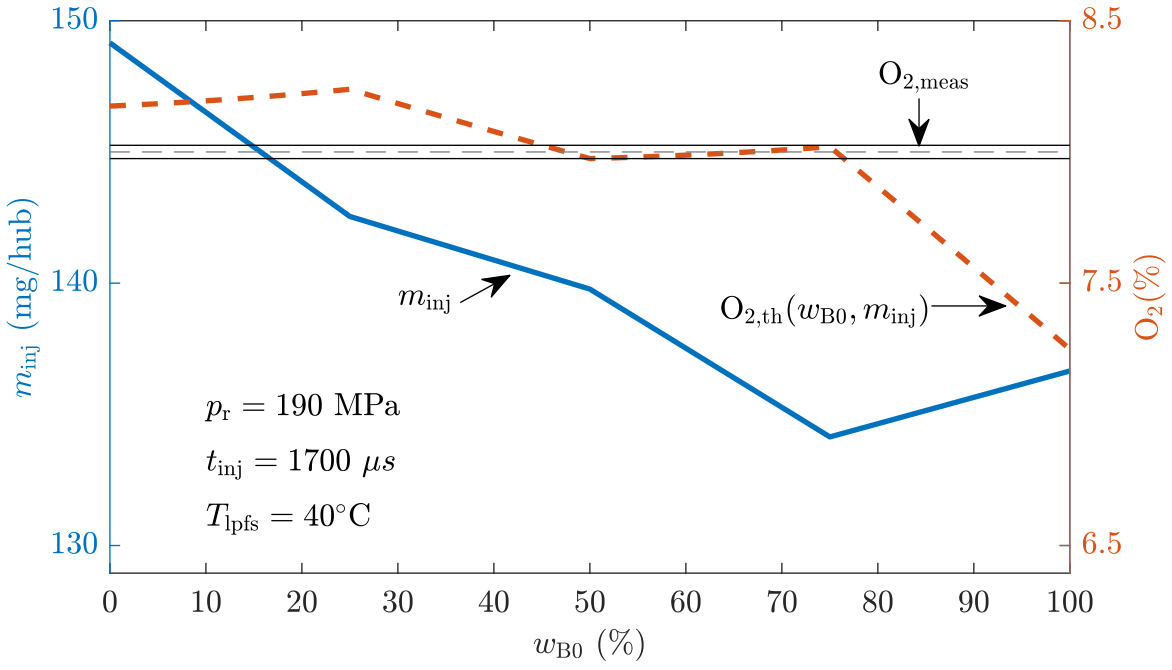

Figure A.2: Not used load point

A.6 Engine Oil Analysis

The engine oil analyses were also carried out externally. The analysis results are shown below. Since the engine oil was not renewed before each analysis, the fuel mass previously contained in the engine oil must be deducted for the fuel entry into the engine oil.

Parameter	Unit	New Oil	100_0_0	50_0_50	0_0_100	50_50_0	0_100_0	0_0_100	0_0_100	0_0_100	0_0_100
Hour of operation	h	60.3	61.3	62.3	63.3	64.3	65.3	68.4	72.4	73.4	74.4
Wear											
Iron	mg/kg	1	1	1	2	1	1	1	1	0	1
Chrome	mg/kg	0	0	0	0	0	0	0	0	0	0
Tin	mg/kg	0	0	0	0	0	0	0	0	0	0
Aluminium	mg/kg	1	1	1	1	1	1	1	1	0	1
Nickel	mg/kg	0	0	0	0	0	0	0	0	0	0
Copper	mg/kg	0	1	0	1	0	0	0	0	0	0
Lead	mg/kg	0	0	0	0	0	0	0	0	0	0
Manganese	mg/kg	0	0	0	0	0	0	0	0	0	0
PQ Index	mg/kg	<25	<25	<25	<25	<25	<25	<25	<25	<25	<25
Pollution											
Silicon	mg/kg	4	5	4	4	5	4	4	4	3	4
Potassium	mg/kg	0	1	0	1	1	1	1	1	1	1
Sodium	mg/kg	1	1	1	2	1	1	1	1	1	1
Water	%	<0.1	<0.1	<0.1	<0.1	<0.1	<0.1	<0.1	<0.1	<0.1	<0.1
IR glycol	(-)	negative	negative	negative	negative	negative	negative	negative	negative	negative	negative
Canola fuel	%	<0.1	<0.1	0.54	2.33	2.25	2.16	3.04	4.16	1.71	1.99
RME fuel	%	<0.1	<0.1	<0.1	<0.1	0.19	0.79	0.79	0.51	<0.1	<0.1
Diesel fuel	%	<0.1	0.36	0.89	0.87	1.03	0.99	0.99	0.61	<0.1	<0.1
Soot content	%	<0.1	<0.1	<0.1	<0.1	<0.1	<0.1	<0.1	<0.1	<0.1	<0.1
Oil condition											
Viscosity at 40°C	mm²/s	112.14	108.1	107.12	101.48	100.51	98.45	94.45	91.47	102.76	98.45
Viscosity at 100°C	mm²/s	15.21	14.95	1492	13.96	13.71	13.21	12.97	12.43	14.75	14.35
Oxidation	A/cm	1	1	2	3	2	2	3	3	2	2
Nitration	A/cm	0	1	0	1	0	0	0	0	0	0
Sulphation	A/cm	0	0	0	0	0	0	0	0	0	0
Dirt holding capacity	%	100	100	100	100	100	100	100	100	100	100
Additives											
Calcium	mg/kg	1114	1098	1104	1081	1076	1054	1014	992	1092	1077
Magnesium	mg/kg	618	607	598	592	588	589	569	511	612	596
Boron	mg/kg	204	206	205	196	194	192	196	184	206	192
Zinc	mg/kg	908	897	896	902	901	896	888	891	896	889
Phosphorus	mg/kg	778	756	761	771	768	764	746	761	764	768
Barium	mg/kg	0	0	0	0	0	0	0	0	0	0
Molybdenum	mg/kg	211	205	196	191	192	189	188	187	201	198
Sulphur	mg/kg	2374	2311	2291	2164	2169	2142	2134	2139	2234	2176

Figure A.3: Oil analysis performed in this research work

A.7 Neglecting the Leakage Quantity for Injection Models

Leakage quantity is determined via look-up tables based on rail pressure and injector pulse duration, similar to the state-of-the-art total injection quantity determination (section 3.5). Since rail pressure or injector pulse duration can be wrong during engine tuning, calculated leakage quantity is not exact.

However, leakage quantity is very small compared to the injected fuel mass (Table A.3). The injector was optimized for small leakage quantities since the leakage worsens the efficiency of

Table A.3: Fuel quantity comparsion

	m_{inj} (mg/str)	m_{leak} (mg/str)
series engine configuration	105	3.5
injector-pulse-tuning	115	3.8
rail-pressure-tuning	113	3.6

the engine [75]. For example, leakage quantity $m_{\text{leak,real}}$ is approx. 3.5 mg/str with a real injection of $m_{\text{inj,real}} = 105$ mg/str into the combustion chamber. If there is engine tuning, like extended injector pulse durations or a falsified rail pressure, calculated injection quantity has an error due to difference in leakage. Real fuel mass injected into the cylinder is 115 mg/str with injector-pulse-tuning. Real leakage quantity is 3.8 mg/str.
Since leakage quantity is calculated with the ECU value of the injector pulse duration (3.5 mg/str), error of leakage quantity would therefore be 0.3 mg/str. This is negligible in comparison to real injected fuel mass of 115 mg/str.

A.8 Restrictions of the RBFE-Model

Rail-pressure-tuning cannot be detected with the RBFE-Model. This effect can be illustrated by Figure A.4. If slight fuel temperature changes in the rail (due slightly falsified rail pressure) are neglected, fuel density depends only on rail pressure. In a small range such as a e.g. 10% increase in rail pressure, density change can be assumed to be linear (shown in red in Figure A.4). Definition of the RTF (Equation 7.1) leads to the rail pressure

$$p_{\text{r,bi}} = p_{\text{r,bi,ECU}} \cdot \text{RTF} \tag{A.17}$$

$$p_{\text{r,ai},i} = p_{\text{r,ai,ECU}} \cdot \text{RTF} \tag{A.18}$$

before and after an injection.
In the ECU density difference $\Delta\rho_{\text{ECU}}$ can be calculated using angular relationship.

$$\Delta\rho_{\text{ECU}} = (p_{\text{r,bi,ECU}} - p_{\text{r,ai,ECU}}) \cdot \tan(\alpha) \tag{A.19}$$

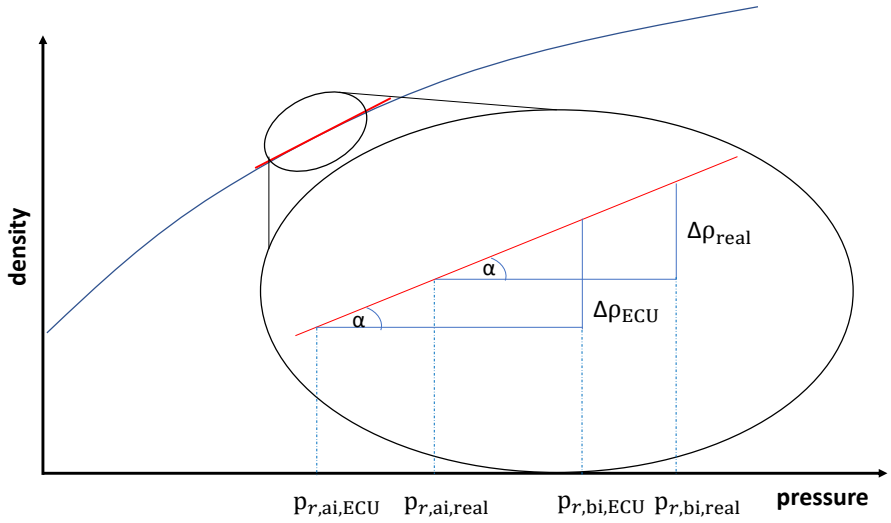

Figure A.4: Simplified density curve

Angle α can be calculated with real density difference and real rail pressure via angular relationship:

$$\alpha = \arctan\left(\frac{\Delta\rho_{\text{real}}}{p_{\text{r,bi}} - p_{\text{r,ai},i}}\right) \tag{A.20}$$

If α is inserted in Equation A.19 result is

$$\Delta\rho_{\text{ECU}} = (p_{\text{r,bi,ECU}} - p_{\text{r,ai,ECU}}) \cdot \tan\left(\arctan\left(\frac{\Delta\rho_{\text{real}}}{p_{\text{r,bi}} - p_{\text{r,ai},i}}\right)\right). \tag{A.21}$$

Equation A.21 becomes simpler after inserting Equation A.17 and Equation A.18:

$$\Delta\rho_{\text{ECU}} = \frac{\Delta\rho_{\text{real}}}{\text{RTF}} \tag{A.22}$$

If injected fuel mass is increased, due to a falsified rail pressure, measured pressure and density differences are reduced by just this factor. To illustrate effects, following assumptions are made:

- The course of the fuel density is linear to the rail pressure (red line in Figure A.4)
- A rail pressure increased by 10 % results in an increased injection quantity by 10 %.
- No injector leakage

This corresponds to a complete linearization. Measured pressure drop, or density difference at the ECU according to Equation A.22, would be reduced by the factor RTF (in this case 1.1) compared to real (tuned) pressured drop. Thus calculated RBFE value would correspond exactly to desired fuel quantity. Since in reality injected fuel quantity does not depend linearly on rail pressure, following assumptions

- The course of the fuel density is linear to the rail pressure (red line in Figure A.4)
- A rail pressure increased by 10 % results in an increased injection quantity by e.g. 7 % (depending on load point)
- No injector leakage

lead to an underestimation of the desired fuel. If it is further assumed the fuel density curve is linear, an increase in fuel mass by 7 % leads to an increase in pressure drop by 7 % at a rail pressure increased by 10 %. Since density difference according to Equation A.22 is reduced by the factor RTF (in this case 1.1) calculated model value of the *RBFE Model* is smaller than the desired fuel quantity.
If no more assumptions are made, but real values for fuel density and increase of the injection quantity are used

- The fuel density curve is degressive

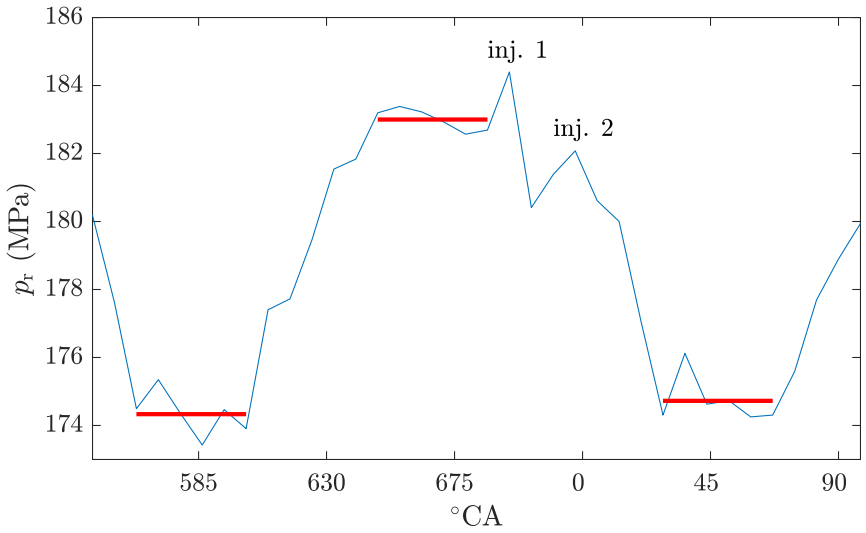

Figure A.5: Rail pressure depending on crankshaft angles with multi injection

- A rail pressure increased by 10 % results in an increased injection quantity by e.g. 7 % (depending on load point)
- Injector leakage present

there are two opposite effects. An injection quantity increased by 7 % theoretically still leads to smaller measured pressure drop, but the degressive course of fuel density leads to a larger pressure drop (if 7 % more fuel is injected, pressure drop must increase due to degressive course of density). Since real injector leakage is not known, the model would tend to overestimate desired fuel quantity.
Slope of fuel density and increase of injected fuel mass during rail-pressure-tuning depending on the respective load point. Even with a perfect *RBFE Model* (injector leakage exactly, no noise, density and temperatures exactly calculated for all load points) modeled value fluctuates around desired fuel quantity. It becomes clear that no rail-pressure-tuning can be detected with the RBFE model.

Another small limitation is the lack of handling multiple injections. For comparison, Figure A.5 shows the same load point as Figure 7.6, with an additional pre-injection. It becomes clear that the course is much more disturbed. With the method presented in Table 7.1 constant rail pressure zones can be determined. In the rail pressure course two injector pulses can be seen (peaks due to interference). If there are up to 5 injections, the model cannot be used.
However, the model works particularly well with large injection quantities. Here, multi injections are deactivated as standard, so only one large injection takes place. This results in a less disturbed signal and longer constant pressure zones. If the model is used in series production even with smaller injection quantities, it is possible to deactivate multiple injections for the use of the model only.

Bibliography

[1] A. Liaquat et al. “Impact of palm biodiesel blend on injector deposit formation”. In: *Applied energy* 111 (2013), pp. 882–893.

[2] H. Aatola et al. “Hydrotreated Vegetable Oil (HVO) as a Renewable Diesel Fuel: Trade-off between NOx, Particulate Emission, and Fuel Consumption of a Heavy Duty Engine”. In: *SAE International Journal of Engines* 1.1 (2009), pp. 1251–1262.

[3] Allcar Tuning. *Chip & Eco Tuning*. 2019. URL: https://allcartuning.com/.

[4] Allgemeiner Deutscher Automobil-Club e.V., ed. *ADAC Pannenstatistik 2018*. München.

[5] B. Argueyrolles et al. “Influence of injector nozzle design and cavitation on coking phenomenon”. In: *SAE Technical Paper Series*. SAE Technical Paper Series. SAE International400 Commonwealth Drive, Warrendale, PA, United States, 2007. DOI: 10.4271/2007-01-1896.

[6] D. Backofen, G. Braungarten, and H. Tschöke. “Nutzung von BCO in Motoren”. In: *Gülzower Fachgespräche* (2008), p. 154.

[7] R. Barbour et al. *Finding a solution to internal diesel injector deposits: Future Mobility : 12. June 2018*. Ostfildern: Technische Akademie Esslingen, 2018. ISBN: 978-3-943563-04-7.

[8] J. Barker et al. “Diesel injector deposits-an issue that has evolved with engine technology”. In: *SAE Technical Paper* 2011 ().

[9] W. Bartz, ed. *Fuels 2007: 6th international colloquium*. Ostfildern: Technische Akademie Esslingen, 2007. ISBN: 3-924813-67-1.

[10] C. Baumgarten et al. *Umwelt und Landwirtschaft: Ausgabe 2018*. Ed. by Umweltbundesamt Fachgebiet 1.5. 2018.

[11] C. Beatrice et al. “Assessment of biodiesel blending detection capability of the on-board diagnostic of the last generation automotive diesel engines”. In: *Fuel* 90.5 (2011), pp. 2039–2044.

[12] O. Bhardwaj et al. “Partikelfilter-Regeneration bei Biokraftstoffen”. In: *MTZ - Motortechnische Zeitschrift* 74.4 (2013), pp. 284–291. ISSN: 2192-8843. DOI: 10.1007/s35146-013-0071-0.

[13] BHP Motorsport. *Chiptuning für Traktoren und Landmachinen*. 18.12.2019. URL: https://www.bhp-chiptuning.com/.

[14] M. Brand, R. Fischer, and Gscheidle T. *Fachkunde Kraftfahrzeugtechnik*. 30., neubearbeitete Auflage. Europa-Fachbuchreihe für Kraftfahrzeugtechnik. Haan-Gruiten: Verlag Europa-Lehrmittel, 2013. ISBN: 978 3 8085 2240 0.

[15] M. Braunschweig and T. Czarnecki. “On-Board-Diagnose bei Dieselmotoren”. In: *MTZ - Motortechnische Zeitschrift* 65.7-8 (2004), pp. 552–557. ISSN: 0024-8525. DOI: 10.1007/BF03227199.

[16] S. Brysch. *Biogene Kraftstoffe in Deutschland: Biodiesel, Bioethanol, Pflanzenöl und Biomass-to-Liquid im Vergleich*. Vol. 12. Reihe Nachhaltigkeit. Hamburg: Diplomica Verl., 2008. ISBN: 3836606712.

[17] Bundesministerium für Ernährung und Landwirtschaft. *Ackerbau Erntebericht 2018*. Berlin.

[18] Bundesministerium für Ernährung und Landwirtschaft. *Ackerbau Erntebericht 2019*. Berlin.

[19] Bundesministerium für Umwelt, Naturschutz und nukleare Sicherheit. *Klimaschutzplan 2050: Klimaschutzpolitische Grundsätze und Ziele der Bundesregierung*. Ed. by Bundesministerium für Umwelt, Naturschutz und nukleare Sicherheit. Berlin, 2019.

[20] Bundesministerium für Wirtschaft und Energie. *Bekanntmachung zur Förderung von Forschung, Entwicklung und Demonstration in den Gebieten der „Angewandten Energieforschung“, der „Neuen Fahrzeug- und Systemtechnologien“ und der „Maritimen Technologien“ Programmübergreifende Förderinitiative „Energiewende im Verkehr: Sektorkopplung durch die Nutzung strombasierter Kraftstoffe“*. 2017.

[21] R. Caprotti et al. “Detergency Requirements of Future Diesel Injection Systems”. In: *SAE Technical Paper Series*. SAE Technical Paper Series. SAE International400 Commonwealth Drive, Warrendale, PA, United States, 2005. DOI: 10.4271/2005-01-3901.

[22] R. Caprotti et al. “RME Behaviour in Current and Future Diesel Fuel FIE’s”. In: *SAE Technical Paper Series*. SAE Technical Paper Series. SAE International400 Commonwealth Drive, Warrendale, PA, United States, 2007. DOI: 10.4271/2007-01-3982.

[23] A. P. Carlucci et al. “Advanced closed loop combustion control of a LTC diesel engine based on in-cylinder pressure signals”. In: *Energy Conversion and Management* 77 (2014), pp. 193–207.

[24] S. Clever. *Model-based fault detection and diagnosis for a common rail diesel engine: Zugl.: Darmstadt, Techn. Univ., Diss., 2011*. Vol. 1202. Berichte aus dem Institut für Automatisierungstechnik und Mechatronik der TU Darmstadt. Düsseldorf: VDI Verl., 2011. ISBN: 9783185202087.

[25] T. Dallmann, F. Posada, and A. Bandivadekar. “Costs of Emission Reduction Technologies for Diesel Engines Used in Non-Road Vehicles and Equipment”. In: *ICCT Work. Pap* 10 (2018).

[26] Das Europäische Parlamaent und der Rat der Europäiuschen Union. *Verordnung über die Anforderungen in Bezug auf die Emissionsgrenzwerte für gasförmige Schadstoffe und luftverunreinigende Partikel und die Typgenehmigung für Verbrennungsmotoren für nicht für den Straßenverkehr bestimmte mobile Maschinen und Geräte, zur Änderung der Verordnungen (EU) Nr. 1024/2012 und (EU) Nr. 167/2013 und zur Änderung und Aufhebung der Richtlinie 97/68/EG: EU2016/1628*. 16.09.2016.

[27] S. Dieringer. *Der Flexfuel Traktor: Untersuchungen zum Verbrennungsverhalten von Pflanzenölkraftstoffen und zur Unterscheidbarkeit fossiler und biogener Kraftstoffe: Zugl.: Hohenheim, Univ., Diss., 2012*. Berichte aus der Agrarwissenschaft. Aachen: Shaker, 2012. ISBN: 3844010106.

[28] P. Dönges and H. Traulsen. *Felderprobung Rapsöl pur*. DEULA Schleswig-Holstein GmbH, 2007.

[29] DTE Systems GmbH. *Innovatives Traktor-Tuning für mehr Leistung*. 2019. URL: https://www.chiptuning.com/.

[30] A. Duncan. "High-Pressure Viscosity of Biodiesel, Diesel, and Biodiesel-Diesel Blends: Experimental Data and Modeling". PhD thesis. University of Kansas.

[31] C. Düsseldorf. *Experimentelle Untersuchungen zur inner- und außermotorischen Partikelreduktion an einen Nutzfahrzeugdieselmotor zur Erfüllung der Abgasstufe IV im Betrieb mit biogenen Kraftstoffen: Zugl.: Kaiserslautern, Techn. Univ., Diss., 2014*. Vol. 15. VKM-Schriftenreihe. Kaiserslautern: Techn. Univ, 2015. ISBN: 9783943995862.

[32] S. Eakle et al. "Investigation of Urea Derived Deposits Composition in SCR Systems and Their Potential Effect on Overall PM Emissions". In: *SAE Technical Paper Series*. SAE Technical Paper Series. SAE International400 Commonwealth Drive, Warrendale, PA, United States, 2016. DOI: 10.4271/2016-01-0989.

[33] Eberl Tuning. *Motoren-Verbrauchsoptimierung*. URL: https://eberl-tuning.de/.

[34] B. Elvers and F. Ullmann, eds. *Ullmann's food and feed*. Weinheim: Wiley-VCH Verlag GmbH & Co. KGaA, 2017. ISBN: 9783527339907.

[35] P. Emberger. *Zünd-, Verbrennungs- und Emissionsverhalten verschiedener Pflanzenöle*. Ed. by Universitäts- Und Landesbibliothek Sachsen-Anhalt. 2013. DOI: 10.25673/914.

[36] J. Ettl et al. "Reale Emissionen eines pflanzenöltauglichen Traktors". In: *ATZoffhighway* 9.4 (2016), pp. 48–55. ISSN: 2191-1843. DOI: 10.1007/s35746-016-0038-4.

[37] Europäische Union. *Richtlinie 2007/46/EG des Europäischen Parlaments und des Rates vom 5. September 2007 zur Schaffung eines Rahmens für die Genehmigung von Kraftfahrzeugen und Kraftfahrzeuganhängern sowie von Systemen, Bauteilen und selbstständigen technischen Einheiten für diese Fahrzeuge*.

[38] W. Frede. *Handbuch für Lebensmittelchemiker: Lebensmittel, Bedarfsgegenstände, Kosmetika, Futtermittel*. 3. Aufl. Dordrecht: Springer, 2010. ISBN: 978-3-642-01684-4.

[39] S. Freitas et al. "Measurement and prediction of high-pressure viscosities of biodiesel fuels". In: *Fuel* 122 (2014), pp. 223–228. DOI: 10.1016/j.fuel.2014.01.031.

[40] M. Frobenius et al. “Interaktion von Injektorströmung und Spraybildung in mittelschnelllaufenden Common-Rail Dieselmotoren: Simulation und experimentelle Validierung”. In: *Diesel-und Benzindirekteinspritzung V: Spraybildung, Simulation, Applikation, Messtechnik: mit 29 Tabellen* 5 (2009), p. 202.

[41] I. Galiev et al. “Increase of efficiency of tractors use in agricultural production”. In: *Proceedings of 17th International Scientific Conference “Engineering for Rural Development*. Vol. 17. 2018, pp. 373–377.

[42] J. Galle et al. “Failure of fuel injectors in a medium speed diesel engine operating on bio-oil”. In: *Biomass and Bioenergy* 40 (2012), pp. 27–35.

[43] C. Gazzarin and M. Lips. “Berechnung und Grunddaten der Maschinenkosten”. In: *Agroscope-Reckenholz-Tänikon - Maschinenkostenbericht* (2013).

[44] C. Guardiola et al. “Closed-loop control of a dual-fuel engine working with different combustion modes using in-cylinder pressure feedback”. In: *International Journal of Engine Research* 21.3 (2020), pp. 484–496.

[45] C. Guido, C. Beatrice, and P. Napolitano. “Application of bioethanol/RME/diesel blend in a Euro5 automotive diesel engine: potentiality of closed loop combustion control technology”. In: *Applied energy* 102 (2013), pp. 13–23.

[46] G. Haarlemmer et al. “Investment and production costs of synthetic fuels–A literature survey”. In: *Energy* 66 (2014), pp. 667–676.

[47] M. Habrioux et al. “High pressure density and speed of sound in two biodiesel fuels”. In: *Journal of Chemical & Engineering Data* 58.12 (2013), pp. 3392–3398.

[48] J. Hagen et al. “Optimierung der dieselmotorischen Verbrennung durch Weiterentwicklung des Injektors”. In: *MTZ-Motortechnische Zeitschrift* 77.4 (2016), pp. 16–23.

[49] E. Hassel and V. Wichmann. “Ergebnisse des Demonstrationsvorhabens „Praxiseinsatz von serienmäßigen neuen rapsöltauglichen Traktoren “”. In: (2005). URL: http://www.%20biotrieb.%20org/fileadmin/user%5Ctextunderscore%20upload/biotrieb/pdf/100traktorenErgebnisse.%20pdf.

[50] P. Hendriksen et al. “Alternative Fuels”. In: *Transforming Urban Mobility* (2019), p. 87.

[51] A. Hoang and A. Le. “Trilateral correlation of spray characteristics, combustion parameters, and deposit formation in the injector hole of a diesel engine running on preheated Jatropha oil and fossil diesel fuel”. In: *Biofuel Research Journal* 6.1 (2019), pp. 909–919. DOI: 10.18331/BRJ2019.6.1.2.

[52] Hochschule Amberg-Weiden. “Rapsöl DIN 51605 Messungen”. Messdaten in Kooperation mit Flucon. Amberg-Weiden, 2013.

[53] H. Hoffmann. *A contribution to the investigation of internal Diesel injector deposits: Dissertation*. Vol. Band 39. Berichte aus der Verbrennungstechnik. 2018. ISBN: 978-3-8440-5953-3.

[54] O. Hofmann et al. “Optimal Injection Strategies to Compensate for Injector Aging in Common Rail Fuel Systems”. In: *SAE International Journal of Engines* 11.6 (2018), pp. 1083–1092.

[55] U. Hofmann, P. Reinhardt, and M. Evtimova. “Untersuchungen zum Einsatz eines Partikelfiltersystems beim Betrieb eines Dieselmotors mit Rapsmethylester und Rapsöl”. In: *Chemie Ingenieur Technik* 78.6 (2006), pp. 709–714. ISSN: 0009-286X. DOI: 10.1002/cite.200500188.

[56] H. Holzmann. *Business Unit Sensors & Actuators: Smart NOx Sensor*. Ed. by Continental Division Powertrain. 2009.

[57] H. Holzmann. *Smart NOx Sensor: 3rd Generation*. Ed. by Continental Division Powertrain. 2013.

[58] A. Hoy et al. “The extreme European summer of 2015 in a long-term perspective”. In: *International Journal of Climatology* 37.2 (2017), pp. 943–962.

[59] Y. Hu et al. “Accommodation closed-loop control of dieseline fueled flexible fuel engine based on in-cylinder pressure sensor”. In: *IFAC-PapersOnLine* 49.11 (2016), pp. 202–209.

[60] Benedikt Huber and Heinz Ulbrich. “Modeling and Experimental Validation of the Solenoid Valve of a Common Rail Diesel Injector”. In: *SAE Technical Paper Series*. SAE Technical Paper Series. SAE International400 Commonwealth Drive, Warrendale, PA, United States, 2014. DOI: 10.4271/2014-01-0195.

[61] R. Isermann. “Combustion engine diagnosis: Model-based condition monitoring of gasoline and diesel engines and their components”. In: *ATZ / MTZ-Fachbuch* (2017). DOI: 10.1007/978-3-662-49467-7. URL: http://dx.doi.org/10.1007/978-3-662-49467-7.

[62] R. Isermann. “Fault diagnosis of diesel engines”. In: *Mechanical Engineering-CIME* 135.12 (2013), S6–S6.

[63] R. Isermann. *Mechatronische Systeme: Grundlagen*. 2., vollst. neu bearb. Aufl. Berlin: Springer, 2008. ISBN: 978-3-540-32336-5. DOI: 10.1007/978-3-540-32512-3.

[64] R. Isermann. “Modellbasierte Diagnose von Dieselmotoren”. In: *MTZ-Motortechnische Zeitschrift* 78.4 (2017), pp. 70–77.

[65] A. Janssen et al. “Tailor-Made Fuels from Biomass for Homogeneous Low-Temperature Diesel Combustion”. In: *Energy & Fuels* 25.10 (2011), pp. 4734–4744. ISSN: 0887-0624. DOI: 10.1021/ef2010139.

[66] A. Joedicke et al. “Understanding the Effect of DISI Injector Deposits on Vehicle Performance”. In: *SAE Technical Paper Series*. SAE Technical Paper Series. SAE International400 Commonwealth Drive, Warrendale, PA, United States, 2012. DOI: 10.4271/2012-01-0391.

[67] John Deere Product configurator. *List prices: Configure your tractor*. 2019. URL: https://configurator.deere.com/.

[68] R. Junk et al. *Ablagerungen in Common Rail Injektoren-kraftstoffseitige und konstruktive Maßnahmen: Schlussbericht zum Vorhaben*. Universität Rostock, Lehrstuhl für Kolbenmaschinen und Verbrennungsmotoren, 2018.

[69] Karlheinz KORBEL Gesmbh. *KORBEL Racing: Chiptuning*. URL: https://www.autokorbel.at/.

[70] M. Keskin and Y. ŞEKERLI. "An evaluation of combine harvester accidents in turkey". In: *Mustafa Kemal Üniversitesi Ziraat Fakültesi Dergisi* 23.2 (2018), pp. 137–147.

[71] M. Klaissle. "Ablagerungsbildung beim Betrieb eines Dieselmotors mit Rapsölkraftstoff". München, Technische Universität München, Diss., 2013. München: Universitätsbibliothek der TU München, 2013. URL: http://nbn-resolving.de/urn/resolver.pl?urn:nbn:de:bvb:91-diss-20131010-1115826-0-8.

[72] P. Lacey et al. "Fuel quality and diesel injector deposits". In: *SAE International Journal of Fuels and Lubricants* 5.3 (2012), pp. 1187–1198.

[73] M. Lecompte et al. "The Benefits of Diesel Exhaust Fluid (DEF) Additivation on Urea-Derived Deposits Formation in a Close-Coupled Diesel SCR on Filter Exhaust Line". In: *SAE International Journal of Fuels and Lubricants* 10.3 (2017), pp. 864–876.

[74] H. Li et al. "Effect of Multifunctional Fuel Additive Package on fuel injector deposit, combustion and emissions using pure rape seed oil for a DI diesel". In: *SAE International Journal of Fuels and Lubricants* 2.2 (2010), pp. 54–65.

[75] S. Matsumoto et al. "The New Denso Common Rail Diesel Solenoid Injector". In: *MTZ worldwide* 74.2 (2013), pp. 44–48. ISSN: 2192-9114. DOI: 10.1007/s38313-013-0018-3.

[76] K. Maurer. "Motorprüflauf mit Rapsöl-Diesel-Mischungen: Förderkennzeichen: FNR220268000". In: *Schlussbericht, Universität Hohenheim* (2003).

[77] G. Merker and R. Teichmann, eds. *Grundlagen Verbrennungsmotoren: Funktionsweise und alternative Antriebssysteme : Verbrennung, Messtechnik und Simulation*. 8., vollständig überarbeitete und erweiterte Auflage. ATZ/MTZ-Fachbuch. Wiesbaden: Springer Vieweg, 2018. ISBN: 978-3-658-19211-2. DOI: 10.1007/978-3-658-19212-9.

[78] K. Min, J. Chung, and M. Sunwoo. "Torque balance control for light-duty diesel engines using an individual cylinder IMEP estimation model with a single cylinder pressure sensor". In: *Applied Thermal Engineering* 109 (2016), pp. 440–448.

[79] M. Mudersbach et al. *Jahresbericht des BDL: Zahlen und Fakten zum Leasing-Markt*. Ed. by Bundesverband Deutscher Leasing Unternehmen. Berlin, 2019.

[80] T. Nguyen, J. Bazile, and D. Bessières. "Density measurements of waste cooking oil biodiesel and diesel blends over extended pressure and temperature ranges". In: *Energies* 11.5 (2018), p. 1212.

[81] B. Nikolić et al. “Function K – as a Link between Fuel Flow Velocity and Fuel Pressure, Depending on the Type of Fuel”. In: *Facta Universitatis, Series: Mechanical Engineering* 15.1 (2017), p. 119. ISSN: 0354-2025. DOI: 10.22190/FUME160628003N.

[82] B. Osterburg et al. “Erfassung, Bewertung und Minderung von Treibhausgasemissionen des deutschen Agrar- und Ernährungssektors: Studie im Auftrag des Bundesministeriums für Ernährung, Landwirtschaft und Verbraucherschutz”. In: *Arbeitsberichte aus der VTI-Agrarökonomie* (2009).

[83] R. Payri et al. “The effect of temperature and pressure on thermodynamic properties of diesel and biodiesel fuels”. In: *Fuel* Volume 90 (2011), pp. 1172–1180.

[84] P. Pickel. “Ackerbauliche Elektromobilität–mobile Maschinen am Netz: Kuratorium für Technik und Bauwesen in der Landwirtschaft e. V. (KTBL)”. In: *Mit Energie in die Zukunft-Strom, Wärme und Kraftstoffe in der Landwirtschaft* (2020), p. 50.

[85] P. Pickel and G. Höner. “Hirsche mit Akku”. In: *Top Agrar 45 (2018)*, pp. 106–108.

[86] S. Pischinger. “Die Zeit ist reif für neue Generationen von Kraftstoffen: Wiesbaden, Springer Fachmedien”. In: *MTZ-Motortechnische Zeitschrift* 77 (2016), pp. 24–27.

[87] H. Prankl and H. Schaufler. “Motortuning zur Leistungssteigerung an Traktoren”. In: *Bericht BLT053322, Francisco Josephinum Wieselburg* (2006).

[88] Prof. Heinz Flessa. *Treibhausgasemissionen der deutschen Landwirtschaft: Quellen, Entwicklungen, Minderungen: Fachtagung Klimaschutz*. Braunschweig, 2019.

[89] V. Quaschning. *Regenerative Energiesysteme: Technologie – Berechnung – Klimaschutz*. 10., aktualisierte und erweiterte Auflage. 2019. ISBN: 978-3-446-46113-0.

[90] R. Quigley et al. *A study of the internal injector deposit phenomenon*. Ed. by Lubrizol Corporation. 2010.

[91] A. Ramadhas. *Alternative Fuels for Transportation*. Mechanical and Aerospace Engineering Series. Boca Raton: CRC Press, 2016. ISBN: 1439819572.

[92] C. Rapp. *Hydraulik für Ingenieure und Naturwissenschaftler: Ein Kurs mit Experimenten und Open-Source Codes*. Lehrbuch. Wiesbaden: Springer Vieweg, 2017. ISBN: 978-3-658-18618-0. DOI: 10.1007/978-3-658-18619-7.

[93] O. Reichert. *Reichert Racing: Chiptuning für Agrarfahrzeuge, Traktoren, Mähdrescher*. Tittmoning. URL: http://www.chiptuning.tv/.

[94] K. Reif. *Dieselmotor-Management: Systeme, Komponenten, Steuerung und Regelung*. 5., überarbeitete und erweiterte Auflage. SpringerLink Bücher. Wiesbaden: Vieweg+Teubner Verlag, 2012. ISBN: 978-3-8348-2179-9. DOI: 10.1007/978-3-8348-2179-9.

[95] K. Reif, ed. *Dieselmotor-Management: Systeme, Komponenten, Steuerung und Regelung*. 6. Auflage 2019, überarb. u. erw. Bosch Fachinformation Automobil. Wiesbaden: Springer Fachmedien Wiesbaden GmbH, 2019. ISBN: 978-3-658-25071-3.

[96] K. Reif, ed. *Sensoren im Kraftfahrzeug*. 3. Auflage. Bosch Fachinformation Automobil. Wiesbaden: Springer Vieweg, 2016. ISBN: 978-3-658-11210-3.

[97] E. Remmele. *Standardisierung von Rapsöl als Kraftstoff*. München: Hieronymus Buchreproduktions GmbH, 2002.

[98] Remmele et al. “Biodiesel, Rapsöl und Methan als Kraftstoff für Traktoren”. In: *Mit Energie in die Zukunft* (2020), p. 42.

[99] B. Richter et al. “Charakterisierung interner Ablagerungen in Common-Rail-Injektoren”. In: *MTZ-Motortechnische Zeitschrift* 74 (2013), pp. 796–803.

[100] J. Rockström et al. “A roadmap for rapid decarbonization”. In: *Science* 355.6331 (2017), pp. 1269–1271.

[101] S. Schuckert, M. Huthmacher, and G. Wachtmeister. *Compensation Strategies for Aging Effects of Common-Rail Injector Nozzles*. 2019.

[102] W. Schüle. *Leitfaden der Technischen Wärmemechanik: Kurzes Lehrbuch der Mechanik der Gase und Dämpfe und der mechanischen Wärmelehre*. Vierte, vermehrte und verbesserte Auflage. Berlin, Heidelberg: Springer Berlin Heidelberg, 1925. ISBN: 978-3-642-90382-3. DOI: 10.1007/978-3-642-92239-8.

[103] S. Schwab et al. “Internal injector deposits in high-pressure common rail diesel engines”. In: *SAE International Journal of Fuels and Lubricants* 3.2 (2010), pp. 865–878.

[104] T. Sem. “Investigation of Injector Tip Deposits on Transport Refrigeration Units Running on Biodiesel Fuel: SAE 2004 World Congress & Exhibition”. In: *SAE Technical Paper Series*. SAE Technical Paper Series. SAE International400 Commonwealth Drive, Warrendale, PA, United States, 2004. DOI: 10.4271/2004-01-0091.

[105] K. Sethanunt and S. Koetniyom. “Influence of fuel pressure increment in diesel common rail engine using external tuning box”. In: *International Journal of Engineering Science and Innovative Technology (IJESIT) Volume* 2 (2013), pp. 246–253.

[106] P. Singh, V. Goel, and S. Chauhan. “Impact of dual biofuel approach on engine oil dilution in CI engines”. In: *Fuel* 207 (2017), pp. 680–689.

[107] P. Smith et al. “Agriculture, forestry and other land use (AFOLU)”. In: *Climate change 2014: mitigation of climate change. Contribution of Working Group III to the Fifth Assessment Report of the Intergovernmental Panel on Climate Change*. Cambridge University Press, 2014, pp. 811–922.

[108] M. Sosio. *Einfluss der Motorbetriebstemperatur auf die Entstehung der Stickstoffmonoxidemissionen während instationärer Vorgänge am PKW-Dieselmotor*. Research. Wiesbaden: Springer Vieweg, 2020. ISBN: 978-3-658-30471-3.

[109] U. Spicher and M. Lüft. *Optimierung der Kraftstoffstrahlausbreitung für Pflanzenöl, insbesondere natürliches Rapsöl, bei der Verwendung moderner Diesel-Einspritzsysteme: Abschlussbericht: Forschungsvorhaben BWK 25002*. Ed. by Karlsruhe: Institut für Kolbenmaschinen der Universität Karlsruhe. Karlsruhe, 2007.

[110] K. Stephan and F. Mayinger. *Thermodynamik: Band 1: Einstoffsysteme. Grundlagen und technische Anwendungen*. Springer-Verlag, 2013.

[111] M. Stöhr. *Regional-ökonomische Effekte der Nutzung von Pflanzenöl-Kraftstoff in Landmaschinen*. Ed. by B.A.U.M. Consult GmbH. München, 2015. DOI: 10.13140/RG.2.1.4427.1522.

[112] M. Stöhr, S. Giglmaier, and R. Berlet. *Folgenabschätzung zum Einsatz batteriebetriebener vollelektrifizierter Landmaschinen*. Ed. by BAUM Consult GmbH. München, 2015.

[113] M. Stöhr and P. Pickel. *Klimadesign von Pflanzenölkraftstoffen für landwirtschaftliche Maschinen: LANDTECHNIK, Bd. 67 Nr. 1 Seite 65–68*. 2012. DOI: 10.15150/LT.2012.596.

[114] V. Strots et al. "Deposit formation in urea-SCR systems". In: *SAE International Journal of Fuels and Lubricants* 2.2 (2010), pp. 283–289.

[115] KW-Systems. *The Power inside*. URL: https://kw-chiptuning.com/.

[116] J. Tang. "Belagbildung in Einspritzdüsen direkteinspritzender Dieselmotoren". Dissertation. Aachen: RWTH Aachen University, 2010.

[117] J. Tang et al. "Einflüsse auf die Belagsbildung bei Einspritzdüsen von Diesel motoren mit Direkteinspritzung". In: *MTZ - Motortechnische Zeitschrift* 69.9 (2008), pp. 754–761. ISSN: 2192-8843. DOI: 10.1007/BF03227487.

[118] N. Tarasinski, V. Kegel, and J. Daubermann. *GridCON - Development and Testing of a Cable-fed Full Electric and Autonomous Agricultural Machine*. Düsseldorf, 2018.

[119] TEC Power. *Chiptuning Qualität ist programmierbar*. URL: http://www.tec-power.de/.

[120] K. Thuneke and B. Widmann. "Rapsöl als Schlepperkraftstoff–Techniken und Perspektiven". In: *Ackerbau der Zukunft* (2002), p. 23.

[121] H. Tschöke, K. Mollenhauer, and R. Maier, eds. *Handbuch Dieselmotoren*. 4. Auflage. Springer Reference Technik. Wiesbaden: Springer Vieweg, 2018. ISBN: 978-3-658-07697-9. DOI: 10.1007/978-3-658-07697-9.

[122] F. Tubiello et al. *Agriculture, Forestry and Other Land Use Emissions by Sources and Removals by Sinks: 1990-2011 Analysis*. FAO, 2014. DOI: 10.13140/2.1.4143.4245.

[123] GP-Tuning. *Chiptuning- / Leistungsoptimierungs- und Softwaretuning-Partner für Motorsportfahrzeuge*. URL: https://www.gp-tuning.at.

[124] J. Ullmann et al. "Investigation into the Formation and Prevention of Internal Diesel Injector Deposits". In: *SAE International* 2008-01-0926 (2008). DOI: 10.4271/2008-01-0926.

[125] R. van Basshuysen and F. Schäfer, eds. *Handbuch Verbrennungsmotor: Grundlagen, Komponenten, Systeme, Perspektiven*. 8. überarbeitete Auflage. ATZ / MTZ-Fachbuch. Wiesbaden: Springer Vieweg, 2017. ISBN: 978-3-658-10901-1. DOI: 10.1007/978-3-658-10902-8.

[126] J. Wang et al. *Fuel property-adaptive engine control system with on-board fuel classifier*. Patent Number: 7,266,439, 2007.

[127] G. Wcisło. *Determination of rapeseed oils combustion heat in calorimeter bomb and an assessment of the heat value*. 2005.

[128] C. Weeks et al. “Analytical investigation of urea deposits in SCR system”. In: *SAE International Journal of Engines* 8.3 (2015), pp. 1219–1239.

[129] C. Wolf et al. “Methoden zur Analyse und Bewertung ausgewählter ökologischer und ökonomischer Wirkungen von Produktsystemen aus land-und forstwirtschaftlichen Rohstoffen”. In: *ExpRessBio, Berichte aus dem TFZ* 45 (2016), p. 165.

[130] M. Wörgetter. *Local and Innovative Biodiesel: Final Report: Altener Project No. 4.1030/C/02-22*. Wieselburg, 2006.

[131] R. Zahoransky. “Stationäre Kolbenmotoren für energetischen Einsatz”. In: *Energietechnik*. Springer, 2015, pp. 231–268.

[132] J. Zhao and J. Wang. *Energy-based and oxygen-based biodiesel blend level estimation methods for diesel engines*. 2012.

[133] A. Ziegler. *Ansatzpunkte und Potentiale zur Minderung des Treibhauseffektes aus Sicht der fossilen Energieträger: DGMK-Projekt 448-1; Forschungsbericht 448-1*. Als Ms. gedr. Berichte / Deutsche Wissenschaftliche Gesellschaft für Erdöl, Erdgas und Kohle e.V. Hamburg: DGMK, 1992. ISBN: 3-928164-25-2.

Own Publications

Main Author

ATZ live: Heavy-Duty-, On- und Off-Highway-Motoren 2019, “Model-Based Injector Deposit Detection”, Hinrichs M., Isermann R., Pickel P., Friedrichshafen

VDI Landtechnik 2019: 77.Landtechnik AgEng 2019, “Model-Based Chiptuning Detection of Diesel Engines”, Hinrichs M., Isermann R., Pickel P., Hannover

Fuels of the Future 2020, “Onboard fuel detection of a stage 5 engine”; Hinrichs M., Berlin

ATZ live: Simulation und Test 2019, “modelbasierte Kraftstofferkennung im Dieselmotor”; Hinrichs M., Isermann R., Pickel P., Hanau

Co-Author

Berichte aus dem TFZ 63: Rapsölkraftstoff als Energieträger für den Betrieb eines forstwirtschaftlichen Vollernters (Harvester); Emberger P., Mautner S., Hinrichs M., Thuneke K., Remmele E.

Field tests and real-world exhaust gas emissions of a pure rapeseed oil-fuelled harvester in forestry: Testing a solution for combined water, soil, and climate protection; Emberger P., Hinrichs M., Huber G., Emberger-Klein A., Thuneke K., Pickel P., Remmele E.

Supervised student Theses

Erkennen eines fehlerbehafteten Luftpfades eines Dieselmotors der Abgasstufe 4, im Betrieb mit sauerstoffhaltigen Kraftstoffen, Bachelorthesis; Moellmann J.

Isolation geeigneter Sensoren zur Kraftstoffdetektion und zum Einsatz für beliebige Kraftstoffgemische in einem Dieselmotor, Bachelorthesis; Ruland F.

Aufbau eines Simulationsmodels zur Erstellung von Injektorkennfeldern für verschiedene Kraftstoffmischungen, Masterthesis; Schroeder A.

Emissionsanalyse eines Final Tier 4 Nutzfahrzeugdieselmotors im Rapsöl- und Dieselbetrieb unter Variation des Lambda-Wertes, Diplomarbeit; Hinkelmann P.